# Pullout Resistance of Mechanically Stabilized Reinforcements in Backfills Typically Used in Texas: Volume 1

Priyantha Jayawickrama, James G. Surles,
Timothy D. Wood, William D. Lawson

Texas Department of Transportation

**NOTICE**

The United States Government and the State of Texas do not endorse products or manufacturers. Trade or manufacturers' names appear herein solely because they are considered essential to the object of this report.

**Technical Report Documentation Page**

| 1. Report No.:<br><br>FHWA/TX-13/0-6493-1 | 2. Government Accession No.: | 3. Recipient's Catalog No.: |
|---|---|---|
| 4. Title and Subtitle:<br>Pullout Resistance of MSE Reinforcements in Backfills Typically Used in Texas: Volume 1, Research Report | | 5. Report Date:<br>August 15, 2013 |
| | | 6. Performing Organization Code: |
| 7. Author(s): Jayawickrama, P.W., J.G. Surles, T.A. Wood, and W.D. Lawson | | 8. Performing Organization Report No. 0-6493-R1 |
| 9. Performing Organization Name and Address:<br>   Center for Multidisciplinary Research in Transportation<br>   Texas Tech University<br>   Box 41023<br>   Lubbock, Texas 79409-1023 | | 10. Work Unit No. (TRAIS): |
| | | 11. Contract or Grant No. :<br>   Project 0-6493 |
| 12. Sponsoring Agency Name and Address<br>   Texas Department of Transportation<br>   Research and Technology<br>   P. O. Box 5080<br>   Austin, TX 78763-5080 | | 13. Type of Report and Period Cover:  Technical Report |
| | | 14. Sponsoring Agency Code: |
| 15. Supplementary Notes:<br>   This study was conducted in cooperation with the Texas Department of Transportation | | |

16. Abstract:

   This report documents findings from a three-year research study that examined the pullout resistance of inextensible MSE reinforcements in backfills typically used in Texas. The study involved an extensive laboratory test program in which a total of 650 pullout tests were completed. These tests were conducted using a large scale pullout test system that consisted of a test box with dimensions of 12ft x 12ft x 4ft and capability to simulate overburden pressures equivalent to 40 feet of fill. Tests were conducted on ribbed strip reinforcements, welded steel grid reinforcements, and a limited number of smooth bars embedded in two types of backfill, designated as Type A (gravelly) and Type B (sandy) select backfill as per TxDOT specifications. A subset of strip and grid reinforcements in each backfill type was instrumented with strain gages to provide further insight into mechanisms that control pullout resistance. The research design evaluated pullout resistance factors for both strip and grid reinforcements for a variety of independent variables including overburden pressure, reinforcement length, skew or splay angle, grid wire size, and grid geometry including both transverse and longitudinal wire spacing. Appropriate statistical analyses were used to interpret the data within the context of published AASHTO design guidance for inextensible MSE reinforcements.  This volume, Volume 1, summarizes the research findings. Volume 2 and Volume 3 present the test reports for MSE reinforcements in Type B and Type A backfill, respectively.

| 17. Key Words<br>  Pullout Resistance, MSE Walls, Internal Stability, Inextensible Reinforcement, TxDOT | | 18. Distribution Statement<br>   No restrictions.  This document is available to the public through the National Technical Information Service, Springfield, Virginia 22161, www.ntis.gov | |
|---|---|---|---|
| 19. Security Classif. (of this report)<br>   Unclassified | 20. Security Classif. (of this page)<br>   Unclassified | 21. No. of Pages<br>274 | 22. Price |

Form DOT F 1700.7 (8-72)

# Pullout Resistance of Mechanically Stabilized Reinforcements in Backfills Typically Used in Texas

By

Priyantha W. Jayawickrama

James G. Surles

Timothy A. Wood

William D. Lawson

Research Project Number 0-6493

Research Report Number 0-6493-1, Volume 1

**AUTHOR'S DISCLAIMER**

The contents of this report reflect the views of the authors who are responsible for the facts and the accuracy of the data presented herein. The contents do not necessarily reflect the official view of policies of the Texas Department of Transportation or the Federal Highway Administration. This report does not constitute a standard, specification, or regulation.

**PATENT DISCLAIMER**

There was no invention or discovery conceived or first actually reduced to practice in the course of or under this contract, including any art, method, process, machine, manufacture, design or composition of matter, or any new useful improvement thereof, or any variety of plant which is or may be patentable under the patent laws of the United States of America or any foreign country.

**ENGINEERING DISCLAIMER**

Not intended for construction, bidding, or permit purposes.

**TRADE NAMES AND MANUFACTURERS' NAMES**

The United States Government and the State of Texas do not endorse products or manufacturers. Trade or manufacturers' names appear herein solely because they are considered essential to the object of this report.

# Table of Contents

# List of Figures

# List of Tables

# Volume 2: Test Reports for MSE Reinforcements in Type B (Sandy) Backfill

Appendix F: MSE Reinforcements Pullout Test Reports: Ribbed Strips in Type B Backfill

Appendix G: MSE Reinforcement Pullout Test Reports: Ribbed Strips in Type B Backfill – Under-Compacted

Appendix H: MSE Reinforcement Pullout Test Reports: Welded Steel Grids in Type B Backfill

Appendix I: MSE Reinforcement Pullout Test Reports: Smooth Bars in Type B Backfill

Appendix J: MSE Reinforcement Pullout Test Strain Gage Reports: Ribbed Strips in Type B Backfill

Appendix K: MSE Reinforcement Pullout Test Strain Gage Reports: Welded Steel Grids in Type B Backfill

# Volume 3: Test Reports for MSE Reinforcements in Type A (Gravelly) Backfill

Appendix L: MSE Reinforcement Pullout Test Reports: Ribbed Strips in Type A Backfill

Appendix M: MSE Reinforcement Pullout Test Reports: Welded Steel Grids in Type A Backfill

Appendix N: MSE Reinforcement Pullout Test Reports: Smooth Bars in Type A Backfill

Appendix O: MSE Reinforcement Pullout Test Strain Gage Reports: Ribbed Strips in Type A Backfill

Appendix P: MSE Reinforcement Pullout Test Strain Gage Reports: Welded Steel Grids in Type A Backfill

# CHAPTER 1
# INTRODUCTION

## 1.1 OVERVIEW

This report documents findings from a three-year research study that examined the pullout resistance of inextensible Mechanically Stabilized Earth (MSE) reinforcements embedded in backfills typically used in Texas. The study involved an extensive laboratory test program in which a total of 650 pullout tests were successfully completed on ribbed strip, welded steel grid, and smooth steel bar MSE reinforcements under a wide range of test conditions.

Mechanically Stabilized Earth Wall (MSE wall or MSEW) is a generic term that is used to describe earth retaining systems that utilize reinforced soil fill (*1*). This type of wall system is constructed from the bottom up by placing alternating layers of soil fill and reinforcing elements. The reinforcements are connected to a wall facing that prevents the soil from raveling out between layers of reinforcement. Figure 1.1 shows the essential components of a generic MSE wall system.
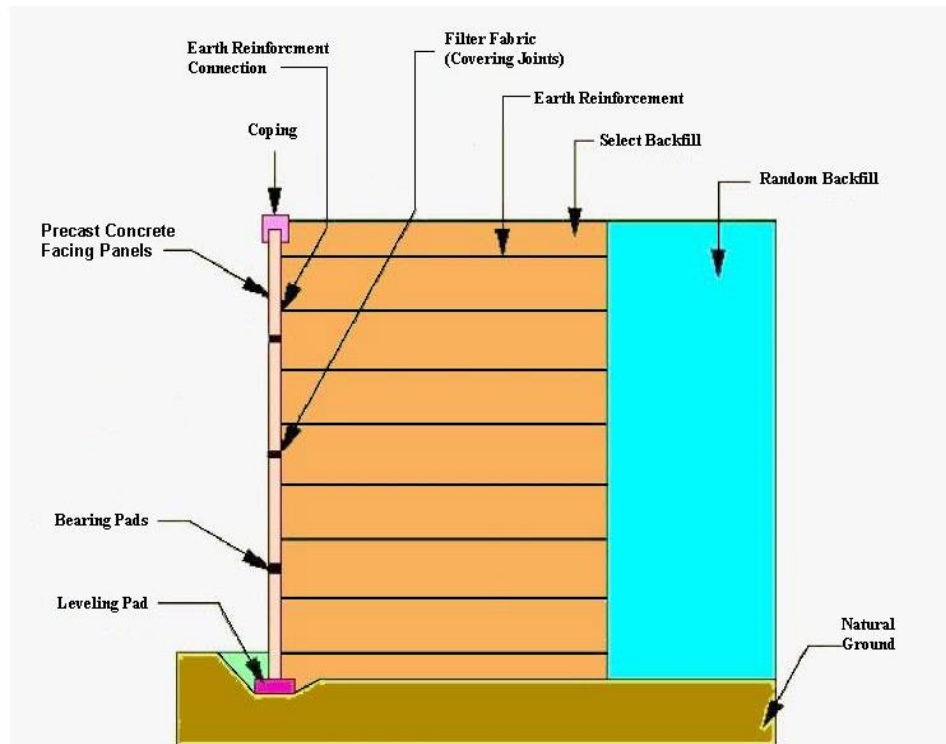
**Figure 1.1** Primary Components of an MSE Retaining Wall System

A broad range of materials are available for use as MSE wall facings: precast concrete panels, dry cast modular blocks, welded wire mesh, wrapped sheets of geosynthetics, and gabions. Similarly, soil reinforcement elements may consist of steel strips, welded steel grids, polymeric grids, and geotextile sheets. Even though the term "MSE wall" is often used generically to describe any wall system that uses reinforced soil fill, the MSE wall system that has gained most widespread application in the transportation industry is the MSE wall with segmental pre-cast concrete facing and galvanized steel strips or welded steel grids as backfill reinforcement. This type of MSE wall system is used in a wide range of applications including retaining walls, bridge abutments, wing walls and access ramps (see Figure 1.2). The popularity of MSE walls is largely due to several important advantages this type of retaining wall offers over conventional walls such as cast-in-place concrete walls with spread footings. These advantages include: (a) ease and speed of construction, (b) cost effectiveness, (c) ability to tolerate larger differential settlements, and (d) aesthetics.



**Figure 1.2** MSE Retaining Walls Used in Transportation Applications

Data compiled by the Texas Department of Transportation (TxDOT) from August 2010 through September 2011 reveal that over 70% of the square footage of earth retaining walls built by the agency belonged to the MSE wall category that utilized precast concrete panels and galvanized steel reinforcement (*3*). Consistent with this application, the research study described in this report focused exclusively on the behavior of MSE wall systems with galvanized steel reinforcements.

The design of MSE walls requires evaluation of the wall system for both *external stability* and *internal* stability. External stability analysis assumes that the wall facing, reinforcement elements, and the reinforced fill remain intact as one coherent unit. Then, necessary analyses are conducted to ensure the stability of this unit against several modes of external failure including (a) sliding, (b) overturning, (c) global stability (or deep-seated shear) and (d) bearing capacity. Next, the integrity of the wall system is examined to ensure internal stability. Internal stability analyses examine two different potential failure mechanisms: (a) reinforcement rupture and (b) reinforcement pullout failure. The work undertaken as a part of this research addressed one aspect of internal stability, namely reinforcement pullout. More specifically, this research examined the pullout resistance of inextensible metallic reinforcements comprised of steel strip and grid type reinforcements embedded in granular backfills typically used in TxDOT retaining walls.

Two separate stress transfer mechanisms are generally believed to be responsible for the development of pullout resistance between metallic reinforcements and MSE backfill material. These are *friction* and *passive resistance*. Friction develops at locations where relative shear displacement occurs between the reinforcement surface and backfill soil. Steel strips and longitudinal bars of welded steel grids are examples of reinforcing elements that produce pullout resistance through friction. Passive resistance occurs through the development of bearing type stresses on reinforcing elements oriented normal to the direction of movement. Transverse bars in a welded steel grid and transverse ridges on ribbed steel strip reinforcement are examples of reinforcing elements that produce pullout resistance through passive resistance.

In common design practice, the pullout resistance of MSE reinforcement is estimated using a parameter called the *pullout resistance factor,* F*. This parameter combines the contributions from both friction and passive resistance rather than treating the two mechanisms separately. The most reliable way to determine the pullout resistance factor, F*, for a specific reinforcement-backfill combination is to conduct project-specific laboratory or field pullout resistance tests (*1*, *2*). However, many practical challenges are associated with project-specific pullout resistance testing under production conditions. First, a specific backfill source may not have been identified at the time the internal stability analysis of the wall system is performed. Second, significant variability will likely exist in large volumes of

backfill used in a particular wall construction project. Therefore, repetitive pullout resistance testing will be necessary to establish the variability in pullout resistance resulting from changes in backfill material. For these reasons, project-specific pullout resistance testing is rarely undertaken in routine MSE wall design practice. Instead, the designers use default $F^*$ values calculated based on empirical relationships found in the AASHTO LRFD Bridge Design Specifications (*4*). These AASHTO empirical relationships for F* have been developed based on historical data that have been collected from tests conducted using a range of backfill materials. They are expected to yield conservative estimates of F*.

## 1.2 STATEMENT OF THE RESEARCH PROBLEM

The specifications for MSE select backfill were significantly revised when TxDOT published their 2004 *Standard Specifications for Construction and Maintenance of Highways, Streets, and Bridges* (referred to hereafter as *Standard Specifications*). Item 423, Retaining Walls, lists the gradation requirements for the select backfill for MSE Walls (*5*). The gradation limits listed in the 2004 *Standard Specifications* for certain backfill categories, such as Item 423 Types A and D, result in backfill materials with much coarser gradation limits than those recommended in FHWA guidelines. It is likely that the nature of interaction taking place between the TxDOT coarse granular backfill and metallic reinforcements are quite different from MSE reinforcement interactions observed for granular backfill with finer gradation. It can be anticipated that coarse granular backfill will result in larger frictional and passive resistance. Furthermore, the reinforcement elements may exhibit different deformation behavior during pullout when they are embedded in coarse granular fill. As a result, wall designs achieved based on AASHTO default F* parameters for TxDOT wall systems may be less than optimal. Therefore, it is desirable to investigate pullout resistance behavior of these backfill-reinforcement combinations through a comprehensive pullout resistance test program. The results from this pullout test program will then be evaluated to determine their implications on the selection of MSE wall type as well as actual design of the particular MSE wall system selected.

A second important concern related to reinforcement pullout resistance arises when the layout of the MSE reinforcements needs to be altered to avoid conflicts between the design layout of MSE reinforcement and obstructions which occur in the reinforced backfill

zone behind the wall facing panels.  Examples of vertical obstructions include foundations for bridge abutments and foundations for traffic sign structures and light poles. Horizontal obstructions include drainage inlets and storm sewers.  Figures 1.3(a) and (b) show examples of each of these types of obstructions.



(a)                                                    (b)

**Figure 1.3.** Obstructions behind MSE Walls (a) Vertical Obstruction, (b) Horizontal Obstruction

Ideally, potential conflicts are identified during preliminary planning stages so the obstructions can be relocated out of the reinforced fill and hence avoid the problem. However, it is not always possible to relocate obstructions to avoid conflicts.  Therefore, wall designers often rely on alternative reinforcement layouts to circumvent obstructions that are found within the reinforced fill.  Such alternative reinforcement layouts have the potential to impact the pullout resistance of the MSE reinforcement.  Little or no data are available in published literature on the influence of alternative reinforcement details on pullout resistance. To help address this need, this study explored pullout resistance impacts associated with avoidance of vertical obstructions. TxDOT requested that horizontal obstruction avoidance not be included in the research program.

In summary, this research study was initiated with two primary research objectives in mind:

(a) To conduct a comprehensive pullout test program and hence identify pullout resistance factor, F*, values applicable to specific backfill-reinforcement combinations used by TxDOT

(b) To explore how pullout resistance is impacted by alternative reinforcement layouts that are commonly used to circumvent vertical obstructions behind the wall facing.

## 1.3 RESEARCH APPROACH

The research plan used to accomplish the objectives involved the following essential tasks:

1. Collect and review pertinent background literature: As a part of this effort, a large body of literature that included policy documents, reports and articles related to pullout behavior of MSE reinforcements was collected and reviewed in detail. The research team placed special emphasis on reports and articles dealing with previous research studies on pullout resistance testing.

2. Development of the Pullout Resistance Test Matrix: The centerpiece of this research study is a comprehensive pullout resistance test program that included 650 pullout resistance tests. Before this test program could be launched it was necessary to carefully evaluate all test variables of interest, identify those that were most critical, and then design a test matrix that would adequately capture the effects of these variables on the pullout resistance of MSE reinforcements.

3. Design and Construction of the Pullout Resistance Test System: Recommendations found in FHWA Publication FHWA NHI-00-043 specify that test systems used for pullout resistance testing should include a soil box with a minimum length of 4ft, a minimum width of 2.5ft and a minimum depth of 1.5ft (5). However, a test box meeting those minimum requirements would not be large enough for testing the pullout resistance of alternative reinforcement arrangements around vertical obstructions. Therefore, as

part of this research project, a large-scale pullout load test system with dimensions 12ft by 12ft in plan area and 4ft in depth was designed and fabricated.

4. Pullout Resistance Test Program:  As mentioned above, a comprehensive pullout resistance test program that included 650 pullout tests was completed as a part this research study.  Tests were conducted with two different backfill materials, namely, Type A select backfill and Type B select backfill material according to TxDOT *Standard Specification* Item 423.  Also, tests were conducted on two types of inextensible reinforcement: ribbed steel strips and welded steel grids.  Since welded steel grids of various transverse and longitudinal bar sizes and spacings are available, tests representing a wide range of these parameters were included in the test program.  A subset of the pullout tests was devoted to testing reinforcements fitted with strain gages.  The purpose of the strain gaged tests was to gain better insight into the stresses, strains, forces and displacements of reinforcement.  A limited number of pullout tests were conducted on smooth straight bars to determine the relative contribution made by longitudinal bars to overall pullout resistance capacity of welded steel grids.  In addition, the program included a series of tests involving two specific alternative reinforcement layouts commonly used to avoid vertical obstructions: strips placed at selected skew angles and grids that were cut and splayed.

5. Data Reduction and Statistical Analysis:  The raw data collected from each pullout test were appropriately processed to obtain the pullout resistance factor, $F^*$, along with many other test variables.  The database containing all of the $F^*$-values was then subjected to detailed statistical analyses.  The statistical analyses were used to identify the independent variables that significantly influence $F^*$, develop predictive models for $F^*$, and determine confidence intervals corresponding to each predictive model.

## 1.4  REPORT ORGANIZATION

This report provides complete documentation of work performed for TxDOT Research Study 0-6493: Pullout Resistance of Mechanically Stabilized Earth Reinforcements in Backfills Typically Used in Texas.  The report is presented in three volumes.  Volume 1 is the report narrative and provides both the breadth and detail of the research findings. Volume 2 consists of a series of appendices which present test reports and data for pullout tests of MSE reinforcements embedded in TxDOT Item 423, Type B (sandy) backfill. Volume 3 consists of a series of appendices which present test reports and data for pullout tests of MSE reinforcements embedded in TxDOT Item 423, Type A (gravelly) backfill.

Relative to Volume 1, Chapter 1 introduces the research problem and provides an overview of the study. Chapter 2 presents a comprehensive review of background information related to pullout resistance of MSE reinforcement.  It includes sub-sections dealing with pullout resistance concepts and theory, current AASHTO and TxDOT design practice with respect to the estimation of pullout resistance, as well as strategies used when dealing with vertical obstructions behind the wall facing.  Detailed information related to previous research studies that involved pullout resistance testing is presented in Chapter 3, which reviews and synthesizes data collected from pullout resistance testing conducted in the laboratory environment as well as in the field.  Chapter 4 describes the pullout resistance test program completed in this research study.  It includes detailed information on the development of the test matrix, design and fabrication of the pullout resistance test system, the test procedures and data processing methods used.  Chapter 5 is devoted to presentation of data obtained through the pullout test program, documenting material quality control data and providing a synthesis of pullout resistance factors obtained; Chapter 5 also presents general observations made during pullout resistance testing.  Detailed statistical analyses of data and inferences made based on such analyses are presented in Chapter 6.  Chapter 7 presents the conclusions and recommendations from the research.

Appendices in Volume 1 include backfill gradation data, quality control data for the MSE reinforcements tested in this study, summary data tables for MSE pullout tests in Type B backfill, summary data tables for MSE pullout tests in Type A backfill, and summary data tables for strain-gaged pullout tests in both Type B and Type A backfill.

# CHAPTER 2
# REVIEW OF PERTINENT BACKGROUND INFORMATION

## 2.1 OVERVIEW

This chapter presents a review of essential background information related to pullout resistance behavior of metallic MSE reinforcement embedded in soil backfill. It begins with a general overview of the concept of reinforced earth and the theoretical background on soil-reinforcement interactions and mechanisms governing pullout resistance. This section is followed by a review of current policy and design practice related to the estimation of pullout resistance of MSE reinforcements. The last section of this chapter deals with alternative reinforcement layouts that are commonly used to circumvent vertical obstructions found behind MSE wall facing panels. It should be noted that findings from review of previous research studies involving pullout resistance testing is not included in this chapter. Instead, a detailed review of pullout resistance test programs conducted by previous researchers and data collected is presented in Chapter 3.

## 2.2 MECHANISMS GOVERNING PULLOUT RESISTANCE

People have long recognized that strength properties of soils can be greatly enhanced by mixing them with suitable reinforcing materials. For example, ancient Egyptians used straw as an additive to clay to make stronger bricks. Similarly, ancient Chinese and French settlers in Canada used tree branches to reinforce mud dikes. During medieval times, alternating layers of earth and logs were used when building fortifications. In the early 1900s, layers of metallic reinforcements were embedded in soil to strengthen the downstream slopes of earth dams.

However, it was not until the 1960s when a rational design method for reinforced earth structures was developed by the French architect and engineer, Henri Vidal, based on concepts of reinforced earth (*6*). Vidal's research led to the development of a patented soil reinforcement system that is known today as Reinforced Earth®. This system uses flat strips of steel embedded in granular material to form the reinforced earth mass. Vidal recognized that a granular soil cannot maintain stability of a vertical cut or a steep slope because of its inability to withstand tensile stresses. He demonstrated that when elongated steel reinforcing

elements are embedded within the granular soil mass, the tensile stresses within the soil are transferred to the reinforcements. In other words, a reinforced soil mass would behave very much the same way as reinforced concrete does. However, Vidal pointed out that, for the reinforced soil to function in this manner, it is critical that proper "bonding" exists at the interface between steel reinforcement and the soil grains. In the case of granular soils reinforced with steel strips, such bonding would develop through friction that is mobilized on either side of the metallic strip as shown in Figure 2.1. Thus it is important that slippage does not occur at the soil-reinforcement interface. According to Vidal, appropriate bond between the soil and reinforcement can only be achieved if the non-cohesive backfill has an internal angle of friction of 25° or greater.



$$tg\,\alpha < f \qquad tg\,\alpha' < f$$
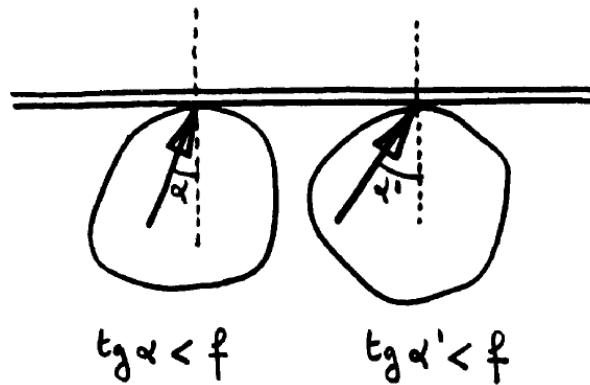
**Figure 2.1** Stress Transfer at Points of Contact between Soil and Reinforcement (*6*)

Vidal also suggested that, if steel reinforcement are embedded within the soil mass at an appropriate spacing, then stress transfer would occur between adjacent reinforcement through a phenomenon known as *soil arching* as shown in Figure 2.2. Vidal used the soil arching concept to explain how reinforcement of the entire soil mass could be achieved with discrete earth reinforcements placed at appropriate spacing. In other words, he used soil arching to demonstrate that it is not necessary for the reinforcement to be continuous.
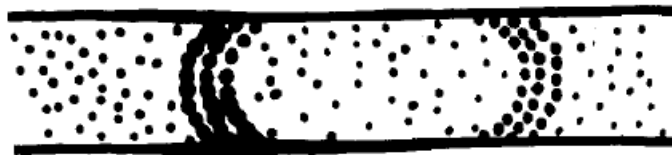


**Figure 2.2** Stress Transfer between Adjacent Layers of Reinforcement through Soil Arching (*6*)

Since the introduction of the Reinforced Earth® system by Vidal in the 1960s, several other researchers have investigated the viability of using other systems of soil reinforcement. One such system that later gained widespread application is the welded wire soil reinforcement scheme envisioned by William K. Hilfiker (7). In this system, a welded wire mesh serves as the soil reinforcement instead of flat steel strips. The diameter of the wire and the dimensions of the mesh openings can be varied depending on the specific application in which this type of soil reinforcement is used. Pullout resistance behavior of welded wire mesh type reinforcement was investigated experimentally by Chang *et el.*, 1977 (*8*) and then by Bishop and Anderson, 1979 (*9*). Both of these studies concluded that welded mesh reinforcement provided much larger pullout resistance than strip type reinforcement for the same reinforcement surface area. They attributed the increase in pullout resistance to the anchorage effect of transverse wires. However, neither of these research studies attempted to examine the fundamental mechanisms contributing to pullout resistance. Instead, they determined pullout resistance empirically based on laboratory test results.

A detailed study of the soil-reinforcement interactions that contribute to pullout resistance of welded wire mesh reinforcement was undertaken by Peterson in 1980 (*7*). In welded wire mesh, two separate mechanisms are responsible for the development of pullout resistance. The first mechanism involves friction between the longitudinal wires and the soil particles. The second mechanism is developed from the "anchorage" of transverse wires embedded in the soil.

Eq. 2.1 provides the relationship between frictional resistance, $F_f$ developed along the length, *l* of a single longitudinal wire in a welded wire mat.

$$F_f = \sigma \left( \pi \, d \, l \right) \tan \delta \qquad (2.1)$$

where:

$\sigma$ = average overburden pressure $= \dfrac{\sigma_v + \sigma_h}{2} = \dfrac{\sigma_v + 0.5\sigma_v}{2} = 0.75\sigma_v$

d = diameter of longitudinal wire

$\delta$ = angle of friction between reinforcement and soil

Peterson (1980) argued that the mechanisms controlling pullout resistance of a transverse reinforcement element will be the same as those governing the bearing capacity of a strip footing. Accordingly, the Terzaghi-Buisman equation (*i.e.*, Eq. 2.2) for ultimate bearing capacity of a strip footing of width B, can be used to determine pullout resistance of a transverse bar (See Figure 2.3).

$$q_{ult} = cN_c + \gamma DN_q + \frac{1}{2} \gamma BN_\gamma \qquad (2.2)$$

where:
$q_{ult}$ = ultimate bearing capacity
D = depth of embedment
B = width of the strip footing
c = soil cohesion
$\gamma$ = soil unit weight
$N_c$, $N_q$ and $N_\gamma$ = bearing capacity factors
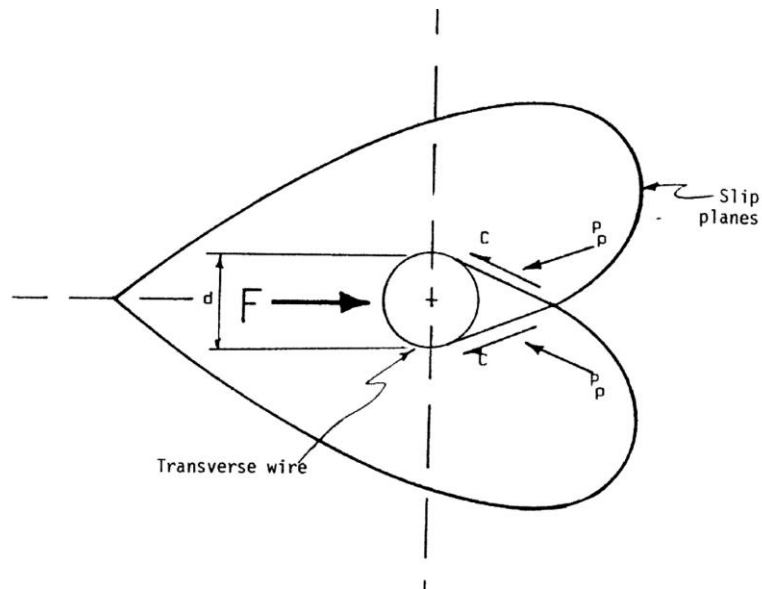


**Figure 2.3** Slip Surfaces Associated with Bearing Capacity Type Pullout Failure Mechanism (*7*)

When Eq. 2.2 is applied to a transverse bar embedded in soil, the unit ultimate bearing resistance, q for the bar can be determined.

$$q_{ult} = cN_c + \sigma_n N_q + 0.5\gamma d N_\gamma \qquad (2.3)$$

where:

$\sigma_n$ = normal pressure due to soil overburden

d = diameter of transverse wire

By applying Eq. 2.3 to a single transverse bar, the ultimate bearing resistance per unit width of reinforcement, $\sigma_b$ can be determined.

$$\sigma_b = cN_c d + \sigma_n d N_q + 0.5\gamma d^2 N_\gamma \qquad (2.4)$$

Eq. 2.4 can be further simplified based on the following considerations: for cohesionless backfill c = 0 and the third term in Eq. 2.4 can be disregarded because $d^2$ is small. Rewriting Eq. 2.4,

$$\sigma_b = \sigma_n d N_q \qquad (2.5)$$

If there are N transverse bars embedded in the backfill, then the pullout resistance per unit width of the reinforcement is given by Eq. 2.6a (expressed in terms of force) and Eq. 2.6b (expressed in terms of stress):

$$P_p = N\sigma_n d N_q \qquad (2.6a)$$

$$\sigma_p = N\sigma_n N_q \qquad (2.6b)$$

The bearing capacity factor, $N_q$ in the above formulation is a function of angle of friction, $\phi$. Peterson (1980) used the function $N_q$ shown in Eq. 2.7 which is based on Terzaghi's theory of general shear failure. Jewel (1984) used the functional form presented in Eq. 2.8 for $N_q$ (*5*). Eq. 2.8 is based on punching shear failure (*10*).

$$N_q = e^{\pi \tan \phi} \tan^2\left(\frac{\pi}{4} + \frac{\phi}{2}\right) \qquad (2.7)$$

$$N_q = e^{(\pi/2+\phi)\tan\phi} \tan\left(\frac{\pi}{4} + \frac{\phi}{2}\right) \qquad (2.8)$$

Jewel (1984) also proposed the use of an adjustment factor to account for soil dilatancy, anchor roughness and initial stress state in the soil.  Bergado (1992) studied the pullout behavior of grid reinforcement in clayey backfill material and used a formulation that retained the cohesion term in Eq. 2.2 (*11*).

From the above discussion, it is clear that different approaches and design equations have been proposed for estimating the pullout resistance of MSE reinforcements.  However, these equations are based on different interaction parameters and as a result, comparison of pullout performance of different reinforcements for a given application based on these equations is difficult.  To overcome this difficulty, a normalized definition of pullout resistance is introduced in the FHWA-NHI-10-024 manual (*2*).  This normalized definition is based on a single parameter called Pullout Resistance Factor, F*, which combines the contributions from both friction and bearing mechanisms.  Moreover, the generalized equation presented in the FHWA-NHI-10-024 manual is applicable to all types of inextensible and extensible reinforcements.  Eq. 2.9 represents the generalized pullout resistance equation described above:

$$P_r = F^* \alpha \, \sigma'_v \, L_e \, C \qquad\qquad (2.9)$$

where:

$P_r$    = Pullout resistance per unit width of reinforcement

$L_eC$ = Total surface area per unit width of the reinforcement in the resistive zone behind the failure surface

$L_e$   = Embedment length in the resisting zone behind the failure surface

$C$    = Effective unit perimeter; C=2 for sheets, strips and grids

$F^*$   = Pullout resistance factor

$\alpha$    = A scale correction factor (generally 1.0 for metallic reinforcement, 0.6-1.0 for geosynthetic reinforcements)

$\sigma'_v$  = Effective vertical stress at the soil-reinforcement interfaces

Figure 2.4 shows the frictional and bearing (passive) resistance mechanisms that contribute to pullout resistance of ribbed steel strips and welded steel grids.



(a)



(b)
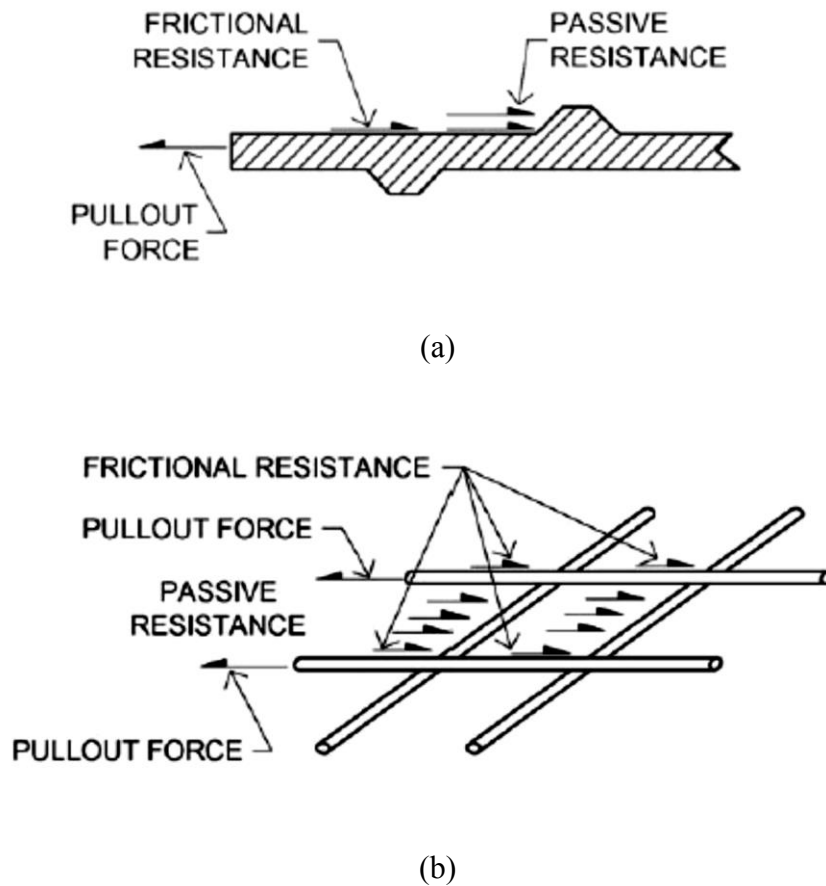
**Figure 2.4**  Frictional and Bearing Resistance on Reinforcements: (a) Ribbed Steel Strips, (b) Welded Steel Grids

## 2.3 CURRENT DESIGN PRACTICE

This section provides an overview of the current policy and design practice applicable to the design of MSE walls to safeguard against pullout resistance failure. The discussion includes a review of relevant TxDOT policy documents as well as AASHTO design and construction guidelines.

### 2.3.1 Texas Department of Transportation (TxDOT) Design Practice

TxDOT policy and specifications related to MSE retaining wall design and construction are documented in two separate publications: (a) TxDOT *Standard Specifications* Item 423-Retaining Walls (*12*), and (b) TxDOT *Geotechnical Manual*, 2006 (*13*). The TxDOT *Standard Specifications* Item 423 governs all aspects of wall construction; it provides specific requirements to be met in the selection of materials as well as during wall construction. The TxDOT *Geotechnical Manual* provides necessary guidance to district personnel in conducting geotechnical investigations and design for project development purposes.

Pullout resistance of MSE reinforcements depends on the characteristics of the specific backfill material used as well as its placement conditions. Therefore, it is pertinent to review TxDOT's specifications for MSE select backfill material. TxDOT *Standard Specifications* Item 423 requires select backfill to be free from organic or otherwise deleterious materials. It should also conform to the gradation limits in Table 2.1 as determined by Tex-110-E (*14*). It should not contain shale, caliche, or other soft, poor-durability coarse aggregate particles. Backfill appearing to contain such particles is tested for soundness. Materials with a five-cycle magnesium sulfate soundness test value of more than 30%, when tested in accordance with Tex-411-A (*15*), are rejected. In Types A, B, and D backfill materials, particles larger than 1/4 in. must be angular or crushed. Rounded rock or gravel are not allowed. When the backfill gradation results in 85% or more material retained on the No. 4 sieve, the backfill will be considered rock backfill. All Type D backfill is considered rock backfill.

MSE select backfill used in the construction of permanent MSE retaining walls with galvanized metal reinforcements should also be tested for corrosion potential based on pH, resistivity and chloride and sulfate contents.   The specific requirements are as follows:

(a) The pH of the backfill soil material shall be from 5.5 to 10.0, as determined by Test Method Tex-128-E (*16*).

(b) The resistivity of the backfill soil shall not be less than 3000 ohms-cm as determined by Test Method Tex-129-E (*17*).  Materials with a resistivity between 1500 and 3000 ohms-cm may be used, provided the chloride content does not exceed 100ppm and the sulfate content does not exceed 200ppm as determined by Tex-620-J (*18*).

**Table 2.1** TxDOT Select Backfill Gradation Limits (*12*)

| TYPE | Applications | Sieve Size | Percent Retained |
|------|-------------|------------|------------------|
| A | Permanent Walls Enhanced Performance | 3.0-in | 0 |
| | | 1/2-in | 50-100 |
| | | No.40 | 85-100 |
| B | Permanent Walls | 3.0-in | 0 |
| | | No.40 | 40-100 |
| | | No.200 | 85-100 |
| C | Temporary MSE Walls | 3.0-in | 0 |
| | | No.200 | 70-100 |
| D | For Areas of walls subject to inundation or below 100-yr flood plain | 3.0-in | 0 |
| | | 3/8-in | 85-100 |

TxDOT *Standard Specifications* Item 423 requires MSE select backfill to be compacted to achieve a minimum of 95% of the maximum dry unit weight established based on Tex-114-E (*19*).   Rock backfill or material that is too coarse for density testing shall be placed by the ordinary compaction method described in Specification Item 132 (*20*).  When ordinary compaction is used, the contractor is required to use approved rolling equipment,

place material in lifts of loose thickness no more than 8-in, bring the material to appropriate moisture content as specified in plans and compact the soil until there is no further evidence of consolidation.

When TxDOT specifies an MSE Wall in the construction plans, the wall has been checked for external stability including global stability. The internal stability and reinforcement lengths are not included in the plans and are the responsibility of the proprietary wall manufacturer that is selected by the contractor. The TxDOT *Geotechnical Manual* (*13)* does not identify a specific procedure to be used in the design of earth retaining walls. Instead it states that the design and analysis should be accomplished using accepted geotechnical engineering industry standards. Accordingly, these designs are performed according to procedures outlined in the AASHTO *Standard Specifications for Highway Bridges* (*21*). A review of relevant sections of AASHTO involving pullout resistance of MSE reinforcement is provided below.

### 2.3.2 MSE Retaining Walls: AASHTO Design

Procedures to be used in the design of MSE retaining walls are described in Section 5.8 of the AASHTO *Standard Specifications for Highway Bridges* (*21*). As mentioned in the introductory chapter of this report, the design must address both external and internal stability of the wall system. External stability analyses, described in AASHTO Sec. 5.8.2, are conducted assuming that the entire wall system including the wall facing and the reinforced earth mass behaves as a rigid body. Stability analyses investigate wall stability against sliding, overturning, bearing capacity and deep seated shear failure. As mentioned earlier, the primary thrust in this research study is on internal stability, or more specifically on failure by reinforcement pullout. Therefore, external stability analysis procedures are not discussed here in further detail.

The procedures to be used in internal stability analysis are found in AASHTO Sec. 5.8.4 (*21*). Internal stability analyses investigate two potential failure mechanisms: reinforcement pullout and reinforcement rupture. Analysis of the MSE wall system for reinforcement pullout failure requires calculation of maximum reinforcement load and estimation of reinforcement pullout capacity. AASHTO recommends the use of the *Simplified Coherent Gravity* approach to calculate the maximum reinforcement loads. Other

widely accepted methods may be used at the discretion of the wall owner or the approving agency. In the Simplified Coherent Gravity approach, the load in the reinforcements is obtained by multiplying a lateral earth pressure coefficient by the vertical stress at the reinforcement location, and then applying the resulting lateral pressure to a tributary area that transfers the load to the reinforcement. The lateral earth pressure coefficient to be used in the above analysis is designated "$K_r$". $K_r$ is determined by first calculating the coefficient of lateral earth pressure for active conditions (*i.e.* $K_a$) for the backfill and then applying a multiplier which is presented in Figure 2.5. According to this figure, the multiplier $K_r/K_a$ is a function of the depth and the type of reinforcement used.

Accordingly, the lateral earth pressure ($\sigma_h$) is given by the following equation,

$$\sigma_h = K_r \sigma_v + \Delta \sigma_h \tag{2.10}$$

where:

$\sigma_v$ = vertical soil pressure

$\Delta \sigma_h$ = horizontal pressure resulting from concentrated surcharge loads

$K_r$ = lateral earth pressure coefficient
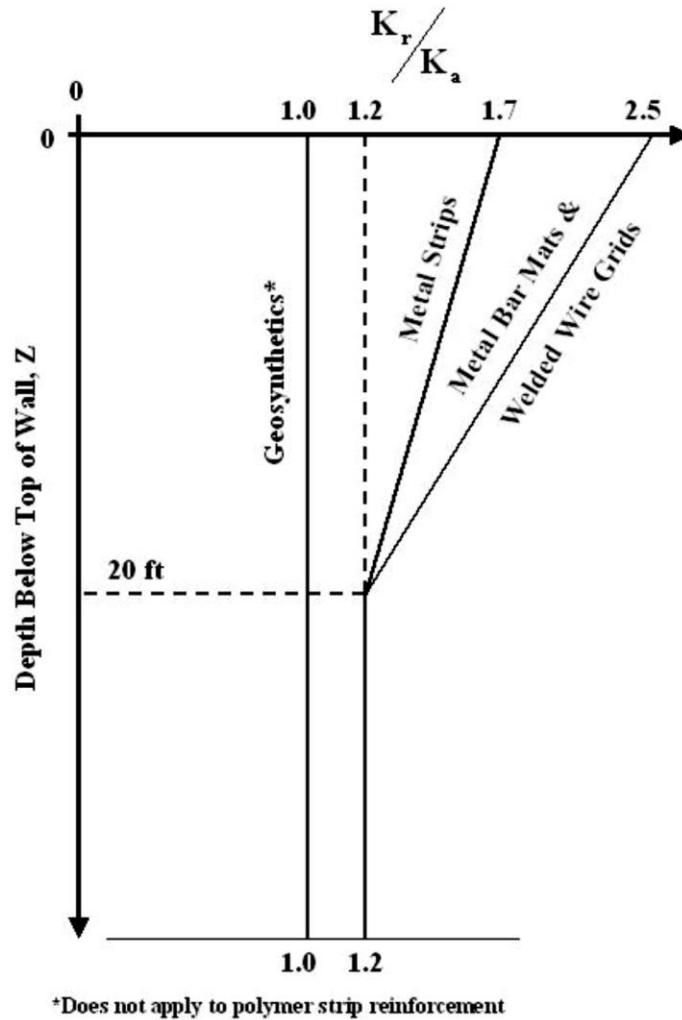
**Figure 2.5** Variation of the Coefficient of Lateral Stress Ratio $K_r/K_a$ with Depth in a Mechanically Stabilized Earth Wall (*21*)

In the next step, the lateral stress, $\sigma_h$ is multiplied by the tributary area to obtain the maximum tensile load on the reinforcement per unit width.

$$T_{max} = \sigma_h (S_v \times 1) = \sigma_h S_v \qquad (2.11)$$

where:

$T_{max}$ = maximum tensile load per unit width

$S_v$ = vertical spacing between reinforcement layers

The next step in the pullout resistance design involves calculation of the pullout resistance capacity. This calculation begins with an *a priori* assumption regarding the location of the *line of maximum tensile stress* or *potential failure surface* within the reinforced backfill. This line of maximum tensile stress separates the reinforced fill into two zones: active zone and resistant zone. Data collected from instrumented MSE walls have shown that the location of the line of maximum stress varies depending on whether *inextensible* (*e.g.* steel) or *extensible* (*e.g.* polymeric) reinforcement are used. Figure 2.6 shows the lines of maximum stress commonly used in MSE wall design (*21*). The pullout resistance capacity is the resisting force that would develop on the length of reinforcement embedded in the resistant zone. Finally, the factor of safety with respect to pullout failure is estimated as shown below. The length of the reinforcement is adjusted so that a minimum factor of safety of 1.5 is achieved.

$$FS_{PO} = \frac{P_r}{T_{max}}$$
(2.12)

where:

$FS_{PO}$ = Factor of safety against pullout failure

AASHTO specifications allow the pullout resistance factor, F* in Eq. 2.9 to be obtained from product-specific pullout resistance testing or through empirical equations. As noted previously, performing product-specific pullout resistance testing under production conditions for a specific MSE wall project is problematic. Accordingly, the designer may use the following equations found in AASHTO to obtain conservative estimates of F* for ribbed steel strips and grids embedded in standard backfill with the exception of uniform (coefficient of uniformity, $C_u$ <4) sands.
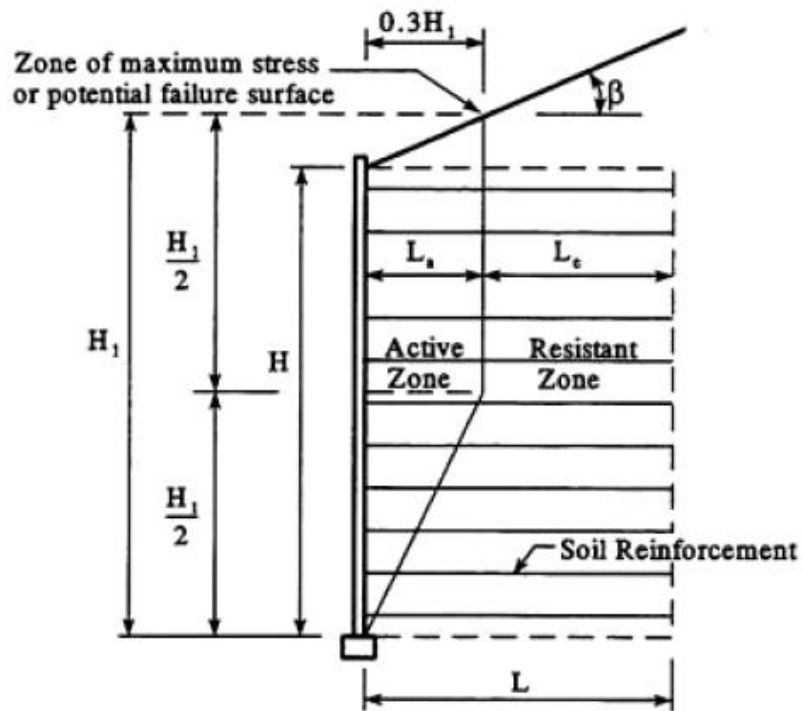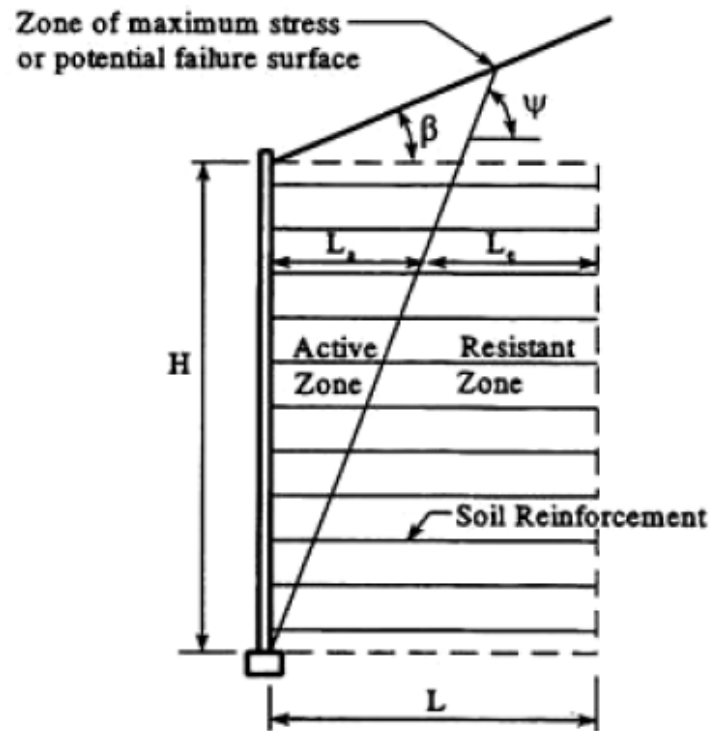
**Figure 2.6** Line of Maximum Tensile Stress Walls with No Significant Batter (a) Inextensible Soil Reinforcement and (b) Extensible Soil Reinforcement (*21*)

**For steel ribbed reinforcement**:

$$F^* = 1.2 + \log \cdot C_u \leq 2.0 \quad \text{at the top of the wall} \tag{2.13a}$$

$$F^* = \tan \phi \quad \text{at a depth 20ft and below} \tag{2.13b}$$

where:

$\quad\quad C_u$ = Coefficient of uniformity for backfill

$\quad\quad \phi$ = Angle of internal friction for backfill

If the specific value for $C_u$ for the actual backfill used is not known at the time of the design, $C_u = 4$ may be assumed; the maximum value of $\phi$ to be used in Eq.2.13b is 34°.

**For steel grid reinforcement**:

$$F^* = 20 \left( \frac{t}{S_t} \right) \text{at the top of the wall} \tag{2.14a}$$

$$F^* = 10 \left( \frac{t}{S_t} \right) \text{at a depth 20ft and below} \tag{2.14b}$$

where:

$\quad\quad t$ = diameter of the transverse bar

$\quad\quad S_t$ = transverse bar spacing

The relationships represented by Eq. 2.13 and Eq. 2.14 are also shown graphically in Figure 2.7.

The AASHTO Reference F* function identified here and presented for comparison in charts throughout this report is based on these formulations. For strips, the design assumptions of $C_u = 4$ and $\phi = 34°$ have been used throughout. Equation 2.13, Equation 2.14 and Figure 2.7 have been taken from the AASHTO *Standard Specifications for Highway Bridges*, 17th Edition (*21*), consistent with TxDOT's continued reliance on LFD and ASD design methods for MSE walls. The AASHTO *LRFD Bridge Design Specifications*, 5th Edition (*4*) uses the same equations and figures for describing F*.
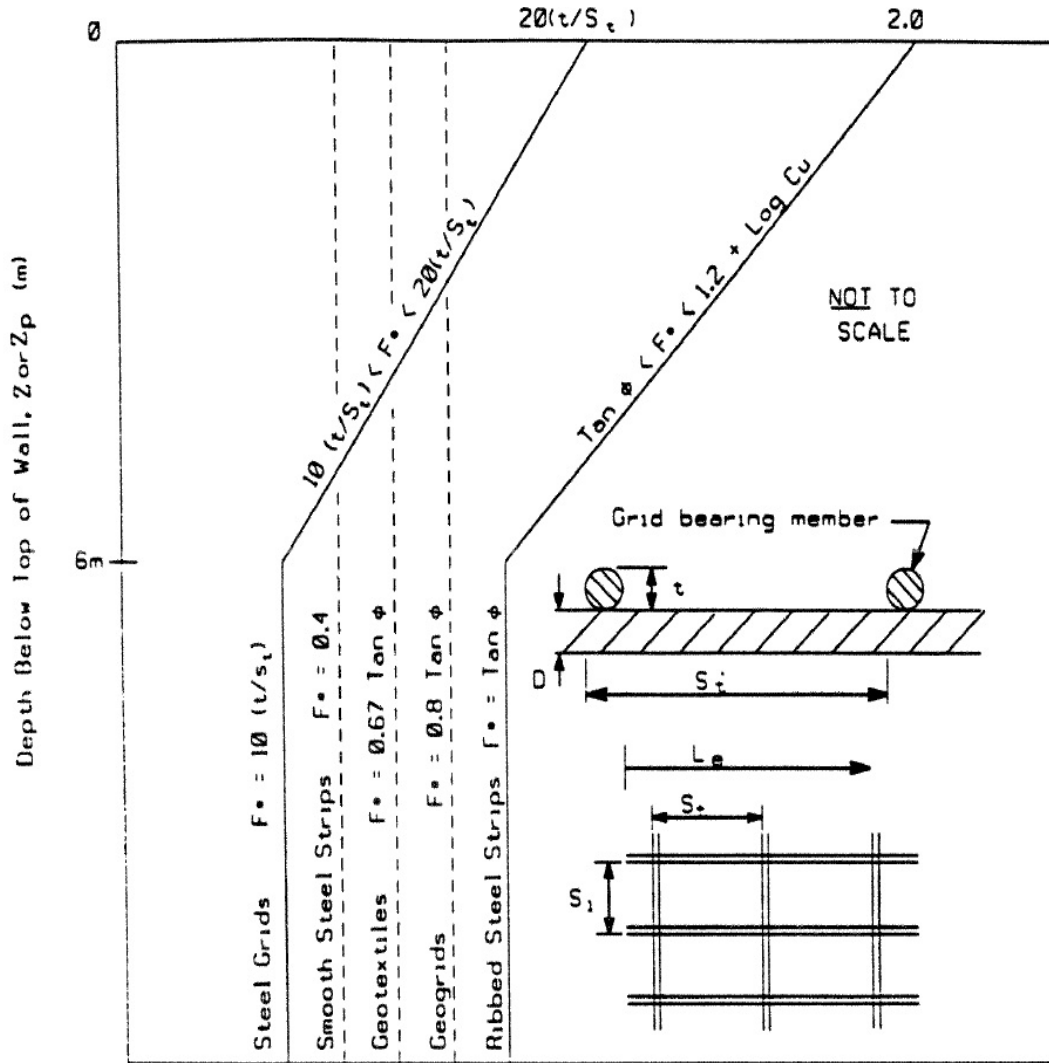
**Figure 2.7** Default Values for Pullout Resistance Factor, F* (*21*)

## 2.4  ALTERNATIVE REINFORCEMENTS TO AVOID OBSTRUCTIONS

Obstructions such as drilled shafts, driven piles, drainage inlets, and storm sewers often prevent MSE backfill reinforcements from being placed in their preferred or optimum configurations.  In some situations, the conflict can be resolved through early recognition of the problem.  For example, a drainage pipe can be relocated away from the reinforced fill thereby eliminating the need for reconfiguration of reinforcements.  At other times avoiding the obstruction may not be possible.  An example of such a situation is an MSE wall that is being built close to a drilled shaft or pile-supported bridge abutment.  In these instances the conflict should be appropriately addressed during the design of the structure so that the

service life or safety of the wall system will not be compromised. Unfortunately, all too often such conflicts are left to be resolved in the field during construction.

Conflicts may occur due to vertical obstructions (*e.g.*, drilled shafts, piles) or horizontal obstructions (*e.g.*, horizontal drainage pipe). There are a number of strategies commonly used to resolve these conflict situations. The appropriate strategy generally depends on type/size of the obstruction, the type of reinforcement (individual reinforcing strips or bar mats) and type of connection between the reinforcement and the facing (pinned, fixed or bolted connections). The following is a brief discussion of some commonly used strategies and problems arising from implementing the strategies *incorrectly*.

### 2.4.1 Lateral Shifting of the Reinforcement

One of the common strategies used to avoid obstructions involves relocation of the reinforcement by shifting it laterally to avoid the conflict. When this approach is used, the wall facing is fitted with additional connectors and then the soil reinforcing is attached to the connectors away from the obstruction. This strategy allows the total pullout resistance capacity of all reinforcement attached to each wall panel to be maintained at the original design value. Figure 2.8 shows an alternative reinforcement layout that could be used with welded steel grids. In this case, the facing panel has been provided with extra clevis loops so that reinforcing grid can be shifted laterally and attached to the panel at a different location, avoiding the conflict with the obstruction. Figure 2.9 shows a variation of this strategy that can be used when obstruction is so large that pullout capacity equivalency cannot be established for each single panel. In this case, a galvanized steel angle has been used to achieve mechanical connection between two adjacent facing panels of an MSE wall system. The reinforcing strips are then attached to the angle away from the obstruction (*i.e.,* inlet structure).

### 2.4.2 Skewing of Strip Reinforcements

Skewing strip reinforcements to avoid an obstruction is an acceptable approach when the reinforcement connections are designed to allow rotation (*i.e.*, bolted connections). Figure 2.10 illustrates this reinforcement layout. Typically, the skew angle is limited to 15º so that skewing does not generate bending moments in the reinforcement and connections.

Further, the tensile resistance of the reinforcement must be reduced by the cosine of the skew angle (*4, 21*).
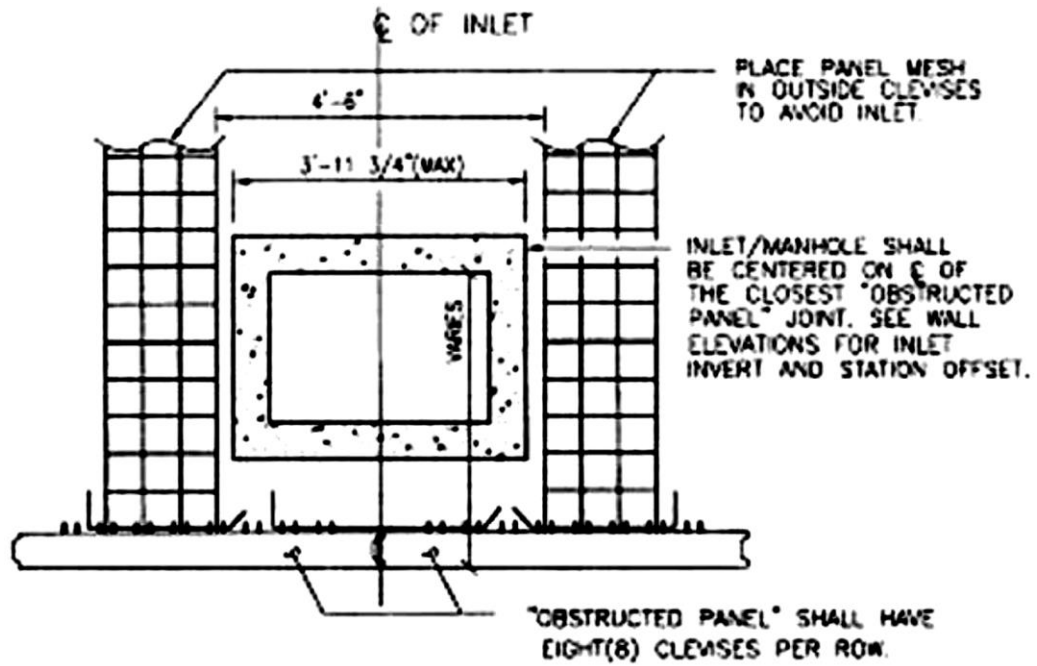


**Figure 2.8**  Lateral Shifting of Grid Type Reinforcement to Avoid Obstruction (*2*)
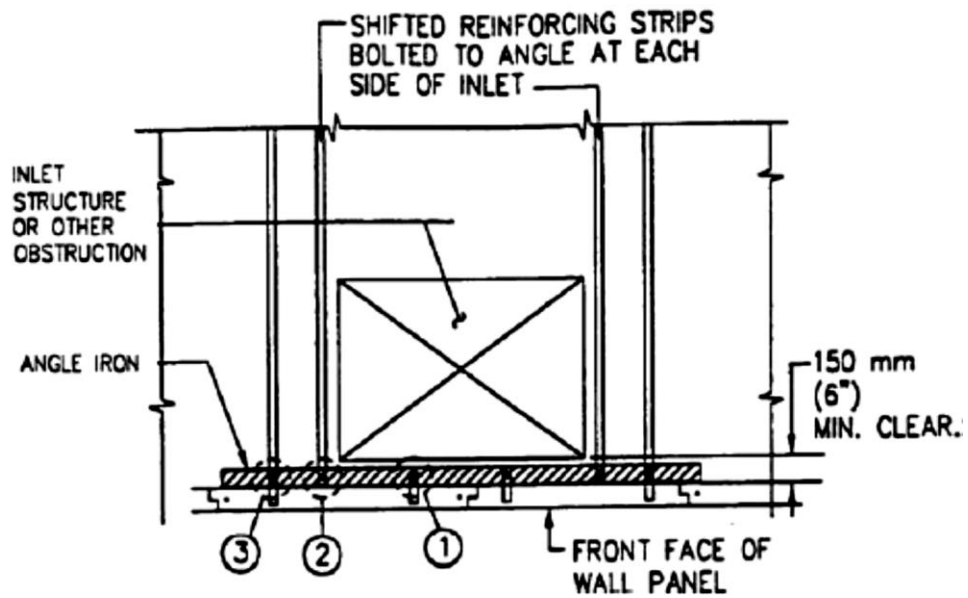


**Figure 2.9**  Lateral Shifting of Strip Reinforcement to Avoid Obstruction (*2*)
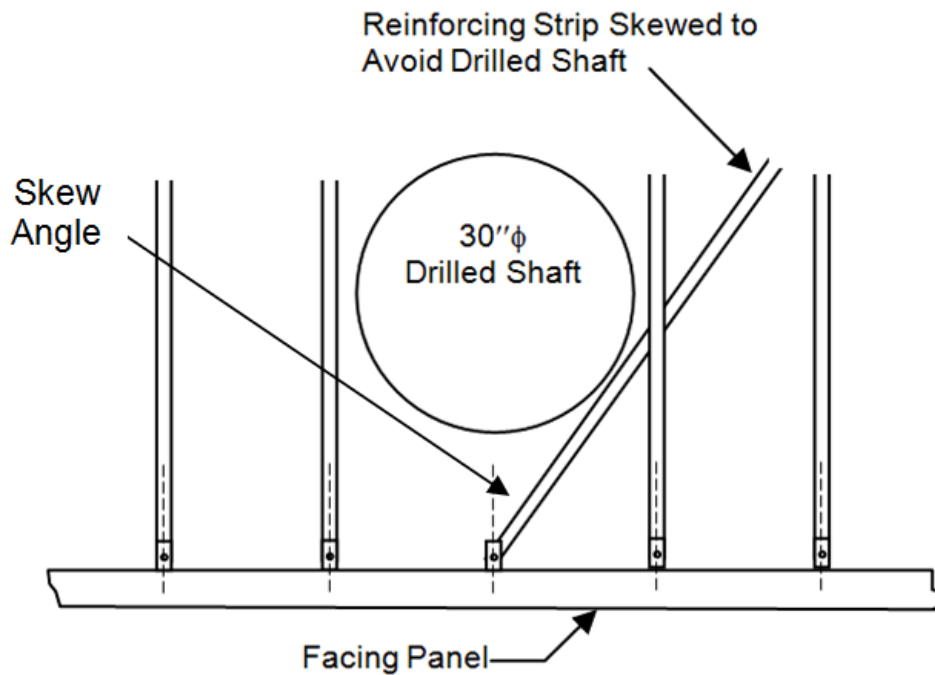
**Figure 2.10** Skewing Strip Type Reinforcement to Avoid Vertical Obstructions

Skewing of strip reinforcement must start at the bolted connection. Bending the reinforcement to avoid obstructions is not skewing and bending can have an adverse effect on the stress transfer and stress distribution at the connection.

### 2.4.3 Cutting and Splaying of Grid Reinforcements to Avoid Obstructions

Two types of cuttings are used as a means of working around obstructions. The first involves cutting longitudinal members of the soil reinforcements. While this type of cut may simplify construction, it clearly increases the stresses in the remaining longitudinal members, and <u>therefore should not be used</u>.

The second type of cut involves severing the transverse members of a grid type reinforcement. This practice allows the grid to be separated so that longitudinal members can be splayed around the obstruction (see Figure 2.11). This splay configuration changes the soil-reinforcement interaction characteristics and therefore its effect must be evaluated

through pullout testing. Splaying bar mat reinforcements is permitted in the AASHTO *Standard Specifications for Highway Bridges,* 17th Edition (*21*), which provides allowable stress design guidance for MSE walls. Therefore, consistent with TxDOT policy, cut and splay behavior of welded steel grids (bar mats) has been evaluated through pullout testing in this study. However, it should be noted that AASHTO *LRFD Bridge Design Specifications*, 5th Edition does not permit the cutting grids without modification to the wall design (*4*).
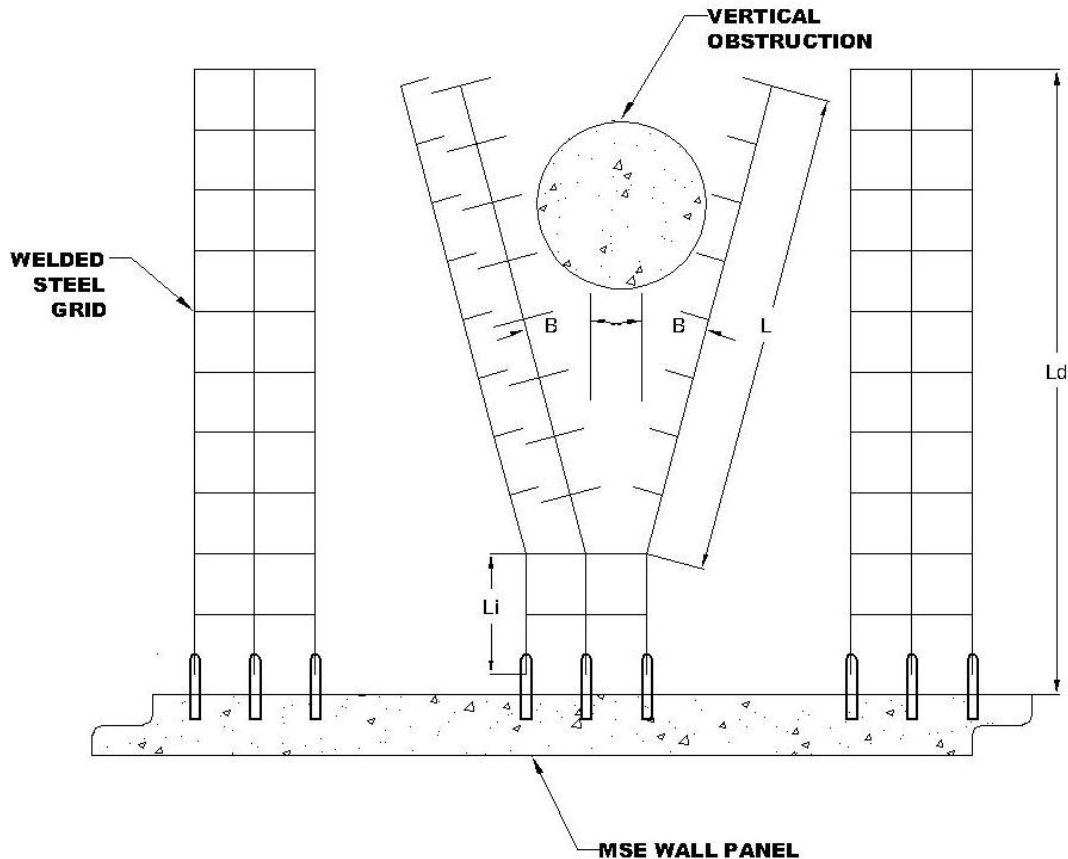


**Figure 2.11** Cutting Transverse Members to Allow Splaying Longitudinal Members Around Obstructions

### 2.4.4 Use of a Structural Yoke

Use of a structural yoke is another approach that is used with bar mat type reinforcements. Figure 2.12 illustrates this approach. An extension may be designed and constructed with structural steel plates to allow the standard reinforcement connection to be made behind a vertical obstruction. FHWA-NHI-10-024, 2009 specifies that, when this approach is used, the structural frame and the connections must be designed in accordance

with AASHTO Specifications for steel structures for the maximum tensile loads at any level of reinforcement with the reinforced soil mass (*2*). TxDOT does not allow the use of structural yoke to avoid obstructions during MSE wall construction.
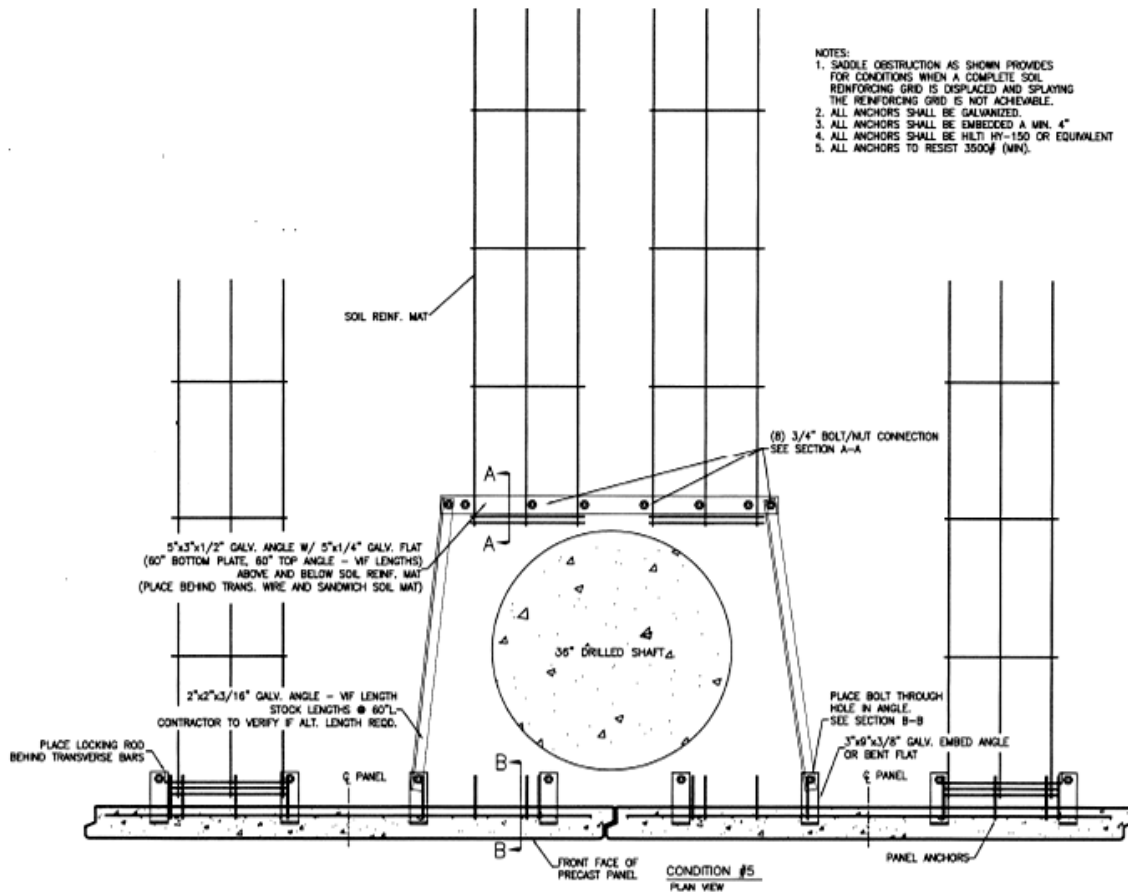


**Figure 2.12.** Use of a Structural Yoke

### 2.4.5 Bending of MSE Reinforcements

TxDOT has seen various attempts by wall designers to avoid both horizontal and vertical obstructions in the reinforced backfill zone by bending the MSE reinforcements. AASTHO policy does not *directly* address bending of MSE reinforcements. However, in their guidance on splaying strip and bar mat reinforcements, AASHTO explicitly forbids generating moment "…in the reinforcement or the connection of the reinforcement to the wall face" (*21*). Another consideration against bending is avoidance of damage to the galvanized protective coating on the reinforcements.

### 2.4.6    Connecting the Soil Reinforcements to Obstruction

A strategy that has been used to deal with drilled shafts, piles, and large inlet structures that are in the path of the MSE reinforcement is to sever the reinforcement and connect it to the structure.  There are two problems with this strategy.  First, the obstructing structure (*i.e.*, drilled shaft, pile, or drainage inlet) has likely *not* been designed to carry additional lateral loads transferred to it by the MSE reinforcements.  Second, any differential settlement that may occur in the MSE wall with respect to the existing structure can cause overstresses in the reinforcement or the connection and lead to rupture of these elements. Therefore, cutting MSE reinforcements and connecting the reinforcement to structures is not considered an acceptable strategy.

**CHAPTER 3**

**REVIEW OF PUBLISHED LITERATURE ON PULLOUT TESTING**

**3.1 OVERVIEW**

Since the introduction of reinforced earth concepts to retaining wall construction in the 1960s, numerous research studies have examined pullout resistance behavior of MSE reinforcements. Some of these research studies involved pullout resistance testing in the laboratory environment while others involved measurement of pullout resistance in the field. As a part of the literature survey completed in this research, technical reports and articles published based on previous pullout resistance test programs were collected and reviewed in detail. The objectives of this literature review were twofold: (a) to compile information on pullout test equipment and test procedures used in previous research, and (b) to synthesize the data available through previous test programs so that they can be compared with the data obtained from the current study. The findings from this literature review effort are presented in this chapter.

**3.2 LABORATORY TESTING TO DETERMINE PULLOUT RESISTANCE**

This section summarizes the findings from review of previous laboratory studies that examined pullout resistance of MSE reinforcements. A total of 22 reports and articles dealing with laboratory pullout testing are included in this review. An overview of the findings from this review is given below. Specific information related to each laboratory test study is presented in Table 3.1. This information includes: (a) type of backfill material used in testing, (b) type of reinforcement tested, (c) total number of pullout resistance tests completed, (d) dimensions of the test box and test system detail, (e) magnitude of overburden stress simulated during testing and the method used to apply the stress, (f) equipment used to apply the pullout load and (g) instrumentation used to measure pullout load and displacement, and (h) significant findings. In Table 3.1 articles are presented in chronological order. It should be noted that information reported in the original references has been converted to a consistent system of units to allow easy comparison.

**Table 3.1** Previous Laboratory Research Studies on Pullout Resistance of MSE Reinforcements

| | |
|---|---|
| **Ref: Chang et.al. 1977 (*8*)** | |
| Type of Backfill | Poorly graded gravelly sand |
| Type of Reinforcement | Galvanized steel strips (2.3-in wide, 0.125-in thickness); bar mesh reinforcements (0.375-in dia. wires and 4in by 8in opening), smooth bars (0.375-in dia), Solid steel plate (28-in wide and 0.125-in thickness) |
| Test System Dimensions and Detail | 3-ft (Width) x 4.5-ft (Length) x 1.5-ft (Height) |
| No. of Tests Completed | 10 tests |
| Overburden Pressure | Applied using a hydraulic jack; Overburden pressures of 720, 1440, 2880, 3600 psf |
| Pullout Force Application | Pullout force was applied using hydraulic jack at a constant strain rate of 0.002 in/min; The load was measured using load cells; Displacement measured at both front and back using extensometers; Front face of the test box removed prior to pullout load application |
| Comments | Gradation data for backfill was not presented in the original reference; Original article provided load-displacement curves; therefore, the pullout force corresponding to a particular displacement could be determined. |
| | |
| **Ref: Bishop and Anderson, 1979 (*9*); Peterson, L. M., 1980 (*7*)** | |
| Type of Backfill | Tests were conducted on two separate types of backfill materials: Silty Sand and Gravelly Sand |
| Type of Reinforcement | Welded Wire Mesh with bar sizes 0.15-in, 0.177-in, 0.207-in and 0.252-in and mesh opening 2-in by 6-in |
| Test System Detail | 6-ft (Width) x 5-ft (Length) x 4-ft (Height) |
| No. of Tests Completed | 60 tests |
| Overburden Pressure | Applied using sixteen hydraulic rams mounted on four I-beams (4 rams per I-beam); rams jack against 1.0-in thick steel plates placed on top of the soil; Overburden pressure range: was 800-9700psf |
| Pullout Force Application | Hydraulic ram jacked against test cell; Load increased by 500-lb or 1,000-lb increments once every 30 seconds; A seating load of 500-lb was used; Pullout load calculated using axial strains measured on pull rod; displacements measured using dial gage with an accuracy of 0.001-in. |
| Comments | Pullout forces were determined at a displacement of 0.2-in.; Tests terminated at maximum displacement of 0.5-in or less; Pullout force due to bearing was determined by subtracting frictional force from the total force |

**Ref.: Nielson and Anderson, 1984 (*22*)**

| | |
|---|---|
| Type of Backfill | Tests were conducted on three separate types of backfill materials: Silty Sand, Washed Sand, and Pea Gravel; Sands compacted to achieve 90% and pea gravel to 100% maximum dry density |
| Type of Reinforcement | Welded Wire Mesh with bar sizes 0.25 and 0.375-in and with transverse bar spacings of 12, 18, 24-in; wire mesh with bar sizes 0.15-in and 0.177-in and mesh opening 2-in by 6-in. |
| Test System Detail | 6-ft (Width) x 5-ft (Length) x 4-ft (Height) |
| No. of Tests Completed | 93 tests |
| Overburden Pressure | Applied using sixteen hydraulic rams mounted on four I-beams (4 rams per I-beam); rams jack against 1.0-in thick steel plates placed on top of the soil; Overburden pressure range: 605-3627 psf |
| Pullout Force Application | Hydraulic ram against test cell; Strain rate: 0.067in/min; A seating load of 500-lb was used; Pullout load calculated using axial strains measured on pull rod; displacements measured using dial gage with an accuracy of 0.001-in. |
| Comments | Pullout force corresponding to 0.75-in displacement was reported; This study reported weld breaks; Pullout force due to bearing was determined by subtracting frictional force from the total force |

**Ref.: Hannon and Forsyth, 1984 (*23*)**

| | |
|---|---|
| Type of Backfill | Silt with low plasticity compacted to achieve 90% maximum dry density |
| Type of Reinforcement | Bar mesh with transverse bar size 0.3-in; 6-in by 24-in grid |
| Test System Detail | 3-ft (Width) x 4.5-ft (Length)x 1.5-ft (Height) |
| No. of Tests Completed | 3 tests |
| Overburden Pressure | Applied using a hydraulic jack; Overburden pressures equivalent to 8-ft of fill; approximately 1,000psf |
| Pullout Force Application | Pullout force was applied using hydraulic jack at a constant strain rate of 0.002 in/min; The load was measured using load cells; Displacement measured at both front and back using extensometers; Front face of the test box removed prior to pullout load application |
| Comments | This reference primarily deals with instrumentation and pullout testing conducted in the field; Limited laboratory testing was conducted to validate field measured parameters; Lab testing was conducted using the same test equipment and test protocol as in Reference No. 1. |

**Ref.: VSL Pullout Tests (*24, 25, 26, 27, 28, and 29*)**

| | |
|---|---|
| Type of Backfill | Fine to medium sand with gravel; crushed stone; Due to coarse granular nature compacted densities were not measured in all of the testing; It is estimated that compaction procedure would have achieved relative compaction of 95% or greater |
| Type of Reinforcement | Mesh type reinforcement (specific mesh dimensions and bar sizes not provided) |
| Test System Detail | Rigid metal box (dimensions not provided) |
| No. of Tests Completed | 33 tests |
| Overburden Pressure | Applied using a hydraulic jack; A range of overburden pressures equivalent to 5ft – 40ft of fill were used; approximately 550psf-5400psf |
| Pullout Force Application | Pullout force was applied using hydraulic jack (strain rate not specified); The load was measured using load cells and digital strain indicators; Displacements were recorded using dial gages |
| Comments | This reference represents a collection of six reports that document data obtained from project specific pullout testing conducted for VSL corporation by several different independent test laboratories. |

**Ref.: Bergado et.al. 1990 (*30*), Bergado et.al. 1992 (*31*)**

| | |
|---|---|
| Type of Backfill | Tests were conducted on weathered clay (CL) with low plasticity, lateritic residual soil (GC); material compacted to achieve 95% standard Proctor density |
| Type of Reinforcement | Welded bar mats fabricated using ¼-in and 3/8-in mild steel bars with mesh openings of 6-in x 9-in, 6-in x 12-in, and 6in-18-in |
| Test System Detail | 2.5-ft (Width) x 4.17-ft (Length) x 1.67-ft (Height) test cell made with 0.5-in thick steel plates |
| No. of Tests Completed | 87 tests on weathered clay backfill and 48 tests on lateritic residual soil |
| Overburden Pressure | Applied using inflated air bag fitted to the pullout box shape and size; Overburden pressure used: 204, 1025, 1845, 2662 psf |
| Pullout Force Application | Applied using electric hydraulic ram and measured using a load cell; displacements measured using LVDT; strain rate used was 0.04in/ min |
| Comments | Backfill used in this study is described as poor quality material which is not representative of MSE select backfill used in TxDOT construction. The researchers were investigating possible use of grid type reinforcement to stabilize earth embankments |

**Ref.: Bergado et.al., 1993 (*32*)**

| | |
|---|---|
| Type of Backfill | Tests were conducted on weathered clay with Plasticity Index 48-68%; material compacted to achieve 95% standard Proctor density |
| Type of Reinforcement | Welded bar mats fabricated using ¼-in and 1/2-in mild steel bars with mesh openings of 6-in x 9-in |
| Test System Detail | 2.5-ft (Width) x 4.17-ft (Length) x 1.67-ft (Height) test cell made with 0.5-in thick steel plates |
| No. of Tests Completed | 9 tests (a total of 52 tests including other types of reinforcement) |
| Overburden Pressure | Applied using Inflated air bag fitted to the pullout box shape and size; Overburden pressure used: 208 and 2715 psf |
| Pullout Force Application | Applied using electric hydraulic ram and measured using a load cell; displacements measured using LVDT; strain rate used was 0.04in/ min |
| Comments | Backfill used in this study was medium to highly plastic clay soils which are not representative of MSE select backfill used in TxDOT construction. |

**Ref.: Bergado et. al., 1996 (*33*)**

| | |
|---|---|
| Type of Backfill | Tests were conducted on three types of backfill material: weathered Bangkok clay, clayey sand and lateritic soil; material compacted to achieve 100% standard Proctor density |
| Type of Reinforcement | Welded wire steel grid; bar sizes of 0.25in, 0.30in and 0.5 in and grid opening sizes (6inx9in) |
| Test System Detail | 2.5-ft (Width) x 4.17-ft (Length) x 1.67-ft (Height) test cell made with 0.5-in thick steel plates |
| No. of Tests Completed | 60 tests (some of the tests reported may have been included in previous articles) |
| Overburden Pressure | Applied using inflated air bag fitted to the pullout box shape and size; Overburden pressure range used: 208 to 2715 psf |
| Pullout Force Application | Applied using Electric hydraulic ram; with a strain rate of 0.04 in/ min |
| Comments | Only one of the three backfill soils used in this study, i.e. clayey sand, classified as a coarse grained soil; even that material has a fines content of 44% and therefore does not meet TxDOT specification for MSE select backfill. The primary focus in this paper is on the development of a theoretical basis for prediction of pullout resistance rather than on experimental detail. |

**Ref.: Matsui et al., 1996a (*34*), Matsui et al. 1996b, (*35*), and Matsui et al. 1996c, (*36*)**

| | |
|---|---|
| Type of Backfill | Tests were conducted on one type of backfill material: Granular Sand; Sand was poured from hopper to achieve 80% relative density |
| Type of Reinforcement | Welded wire steel grid with wire dia. of 0.24in and 6-in by 9-in grid opening; Reinforcements were tested with and without an initial vertical bend |
| Test System Detail | 2.47-ft (Width) x 3.44-ft (Length) x 1.56-ft (Height) test cell |
| No. of Tests Completed | 18 tests |
| Overburden Pressure | Applied using inflated air bag fitted to the pullout box shape and size; Overburden pressure used: 1023, 2048, 3074 psf |
| Pullout Force Application | Applied using a hydraulic jack with a capacity of 67.4kips; pullout load was applied at a constant loading rate of 0.225 kips/min; Pullout load measured using a tension load cell with 22.48kip capacity |
| Comments | Welded wire grids were tested with and without a vertical bend, with 1, 2 and 3 embedded transverse bars under three different normal pressures |

**Ref.: Nabeshima and Matsui, 1998 (*37*)**

| | |
|---|---|
| Type of Backfill | Tests were conducted on one type of backfill material: Granular Sand; Sand was poured from hopper to achieve 80% relative density |
| Type of Reinforcement | Welded wire steel grid with wire dia. of 0.30in and 0.35in and 6-in by 9-in grid opening; Reinforcements were tested with and without an initial vertical bend |
| Test System Detail | 2.47-ft (Width) x 3.44-ft (Length) x 1.56-ft (Height) test cell |
| No. of Tests Completed | 9 tests |
| Overburden Pressure | Applied using inflated air bag fitted to the pullout box shape and size; Overburden pressure used: 1023, 2048, 3074 psf |
| Pullout Force Application | Applied using a hydraulic jack with a capacity of 67.4kips; pullout load was applied at a constant loading rate of 0.225 kips/min; Pullout load measured using a tension load cell with 22.48kip capacity |
| Comments | The tests described in this article were conducted using the same test apparatus and procedure as in previous studies by Matsui at al. (*15, 16* and *17*). The current study involved additional tests to examine the effects of the transverse bar diameter. |

**Ref.: Teerawattanasuk et.al., 2003 (*38*)**

| | |
|---|---|
| Type of Backfill | Tests were conducted on sandy backfill material compacted to achieve 95% standard Proctor density |
| Type of Reinforcement | Galvanized and PVC coated hexagonal wire mesh; wire diameter of 0.12-in and mesh opening 3.14in x 3.93in |
| Test System Detail | 2.5-ft (Width) x 4.17-ft (Length) x 1.67-ft (Height) test cell made with 0.5-in thick steel plates |
| No. of Tests Completed | 3 |
| Overburden Pressure | Applied using inflated air bag fitted to the pullout box shape and size with a pressure range of: 1148 to 2192 psf |
| Pullout Force Application | Applied using hydraulic jack with a strain rate of 0.04 in/ min; a seating load of 45.5lb was used. |
| Comments | In this study significant effort was devoted to development of analytical and numerical model to predict pullout resistance of hexagonal wire mesh type reinforcement |

**Ref.: Lee and Bobet 2005 (*39*)**

| | |
|---|---|
| Type of Backfill | Tests were conducted on two types of backfill material: clean sand compacted to achieve 100% standard Proctor density and silty sands compacted to achieve 95% standard Proctor density |
| Type of Reinforcement | 2-in wide and 120mil thick steel strip reinforcement; 2.5ft length embedded in soil |
| Test System Detail | Pullout test system included two separate chambers: (a) soil chamber, and (b) water chamber. The soil chamber had following dimensions: 1.31ft (Width) x 3.28 ft (length) x 1.64ft (Height) |
| No. of Tests Completed | 30 tests |
| Overburden Pressure | Applied using inflated air bag fitted to the pullout box shape and size; three overburden pressures 626.5psf, 2088 psf, and 4177psf were used |
| Pullout Force Application | Applied using electric hydraulic ram with a strain rate of 0.04 in/min for drained tests and 0.39 in/min for undrained tests |
| Comments | The test system used in this research study had the unique capability to incorporate the effects of saturation of the backfill. This will be a particular concern for fine grained soils in which undrained conditions may develop. |

| Ref.: Horpibulsuk and Niramitkornburee, 2010 (40) | |
| --- | --- |
| Type of Backfill | Tests were conducted on clean sand (0.3% gravel, 97% sand and 2.7% silt) |
| Type of Reinforcement | Bearing reinforcement produced by welding steel angles (transverse element) to a deformed steel bar (longitudinal element) |
| Test System Detail | Tests apparatus consisted of a test cell with following dimensions: 1.96-ft (Width) x 8.50-ft (length) x 2.62-ft (Height) |
| No. of Tests Completed | 8 tests |
| Overburden Pressure | Applied using pressurized air bag positioned between compacted sand and top cover; overburden pressure used 626, 1044 and 1880 psf |
| Pullout Force Application | Applied using an electric hydraulic ram with 45kip capacity; load applied at a strain rate of 0.04in/min |
| Comments | The pullout tests described in this reference were conducted on a unique reinforcement that is not used in US MSE wall construction |

The literature review included twenty-two separate studies involving laboratory testing of MSE reinforcement to determine their pullout resistance capacity. However, it is worth noting that not all of these studies have been conducted independently of each other at different testing laboratories. Instead, many have been conducted at the same laboratory using the same equipment and test protocol. These testing laboratories are: Transportation Research Laboratory, California Department of Transportation (CALTRANS) (8, 23), Utah State University (7, 9, 22), VSL Corporation (24, 25, 26, 27, 28, and 29), Asian Institute of Technology (AIT), Thailand (30, 31, 32, 33, 38), Osaka University, Japan (34, 35, 36, 37), Purdue University (39) and Suranaree University of Technology, Thailand (40). Nearly all of these studies used test cells with rigid walls that remained closed during filling of the box as well as during reinforcement pullout. The only exception to this was the test system used by CALTRANS researchers. In these tests the front wall of the test box was removed before pullout load was applied on the reinforcement.

The dimensions of the test cells used varied from one study to another. The typical lengths of the test cells varied from 3.0 to 5.0ft, while the typical widths varied from 2.0ft to 3.0ft. The most commonly used test cell height was 1.5ft. The test cell developed and used by researchers at Utah State University had dimensions of 5ft (Length) x 6ft (Width) x 4ft

(Height) and therefore, had larger width and height than typical dimensions mentioned above.

With the exception of the pullout test programs conducted at AIT, Thailand, most test programs used granular soils as backfill. Backfill was typically placed and compacted to achieve 90-100% of Standard Proctor density. However, in many cases, the information provided was not sufficient to determine whether the granular backfill material used actually met the current AASHTO gradation requirements for select MSE backfill. The test programs conducted at the AIT specifically focused on pullout resistance of reinforcements embedded in low quality backfill (*e.g.*, clays with low to medium plasticity). Two different methods were used to simulate additional overburden soil pressure on the reinforcement. The first method involved the use of hydraulic rams that were jacked against a reaction frame to generate a vertical force that was transferred to steel plates resting on soil. The second involved the use of a pressurized air bag that is positioned between compacted soil backfill and a cover plate of the soil cell. The maximum overburden pressures simulated in this manner were typically in the range of 3,000-5,000 psf (equivalent to approximately 25-40ft feet of soil fill).

Pullout forces were applied using hydraulic loading rams. Most of the research studies used the constant strain rate approach when applying the pullout loads. A strain rate of 0.04 in/min was used almost universally in recent testing. In the testing conducted at Utah State University, the pullout load was applied in a stepwise fashion in 500 or 1,000lb load increments. The researchers at Osaka University used a constant loading rate of 0.225 kips/min when applying the pullout load. The pullout loads were measured either by using load cells or through the measurement of axial strains within the reinforcement. The pullout displacements were measured by dial indicators, LVDTs, or other types of digital displacement sensors.

## 3.3  SYNTHESIS OF LABORATORY PULLOUT TEST DATA

The next step in the literature review effort involved synthesis of the pullout test data reported by previous researchers so that published data could be easily compared with current AASHTO recommendations as well as with data collected in the present research

study.   It was determined that these data would be compiled and presented in the form of F* versus Depth of Fill (DOF) charts.  It is important to point out that only a subset of the available data could be included in the data synthesis.   There are several reasons for this. First, some of the previous pullout test programs involved MSE reinforcements that are not typical of those used in TxDOT MSE wall construction.   Examples of such MSE reinforcements are hexagonal wire reinforcements and unconventional reinforcements that were specially fabricated by the researchers (*e.g.*, steel angles welded to deformed bars). Also excluded were wire mesh type reinforcements that were not representative of the welded steel grids tested in the current study.  Grid reinforcements tested in this research project had the following configurations:  the longitudinal bar spacing ($S_L$) 2 to 12-in, transverse bar spacing ($S_t$) 6 to 12-in,  transverse bar diameter W7.5 to W15 (0.31-0.44 in), and longitudinal bar diameter W9.5 to W20 (0.35-0.50 in).   Only those data obtained from testing of MSE grid reinforcements with similar bar sizes and spacings were included in the data synthesis.  Second, it is important to note that most previous research studies did not report pullout test data in the form of F* values.  Therefore, it was necessary to calculate pullout resistance factor ( F*) values based on Eq. 2.9 using data available in the original articles and reports.  The following data are needed to calculate F* parameters using Eq. 2.9: (a) pullout load ($P_r$), (b) vertical overburden pressure ($\sigma_v$), (c) reinforcement length ($L_e$) and width (*b*).   According to the definition used throughout this study, pullout load ($P_r$) is the maximum pullout force measured at or prior to 0.75-in displacement.  Some difficulties were encountered during the calculation of pullout resistance factors using data reported by previous researchers.  These difficulties included: (a) pullout tests were terminated at maximum displacements less than 0.75-in, (b) the pullout load reported was not determined based on the load measured at 0.75-in displacement and the article did not present the load-displacement data so that pullout load consistent with the current definition could be derived, (c) overburden pressure, $\sigma_v$ could not be reliably determined, (d) embedded length and width of the reinforcements were not clearly defined.  Whenever F* could not be estimated with a reasonable degree of accuracy, data were not included in the composite F* versus Depth of Fill (DOF) plots.

Figure 3.1 and Figure 3.2 present the F* versus DOF charts for ribbed steel strips embedded in sandy and gravelly backfill, respectively.  The AASHTO reference line for

default F* (Eq. 2.13a and 2.13b) corresponding to a soil friction angle, $\phi$=34° and coefficient of uniformity, $C_u$=4.0 is also shown on this plot. The data available for ribbed steel reinforcement through previous laboratory studies were very limited. The source for the data shown in Figures 3.1 and 3.2 is the Reinforced Earth Company (RECo) Technical Bulletin MSE-6 (*41*). The data presented in this technical bulletin are described as a compilation of available F* data obtained from a number of different sources. No information other than a general description of the backfill (*e.g.*, sandy gravel, fine sand, etc.) was available on the material tested. Most importantly, the original reference did not include data related to complete gradation or degree of compaction for these backfill materials. Accordingly, classification of these backfills as sandy and gravelly backfill is based on material description only. It was not possible to establish direct correspondence between these materials and different types select backfills found in TxDOT specifications.
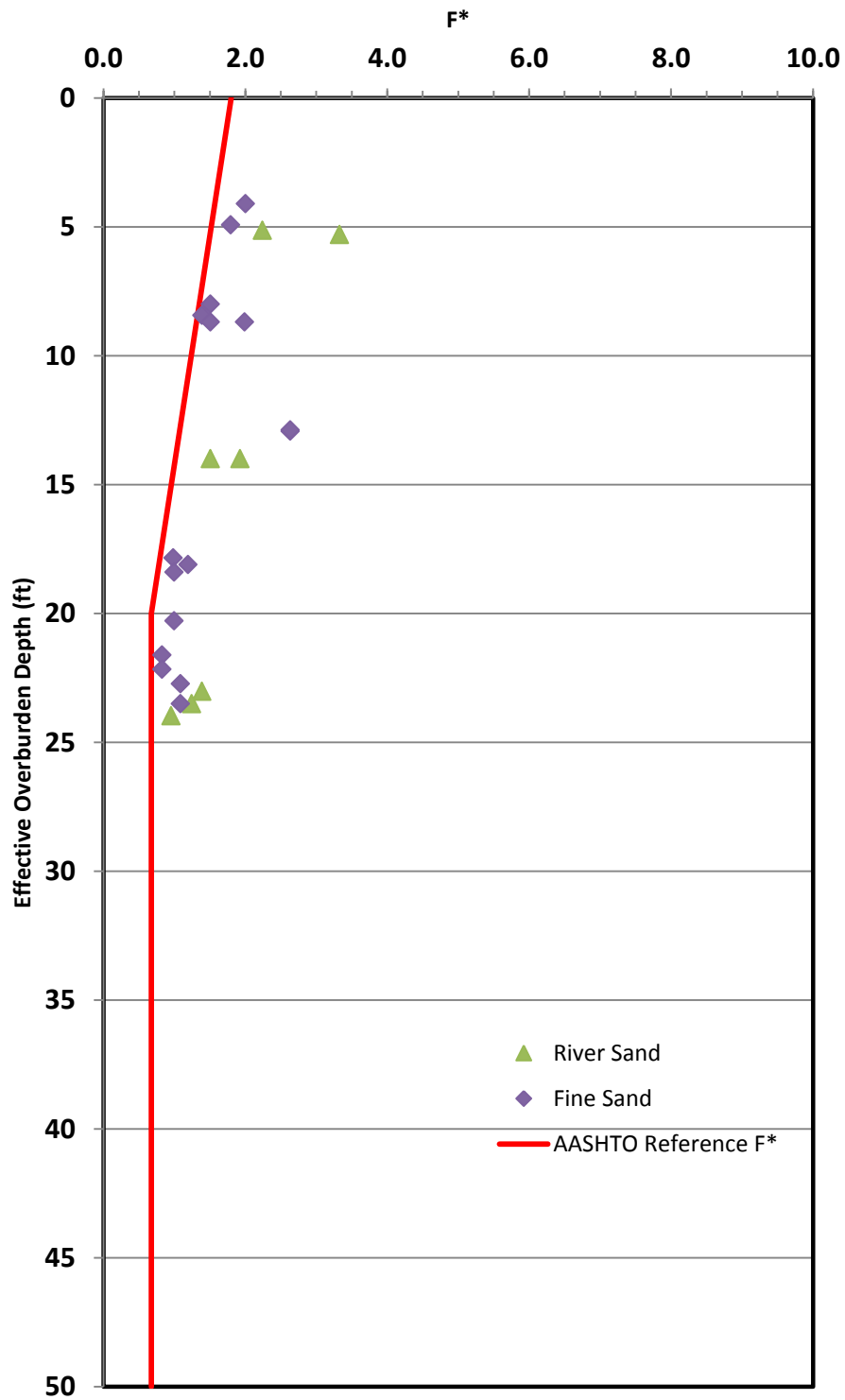
**Figure 3.1** F* versus Depth of Fill Chart for Ribbed Steel Strips; Based on Laboratory Pullout Tests Conducted Using Sandy Backfill (*41*)
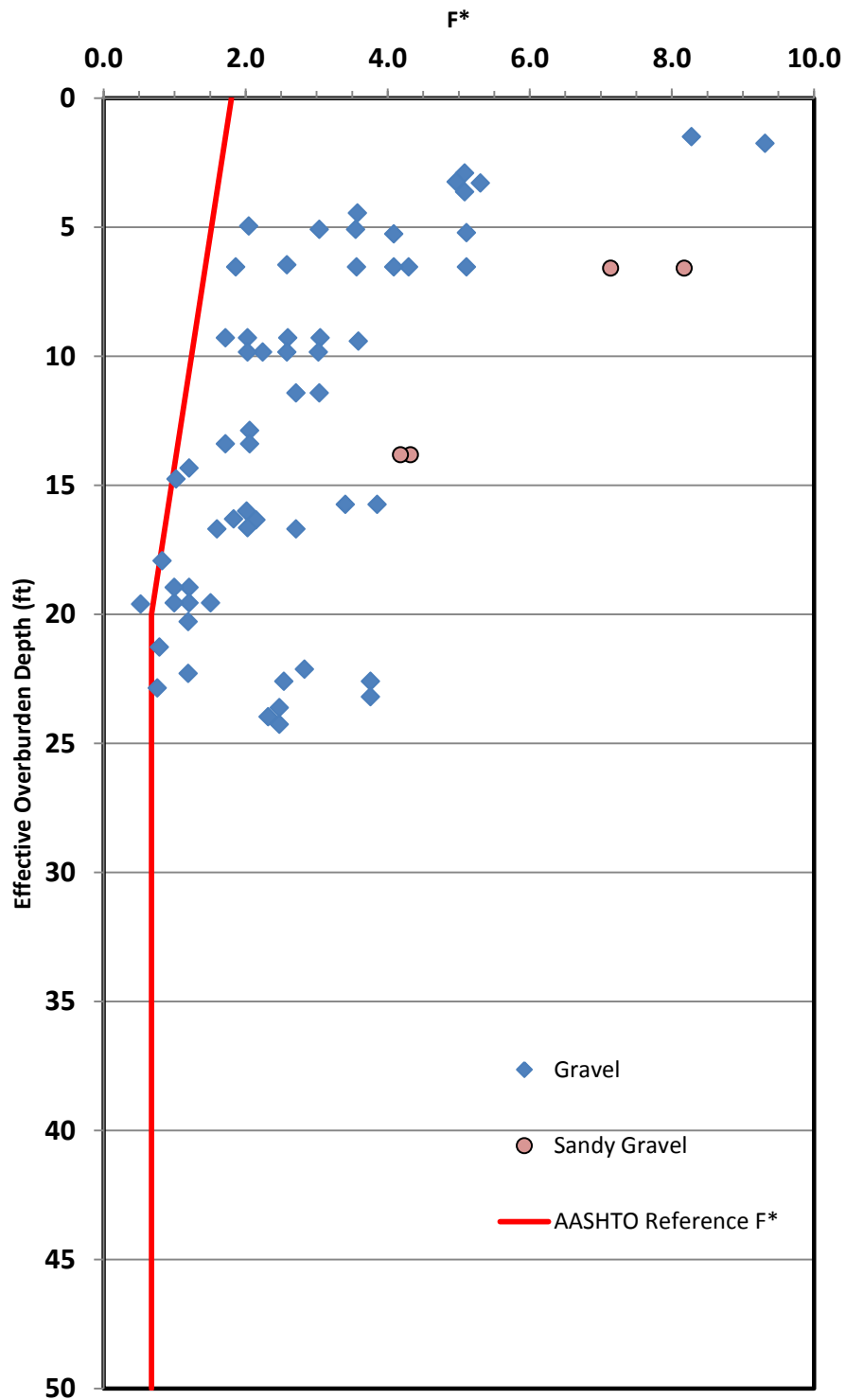
**Figure 3.2** F* versus Depth of Fill Chart for Ribbed Steel Strips; Based on Laboratory Pullout Tests Conducted Using Gravelly Backfill (*41*)

Figures 3.3 and 3.4 present pullout resistance data for tests on welded steel grids. According to the AASHTO reference line for default F* for inextensible grids (Eq. 2.14a and 2.14b), F* is primarily a function of transverse bar spacing/transverse bar diameter ratio (*i.e.*, $t/S_t$). Normalization of F* factor through dividing by $t/S_t$ allows direct comparison of normalized F* values for grids with various bar sizes and spacings. For this reason, Figures 3.3 and 3.4 are presented in the form of normalized F* (*i.e.*, $F^*S_t/t$) versus DOF charts.

Also, using the same approach as that described earlier for ribbed strips, the data points for welded steel grids were differentiated based on type of backfill used in testing, namely, sandy backfill and gravelly backfill. The backfill types that have the group symbols SP, SM, and SW according to the USCS soil classification system were considered as sandy backfill while GP, GC, GW materials were grouped into gravelly backfill. Data obtained for backfills with group symbols CL and ML according to USCS classification are not presented in this report.

When the pullout resistance data are examined cumulatively, it can be observed that a large percentage of data points lie to the left side of AASHTO reference line. Once again, it should be emphasized that, with the data available, it was not possible to ascertain whether the backfill materials labeled as sandy and gravelly backfill met the gradation requirements of current AASHTO (or TxDOT) specifications.
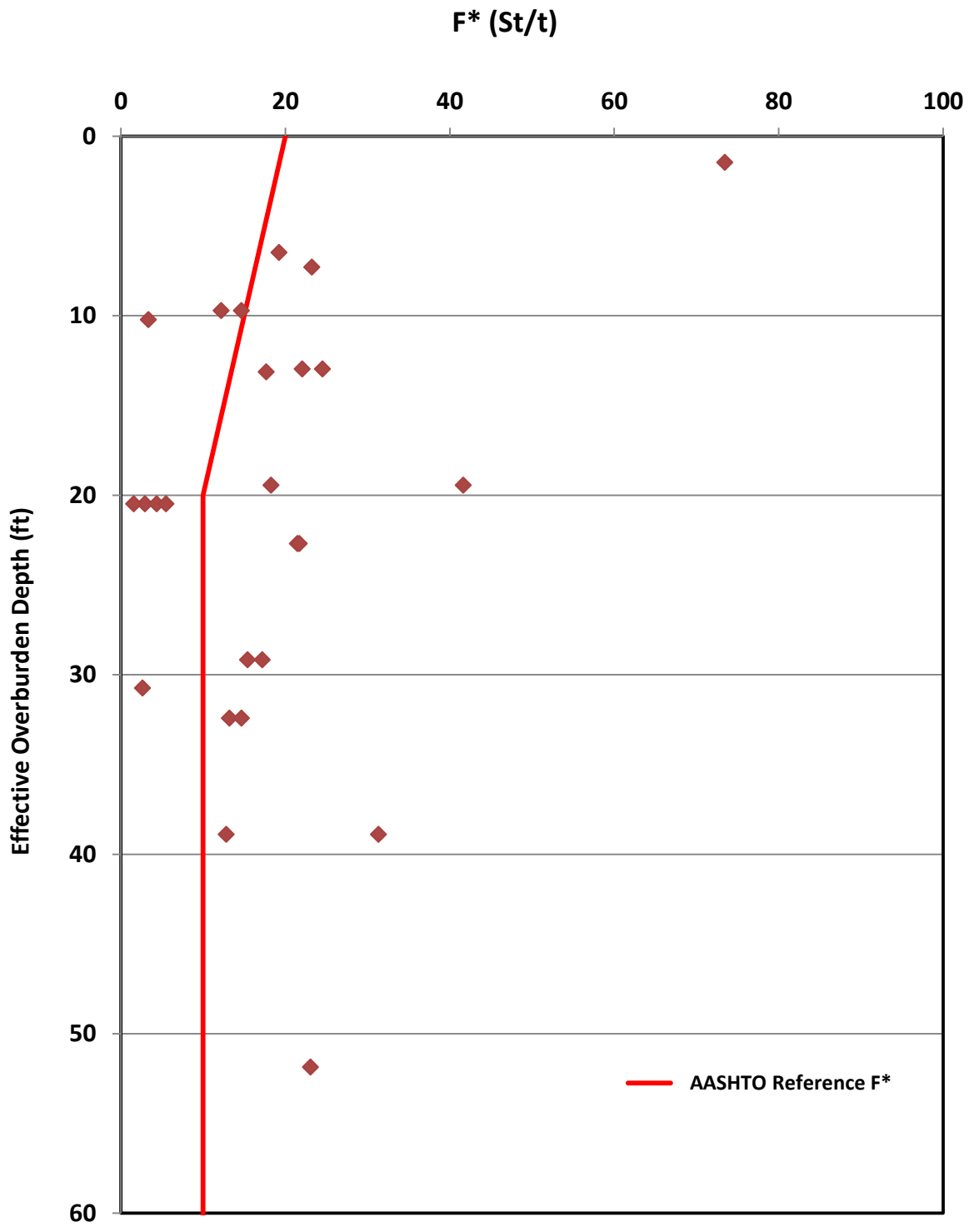
**Figure 3.3** Normalized F* versus Depth of Fill Chart for Welded Steel Grids;
Based on Laboratory Pullout Tests Conducted Using Sandy Backfill
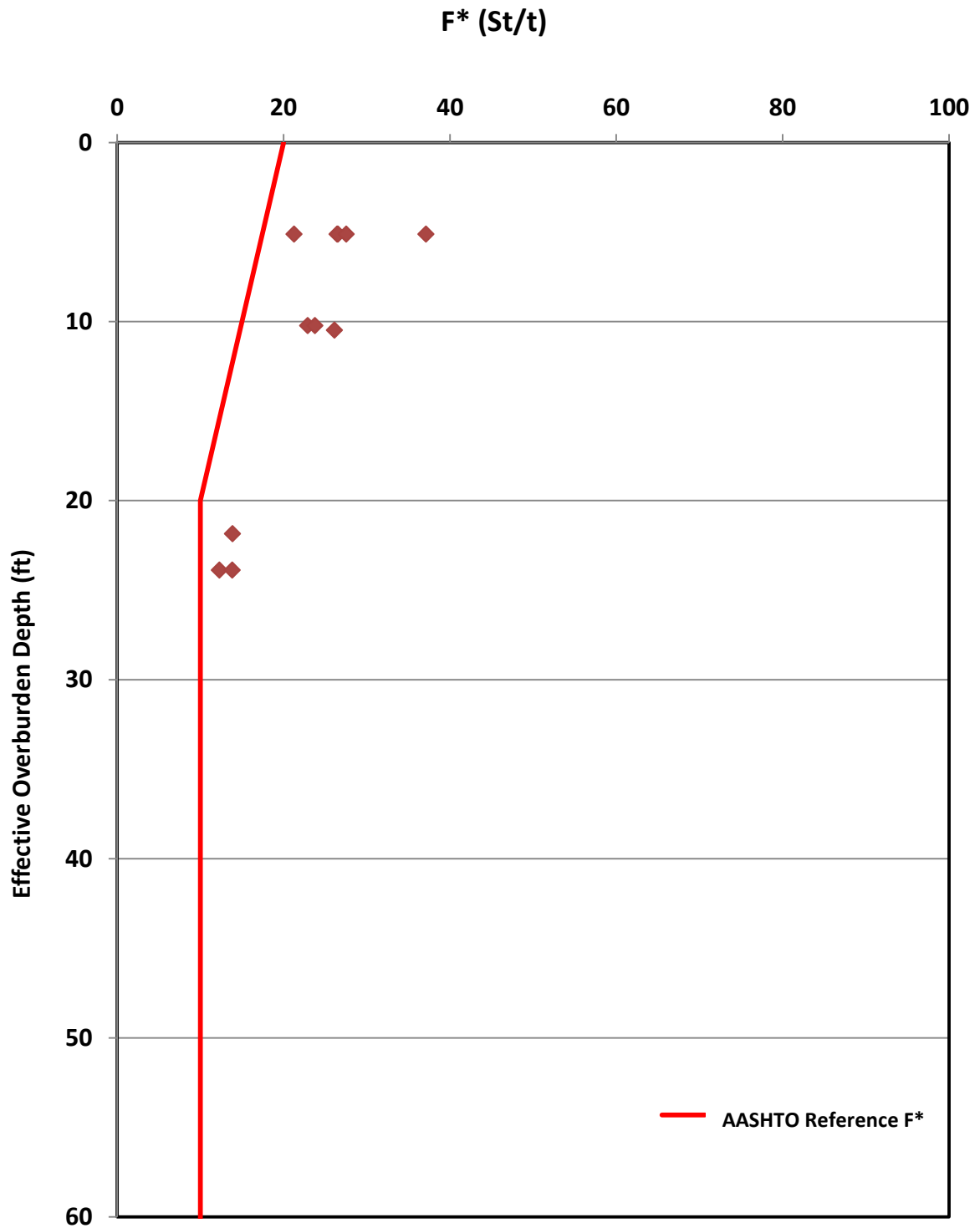
**Fıgure 3.4** Normalized F* versus Depth of Fill Chart for Welded Steel Grids; Based on Laboratory Pullout Tests Conducted Using Gravelly Backfill

## 3.4 FIELD TESTING TO DETERMINE PULLOUT RESISTANCE

Compared to the number of articles and reports available on pullout testing in the laboratory, published literature on pullout testing of MSE reinforcements in the field were very limited. Table 3.2 summarizes the essential information related to three studies that investigated pullout resistance of MSE reinforcements through field testing. One of these studies involved pullout testing of steel strip type reinforcemnt while the other two involved welded steel grids.

Figure 3.5 presents the F* versus DOF chart developed based on field pullout load tests conducted on steel strips. It is believed that the steel strips used in these tests were *smooth* steel strips rather than *ribbed* strips. Therefore, these F* data should be examined in reference to the AASHTO F* line for smooth strips, which is shown as a dotted line in Figure 3.5 (F* = 0.4 at all fill depths). The majority of the measured F* values are found to be higher than that predicted by the AASHTO. However, the incidence of field measured F* falling below the AASHTO recommended value is much more prevalent.

Similarly, Figure 3.6 presents data corresponding to field pullout tests on welded steel grids. Once again, this figure is presented in the form of a normalized F* (*i.e.*, $F^*S_t/t$) versus DOF chart. In this case, the field pullout resistance data were separated into two categories: sandy backfill (USCS group symbols SP, SM, SW) and fine-grained backfill (USCS group symbols ML and CL). Only the field pullout data collected in sandy backfill are shown in Figure 3.6. These data compare favorably against the AASHTO reference line.

**Table 3.2** Pullout Resistance Testing of MSE Reinforcements in the Field

| | |
|---|---|
| **Ref: Chang et.al. 1977 (*8*)** | |
| Test location | Reinforced earth wall constructed on Cal-39 in the San Gabriel Mountains |
| Type of Backfill | Decomposed granite |
| Type of Reinforcement | Galvanized steel strips; Additional dummy strips were installed for pullout load testing (2.362-in wide, 0.118-in thickness); strips were 5, 10, 15, 23 and 46ft long |
| No. of Tests Completed | 9 tests |
| Depth of Fill | 5ft long strip at 7.5-ft depth, 10ft long strip at 12.4-ft depth, 15-ft long strip at 18.2-ft depth, three 23-ft long strips at 18.0-ft depth and three 46-ft long strips at 38.0ft depth |
| Pullout Force Application | Details not found in the article |
| Comments | Four out of the nine strips ruptured at approximately 14.0-kip load; Load displacement curves for successful pullout tests are found in the reference |
| | |
| **Ref.: Hannon and Forsyth, 1984 (*23*)** | |
| Test location | MSE Wall constructed on eastbound I-80 near Baxter, CA |
| Type of Backfill | Low quality backfill; low plastic fine-grained soil |
| Type of Reinforcement | Dummy bar mats were installed in wall for pullout testing; bar mats had three longitudinal bars and one, two or three transverse bars to form 6in x 24-in grid |
| No. of Tests Completed | 15 tests |
| Depth of Fill | Overburden heights of 4, 6, 8, 10 and 12-ft |
| Pullout Force Application | Pullout force was applied by attaching a hydraulic jack and load and then applying the load to the wall face through a timber frame |
| Comments | Field pullout test results were compared with laboratory pullout test results; field pullout tests yielded higher capacity |

| | **Ref.: Bergado et al. , 1991 (_42_), Bergado et.al. 1992 (_43_)** |
|---|---|
| Test location | 18.7ft tall experimental MSE wall built at the campus of Asian Institute of Technology (AIT) using welded wire reinforcement and poor-quality backfill |
| Type of Backfill | Three different backfill soils: Clayey sand, lateritic residual soil and weathered clay; Backfill compacted to achieve 95% of the standard Proctor density |
| Type of Reinforcement | 16.4-ft long, 8-ft wide grid reinforcement W4.5xW3.5 bars and 6inx9in opening |
| No. of Tests Completed | 5 tests |
| Depth of Fill | Overburden heights varied from 4.92-ft to 12.5-ft |
| Pullout Force Application | Pullout loads were applied at constant rate of strain (0.04in/min) using electro-hydraulic servo controlled loading ram through a steel frame butted against the wall face; loads were measured with load cell 50-kip capacity and displacements were measured using LVDTs |
| Comments | A significant observation made in this study was that, unlike in laboratory pullout resistance measurements, the field pullout resistance did not increase with increasing overburden |
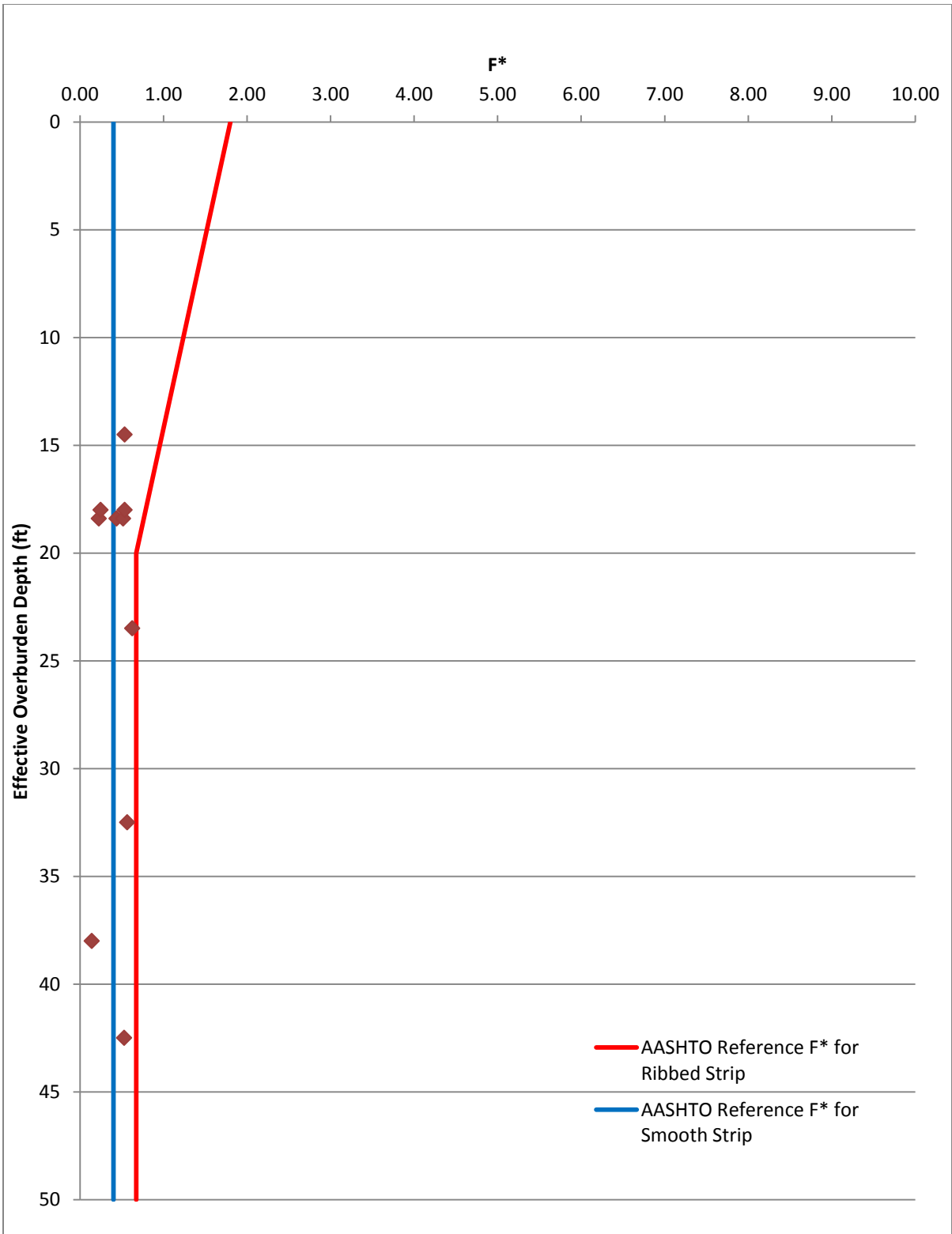
**Figure 3.5** F* versus Depth of Fill Chart for Steel Strips; Based on Field Pullout Tests Conducted in Sandy Backfill

**F\* (St/t)**
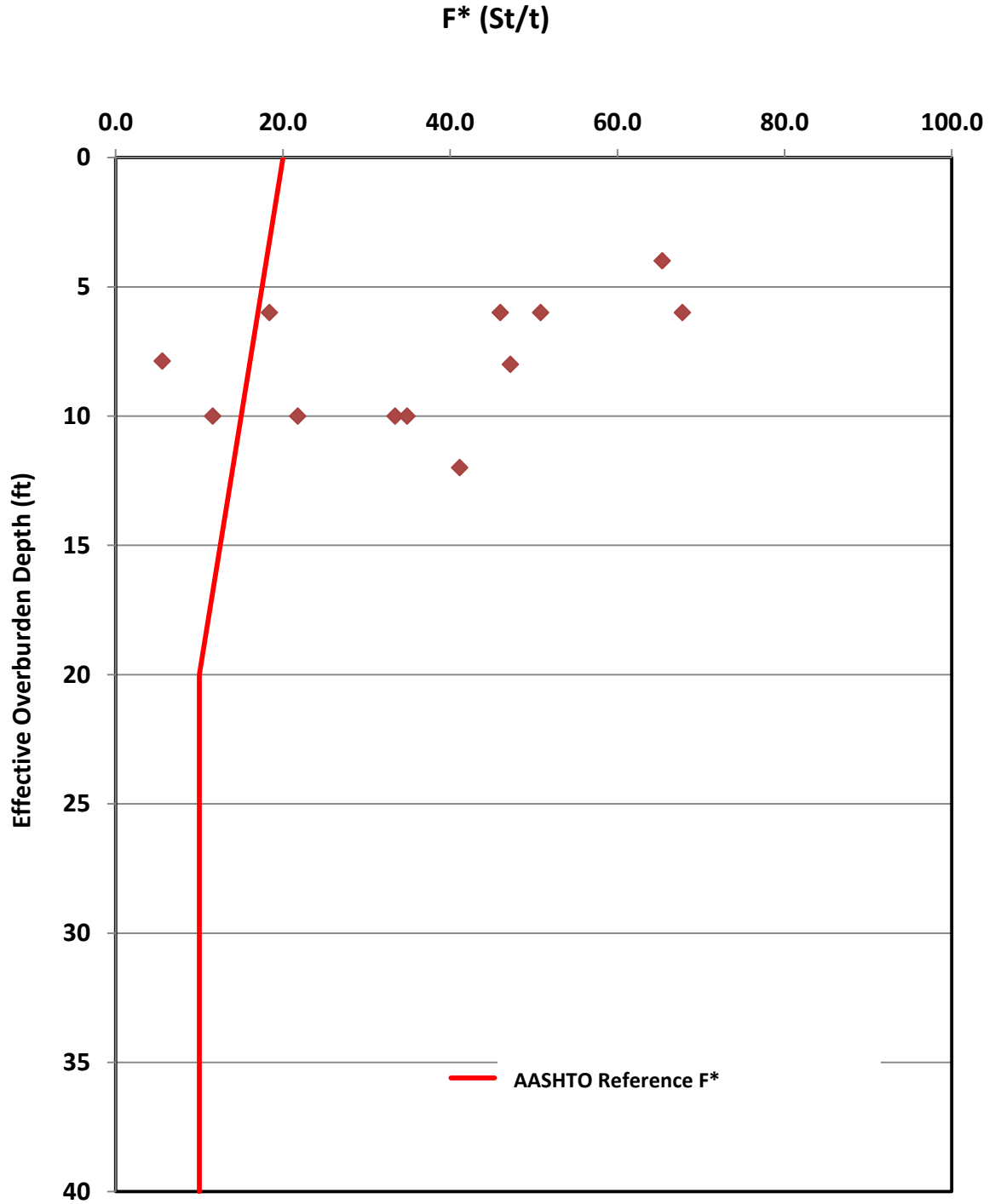


**Figure 3.6** Normalized F* versus Depth of Fill Chart for Welded Steel Grids; Based on Field Pullout Tests Conducted in Sandy Backfill

# CHAPTER 4
# DEVELOPMENT OF THE TEST MATRIX AND MATERIAL CHARACTERIZATION

## 4.1 OVERVIEW

Broadly stated, the principal objective of this study was to determine pullout resistance factors, *i.e*. F* values, for MSE backfill materials and MSE reinforcement elements commonly used in Texas. As discussed in Chapter 2, TxDOT *Standard Specifications* Item 423 allows the use of three different types of select backfill materials, Types A, B and D in the construction of permanent MSE structures (*5*). While the requirements for Type B backfill material are identical to those recommended by the FHWA and AASHTO (*4*), the specifications for Types A and D are significantly more stringent. Specifically, Types A and D backfill represent material with much coarser gradation. In spite of this fact, the same procedure (based on Eq. 2.13 and 2.14) is used in the estimation of the pullout resistance in all MSE wall designs regardless of the type of backfill used. Accordingly, one primary objective of this study was to perform pullout testing and hence investigate the F* values obtained from the placement of inextensible reinforcements in TxDOT's coarse granular backfills and compare the measured values against FHWA/AASHTO recommended values. A second important objective was to evaluate the impact of alternative reinforcement layouts on pullout resistance of MSE reinforcement. Of special interest to this study were skewing of strip type reinforcement and cutting and splaying of grid type reinforcements to avoid vertical obstructions. This chapter describes the development of a suitable test matrix that adequately captures the influence of variables that potentially impact the pullout resistance factor, F*. It also includes a detailed discussion on the selection and characterization of materials used.

## 4.2 SELECTION OF TEST VARIABLES

### 4.2.1 Backfill Material

Input received from the TxDOT project monitoring committee for this research study suggested that the vast majority of MSE retaining walls built by the agency utilize either Type A or Type B select backfill material. Type D backfill (or "rock backfill") is only

required by specification for wall systems that are located within the 100-year flood zone, and the use of Type D backfill is much less common. Therefore, it was determined that primary emphasis for pullout testing would be placed on Type A and Type B backfill materials. It was further determined that the gradation of the material used in testing would represent the finer limits of the gradation band specified for each backfill type to ensure that the test results will be applicable to the worst-case material belonging in that backfill category. Compaction of the backfill in the MSE test box would be conducted according to construction specifications. Accordingly, Type A material was placed and compacted using the ordinary compaction method and Type B material was compacted using the density control method. A relative compaction of 95 percent of maximum dry unit weight as determined per Test Method TEX-114-E, at a moisture content near optimum was used for Type B backfill. Additional overburden stress, intended to model specified backfill overburden depths, was applied using hydraulic jacks and a load frame. Overburden depths of 5, 12, 20 and 40ft were used in this study.

### 4.2.2  MSE Reinforcement

Two types of MSE reinforcement widely used in TxDOT wall construction were selected for testing. They are steel strip reinforcements and welded steel grid reinforcements. The MSE reinforcement strips commonly used by TxDOT are approximately 2.0 inches wide and 5/32-inch thick. They are galvanized and have ribs on both the top and bottom of the strip to enhance pullout resistance. While other types of MSE reinforcing strips exist, 2-inch ribbed strips were tested in this study.

Unlike ribbed steel strip reinforcements, welded steel grids are available in a wide range of bar sizes and spacings. TxDOT construction projects commonly use grids with longitudinal bar spacing of 9 inches, but some 6-inch wide grids are also used. Longitudinal bar size varies with depth, with smaller longitudinal bars in the upper depths (say, 12 feet and above where pullout controls the design) and larger longitudinal bars in the lower depths (say, 20 feet and below where rupture controls the design). Transverse bar diameters and spacings also vary. Thus, it was necessary to design the test matrix so that the test program could explore a reasonable sample of bar sizes and spacings. The development of the test matrix for MSE grids is explained in detail in Section 4.3.2.

### 4.2.3  Alternative Reinforcement Layouts

As described in Chapter 2, alternative reinforcement layouts are often used in the field during MSE wall construction to avoid obstructions such as bridge abutments, foundations and drainage inlets.  These obstructions can be broadly classified into two categories: vertical obstructions and horizontal obstructions.   At the time this research project was initiated, TxDOT had adopted the policy that horizontal obstructions such as drainage pipe that run along the length of the wall will no longer be allowed within the reinforced fill.  Therefore, this research did not investigate the impact of alternative reinforcement details that specifically address horizontal obstructions.

Among the alternative reinforcement configurations used to avoid vertical obstructions, lateral shifting of reinforcement did not require any testing.  The structural yoke was excluded because TxDOT policy does not allow the use of this alternative reinforcement configuration.  Accordingly, the primary focus in this test program was on two specific alternative reinforcement layouts: (a) skewing of strip type reinforcements, and (b) cutting and splaying of grid type reinforcements.

The following sections provide more detailed information on the development of each component of the test matrix.

### 4.3  DEVELOPMENT OF THE TEST MATRIX

### 4.3.1  Test Matrix for Strip Reinforcement

According to current MSE wall design practice as described in Chapter 2, the pullout resistance factor, F* for ribbed steel strip reinforcements is estimated based on Eq. 2.13a and 2.13b.  The relationship between F* and depth of fill for strip reinforcements is also shown graphically in Figure 2.7.   This relationship suggests that the pullout resistance factor, F*, for ribbed steel strip type reinforcement is primarily dependent on the depth of overburden. Overburden depths selected in the development of this test matrix represent typical thresholds for MSE pullout testing.  These test overburden depths were 5ft, 12ft, 20ft and 40ft. Most TxDOT walls range from 5ft to 25ft with an average height of approximately 15ft.   The test overburden depths of 5ft, 12ft and 20ft cover the above depth range.  It should also be pointed out that the 20ft test overburden depth was chosen primarily because,

according to published data, changes in F* data trends occur at this depth.  The 40ft test overburden depth was chosen to represent a reasonable ultimate wall height for TxDOT MSE walls.  The overburden depth was considered as a primary variable in all the test matrices described below.  In addition, the test matrix for strip reinforcement specifically focused on two other variables, embedment length and angle of skew.

### 4.3.1.1  Test Matrix for Strips: Effect of Embedment Length

Available guidance for laboratory pullout resistance testing of MSE reinforcement recommends a minimum embedded length of only 2.0ft (*1, 44*).  An assumption that is inherent in this recommendation is that the pullout resistance factor, F* is independent of the embedment length of the reinforcement, and this is reflected in the AASHTO formulation for pullout resistance.  In other words, the F* measured using a short length of reinforcement may be applied when estimating pullout resistance capacity of much longer reinforcements commonly used in the field.  The larger dimensions of the MSE test box used in this research allowed an opportunity to test the validity of this assumption.  Therefore, it was determined that the strip reinforcements will be tested for a range of embedment lengths.  When selecting the embedment lengths it was important to make sure that the maximum load was controlled by reinforcement pullout rather than reinforcement rupture.  The selection of embedment lengths for the test matrix is described below.

As a first step, the pullout loads corresponding to selected lengths and overburden pressures were estimated based on AASHTO F* equations (Eq. 2.13a and 2.13b).  These estimates represent the 95% lower bound confidence limit of available F* data.  Data presented in the previous chapter indicate that actual pullout resistance could be as much as six times greater than that predicted by the AASHTO equation.  Therefore, the embedment lengths to be used in testing were estimated based on F* values multiplied by three different coefficients, 6.0, 4.5, and 3.0, corresponding to what we termed 'short', 'average', and 'long' lengths, respectively.  The proposed embedment lengths were adjusted based on the initial pre-test F* values if such adjustment was found to be necessary.

Table 4.1 presents the embedment length test matrix for MSE strips. Accordingly, this test program explored the effects of two independent variables of interest, embedment length and overburden depth on the dependent variable, F*, for the range investigated. The

proposed test matrix for MSE strips produces twelve unique tests.  These tests were repeated

three times for a total of 36 strips tested.


**Table 4.1.** Test Matrix for MSE Strips

| Depth of Overburden (ft) | Embedment Length (ft) | | |
|---|---|---|---|
| | Short | Average | Long |
| 5 | 4.0 | 8.0 | 12.0 |
| 12 | 4.0 | 8.0 | 12.0 |
| 20 | 4.0 | 8.0 | 12.0 |
| 40 | 4.0 | 6.0 | 8.0 |


*4.3.1.2   Test Matrix for Strips: Effect of Skew Angle*

In addition to the strip reinforcement test program described above, tests were also

conducted with strips laid at selected horizontal skew angles.  As described in Chapter 2,

skew angles of up to 15-degrees are allowed in wall construction.  However, the effect of

skewing on the pullout resistance of the reinforcements has not been previously investigated

through systematic research.  Therefore, in this study, a portion of the pullout test program

was devoted to the study of effect of reinforcement skewing on the pullout resistance.  Two

skew angles, 15° and 30°, were selected.  The test matrix developed for this purpose is shown

in Table 4.2.


**Table 4.2.** Test Matrix for Skew Testing of MSE Strips

| Depth of Overburden (ft) | Angle of Skew, $\beta$ (deg) | | Embedment Length (ft) |
|---|---|---|---|
| 5 | 15 | 30 | 8.0 |
| 12 | 15 | 30 | 4.5 |


Figure 4.1 illustrates the layout of strip reinforcements for pullout testing of skewed

strip reinforcements.  As seen in this figure, two reinforcements were placed at the same

skew angle and pulled from a single connection point.   This helped to maintain symmetry

and avoid eccentric loading in the pullout assembly.  The total measured pullout force can be

divided in half to determine the pullout resistance of a single strip. The tests shown in Table 4.2 were repeated three times for a total of 24 strips tested in tandem.
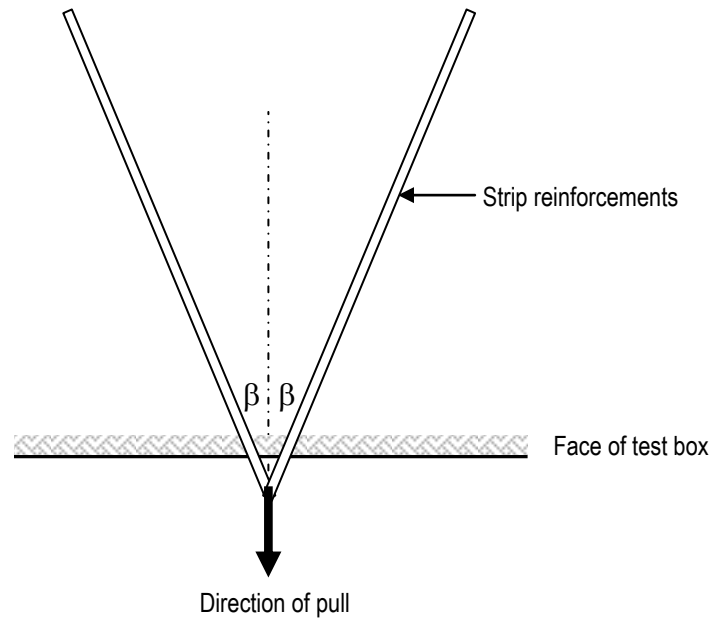


**Figure 4.1** Layout Used in the Pullout Testing of Skewed Strips

### 4.3.2 Text Matrix for Welded Grid Reinforcement

The current procedure for the estimation of pullout resistance factor, F* for grid reinforcement presupposes the following: (a) the primary mechanism that controls pullout resistance in grids is the passive (or bearing) resistance mobilized on transverse bars; in other words, any contribution from frictional resistance on longitudinal bars is negligible, (b) pullout resistance is directly proportional to the number of transverse bars embedded, (c) a single transverse bar subjected to pullout force behaves similarly to a loaded strip footing; therefore, the ultimate resistance mobilized is directly proportional to the diameter of the bar as predicted by classical bearing capacity theory. The findings from previous research studies support the above statements (*7, 9*). The pullout test program undertaken in this research was designed to check the validity of the above assumptions for backfill-reinforcement combinations used in TxDOT construction.

An assumption that is inherent in the existing theory is that the grid remains as a rigid body as it is being pulled through the soil backfill. However, there is reason to believe that significant deformation of the grid occurs when grids embedded in granular backfill are

subjected to pullout forces.  Therefore, parameters that control the rigidity of the welded grid, such as longitudinal and transverse bar sizes and spacings, may impact the pullout resistance of the grids in ways other than that predicted by bearing capacity theory.  For this reason, a second important objective in this test program was to investigate the potential impact that these variables may have on pullout resistance factor of grid reinforcement.

*4.3.2.1   Test Matrix for Grids:  Effect of Embedment Length*

It is generally believed that the pullout resistance of grids increases linearly with the number of transverse bars embedded in the backfill.  This is reflected in the AASHTO procedure for estimating F* for grid reinforcement.  For MSE grids, the embedment length is equal to the transverse bar spacing times the number of bars embedded.  Therefore, when AASHTO F* equations (*i.e.*, Eq. 2.14a and 2.14b) are used in conjunction with Eq. 2.9 to calculate the pullout resistance force $P_r$, the transverse bar spacing, $S_t$ terms cancels out and the number of embedded transverse bars becomes the only independent variable.  This phase of the test program was designed to validate this relationship.  The basic approach was to measure pullout capacity as a function of the number of transverse bars and the depth of backfill while all other variables are held constant.

Table 4.3 represents the test matrix used to investigate the influence of the embedment length.  Table 4.4 provides the test parameters that were held constant during this phase of testing.

**Table 4.3** Test Matrix for Grids: Embedment Length Effect

| Depth of Overburden (ft) | Embedment Length (ft) Transverse bar spacing at 12-in | | |
|---|---|---|---|
| 5 | 6.0 | 9.0 | 12.0 |
| 12 | 3.0 | 6.0 | 9.0 |

**Table 4.4**  Fixed Test Parameters for Embedment Length Testing

| Test Parameter | Fixed Value |
|---|---|
| Grid width, b (in) | 18.0[a] |
| Transverse bar size, t | W11[a] |
| Transverse bar spacing, $S_t$ (in) | 12[b] |
| Longitudinal bar size, d | W 20[c] |
| Longitudinal bar spacing, $S_l$ (in) | 9.0[a] |

Notes:  (a) Most commonly used parameter used in TxDOT construction.

(b) Typical range for $S_t$ is 6-24in. Mid-range value selected

(c) Largest, commercially available bar size selected to ensure test results will not be controlled by rupture capacity of the longitudinal bar.

The number of transverse bars in the backfill zone, which is an expression of embedment length, was selected based on AASHTO F* values with a factor of safety of 2.5. Accordingly, the embedment lengths in Table 4.3 are expected to provide an appropriate range of pullout resistance values without the pullout force being controlled by reinforcement rupture.

The embedment length matrix is a 2×3 matrix which produces six unique tests. Each of these tests was repeated three times for a total of 18 grids tested. This test program quantified the effects of the variables of interest on pullout resistance and allows the F* values to be back-calculated and calibrated according to the soil properties.

*4.3.2.2  Test Matrix for Grids:  Effect of Transverse Bar Size and Spacing*

The AASHTO equations for F* for grids are dependent on three variables: transverse bar size, transverse bar spacing and overburden  depth. The influence of these variables on the pullout resistance of typical TxDOT MSE grids in typical MSE backfill soil is at the core of this testing program. The influence of these three variables was evaluated using a three dimensional test matrix. The total grid width, longitudinal bar size and longitudinal bar spacing were kept constant in this portion of the test program. The test matrix to evaluate effects of transverse bar size, spacing and overburden depth is shown in Table 4.5. The test parameters that were held constant during this phase of testing are shown in Table 4.6.

**Table 4.5** Test Matrix for Grids: Effect of Transverse Bar Size/Spacing

| Depth of Fill (ft) | Transverse Bar Spacing (in) | | | | | | | | | | | | No. of Transverse Bars |
| --- | --- | --- | --- | --- | --- | --- | --- | --- | --- | --- | --- | --- | --- |
| | W7.5 | | | | W11 | | | | W15 | | | | |
| 5 | 6 | 12 | 18 | 24 | 6 | 12 | 18 | 24 | 6 | 12 | 18 | 24 | 6 |
| 12 | 6 | 12 | 18 | 24 | 6 | 12 | 18 | 24 | 6 | 12 | 18 | 24 | 6 |
| 20 | | 12 | 18 | 24 | | 12 | 18 | 24 | | 12 | 18 | 24 | 6 |
| 40 | | | 18 | 24 | | | 18 | 24 | | | 18 | 24 | 3 |

**Table 4.6** Fixed Test Parameters for Transverse Bar Size/Spacing Testing

| Test Parameter | Fixed Value |
| --- | --- |
| Grid width, b (in) | 18.0[a] |
| Longitudinal bar size, d | W20[b] |
| Longitudinal bar spacing, $S_l$ (in) | 9.0[a] |

Notes:  (a) Most commonly used parameter used in TxDOT construction.

(b) Largest, commercially available bar size selected to ensure test results will not be controlled by rupture capacity of the longitudinal bar.

Overburden depths selected in this matrix represent typical thresholds for MSE pullout testing and are consistent with the overburden depths discussed in previous test matrices.  The pullout tests were performed using three transverse bar sizes: W7.5, W11 and W15.  Although the typical transverse bar size for TxDOT MSE grids is W11, variation in bar size is necessary to directly evaluate the $t/S_t$ ratio specific to the F* parameter.  The transverse bar spacing for each transverse bar size varied from 6 inches to 24 inches in 6-inch increments. These transverse bar spacings cover the range of values typical for TxDOT MSE grids. The narrower spacings at deeper fills were not tested because such tight spacing is never used at extreme depths.  When the predicted pullout resistance for the MSE grid was *less than* rupture capacity of the grid, six transverse bars were used in the backfill in an effort to maximize the number of transverse bars in the fill for each test.  Fewer transverse bars were used under 20 feet and 40 feet of fill because these larger overburden pressures increase the pullout resistance.

The pullout resistance factor matrix for MSE grids is a 4x4x3 matrix which produces

39 unique tests, two of which (W11 at 12-inch spacing for 5 feet and 12 feet of overburden) were addressed in the previous sub-matrix. Each of these tests was repeated three times for a total of 111 grids tested. The one extra test was done in an unused slot available within the previous sub-matrix.

### 4.3.2.3 *Test Matrix for Grids: Effect of Longitudinal Bar Size and Spacing*

According to AASHTO equations, the pullout resistance factor, F* for grids is independent of the longitudinal bar size and spacing in the grid. This is consistent with a reinforcement-backfill interaction model in which the welded steel grid remains as a rigid inclusion within the backfill as it is being subjected to pullout forces. In this model, the transverse bars will not undergo any deformation (*i.e.* bending) as they bear against soil backfill to produce pullout resistance. However, when welded steel grids are embedded in properly compacted coarse granular MSE backfill, it is envisioned that the grid does undergo some deformation. Furthermore, it is reasonable to expect that the amount of deformation will be determined by the overall rigidity of the grid. Since the transverse and longitudinal bars in MSE grids are welded together, some portion of the bending moment will be transferred from the transverse bars into the longitudinal bars. Therefore, assuming the welds provide a rigid connection, large longitudinal bars allow less transverse bar deformation than smaller diameter bars. Similarly, closer spacing between longitudinal bars will allow less transverse bar deformation. These effects must be considered. Accordingly, a part of the lab test program conducted in this research was devoted to exploration of the effect of longitudinal bar size and spacing on F*.

Table 4.7 shows the test matrix used to explore the influence of longitudinal bar size and longitudinal bar spacing on the pullout resistance factor, F*. The number of longitudinal bars, transverse bar size and transverse bar spacing were maintained constant during this phase of testing. Table 4.8 provides the test parameters that were held constant.

**Table 4.7** Test Matrix for Grids: Effect of Longitudinal Bar Size/Spacing

| Depth of Fill (ft) | Longitudinal Bar Size | | | | | | | | | |
| --- | --- | --- | --- | --- | --- | --- | --- | --- | --- | --- |
| | W 9.5 | | | | | W 20 | | | | |
| | Longitudinal Bar Spacing (in) | | | | $L_e$ (ft) | Longitudinal Bar Spacing (in) | | | | $L_e$ (ft) |
| 5 | 2 | 6 | 9 | 12 | 6 | 2 | 6 | 9 | 12 | 6 |
| 12 | 2 | 6 | 9 | 12 | 3 | 2 | 6 | 9 | 12 | 6 |
| 20 | | | | | | 2 | 6 | 9 | 12 | 6 |
| 40 | | | | | | 2 | 6 | 9 | 12 | 3 |

**Table 4.8** Fixed Test Parameters for Longitudinal Bar Size/Spacing Testing

| Test Parameter | Fixed Value |
| --- | --- |
| No. of Longitudinal Bars | 3[a] |
| Transverse bar size, t | W11[a] |
| Transverse bar spacing, $S_t$ (in) | 12.0[a] |

Note:   (a) Most commonly used parameter used in TxDOT construction.

Overburden depths selected in this matrix represent typical thresholds for MSE pullout testing and are consistent with the overburden depths discussed in previous test matrices. Two longitudinal bar sizes were used.  W9.5 is a very common longitudinal bar size for shallower overburden depths.  W20 is a typical longitudinal bar size for deeper overburden depths and is the maximum bar size available.  Four different longitudinal bar spacings were used in the test matrix.  They included the two longitudinal bar spacings most commonly used by TxDOT, *i.e.* 6 inches and 9 inches.  Also selected were 2 inches as a minimum spacing and 12 inches as a maximum spacing.  The number of transverse bars in the backfill (embedment length) was varied with depth to avoid rupture of the longitudinal bars.

The longitudinal bar size and spacing test matrix was a 4x2x4 matrix which produced 24 unique tests, three of which (W20 longitudinal bars at 9-inch bar spacing for three overburden depths) were addressed in the previous test matrix.  Each of these tests was repeated three times for a total of 63 grids tested.

*4.3.2.4   Test Matrix for Grids:  Effect of Cut and Splay*

The next phase of the pullout test program explored the influence of cutting and horizontal splaying of grid reinforcement on pullout resistance.  Similar to the lab test program involving skewed strips, splay angles of 15 and 30-degrees were selected for testing.   Table 4.9 represents the test matrix for cut and splay testing while Table 4.10 provides a list of variables held constant during this phase of testing.

**Table 4.9**  Test Matrix for Cut and Splay Testing of MSE Grids

| Depth of Overburden (ft) | Angle of Splay (deg) | | Length, $L_e$ (ft) |
|---|---|---|---|
| 5 | 15 | 30 | 6.0 |
| 12 | 15 | 30 | 6.0 |

**Table 4.10**  Fixed Test Parameters for Cut and Splay Testing

| Test Parameter | Fixed Value |
|---|---|
| Grid width, b (in) | 18.0[a] |
| Transverse bar size, t | W11[a] |
| Transverse bar spacing, $S_t$ (in) | 12[b] |
| Longitudinal bar size, d | W 20[c] |
| Longitudinal bar spacing, $S_l$ (in) | 9.0[a] |

Notes:  (a) Most commonly used parameter used in TxDOT construction.

(b) Typical range for $S_t$ is 6-24in. Mid-range value selected

(c) Largest, commercially available bar size selected to ensure test results will not be controlled by rupture capacity of the longitudinal bar.

The cut and splay test matrix produces four unique tests.  Each of these tests was repeated three times for a total of 18 grids tested.  It should be noted that tests on cut and splayed grids require more space in the MSE test box than straight pullout tests.  This testing provided additional insight into the effects of the cutting and splaying MSE grids on pullout resistance for MSE grids.

### 4.3.3 Test Matrix for Grids: Smooth Straight Bars

The longitudinal bars in welded steel grids can contribute to the pullout resistance of the grid in two possible ways. One of these was discussed in Sec. 4.3.2.3. This involved the contribution of the longitudinal bar to the overall stiffness of the grid and more specifically to the flexural rigidity of the transverse bar. The other involves the frictional resistance that can develop on the surface of the longitudinal bar during pulling. This effect is generally disregarded as frictional resistance is considered to be very small when compared with pullout resistance generated through bearing action. Nevertheless, a limited number of pullout tests were conducted to evaluate this effect. In these tests, the pullout resistance was measured on longitudinal bars that had no transverse bars attached to them. Table 4.11 shows the test matrix used in the evaluation of smooth straight bars. The variables considered were depth of overburden, longitudinal bar size, and length of embedment. The embedment lengths were selected to match with MSE grids tested in previous sub-matrices. It was hoped that this would allow the contributions from frictional and bearing mechanisms to be differentiated from each other.

**Table 4.11** Test Matrix for Pullout Resistance Testing of Single Longitudinal Bars

| Depth of Overburden (ft) | Longitudinal Bar Size | |
|---|---|---|
| | W9.5 | W20 |
| | Embedment length, $L_e$ (ft) | |
| 5 | 6 | 6 |
| 12 | 3 | 6 |
| 20 | | 6 |
| 40 | | 3 |

The longitudinal bar test matrix produced six unique tests. Each of these tests was repeated three times for a total of 18 bars tested.

### 4.3.4 Test Matrix for Strain Gaged Reinforcements

In addition to the pullout test matrices described in Sections 4.3.1 and 4.3.2, the laboratory test program for this research also included a series of pullout load tests on MSE reinforcements that were instrumented with strain gages. The objective of these tests was to

develop better understanding of mechanisms that control development of pullout resistance in MSE reinforcement.

The test matrix developed for strain gaged reinforcements included a total of 16 pullout tests on ribbed strips and 12 tests on welded steel grids. The 16 strip reinforcements consisted of eight 8-ft long strips and eight 12-ft long strips. The test series on welded steel grids included eight tests on 6-ft long grids and four tests on 3-ft long grids.

The test matrix described in Sec. 4.3 represents the overall program for pullout testing conducted in one type of backfill, *i.e.*, Type B. The entire test program was repeated for the second type of MSE backfill, Type A.

## 4.4 MATERIAL CHARACTERIZATION AND QUALITY CONTROL

This section describes procedures used for material characterization and quality control and the results obtained. It is divided into two separate sections. Section 4.4.1 deals with backfill material characterization while Section 4.4.2 deals with the characterization and quality control testing of MSE reinforcements.

### 4.4.1 Backfill Materials

As mentioned in Sec 4.2.1, it was determined that two types of TxDOT MSE backfill – Type A and Type B – would be included in this test program. It was further determined that the material selected for testing would represent the finer limits of the specifications for each backfill type. The shaded zones shown in Figure 4.2 represent the target gradation bands established based on the above requirements.
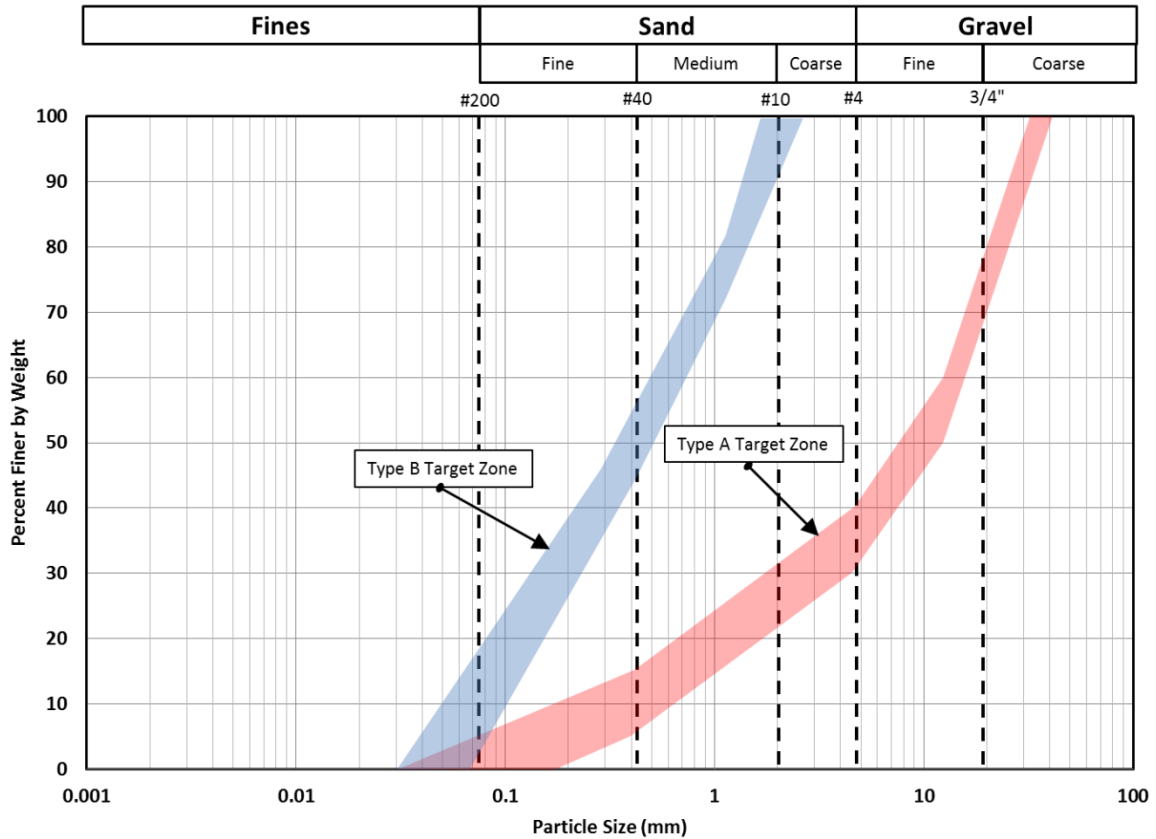
**Figure 4.2** Target Gradation Bands for Type A and Type B Backfill

Material samples were obtained from several local suppliers and particle size distribution tests were conducted to check that they met the applicable gradation requirements. Another important consideration in material selection was the durability and the soundness of the aggregate particles. Hard and durable materials were preferred because such material minimizes the need for periodic replenishment due to material breakdown that occurs during repeated handling. Soil samples were selected primarily based on gradation and soundness criteria. The selected materials were then subjected to a series of other characterization tests including resistivity, pH, moisture-density relationship, Atterberg Limits, and shear strength.

Results obtained from gradation tests conducted on Type B and Type A materials are summarized in Tables A-1 and A-2 respectively in Appendix A. This backfill gradation data is also shown in Figure 4.3. As seen in this figure, the actual gradation of the Type B backfill did not completely fit within the target gradation band that was established in

advance.  Further, this material failed to meet TxDOT Type B gradation requirement for percent passing No.40 sieve (*i.e.* 60 max).   However, after evaluation of seven different locally available natural material sources, this particular material was selected as the best based on following additional project requirements: (a) material should be natural and not a product of artificial blending, (b)  material should be readily available in sufficient quantity so that it could be replenished promptly if such need arises, (c) material should not undergo significant degradation due to repeated use, (d) material should meet resistivity and pH criteria for MSE backfill.  As seen in Figure 4.3, the material maintained its original gradation quite well.

Compliance with the previously established gradation band proved to be an even bigger challenge for  Type A material.  This material required more frequent monitoring to ensure that its gradation remained within specified limits.  Because of the particle composition (*i.e.* crushed limestone) and the larger particle sizes it contained, this material was more susceptible to degradation than the Type B material.  Type A material was replenished two times (*i.e.* a total of three separate batches) during the test program.

In addition to the gradation tests that were conducted at regular intervals throughout the test program, each material was characterized to determine other relevant physical properties such as Atterberg limits, bar linear shrinkage, moisture-density relationship and shear strength,  and electrochemical properties including resistivity and pH.  These tests were performed only one time for each material.  The test standards used and the results obtained are summarized in Table 4.12.
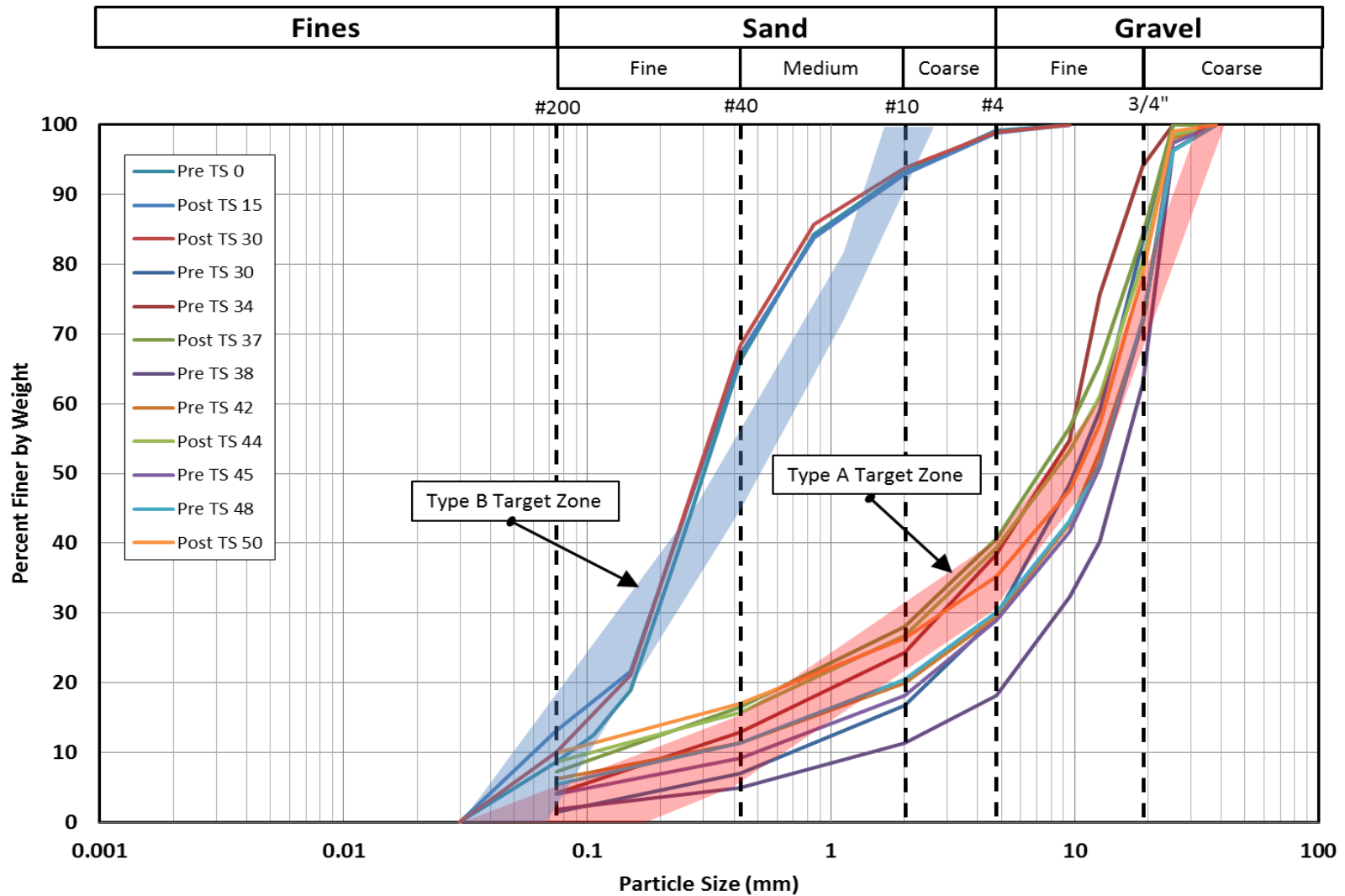
**Figure 4.3** Results from Particle Size Analyses Conducted on Type A and Type B Backfill

**Table 4.12** Physical and Electrochemical Properties of Type A and Type B Backfill

| Test Procedure Description and Standard | Property | TYPE A | TYPE B |
|---|---|---|---|
| Atterberg Limits (Tex-104-E, Tex-105-E, and Tex-106-E) | Liquid Limit (%) | 23 | Non-plastic |
| | Plastic Limit (%) | 20 | Non-plastic |
| | Plasticity Index (%) | 3 | Non-plastic |
| Bar Linear Shrinkage Test (Tex-107-E) | Bar Linear Shrinkage Value (%) | 3 | 2 |
| USCS Classification (ASTM D 2487) | USCS Classification | GW/GP/GP-GM | SP-SM |
| Particle Size Analysis of Soils (Tex-110-E) | Coefficient of Uniformity, $C_u$ | 12.0-180.0 | 4.4 – 7.0 |
| Moisture Density (Tex-114-E) | Optimum moisture content (%) | 6.6 | 7.8 |
| | Maximum Dry Density (pcf) | 122.5 | 124.5 |
| Direct Shear Test (ASTM D3080, ASTM D5321) | Cohesion (psf) | 0-181 | 112 |
| | Angle of Friction (deg) | 51-53 | 39-43 |
| Resistivity (Tex-129-E) | Resistivity (ohm-cm) | 6670 | 8004 |
| Soil pH (Tex-128-E) | pH | 7.6 | 7.9 |

### 4.4.2 MSE Reinforcements

*4.4.2.1 Ribbed Strip Reinforcement*

Two types of MSE reinforcements were included in the pullout testing conducted in this research – ribbed steel strips and welded steel grids. Figure 4.3 shows a schematic of strip type reinforcement as tested. These galvanized steel strips were delivered to Texas Tech University in four separate batches, all in lengths of 14ft. Prior to testing these strips were cut to obtain test specimens of specified lengths as needed for the research study.
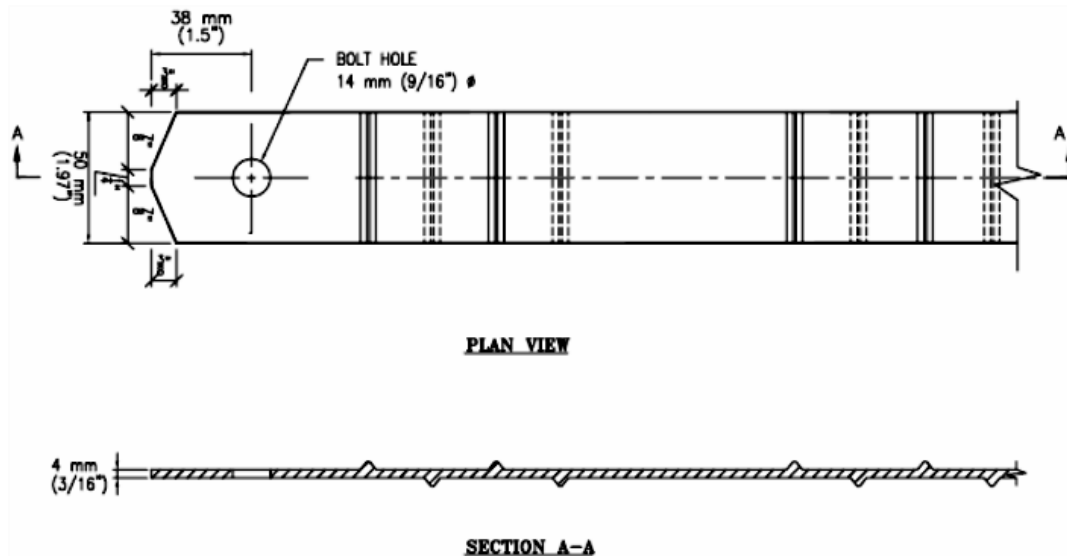


**Figure 4.4** Schematic of Ribbed Steel Strip Reinforcement as Tested (*45*)

The material quality control data for ribbed strip reinforcement used in this research were obtained from the certified mill reports provided by the supplier. The information available in the certified mill reports included yield strength (ksi), tensile strength (ksi), percent elongation, and material composition. The strength and elongation data corresponding to each batch of ribbed strip reinforcement received are found in Table B-1, Appendix B of this report.

### 4.4.2.2   Welded Steel Grid Reinforcement

The welded wire grid reinforcements used in this research were specially fabricated according to specifications provided by Texas Tech researchers.  After fabrication, the grids were galvanized and then transported to the Texas Tech University MSE testing facility.  A schematic of a typical welded grid reinforcement is shown in Figure 4.5.  In grids manufactured and used in field construction, the transverse bars typically extend 1.0in to 1.5in beyond the width of the outer longitudinal bar of the grids as shown in Fig. 4.5.  These overhangs, commonly called "tangs," are an artifact of the manufacturing process and do not meet specific length requirements.   Moreover, tangs are not considered as part of the width of the grid when calculating its pullout load capacity.   For these reasons, in grids used in this research study, the tangs were removed prior to testing by sawing them off.
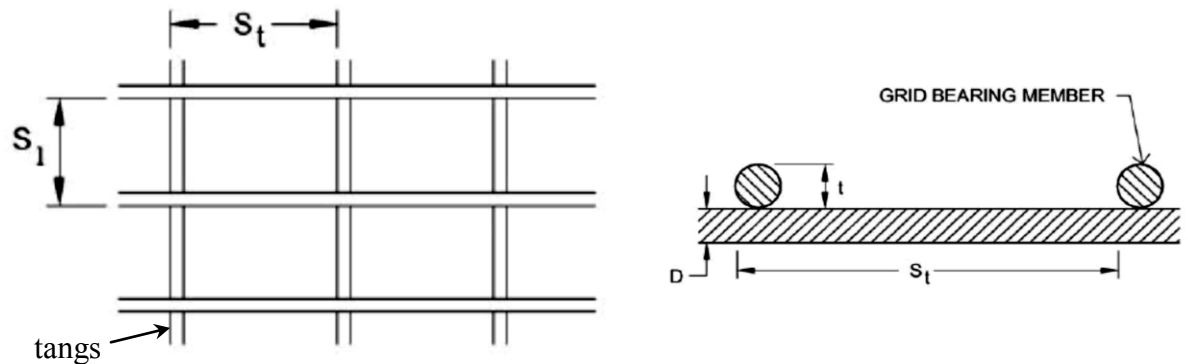


**Figure 4.5**  Schematic of Welded Grid Reinforcement

The welded steel grids used in this test program were received in three separate batches.  The material quality control data for these grids were obtained from the certified mill reports provided by the supplier.  The information available in the certified mill reports included diameter, area, percent reduction of area, breaking strength (ksi), yield strength (ksi), tensile strength (ksi), and weld shear strength for both longitudinal and transverse wires.  The data corresponding to each batch of grid reinforcement received are summarized in Table B-2, Appendix B of this report.

# CHAPTER 5
## PULLOUT RESISTANCE TEST SYSTEM AND TEST PROCEDURE

## 5.1 OVERVIEW

One of the unique features in this research study is the large scale test system that was specially developed for the purpose of pullout testing of MSE reinforcements. Such large scale testing was necessary for two reasons. First, there was a need to simulate alternative reinforcement layouts used in the field to avoid vertical obstructions (*e.g.*, skewed and cut-and-splayed configurations). Second, it was necessary to conduct a large volume of pullout testing within the limited time duration of the project. This chapter describes the test equipment, test procedures and data acquisition and processing methods used for the study. Section 5.2 provides a description of various components of the large scale test system. The next section, Section 5.3, documents the pullout test procedure including test setup preparation, application of overburden pressure, and application of pullout load. Section 5.4 provides a detailed account of the data processing methods used. Section 5.5 presents the steps undertaken during pullout testing of instrumented MSE reinforcements. The last section, Section 5.6, documents general observations made during pullout testing.

## 5.2 PULLOUT RESISTANCE TEST SYSTEM

MSE pullout tests for this study were performed using the large-scale pullout resistance test system erected in the Structures Laboratory of the Department of Civil Engineering at Texas Tech University. The overall dimensions of the MSE test box are 12ft by 12ft in plan area and 4ft in depth. Three of the test box walls were fixed. These walls were constructed by welding steel plates to wide flange stiffening beams. These walls were erected by first bolting six columns (three columns on the east side and three on the west) to the reaction floor in the Texas Tech Civil Engineering Structures Laboratory and then attaching the wall panels to the columns. The fourth wall consisted of hollow structural steel (HSS) sections connected to the box through rigid hinges. This wall, which was removable, was also referred to as the tailgate. Figure 5.1 shows the test box during assembly of the three fixed walls.
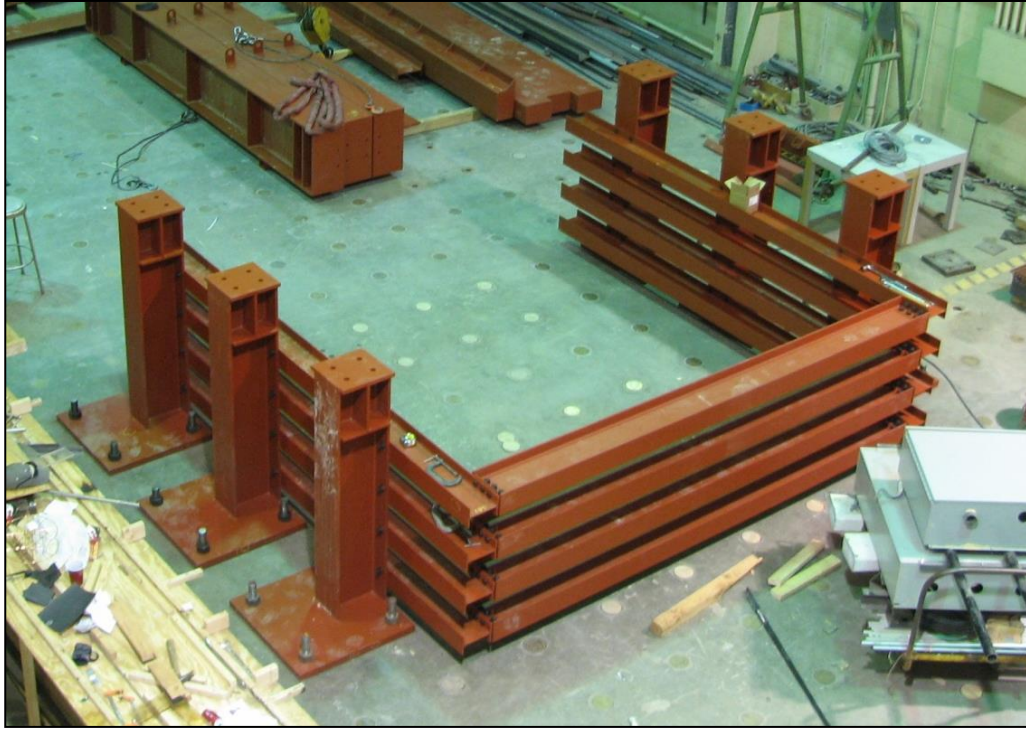
**Figure 5.1** MSE Test Box During Assembly Showing East, West and South Walls

To allow pullout of reinforcements embedded in the box, test slots were cut in the wall plates on the south and east walls. The south wall had 9ft long slots cut at three different heights: 1ft, 2ft and 3ft from the base. The east wall had two 3ft slots at the same three heights providing a total of six test slots. Accordingly, reinforcements could be placed in the MSE test box at three different levels and pulled to the south through slots cut in the south wall (primary test bulkhead) or to the east (secondary test bulkhead), allowing for optimum test space utilization.

In this test system, the soil overburden pressures applied to the embedded earth reinforcement were simulated using a reaction frame assembly which consisted of nine 4ft by 4ft pressure plates that were hydraulically jacked against three wide flange cross beams. This reaction frame assembly was designed to accommodate simulation of overburden pressures up to 40ft of fill. Vertical overburden pressure was monitored throughout the test using five earth pressure cells that were grouted into the bottom slab of the MSE Test Box. A second, independent measurement of the applied overburden was made using a pressure transducer that monitors the fluid pressure in the hydraulic jacks. Figures 5.2 and 5.3 provide isometric views of the pressure plates used to apply additional overburden pressure
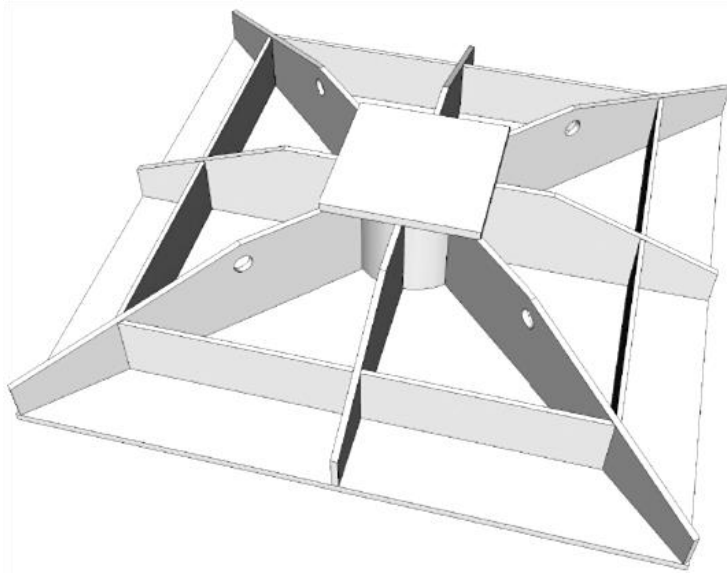
**Figure 5.2**  Isometric View of Pressure Plate
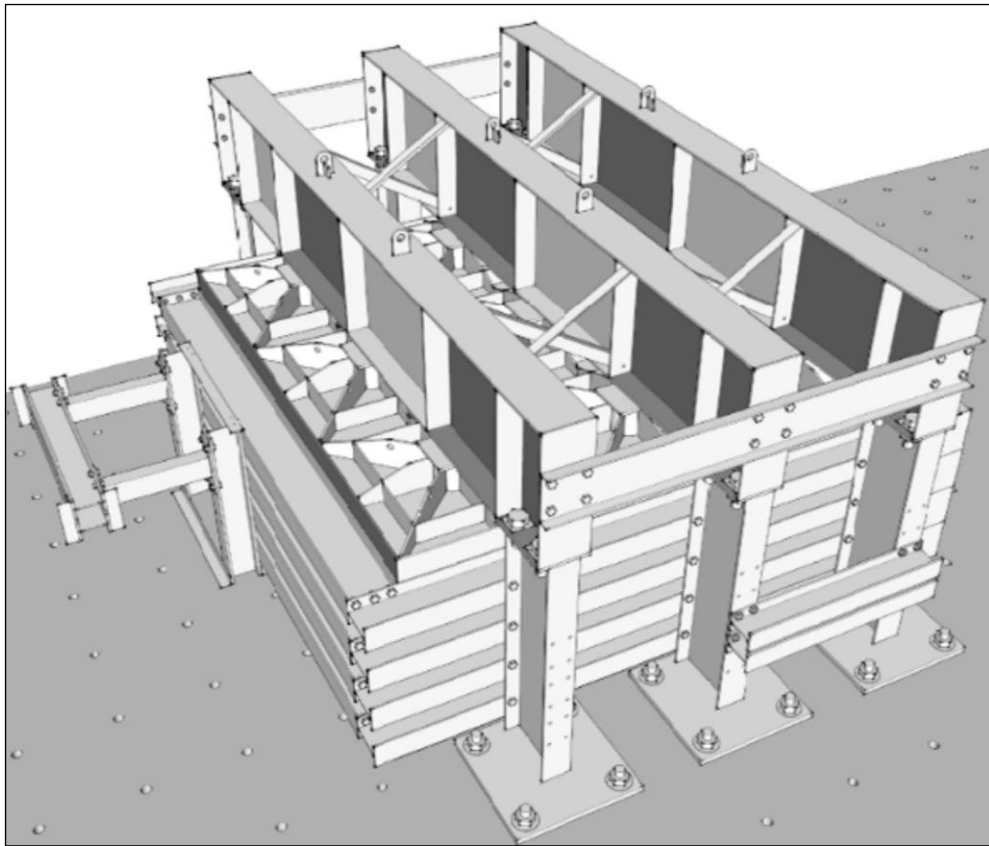


**Figure 5.3**  Fully Assembled Pullout Resistance Test System

and the entire pullout resistance test system after it had been fully assembled.  Figures 5.4 and 5.5 show cross sections through the test system in north-south and east-west directions, respectively.

The pulling system consisted of a reaction frame braced against the south wall, a cross beam between the columns on the east wall and a friction gripper for welded steel grids. As mentioned previously, the MSE test box had the capability to accommodate up to three layers of earth reinforcement in a single filling of the test box with reinforcement layers placed at heights of 1.0ft, 2.0ft and 3.0ft from the base.  The two pulling assemblies could be set to pull at each of the three elevations.

A material storage bin with a 40 cubic yard capacity was constructed on the north end of the pullout resistance test system and used for the purpose of storing backfill material when not in use.  Transferring the backfill material between the storage area and the MSE test box during filling and emptying of the box was accomplished using a skid steer loader. A 10-ton overhead crane was available in the TTU Structures Laboratory for use during test box assembly and disassembly.

Figure 5.6 shows transfer of backfill material from storage bin to the test box using the skid steer loader during filling of the test box.

Pullout testing of each embedded earth reinforcement was accomplished, one at a time, by attaching a pullout load assembly to the reinforcement and then applying the pullout force using a 60-ton hollow core hydraulic jack. MSE strip reinforcements were connected to the pull rod using a simple pin mechanism. Two independent systems were used to measure and record the pullout force. The first was an annular load cell mounted on the pull rod. The second was a pressure transducer that measures hydraulic pressure in the hollow-core jack. Figure 5.7 shows the load cell and hollow core jack.
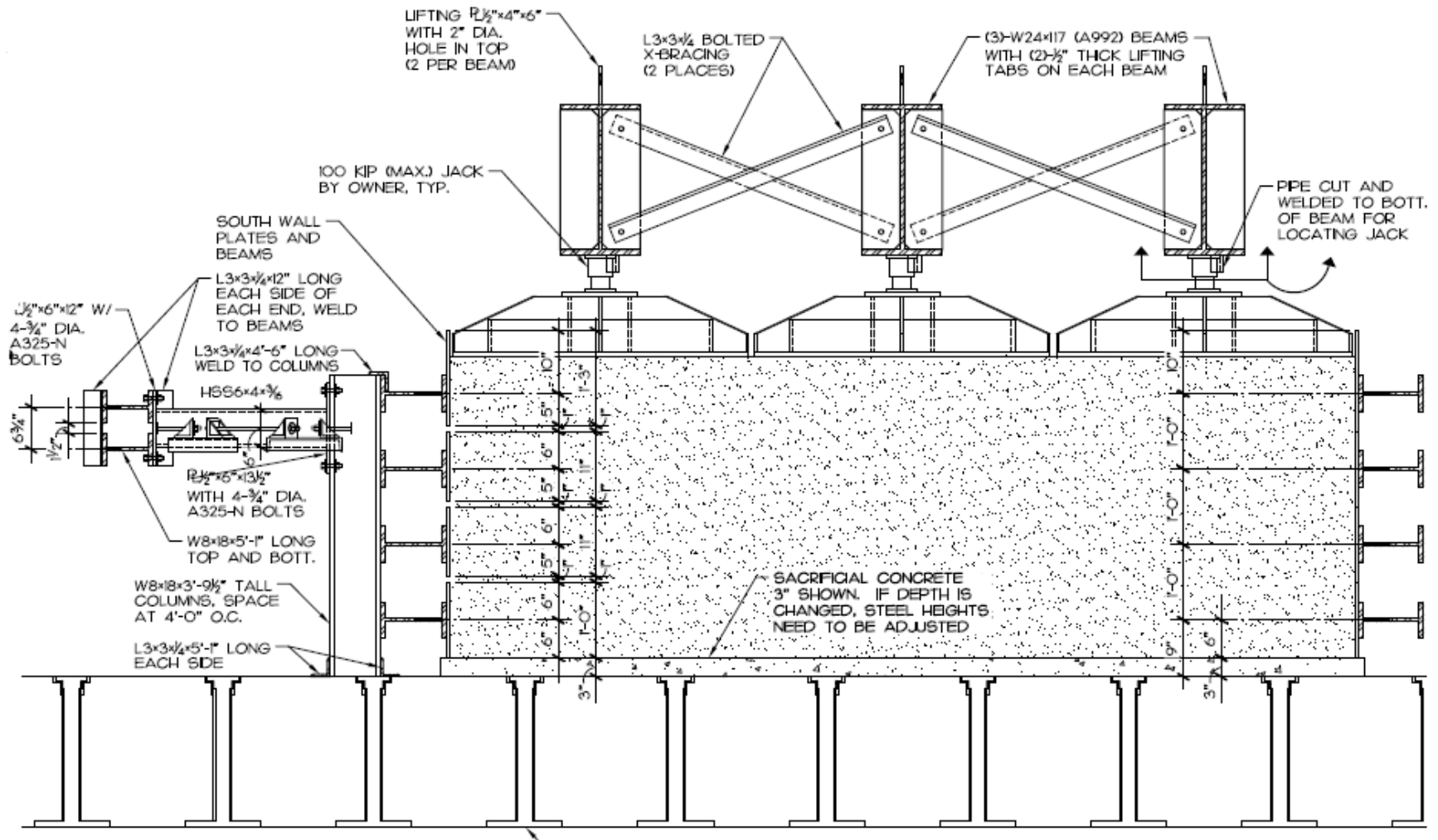
**Figure 5.4** Cross-Sectional View of the Pullout Resistance Test System; North-South Section

**Figure 5.5** Cross-Sectional View of the Pullout Resistance Test System; East-West Section

**Figure 5.6** Skid Steer Loader in Operation during Filling of the Test Box
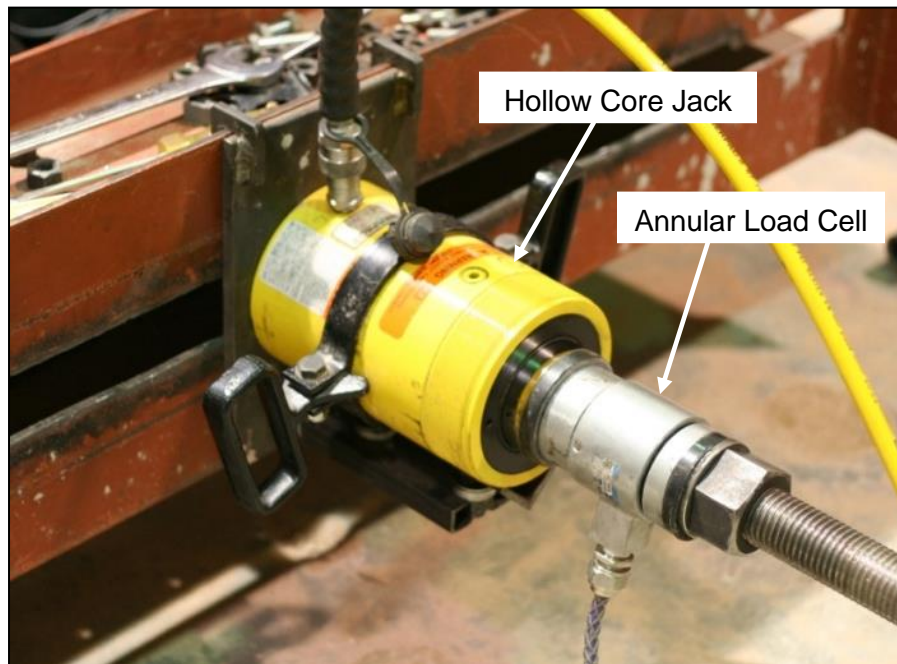


**Figure 5.7** Hollow-Core Jack and Annular Load Cell

Similarly, the displacement of the reinforcement during pullout testing was determined using two independent measurements. The first was an optical measurement of the displacement using a witness marker against a graduated scale. The second measurement system used to record displacement was an electronic displacement gage. To enhance reading accuracy of the optical displacement measurement, a webcam was mounted on the wall of the test box directly over the witness marker. Figure 5.8 shows the witness marker-webcam system used to record optical displacement measurement, while Figure 5.9 shows the digital displacement gage.
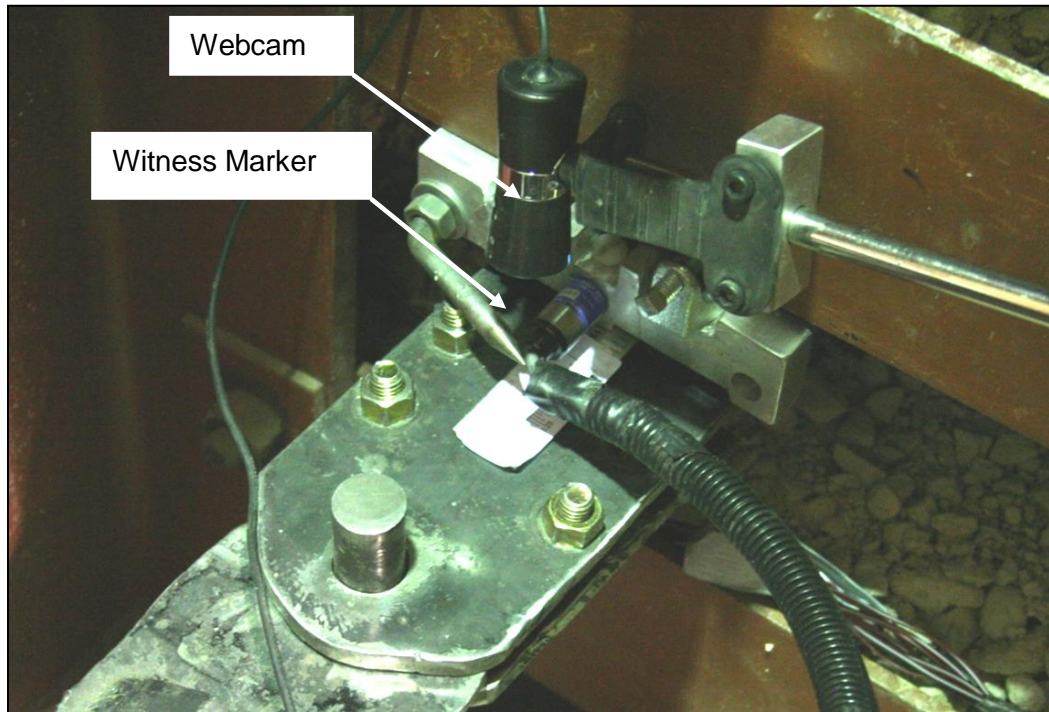


**Figure 5.8** Witness Marker-Webcam System Used to Record Optical Displacement Measurement
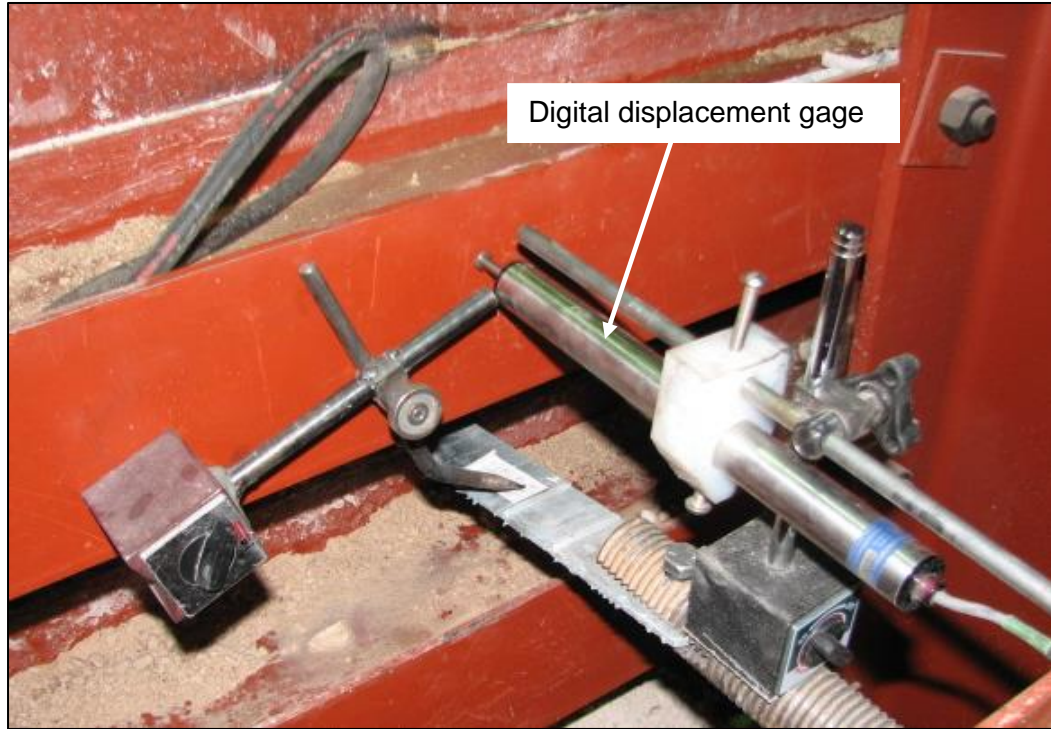
**Figure 5.9** Digital Displacement Gage

## 5.3   PULLOUT RESISTANCE TEST PROCEDURE

This section describes the procedure used during pullout testing of MSE reinforcement. The test procedure was divided into three separate stages: (a) preparation of the test setup, (b) application of the overburden pressure, and (c) application of the pullout load.

### 5.3.1   Preparation of the Test Setup

Test setup preparation involved filling the test box with the backfill and compacting the backfill material to achieve desired density while embedding the MSE reinforcements at appropriate depths within the compacted backfill.  As mentioned previously, the MSE test box was designed with fixed permanent walls on three sides (east, west and south sides) and a removable wall on the north side to allow access for filling the box.  During preparation of a test setup, the north wall was raised in 1-ft lifts as backfill was placed inside the box. Before any backfill was placed in the test box, five Geokon Model 4810 contact earth

pressure cells were affixed to the bottom slab of the test box using cement grout. Figure 5.10 shows the earth pressure cells being placed.



**Figure 5.10**  Mounting Earth Pressure Cells on the Bottom Slab of Test Box

Then the earth pressure cells were covered with Type B backfill (*i.e.*, sandy backfill). The backfill material was placed in the MSE Test Box in lifts of loose fill with approximate thickness of 4-in. Each lift of material was compacted with non-overlapping passes of a vibratory compactor to achieve a compacted thickness of about 3-in. The bottom 6-in of the compacted backfill protecting the earth pressure cells were left undisturbed throughout the duration of the testing program. A different compaction protocol was used for each type of backfill to achieve the final compacted condition. According to TxDOT *Standard Specifications* Item 423, density control approach was used for Type B backfill material. Accordingly, the maximum dry unit weight of the material was determined using Tex-114-E and then the backfill was compacted to achieve a minimum relative compaction of 95%. The compaction moisture content was maintained within 2-3% of the optimum water content during compaction. It was observed that approximately seven passes of the vibratory compactor was needed to reach the desired density. The final compacted density and moisture content was measured using a nuclear density gage. Figure 5.11 shows the

compaction of the backfill in the test box while Figure 5.12 shows the measurement of compacted density using the nuclear density gage.



**Figure 5.11**  Compaction of the Backfill in Test Box



**Figure 5.12**  Measurement of Compacted Density Using the Nuclear Density Gage

Because of the coarse granular nature of Type A backfill, this material was compacted using the ordinary compaction approach. The lift thickness and the compaction procedures used for this material were the same as those used for Type B backfill. Per the ordinary compaction specification, Type A backfill material was compacted until there was no evidence of further volume reduction.

MSE reinforcements were embedded within the backfill at three levels located at heights of 1ft, 2ft and 3ft from the base slab. Each test layer contained no more than four grids placed at equal spacing and with transverse bars facing down. The grids were prepared with an extra 22 inches of longitudinal bar and one extra transverse bar (the zero transverse bar) placed flush with the exterior face of the box. The strips were placed with one foot of extra length outside the box. Wooden shims were inserted between the reinforcement and test slot perimeter as needed to ensure that no steel-on-steel contact occurred between the MSE reinforcement and wall plates. Figure 5.13 depicts a test layer that consisted of both strips and grids. Figure 5.14 shows strip reinforcements placed at skew angles of 15 and 30-deg, while Figure 5.15 shows grid reinforcement laid in the cut and splay configuration.
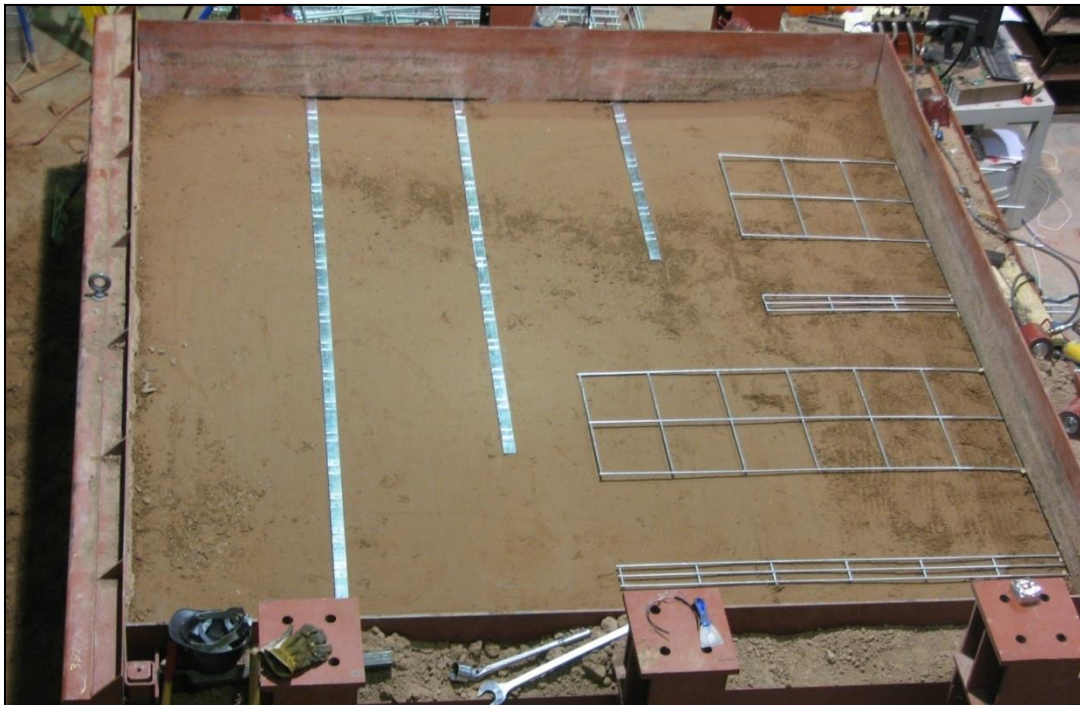


**Figure 5.13** Test Layer with both Strip and Grid Reinforcement
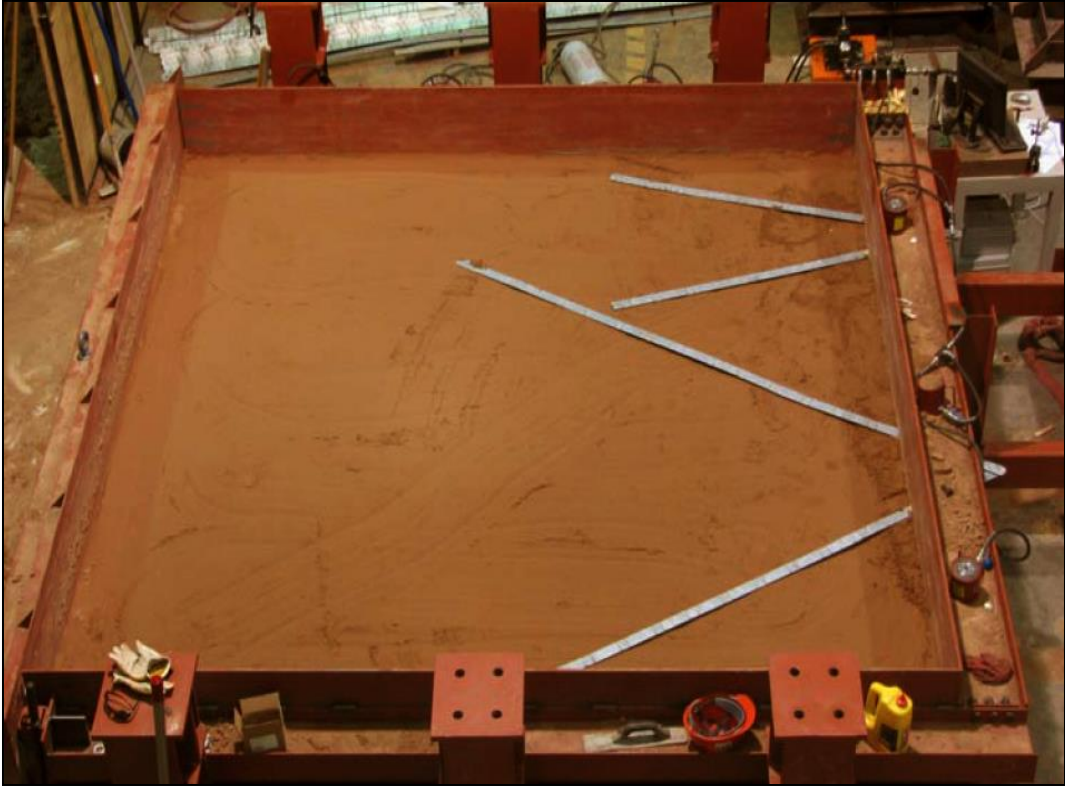
**Figure 5.14** Test Layer with Skewed Strips within the Test Box
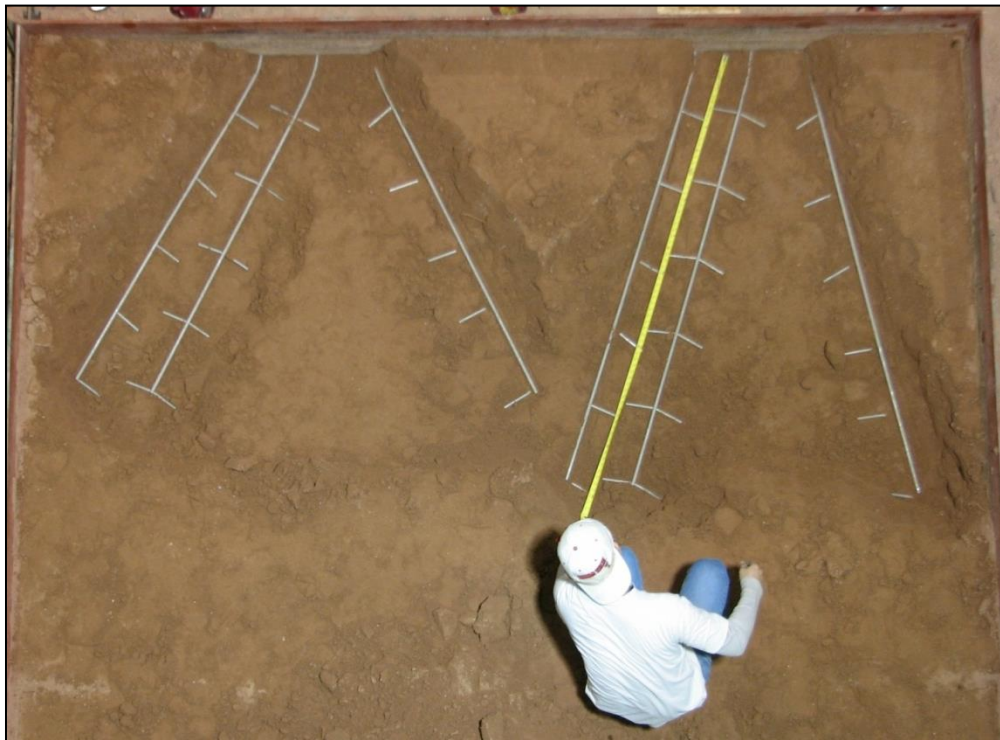


**Figure 5.15** Grid Reinforcement Being Laid in Cut-and-Splay Arrangement

Once the compacted fill was within 3-in of the final fill height, one final lift of backfill material was added. This soil was placed and carefully graded to achieve a level surface as shown in Figure 5.16. The final lift of backfill material was not compacted because its primary purpose was to provide proper seating for the pressure plates, which were placed on top of this layer.

## 5.3.2  Application of the Vertical Overburden Pressure

The large-scale MSE pullout resistance test system is designed such that nine 4ft x 4ft stiffened steel plates are placed on top of the backfill covering the entire surface area of the MSE test box. Then, the three W24x117 wide flange reaction beams are positioned over the pressure plates and the beams bolted to support columns on either side of the test box. Each reaction beam spans over three pressure plates. Hydraulic jacks are placed between the pressure plates and the reaction beams. The hydraulic jacks are then pressurized causing the jacks to apply downward pressure on the soil by pushing against the reaction beams.



**Figure 5.16** Grading the Final Loose Lift of Backfill within the Test Box

The hydraulic jacks are connected to a main hydraulic pump via a manifold so that all nine jacks are pressurized equally and simultaneously. Figure 5.17 shows the pressure plates and hydraulic jacks in place and ready to apply overburden pressure.

It should be noted that the target overburden pressure used to test each MSE reinforcement in a given test setup typically varied from one reinforcement to another. Therefore, it was necessary to adjust the jack pressure before each pullout test to achieve the correct overburden pressure for that specific test. An appropriate allowance to account for the geostatic stress due to weight of the overlying backfill soil was made when calculating the jack-applied pressure.
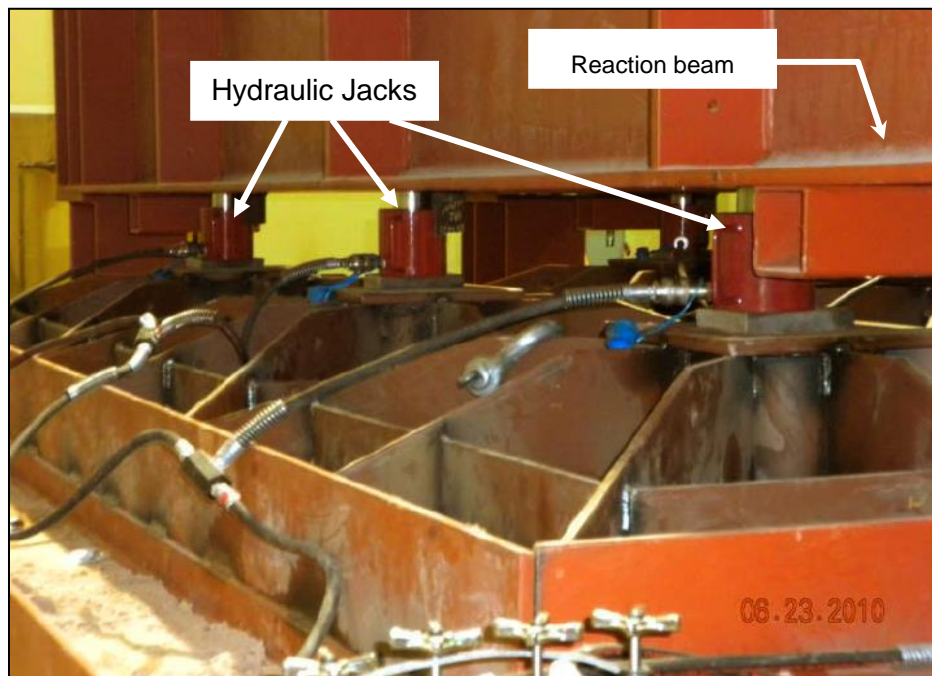


**Figure 5.17** Pressure Plates and Hydraulic Jacks Used to Apply Overburden Pressure

### 5.3.3 Pullout Testing of Embedded MSE Reinforcement

As noted previously, in a typical test setup, the "test overburden stresses" for different MSE reinforcements embedded within that setup would vary from one reinforcement to another. Therefore, it was possible for a given reinforcement to experience an overburden stress larger than its "test overburden stress" prior to being tested. In early stages of testing, the pullout test sequence was designed to achieve maximum efficiency and therefore, the incidence of such over stress was fairly high. However, once the influence of over-stress on

the pullout load capacity was recognized, steps were taken to improve the testing procedure. The improvements implemented were twofold. First, appropriate statistical analyses were conducted so that final predictive models for the pullout resistance factors would be free from undue influence due to over-stress effect existing in early test data. Secondly, the testing sequence used in all subsequent testing was reorganized to ensure that reinforcements would be pulled from the lowest to the highest test overburden stress.

The pullout load on the embedded reinforcements was applied by a hollow core jack that applies tension force to the MSE reinforcement by pushing against a stationary bearing surface, or bulkhead, attached to the MSE test box. Two different pullout load assemblies were used: one for applying pullout loads from the south wall face and the other for applying pullout loads from the east face. Figure 5.18 shows the pullout assembly reaction frame used on the south wall. Due to the large size and weight of this reaction frame, its handling required the use of the overhead crane. This reaction frame and pullout assembly were used for all grid reinforcement tests while a different, smaller unit was used for testing strips through the east face.
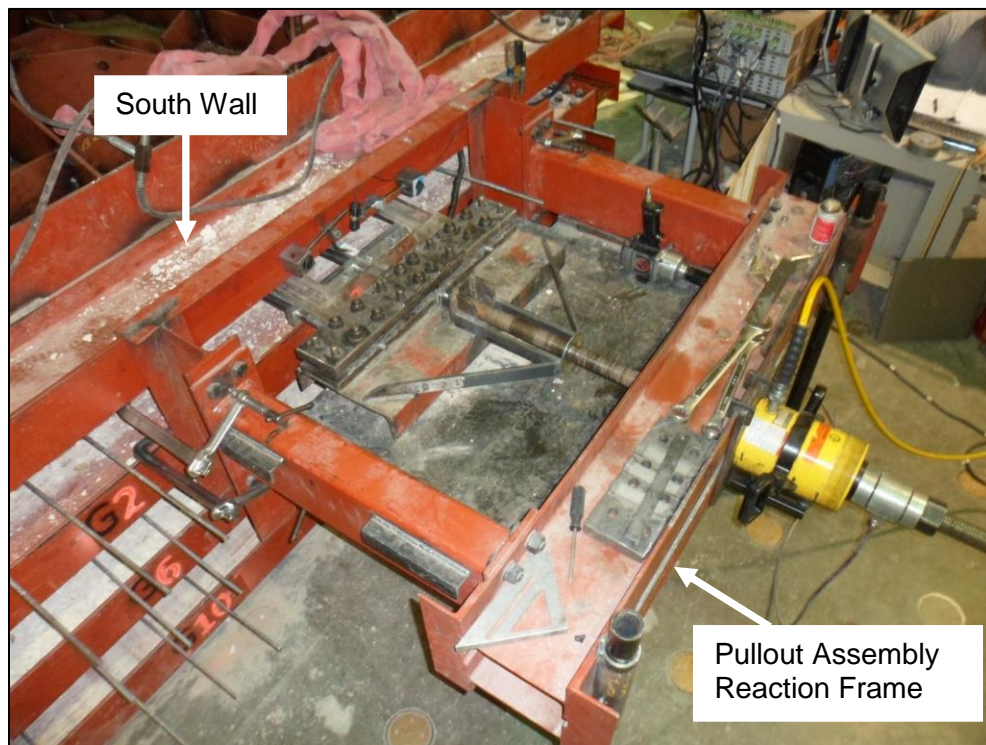


**Figure 5.18** Pullout Assembly and Reaction Frame Used on South Face

The pull force was transmitted to the MSE strip reinforcement through a high tensile strength extension rod. Strip reinforcements were connected to the extension rod by a simple pin-joint to facilitate uniformly-applied, pure axial load without bending. This connection was used effectively for pullout testing conducted in Type B material. However, it was found to be inadequate for pullout testing in Type A backfill because the forces generated were large enough that they caused rupture of the reinforcement at the bolt hole. Therefore, a new frictional gripper was developed and used. The frictional gripper engaged the entire cross section of the strip reinforcement instead of the reduced cross section through the bolt hole. The gripper consisted of two parts that were connected by a hinge. One end of the gripper was clamped to the reinforcement while the other end was threaded onto the end of the pull rod extension. Figures 5.19 depicts the frictional strip gripper.
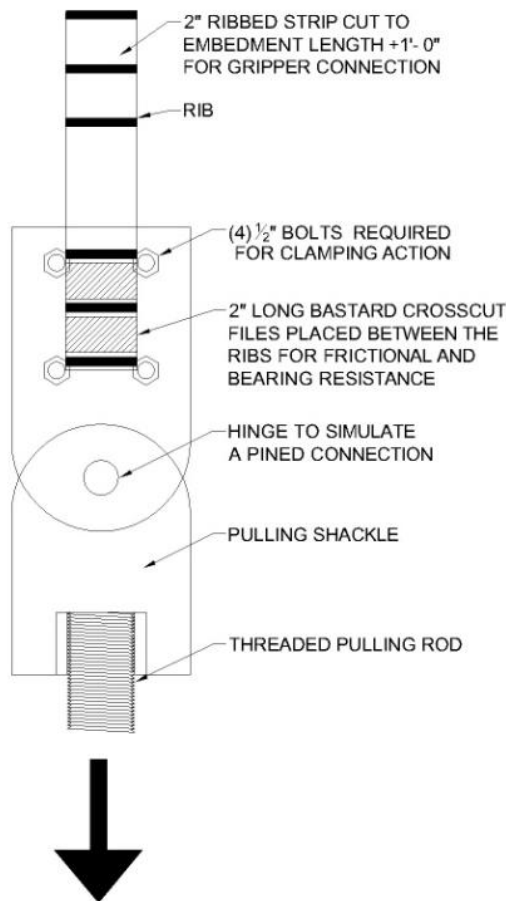


**Figure 5.19** Friction Gripper Used for Testing Strip Reinforcement in Type A Backfill

Connection of grid reinforcements to the pull rod required a much more robust friction gripper. This gripper was designed to accommodate grids with different longitudinal bar spacings. The friction gripper was fabricated by welding a series of flat hardened steel files to two thick steel plates. The grid reinforcements were then sandwiched between the two plates making sure that the longitudinal bars were aligned precisely with the files. The two plates and the reinforcement were then clamped together with bolts. The entire grip assembly was attached to the hollow core hydraulic jack via the same extension rod used for strip reinforcements. Figure 5.20 shows the friction plate gripper used for grid reinforcement testing. The purpose of the spacer seen in the figure was to ensure that the friction gripper was aligned parallel to the test specimen, so that the reinforcement was not subjected to any unintentional skew at the beginning of the test. This precautionary measure however did not eliminate the possibility of incidental skew that resulted from weld breaks that occurred mid-test on one side of the grid. To monitor incidental skew, three displacement gages were placed in front of the test grid, one directly beneath each longitudinal bar. Figure 5.20 also shows these displacement gages.
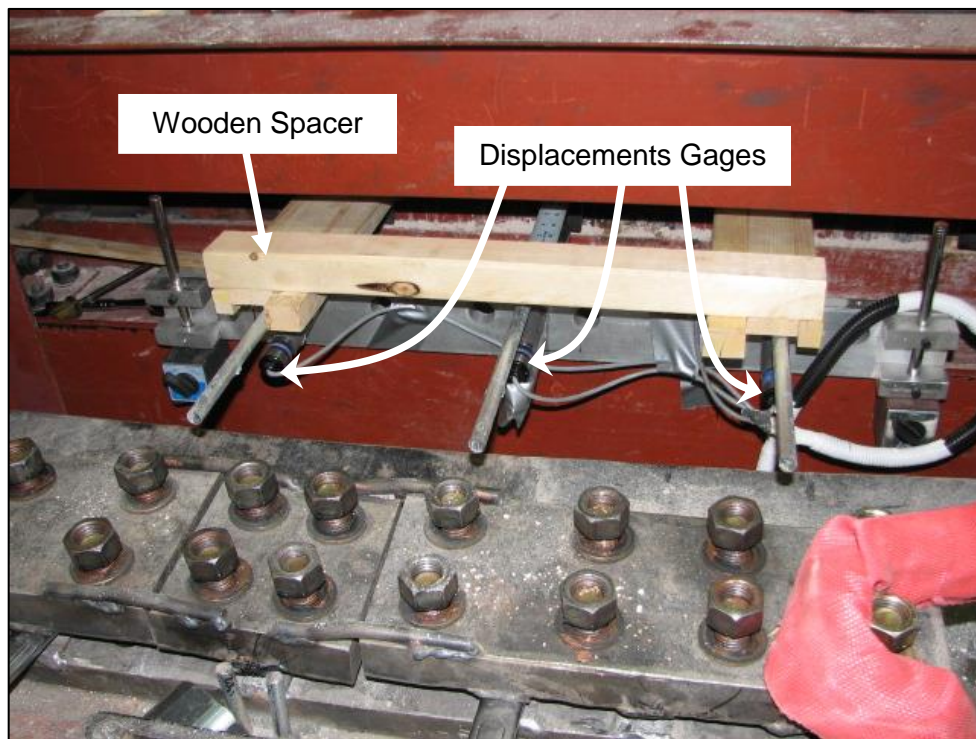


**Figure 5.20** Frictional Plate Gripper Used for Testing Grid Reinforcement Prior to Being Connected to the Grid

Once the extension rod was attached, an optical displacement marker (also called witness marker) was mounted on the wall of the MSE Test Box to facilitate visual measurement of the pullout displacement. The optical displacement marker consisted of a pointer with a magnetic base. The location on the reinforcement to which the witness marker points at this juncture was referred to as "test zero". Test zero is the reference from which both optical and digital displacements during pullout testing were measured. Once "test zero" was established, a reference sticker with 0.125in markings from (-0.25in to +1.50in) was affixed to the reinforcement. In addition to optical displacement measurements, the displacement of the reinforcements during pullout testing was also recorded using a digital displacement gage.

Once the entire pullout mechanism was set up, all sensors were activated allowing the data acquisition system to start recording data. Four channels of digital data were collected during each pullout test in addition to the data from the earth pressure cells. These four channels of data were collected using a Vishay 5000 data acquisition system connected to a personal computer and controlled by "Strain Smart" software. The four digital data channels were:

1. Pullout load from annular load cell
2. Pressure transducer in the hollow core hydraulic jack
3. Linear displacement transducer
4. Pressure transducer in the overburden stress application hydraulics

Data were collected at a frequency of 10Hz on all of these channels. Data from the earth pressure cells were displayed on the computer screen together with the other four data channels during testing, but the actual recording of pressure cell data required a Geokon data-logger, which records earth pressure cell data continuously at a frequency of four times per minute.

Once the data acquisition system was activated, the vertical overburden pressure was applied up to the target value. Testing then began by applying the pullout force via the hollow core hydraulic jack by pumping the jack manually. Reinforcements were pulled until an optical displacement of 1.5" was reached, or until the reinforcement ruptured.

The above procedure was repeated until all MSE reinforcements for a test setup were tested. The test setup was then decommissioned. Decommissioning involved the following activities: archiving the test data, removing the fill from the MSE Test Box, removing and inspecting the condition of the tested earth reinforcements, and cleaning up the system in preparation for the next test setup.

## 5.4 DATA PROCESSING

The data collected during each pullout test included measurements of three different test variables: (a) pullout force, (b) displacement, and (c) vertical overburden pressure. As mentioned previously, two independent measurements were made on each of the above test variables. All of these measurements except for the optical measurement of displacement were made with appropriate electronic data collection devices. Table 5.1 summarizes information related to the specific measurement technique and frequency of measurement for each variable.

**Table 5.1** Measurement Method and Data Collection Frequency for Each Test Variable

| Test Variable | Measurement Method | Frequency of Data Collection |
|---|---|---|
| Pullout Force | Annular Load Cell mounted on pullout rod | 10Hz |
| | Pressure Transducer attached to hollow-core jack | 10Hz |
| Displacement | Optical Measurement using witness marker against graduated scale | 1/16" over 0.0-7/8in 1/8" over 7/8-1.0in 1/4" over 1.0-1.5in |
| | Digital Displacement Sensors and LVDTs (3 sensors for grids) | 10Hz |
| Overburden Pressure | Earth Pressures cells mounted on floor slab | 4 measurements/min |
| | Pressure Transducers attached to overburden pressure jacks | 10Hz |

The data generated required careful management as well as reliable and efficient processing. This was accomplished using a computer program with a database structure.

The first step in the data processing involved the combination of the two independent measurements available for each test variable.

With regard to displacement measurements, it was observed that the digital measurements did not provide stable readings in early stages of the pullout load testing. It is believed that these instabilities were caused by incidental misalignment and erratic movements of the pullout load assembly that typically occurred during the initial seating process. The optical measurement of the displacement, though not capable of providing a high degree of precision, provided stable readings throughout the entire displacement domain. Therefore, these measurements were used to calibrate early digital displacement measurements and hence define zero displacement. To accomplish this, the differences between the optical and corresponding digital displacement readings were first calculated. If the two measurements were offset by the same amount, then this difference was used as the offset correction. Otherwise, the average of these differences was calculated and then the average difference was used as the offset correction. The displacement scale was then zeroed by adding the offset correction to the digital displacements. Once sufficient load had been applied, the digital displacement domain provided stable and accurate readings, allowing it to be used as the primary measurement of the displacement.

With the displacements zeroed, the next step in data processing involved removal of test procedure artifacts from pullout force and overburden pressure measurements. This was done by using purpose-designed data filter. The filter calculated the peak and standard deviation for each continuously measured pullout force and the average and standard deviation for the continuously measured overburden jack pressure for every 0.01in. displacement. This process removed any loss in load due to jack recovery during application of the pullout load. The processed data retained the peak load during each 0.01in displacement, thus producing force measurement equivalent to that expected in a strain controlled test.

Once the data had been filtered, the pullout force and overburden measurements from two independent systems were combined to obtain a single measured value. For this purpose, the average and the variance for each of the two measurements were calculated and then the

calculated averages combined by using the following equation proposed by Lyons, 1991 (*46*).

$$a = \frac{\sum \frac{a_i}{\sigma_i^2}}{\sum \frac{1}{\sigma_i^2}}$$ (5.1)

where: $a$ = Combined measurement,

$a_i$ = Measurement made with a specific measuring system,

$\sigma_i$ = Standard deviation associated with each measurement

Equation 5.1 allows multiple measurements of the same variable to be combined in such a manner that the measuring system providing more consistent data received higher weight and the measuring system with less consistent data received lower weight.  The overall standard deviation corresponding to the combined measurement is given by Eq. 5.2.

$$\frac{1}{\sigma^2} = \sum \frac{1}{\sigma_i^2}$$ (5.2)

To further verify the validity of the above approach for combining independent measurements of the same parameter using Eq. 5.1, the pullout forces measured using the two measurement methods were compared against each other.  Figure 5.21 shows the pullout load measured using the annular load cell plotted against the pullout load measured using the pressure transducer attached to the hydraulic jack. It shows that there was good agreement between the two measurements. Figure 5.22 shows the two independent measurements plotted against the combined measurements. It can be noticed that the slopes of both trendlines are close to 1.0.  The slope of the trendline for the load cell measurement, 0.992 was closer to 1.0 than the slope of the trendline for hydraulic jack measurement, 0.983.  This suggests the load cell measurement provided slightly more consistent measurement and therefore, was favored by Eq. 5.1 when the two measurements were combined.

Figures 5.23 and 5.24 provide similar comparisons for overburden pressure measurement. It is clear that, in this case, the scatter in the earth pressure cell data was much larger compared to values obtained from the overburden jack. Therefore, the overburden jack pressure transducer measurement was heavily favored when calculating the combined measurement for the overburden pressure.  This is evident from the high correlation

($R^2=0.992$) and the slope of 0.997 in the relationship between the combined and jack pressure transducer measurements.
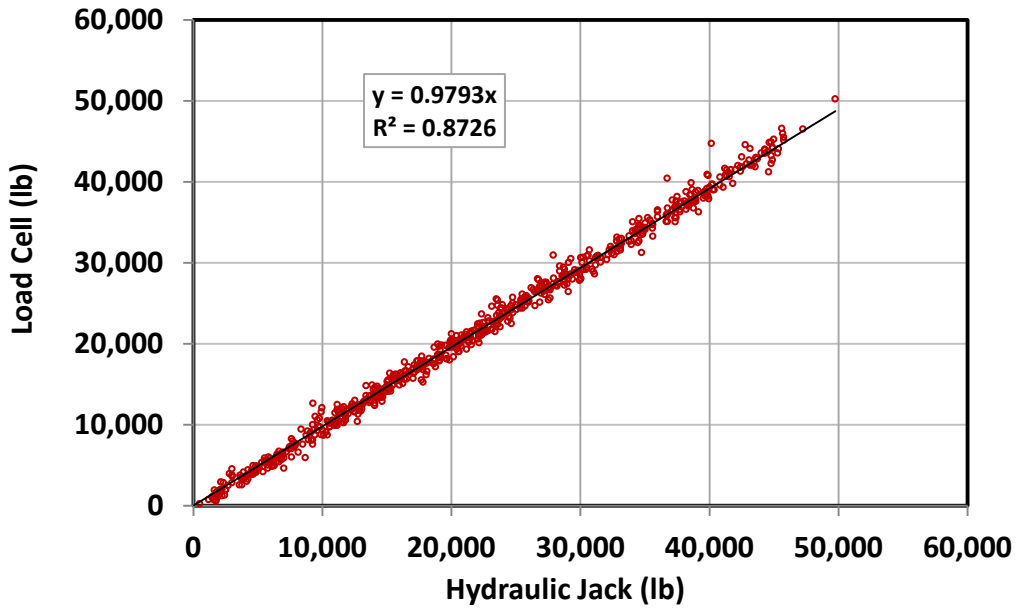


**Figure 5.21** Comparison of the Pullout Forces Measured by the Load Cell and the Hydraulic Jack Pressure Transducer
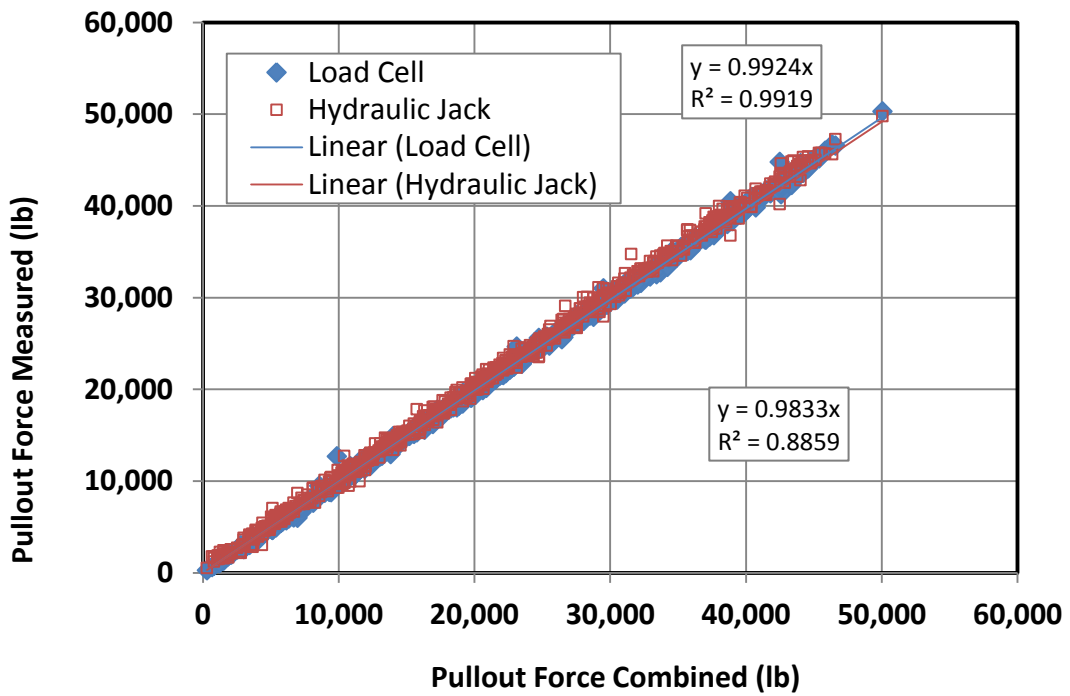


**Figure 5.22** Comparison of the Combined Pullout Load Measurement with the Two Independent Measurements
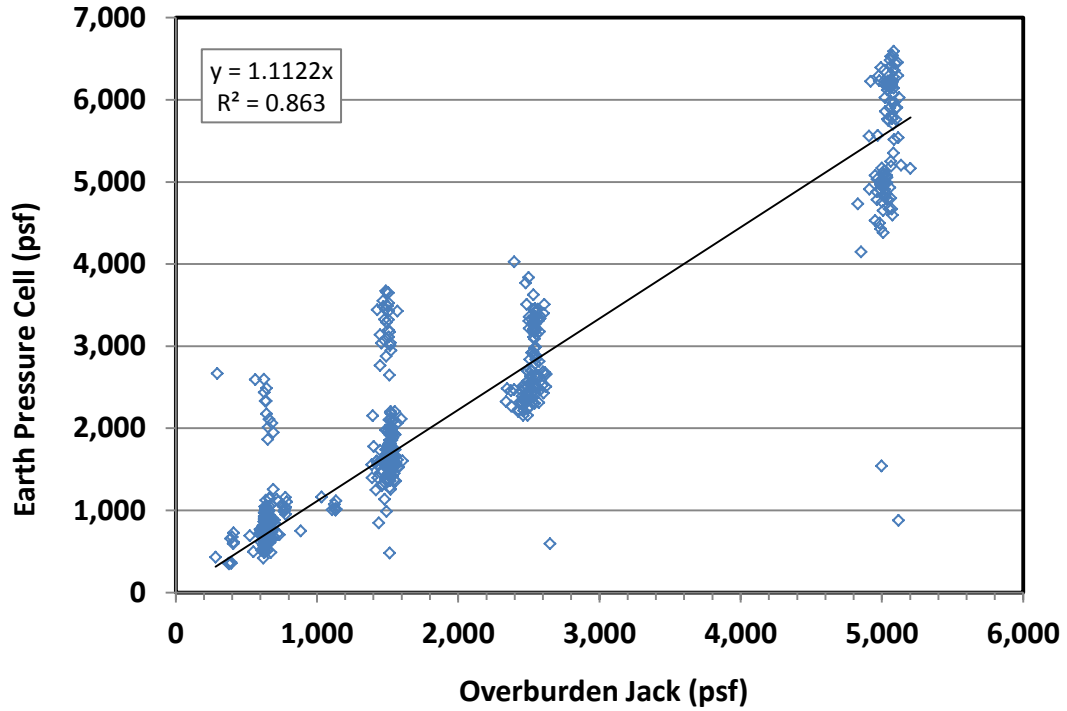
**Figure 5.23** Comparison of the Overburden Pressure Measured by the Earth Pressure Cells and the Overburden Jack Pressure Transducer
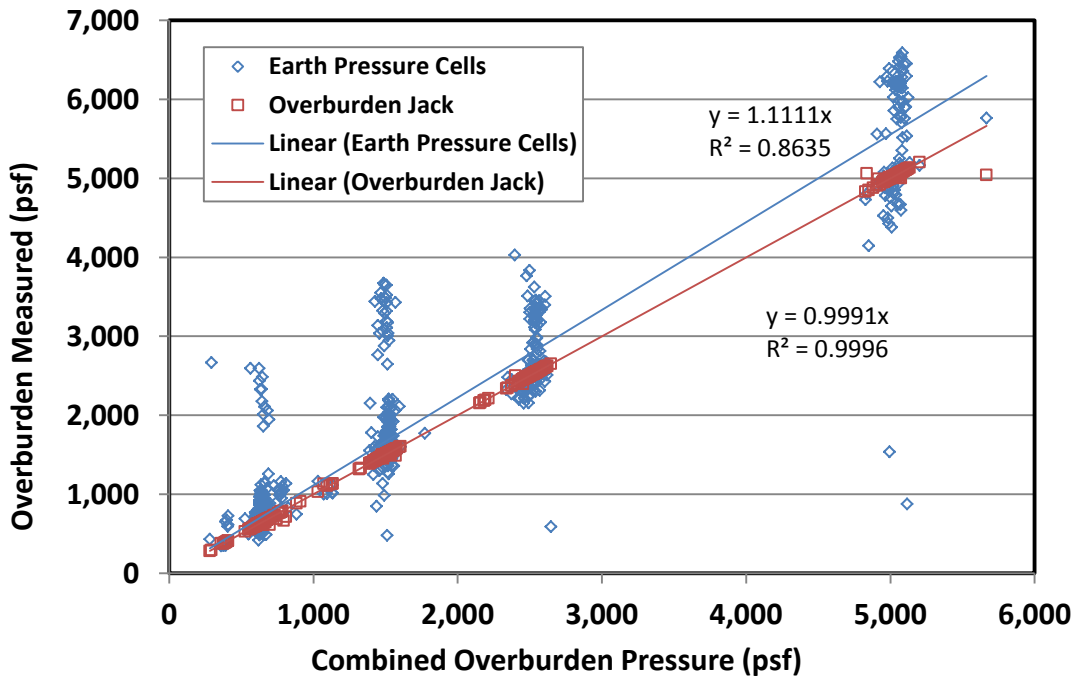


**Figure 5.24** Comparison of the Combined Pullout Load Measurement with the Two Independent Measurements

Figure 5.25 shows a typical load-displacement diagram obtained from an MSE pullout test. This load displacement curve represents a pullout load conducted on a strip type reinforcement.
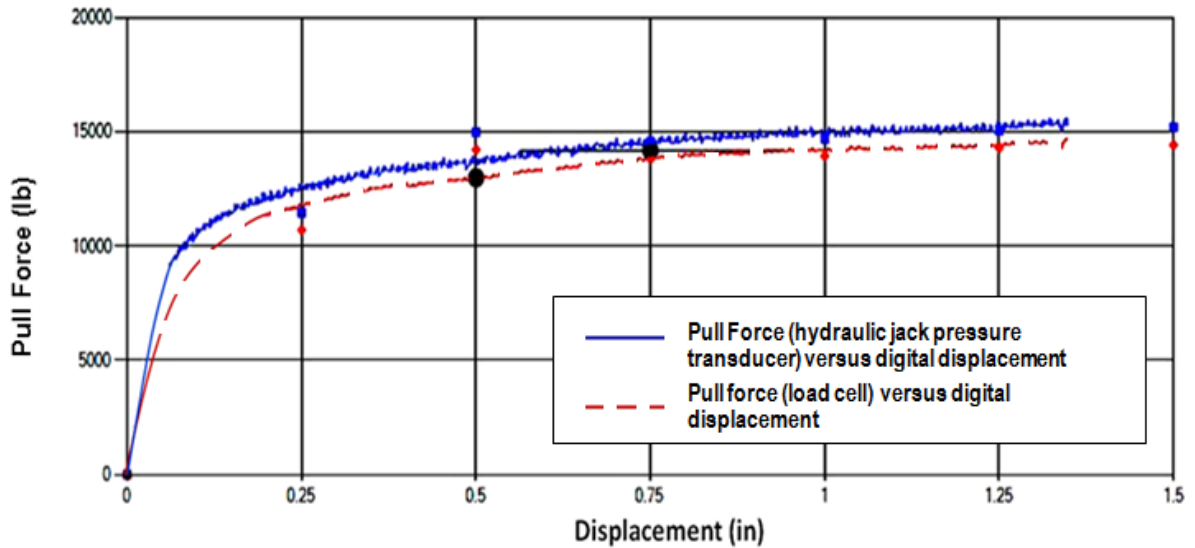


**Figure 5.25**   Typical Load-Displacement Curve for Ribbed Strip Reinforcement

The figure shows two separate plots of load versus displacement: one with the pull force calculated based on hydraulic jack pressure transducer measurements and the other based on pull force calculated from annular load cell readings. Solid black circles represent the combined pull forces calculated using Eq. 5.1 at displacements of 0.5-in and 0.75-in. The peak pullout load measured prior to 0.75in was used to calculate the pullout resistance factor.  Eq. 5.3 was used to calculate the pullout resistance factor, F*.

$$F* = \frac{P_r}{C \; \alpha \; L_e b \; \sigma_v} \tag{5.3}$$

where:

$P_r$   =   Pullout load corresponding to a specific displacement,

$L_e$   =   Length of embedment of the reinforcement,

$b$   =   Width of the reinforcement,

$\sigma_v$   =   Vertical overburden pressure,

$C$   =   2 and $\alpha = 1.0$

## 5.5  PULLOUT TESTING OF STRAIN-GAGED MSE REINFORCEMENTS

In addition to the pullout tests described in previous sections, the pullout test program conducted in this research also included a series of pullout load tests on MSE reinforcements that have been instrumented with strain gages.  The objective of these tests was to develop better understanding of mechanisms that control the development of pullout resistance in MSE reinforcements.  Two separate series of strain-gaged reinforcement tests were performed: one in Type B backfill and the other in Type A backfill.

The strain gaged reinforcement testing in Type B backfill included a total of 16 pullout tests on instrumented ribbed strips.  These included eight 8-ft long strips and eight 12-ft long strips.  The strain gage layout used on a 12-ft long ribbed steel reinforcement is shown in Figure 5.22.  Gages were mounted at distances of 1-ft, 3-ft, 5-ft, 7-ft, 9-ft and 11-ft from the front end of the strip.  Gages were installed in pairs (*i.e.*, both top and bottom) of the strip at each gage location so that any strains induced due to bending of the reinforcement could be eliminated by taking the average of the top and bottom strain readings.

The strain gages used for this study were general-purpose, prewired, Micro-Measurement SR-4, 350ohm SR-4 linear gages. Vishay Precision Group distributes these gages under item identification C2A-13-062LW-350.  The gages were applied to the cleaned steel surface according to Vishay Micro-Measurements Instruction Bulletin B-127-14 using M-Bond 200, a cyanoacrylate bonding system.  The gages were then protected using M-Coat J, a hard-curing polysulfide protective coating system. The M-Coat J is the most robust strain gage protection system distributed by Vishay Precision Group.

The instrumentation layout shown in Figure 5.26 allowed evaluation of the pullout load distribution along the length of the reinforcement.  A uniform distribution would suggest that the reinforcement is behaving in an inextensible manner with uniform slip between the reinforcement and soil at both front and back ends of the strip.

A total of 12 pullout tests were conducted on instrumented grids embedded in Type B backfill.  This test series included eight tests on 6-ft long grids and four tests on 3-ft long grids.  The gage layouts used on these reinforcements are shown in Figure 5.27   The gage layout shown in the figure was designed to produce data on the following aspects of welded grid behavior under pullout load: (a) relative magnitudes of axial loads carried by the

longitudinal bar at the center relative to the longitudinal bars on either side, (b) the pullout load distribution along the length of the grid (from the front to the back), (c) lateral loads carried by transverse bars located at front, middle and back of the grid, (d) magnitudes of moments transferred from transverse bars to the longitudinal bars through welded connections.

The strain gaged reinforcement test series in Type A backfill consisted of four strip reinforcements and eight grid reinforcements. All four strip reinforcements were 8ft long. They were tested at depths of 5ft and 12ft. The gaging plan used was slightly modified from that used previously for tests conducted in Type B material. In this series of tests, an additional pair of strain gages was installed on the leading end of the reinforcement outside the front face of the test box. These strain gages, when averaged, provided an additional measurement of the applied pullout load. The strip reinforcement gage layout used in Type A backfill materials is shown in Figure 5.28.
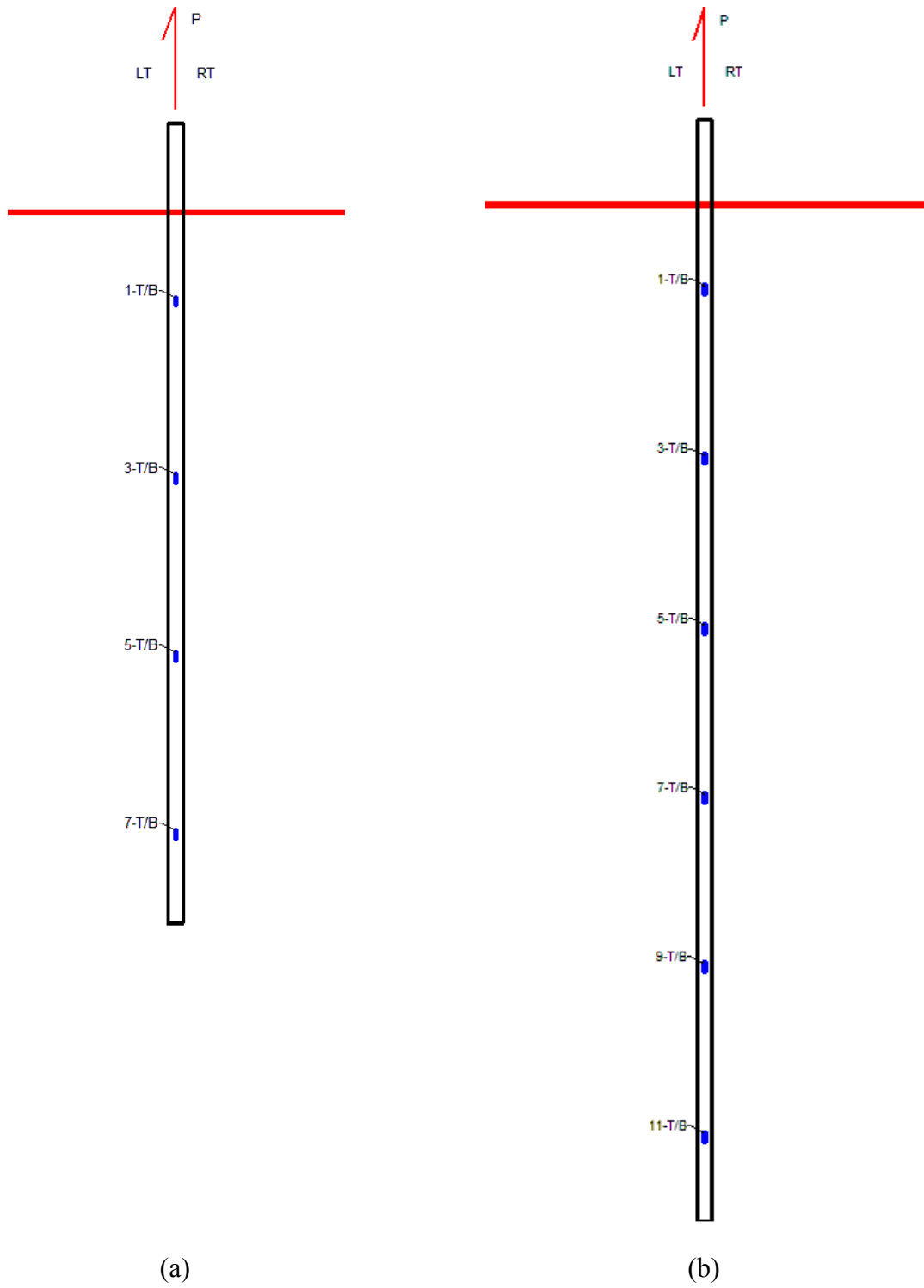
**Figure 5.26** Strain Gage Layouts Used in Strip Reinforcements Tested in Type B Backfill: (a) 8-ft Long Strips, (b) 12-ft Long Strips
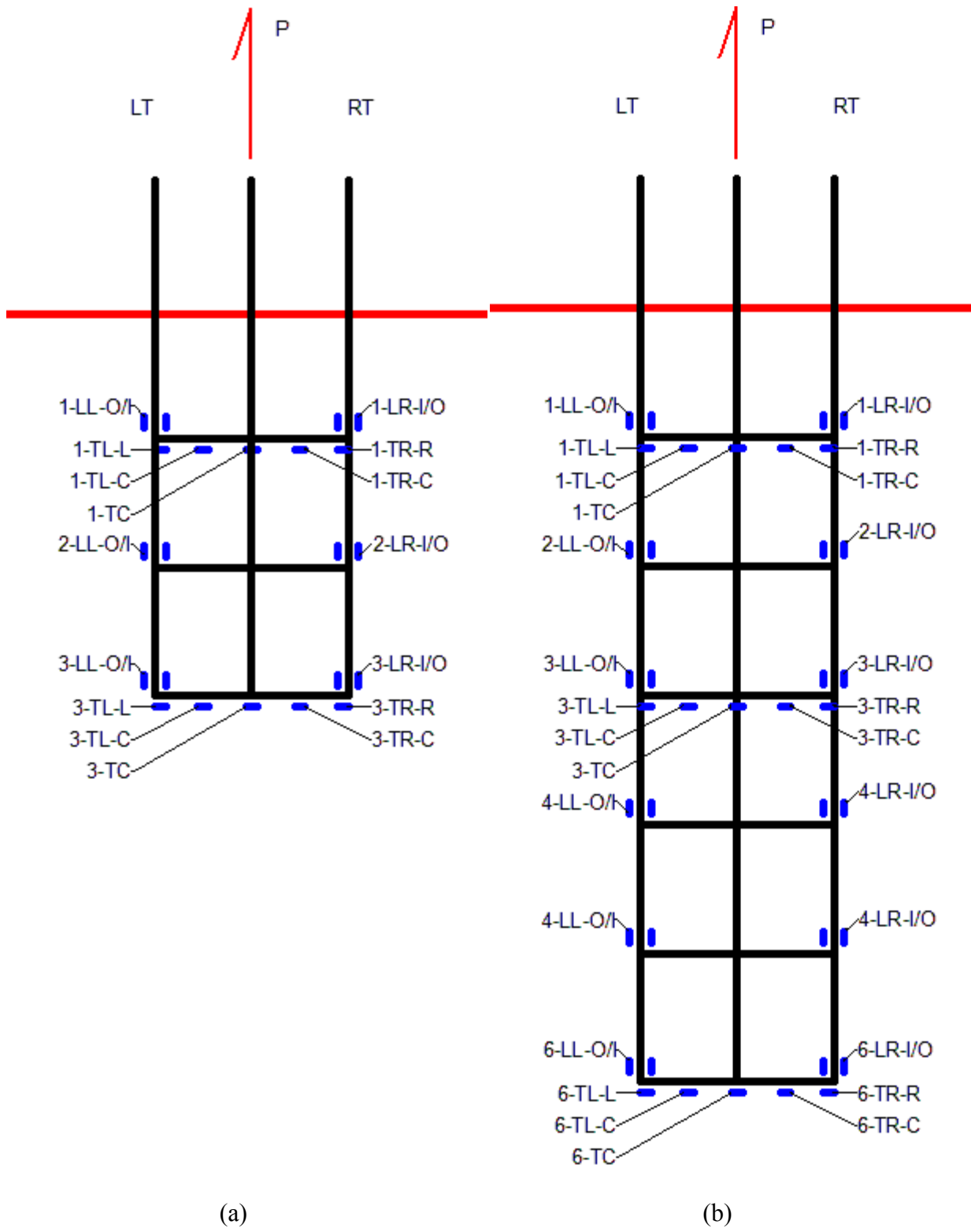
**Figure 5.27** Strain Gage Layouts used in Grid Reinforcements Tested in Type B Backfill: (a) 3-ft Long Grids, (b) 6-ft Long Grids

The gaged grid tests conducted in Type A material included eight 6-ft grids. The gage layouts used in this test series were quite different from those used previously in Type B material. Several significant changes can be noted in this gaging plan when compared with that used for Type B testing. First, the grids were gaged differently to obtain a different type of data. The gage layout used in the first four grids is shown in Figure 5.29(a). This particular gage layout was selected with the objective of collecting data on the bending moments that develop on transverse bars of the grid. The gage layout used in the remaining four grids is shown in Figure 5.29(b). The purpose of this gage layout was to provide data on the distribution of axial load along the length of the grid and between the center and outside bars. In addition, the gage locations were changed by shifting them away from welded connections to avoid possible influence due to stress concentrations at joints.

## 5.6 GENERAL OBSERVATIONS FROM PULLOUT TESTING

This section provides an overview of the general observations made during pullout testing. It is divided into two separate sections. Sec. 5.6.1 includes observations made during pullout testing of ribbed steel strip reinforcement while Sec. 5.6.2 covers observations from pullout testing of grids.

### 5.6.1 Observations from Pullout Testing of Strip Reinforcement

One significant observation made during pullout testing of strips was that this type of reinforcement, in general, tends to gain pullout load capacity rapidly. In other words, strip reinforcements develop a large percentage of their full capacity at relatively small displacements. Although this observation did not hold true for *all* strip reinforcements, many of the strip reinforcements tested reached 80% of the maximum capacity at a displacement of 0.25in. This behavior is evident in the load displacement curve presented in Figure 5.25. It is believed that the observed phenomenon is a result of the primary mechanism that controls pullout resistance of strip type reinforcement, *i.e.* friction.

As explained in Chapter 4, in this study, the reinforcement lengths were selected so that the maximum loads would be controlled by reinforcement pullout rather than by rupture of the reinforcement. However, reinforcement rupture did occur when testing longer lengths
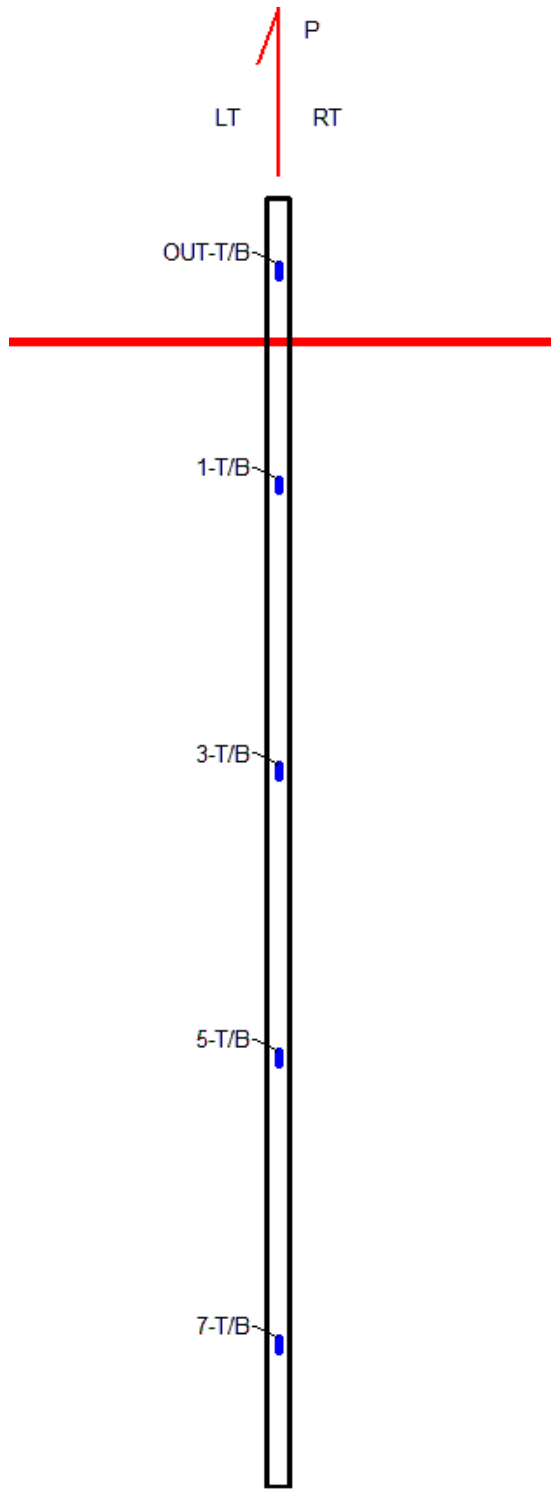
**Figure 5.28** Strain Gage Layouts Used in Strip Reinforcements Tested in Type A Backfill
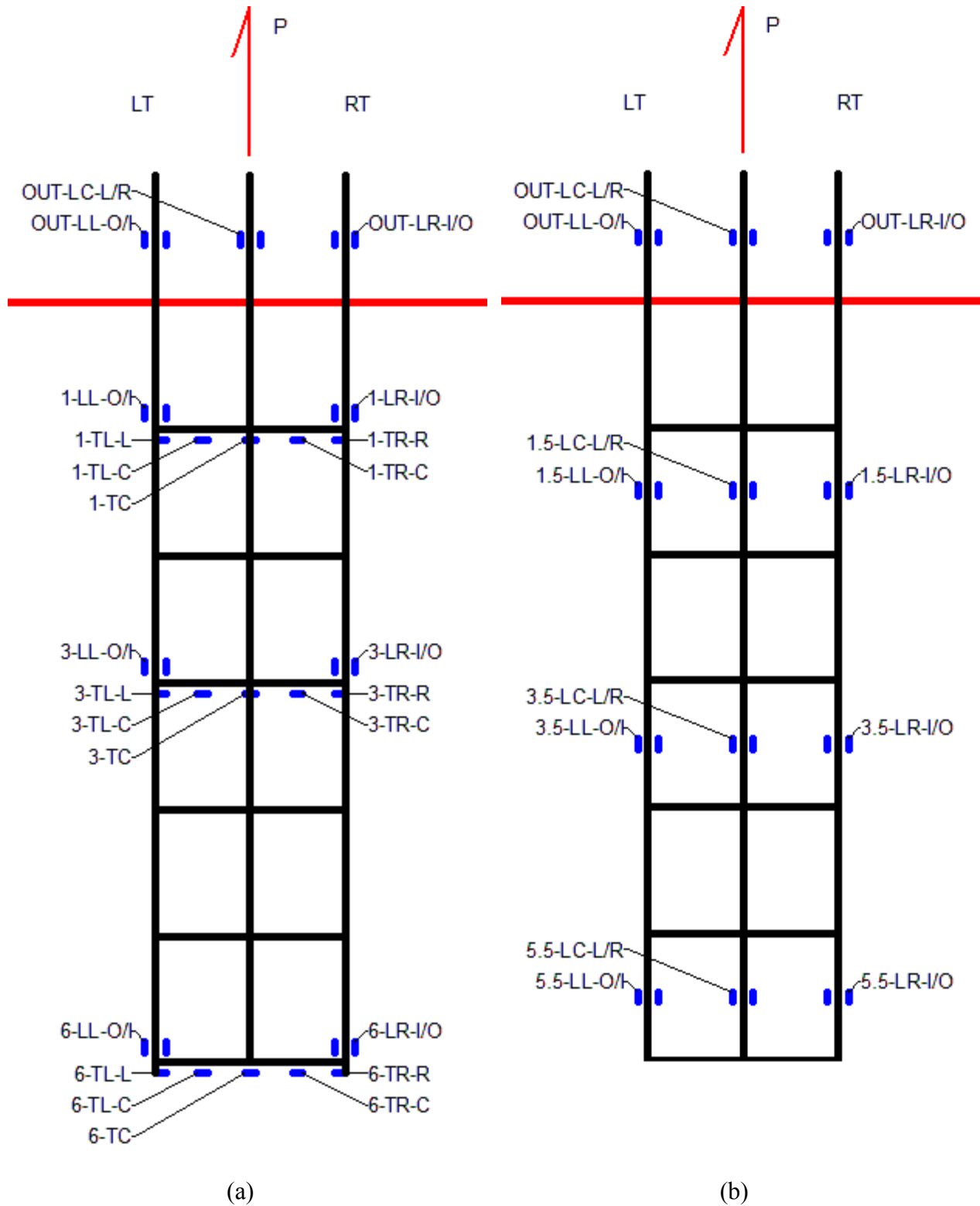
**Figure 5.29** Strain Gage Layouts used in Grid Reinforcements Tested in Type A Backfill:
(a) Bending Moments on Transverse Bars, (b) Axial Loads on Longitudinal Bars

of reinforcement at larger depths of fill.  Initially, these ruptures occurred at the bolt hole where the strip was connected to the pull rod.  The loads corresponding to these ruptures were about 22kips.  This rupture load corresponds to an ultimate steel strength of 83ksi based on the strip reinforcement dimensions shown in Figure 4.4.   In subsequent testing, reinforcement rupture through the reduced cross section at the bolt hole was avoided by using the new frictional rib gripper shown in Figure 5.19.  The new gripper allowed the strip reinforcements to carry pullout loads in excess of 30-kips.

Figure 5.30 shows an example of a strip reinforcement that experienced rupture at the connection.  Based on the definition of the pullout resistance capacity used in this study, the pullout resistance factor, F* for this reinforcement was calculated using the maximum pullout load sustained prior to 0.75-in displacement (2).  A variable called *Rupture Case* was added to the database to identify those pullout tests in which maximum the pullout load was controlled by rupture.  Subsequently, appropriate statistical data analysis techniques were used to determine whether the rupture case had any significant influence on measured F* values.
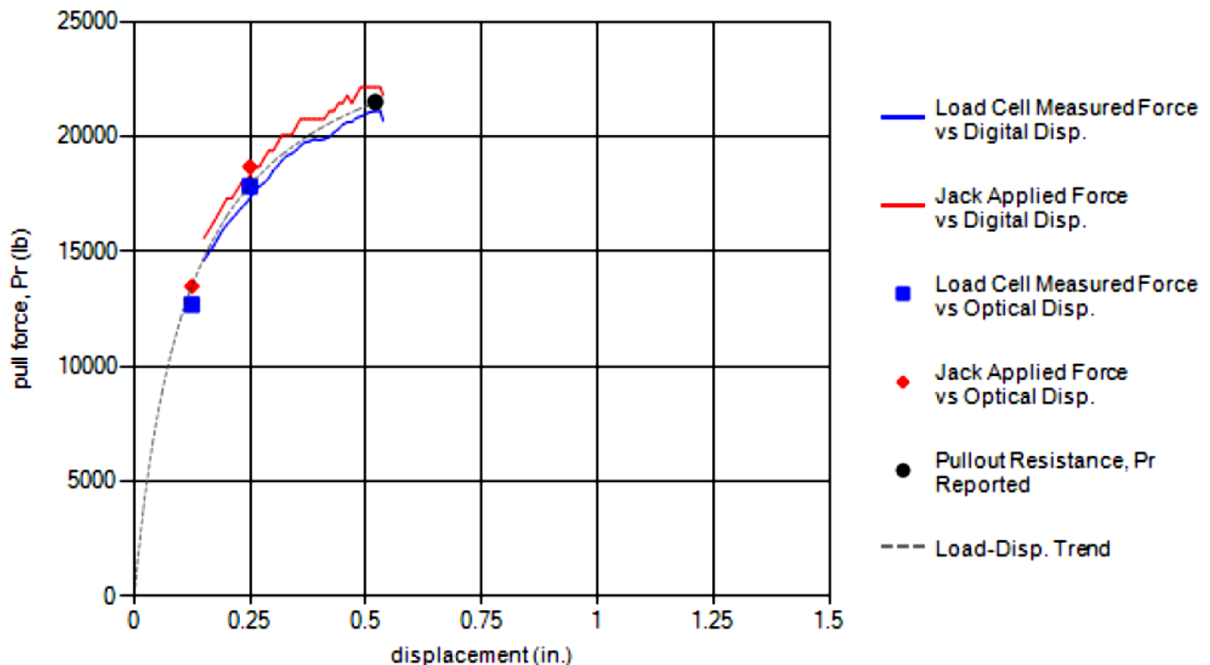


**Figure 5.30**  Load-Displacement Curve for a Strip Reinforcement that Experienced Connection Rupture (Test No. TS31.16-S-L12-Z12-M)

## 5.6.2 Observations from Pullout Testing of Grid Reinforcement

When compared with strip type reinforcement, the grid reinforcement developed pullout load at a slower rate.  In other words, welded steel grids continued to gain capacity beyond 0.25in, 0.50in and sometimes even 0.75in displacement.  This is evident in the grid load-displacement curve shown in Figure 5.31.
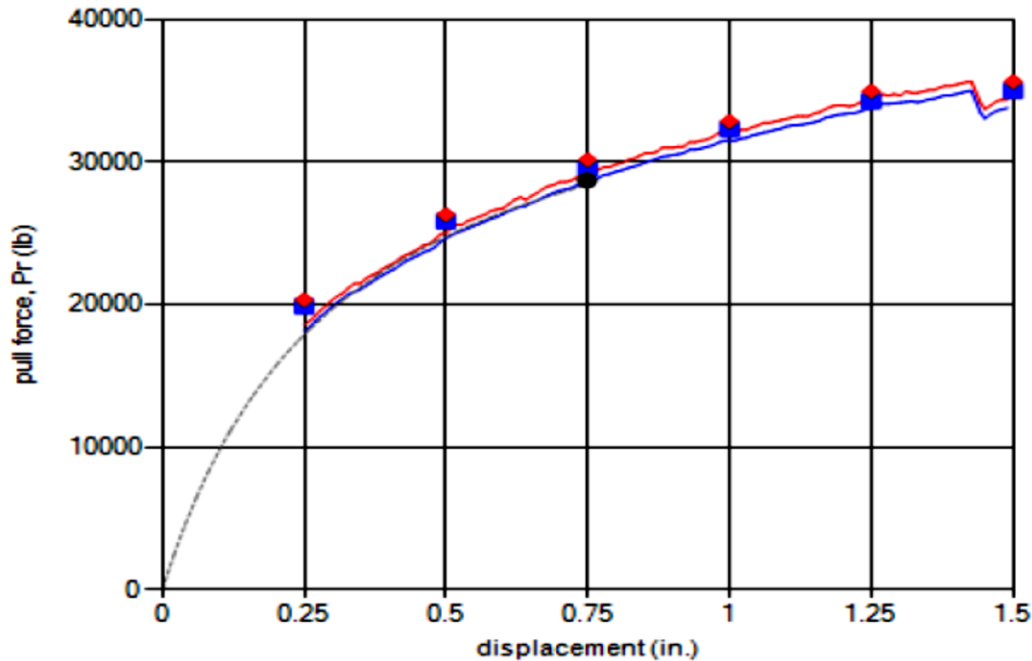


**Figure 5.31**  Load-Displacement Curve for a 9ft long 9x12-W20XW11 grid embedded in Type B backfill

Another important observation made during the pullout testing of grids involved transverse bar deformations noticed during pullout loading. Deformation was observed in nearly all grids as they were being removed from the MSE test box during decommissioning process after the test setup.  To observe this phenomenon more carefully, selected grid reinforcements were carefully exhumed at the conclusion of pullout tests.  Figure 5.32 shows the typical deformed shape of transverse bars as observed in exhumed grid reinforcements.  This observation suggests that plastic deformation of the transverse bars significantly contributes to the overall deformation of the grids.  In some grids, a void had formed behind the deformed transverse bars indicating that the transverse bar had moved relative to the

backfill soil. Figure 5.33 shows this phenomenon. Sec 6.5.2 presents results from strain gaged testing and provides further information about internal stresses within transverse and longitudinal bars and their relation to deformation patterns.
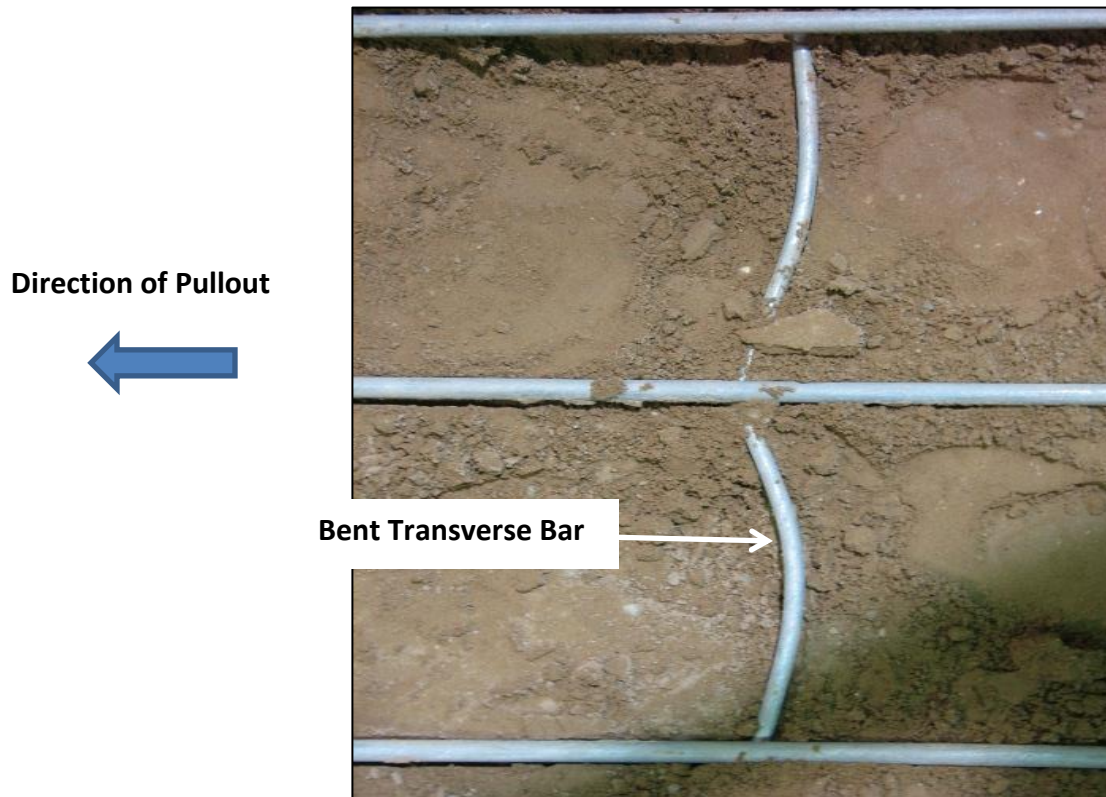


**Figure 5.32** Plastic Deformation of Transverse Bars during Pullout

Thus, it is apparent that the overall grid deformation occurs in two ways: sliding or translational movement of the transverse bar relative to the backfill soil and bending of the transverse bar under the effects of passive soil pressure.

Another very significant observation made during pullout testing of grids has to do with the impact that flexural deformation of the transverse bar had on the welded connections. It was observed that rotational movement of the transverse bar relative to the longitudinal bar created excessive shear stresses on the welded connection often causing connection failure. Figure 5.34 shows an exhumed grid with welded connection failures.
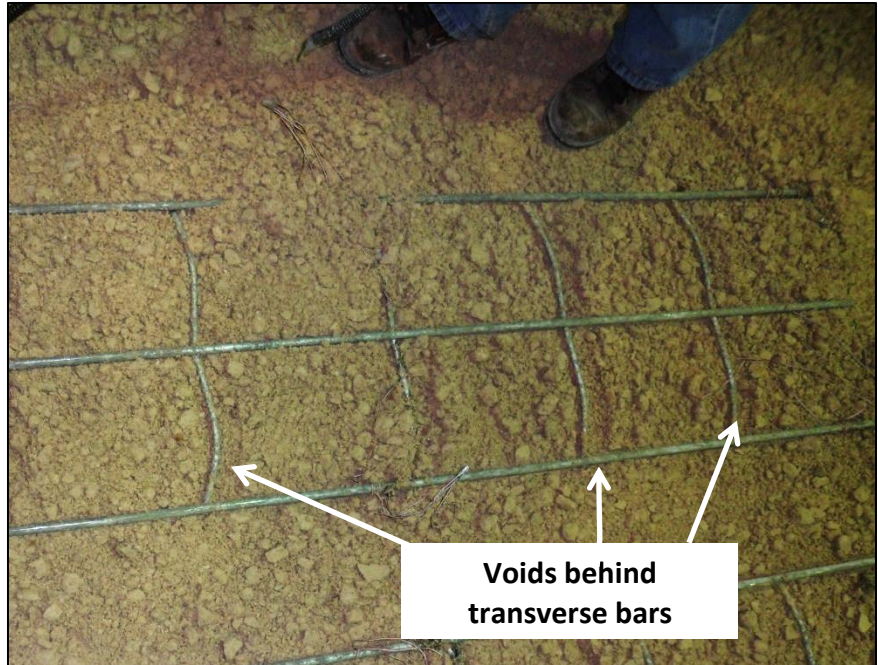
**Figure 5.33**  Voids Formed Behind Transverse Bars during Pullout
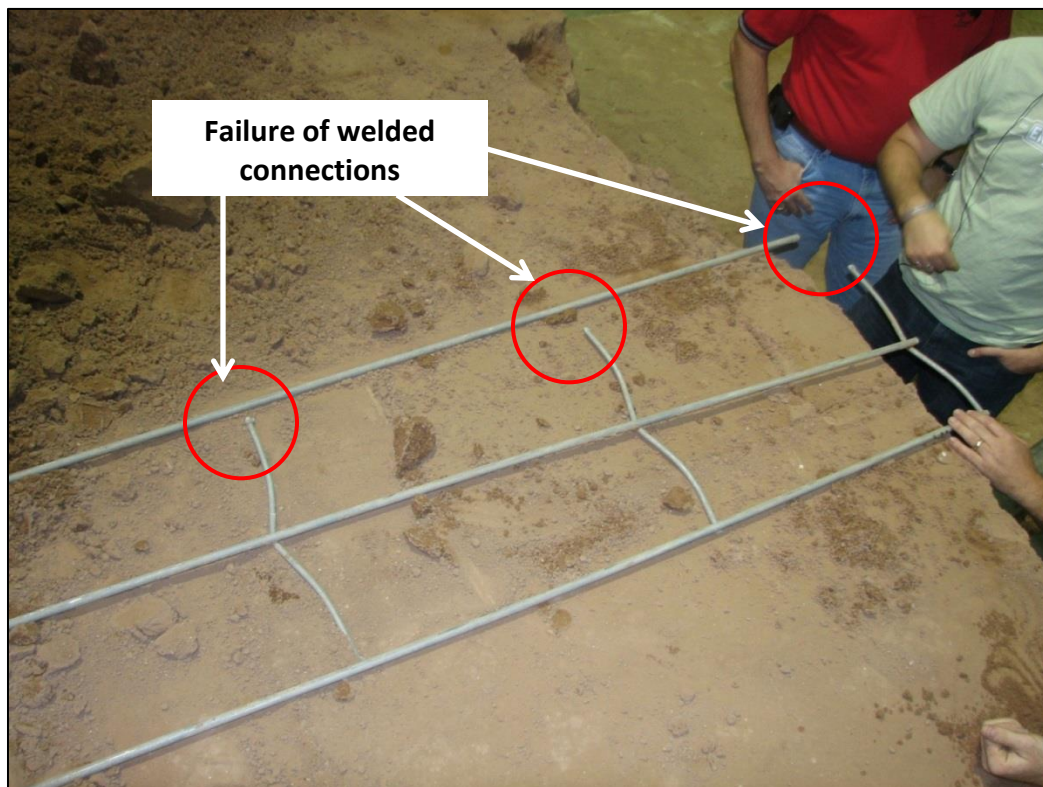


**Figure 5.34**  Exhumed Grid with Failed Weld Connections

Failures of welded connections were marked by a loud popping noise during pullout loading. These were also associated with an abrupt drop in the pullout load and a sudden change in the relative displacement between longitudinal bars. Figure 5.35 shows the abrupt changes in the pullout loads due to weld breaks. It also shows the skewing effect as captured by the changes in the readings of the displacement gages for left, center and right longitudinal bars.
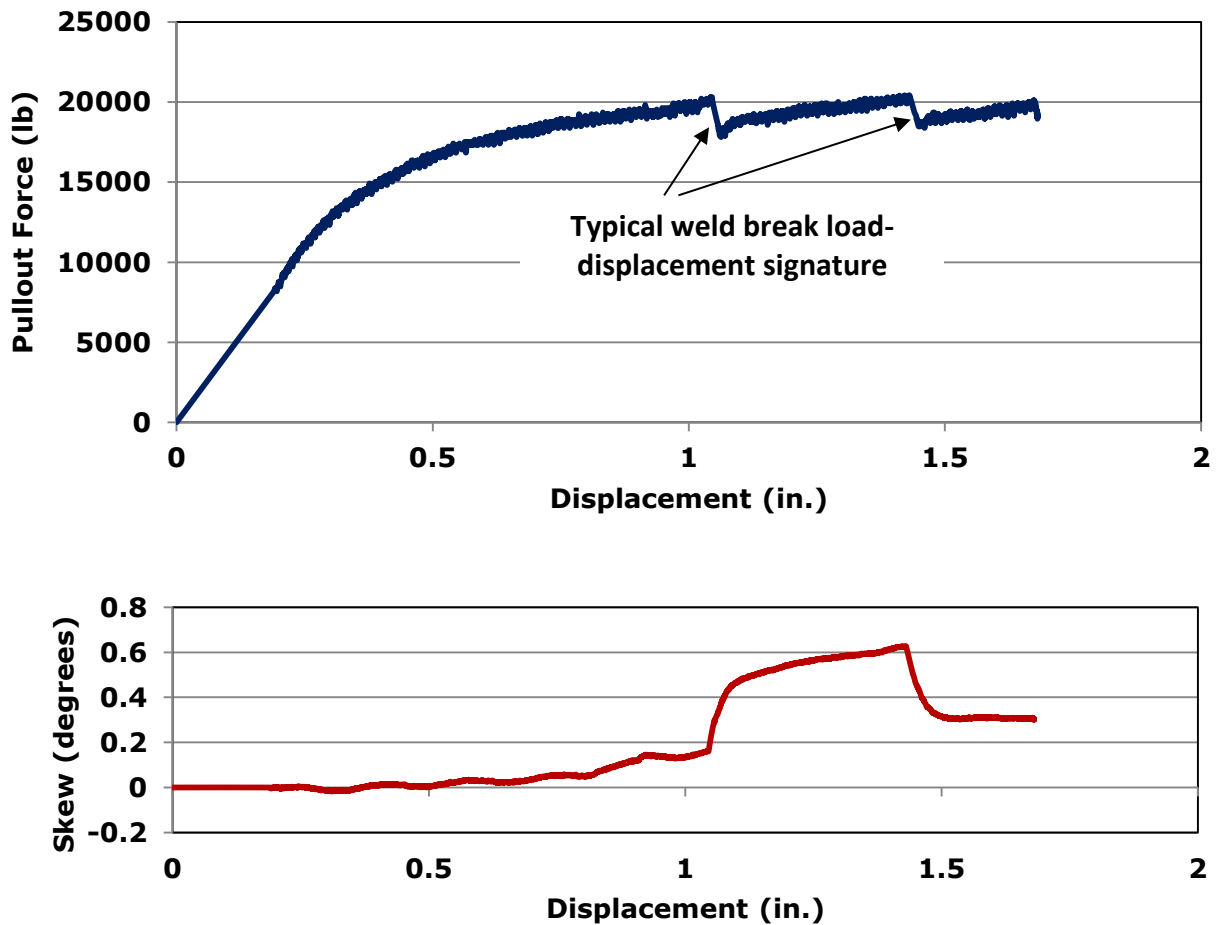


**Figure 5.35** Typical Load-Displacement and Skew Behavior Associated with Weld Breaks

The load-displacement behavior of welded steel grids observed during pullout load testing can be broadly classified into several different types. Examples of grids belonging to each of these different types are shown in Figures 5.36 through 5.39. Figure 5.36 shows the typical load-displacement curve obtained for a grid that did not experience any weld breaks or rupture of longitudinal bars. In this grid, the pullout resistance factor F* would have been controlled by pullout of the grid.
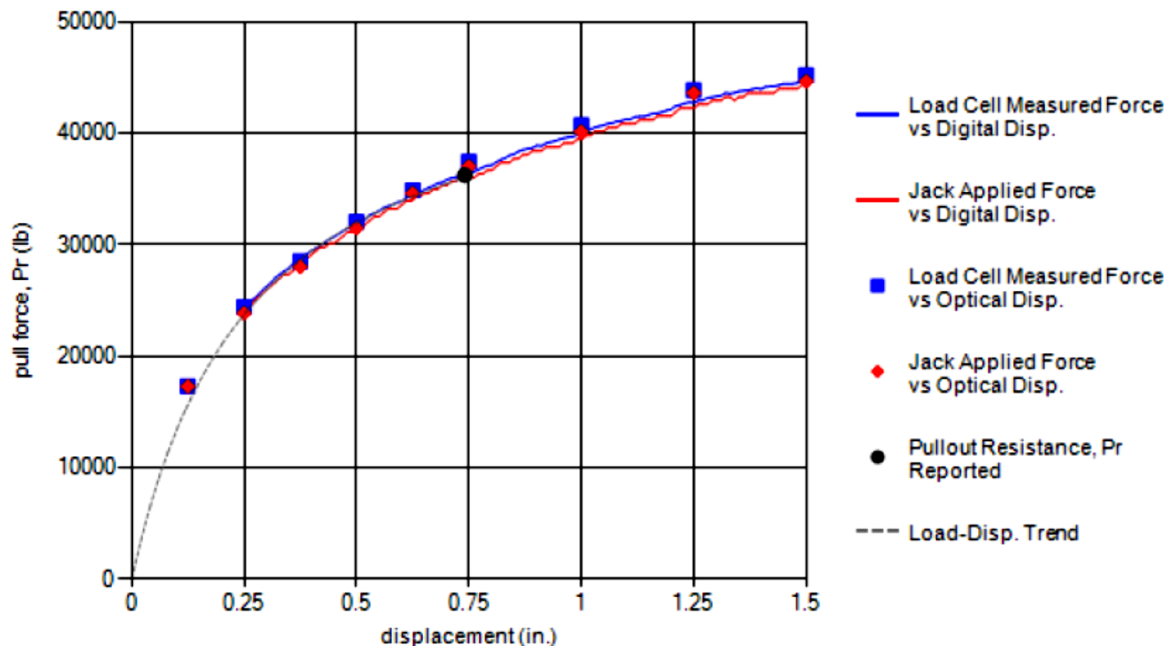


**Figure 5.36** Load-displacement Relationship Corresponding to a Welded Grid that did not Experience Failure of Welded Connections or Rupture of Longitudinal Bars
(Test No. TS 31.07-G-9x12-W20xW11-L6-Z5-M)

Figure 5.37 represents a different type of load-displacement behavior. The abrupt drops in the pullout loads are likely caused by breakage of welded connections. However, in spite of the weld failures, the grid continued to gain capacity up to and even beyond the specified pullout displacement of 0.75-in. Accordingly, the pullout force used in the F* calculation is the value recorded at 0.75-in. The next figure, Figure 5.38, represents a third type of load-displacement behavior. Similar to the previous grid, this grid had also suffered weld failure. However, unlike the previous grid, this grid reached its maximum pullout capacity before the second weld failure (or displacement of 0.63-in). Therefore, the pullout resistance capacity for this grid was calculated based on the peak pullout load at 0.63-in.
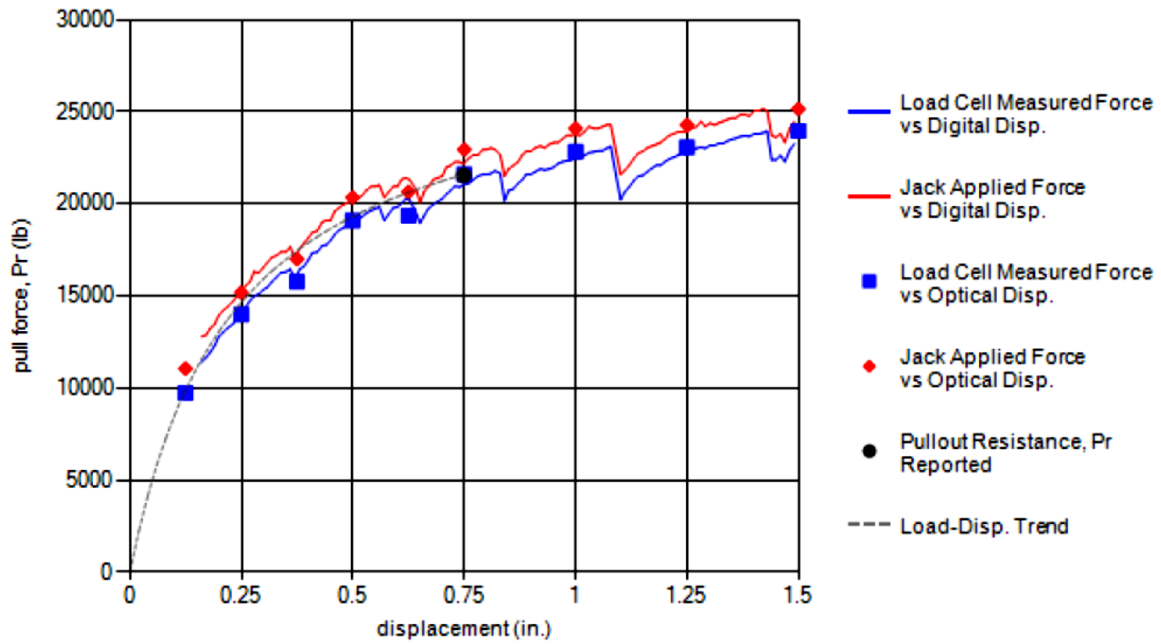
**Figure 5.37** Load-displacement Relationship Corresponding to a Welded Grid that Experienced Progressive Failure of Welded Connections; Peak Pullout Load at δ=0.75in (Test No. TS 32.03-G-9x6-W20xW7.5-L3-Z5-T)
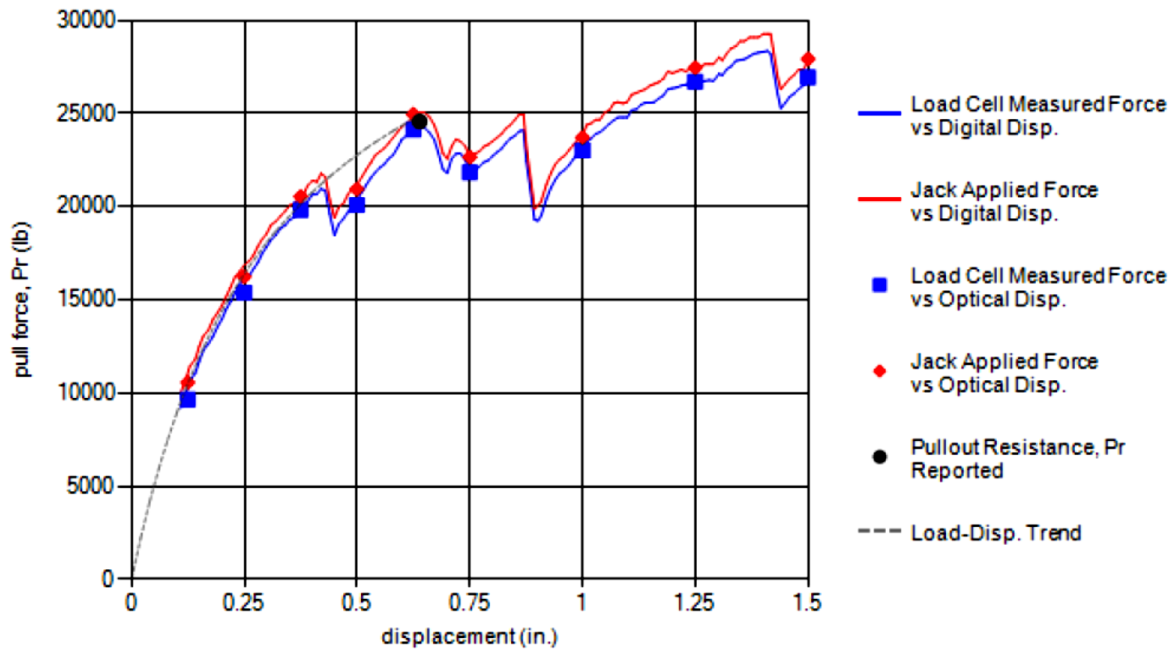


**Figure 5.38** Load-displacement Relationship Corresponding to a Welded Grid that Experienced Progressive Failure of Welded Connections; Peak Pullout Load at δ<0.75in (Test No. TS 32.11-G-9x6-W20xW7.5-L3-Z5-B)

A fourth type of load-displacement behavior for grids occurs when the reinforcement suffers rupture of a longitudinal bar.  This type of ultimate failure is analogous to section rupture of ribbed strips.  An example of a load-displacement relationship of this type is shown in Figure 5.39.  The pullout resistance factor, F* for this grid would be calculated based on the peak load it experienced at a displacement less than 0.75-in.
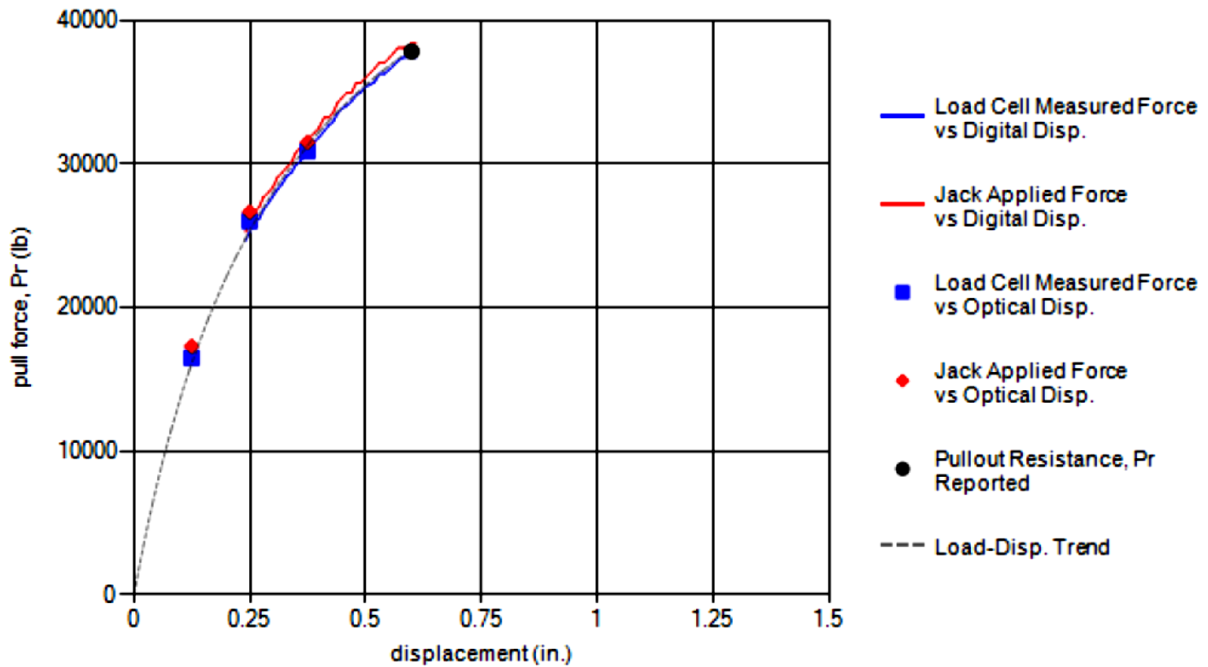


**Figure 5.39** Load-displacement Relationship for a Welded Steel Grid that Experienced Ultimate Rupture; Peak Pullout Load at δ<0.75in (Test No. TS 30.12-G-9x12-W20xW11-L6-Z12-B)

In order to determine potential influence of these different failure modes on F*, a variable called *Load-Displacement Behavior Type* was included in the pullout resistance database.  Subsequently, appropriate statistical data analyses were conducted to determine whether the Load-Displacement Behavior Type had any significant influence on calculated F* values.

# CHAPTER 6
# DATA REVIEW AND ANALYSIS

## 6.1 OVERVIEW

The pullout test program described in previous chapters included a total of 347 successfully completed pullout tests in Type B backfill and 303 successful tests in Type A backfill material. Accordingly, the total number of pullout tests completed in this research project is 650. The tests completed in Type B backfill consisted of 126 pullout tests on ribbed steel strips, 204 tests on welded steel grids and 17 tests on individual smooth bars. Similarly, Type A testing included 73 tests on ribbed steel strips, 214 tests on grids and 16 tests on individual smooth bars. Each one of these tests resulted in a pullout resistance factor, F* for the particular reinforcement-backfill combination. This chapter presents the data generated through the above test program. It also presents a critical review and statistical analysis of the data.

The AASHTO recommendations for default pullout resistance factors or F* parameters for strips and grids are shown in Figure 2.7. This figure presents F* as a function of the depth of embedment of the reinforcement measured from the top of the wall. Therefore, this particular chart format, *i.e.*, F* versus Depth of Fill, was selected as the appropriate format for presentation of data generated through this research. These charts provide a convenient means of comparing new data against AASHTO reference values. It also allows comparative review of data to determine the impact of different test variables on F*. Subsequently, appropriate statistical analyses were performed on the data obtained to determine which variables had the most significant influence on the measured F* and to develop predictive models for each reinforcement-backfill combination.

Section 6.2 provides a general overview of the statistical analysis procedures used. Section 6.3 deals with review and analysis of data collected from pullout tests conducted in Type B backfill material. Similarly, Section 6.4 deals with data corresponding to tests conducted in Type A material. As described in Chapters 4 and 5, this test program also included pullout tests on MSE reinforcement instrumented with strain gages. Data collected from strain gaged reinforcements in Type B and Type A backfill are presented in Section 6.5.

## 6.2    STATISTICAL ANALYSIS OF DATA

The statistical analysis procedures used were *analysis of variance* (ANOVA) and *nonlinear regression analysis*.  These procedures require that the data set meets the following prerequisite conditions: (a) normality, (b) homoscedasticity, and (c) independence.

*Normality:*

ANOVA and regression analysis are fairly robust against departures from the normality criterion. As long as the distribution is not extremely different from a normal distribution, inferences made from the regression line, regression coefficients, and ANOVA will not be seriously compromised.  The data used in this analysis met the normality requirement.

*Homoscedasticity:*

The homoscedasticity criterion is important in regression, especially when the goal is to provide predictions and associated confidence/prediction bounds.  It is also important when comparing several subsets of samples using ANOVA.  This data set clearly did not satisfy the requirement of homoscedasticity, also called uniformity of variance.   This is evidenced by the non-uniform variance in data over the range of depths of fill considered.  In other words, the variance is greatest at a depth of fill of 5ft and then it gradually decreases with increasing depth of fill.  To address this, F* data were transformed into *ln* (F*) which, based on *Box-Cox Transformation*, was found to be the optimum transformation to satisfy the homoscedasticity requirement.

*Independence:*

This condition stipulates that each data point should be independent of all the other data points. In other words, each data point should represent a new piece of information for the statistical model to be valid.

The statistical analysis procedure used with each data set followed the same basic steps.  First, an ANOVA was performed with *ln* (F*) as the *response variable* and the other variables of interest as *factors*.  The factors included those variables that are recognized in the current AASHTO F* equation as key variables.  For example, the current AASHTO F* equation recognizes *depth of fill* as a key variable that influences pullout resistance factor of

ribbed steel strips. Similarly, it recognizes *depth of fill, transverse bar diameter* and *transverse bar spacing* as key variables influencing pullout resistance factor of grid reinforcement. In addition to these variables, other variables that have potential influence on F* were also included in this analysis as factors. The *embedded length of the reinforcement, longitudinal bar spacing* and *longitudinal bar diameter* are examples of such variables. Factors used in ANOVA for both strip and grid type reinforcements are shown in Table 6.1.

**Table 6.1** Factors and Covariates Used in ANOVA

| Type of Reinforcement | Factors | | Covariates |
|---|---|---|---|
| | per AASHTO | Additional | |
| Ribbed Strips | • Depth of fill | • Embedment length<br>• Skew angle | • Test layer (vertical position of reinforcement in the test box)<br>• Overburden stress ratio |
| Welded Steel Grids | • Depth of fill<br>• Transverse bar diameter<br>• Transverse bar spacing | • Embedment length<br>• Longitudinal bar diameter<br>• Longitudinal bar spacing<br>• Splay angle | • Test layer<br>• Overburden stress ratio |

Also shown in Table 6.1 is a second set of variables identified as *covariates*. Covariates represent extraneous variables related to testing. The large test box used in this research could accommodate three layers of reinforcement in a single filling. Moreover, each layer of reinforcement consisted of multiple test specimens. Therefore, it was important to determine whether the position of the reinforcement within the test box (top, middle or bottom layer) had any impact on the measured F*. Another important test variable was the *overburden stress ratio (OSR)*. Once again, this variable becomes relevant because multiple test specimens were embedded and tested in the same test box. Ideally, a test specimen should not experience an overburden stress greater than its test overburden stress prior to being tested. However, this ideal condition could not be achieved for all test specimens in the test series. Therefore, overburden stress ratio was also introduced in the statistical analysis as a covariate. In this manner, any undue influence due to these extraneous variables on the response variable could be filtered out during statistical analysis.

An ANOVA analysis that includes covariates is known as *analysis of covariance*, or ANCOVA. The form of the ANCOVA model used in the present analysis is shown in Eq.6.1. This simple model, used for illustrative purposes, involves one factor A with $k$ levels and one covariate $x$, which is a numeric variable.

$$y_{ij} = \mu + \alpha_i + \beta x_{ij} + \varepsilon_{ij} \qquad\qquad (6.1)$$

where

$y_{ij} = j^{\text{th}}$ observation of the response variable at the $i^{\text{th}}$ level of A

$\mu$ = the intercept

$\alpha_i$ = the effect of the $i^{\text{th}}$ level of the factor A

$\beta$ = a slope parameter associated with the covariate $x_{ij}$ which is measured along with
$\quad y_{ij}$.

$\varepsilon_{ij}$ = the error term that is assumed to be normally distributed with mean zero and
$\quad$ constant variance.

Quite simply, this model allows a different linear regression line between $y$ and $x$ for each level of the factor A.

In cases where a predicted model is desired, the preliminary ANOVA is used to identify which variables are to be included in a nonlinear regression model to relate F* to the other variables. A nonlinear regression was necessary as opposed to linear regression because of the nature of the relationship between F* and Depth of Fill (DOF). It was found that a model of the following form (Eq.6.2) provided a very good fit for the data.

$$\ln(F^*) = \beta_0 + \beta_1 \cdot \exp(\beta_2 \cdot DOF) + \text{linear terms} \qquad\qquad (6.2)$$

where

$\quad\quad \beta_0, \beta_1,$ and $\beta_2$ = regression coefficients

$\quad\quad DOF$ $\quad\quad\quad$ = Depth of Fill

$\quad\quad$ Linear terms $\quad$ = test layer, OSR etc.

MINITAB version 16 was used to perform the nonlinear regression analysis using the Gauss-Newton optimization algorithm to find the least-squares estimators for the parameters.

## 6.3   PULLOUT RESISTANCE FACTORS MEASURED IN TYPE B BACKFILL

This section, which presents pullout resistance factors, *i.e.*, F* values measured in Type B backfill, is further divided into three sub-sections.  Sub-section 6.3.1 reviews pullout test data for strip reinforcement while sub-section 6.3.2 includes a review of pullout test data for grids.  The third section, Section 6.3.3 presents pullout tests data corresponding to smooth straight bars.

### 6.3.1   F* for Strip Reinforcements Embedded in Type B Backfill

F* parameters and other summary data for all strip reinforcements in Type B backfill are found in Appendix C of this volume, Volume 1 (See Tables C1 and C2).  In addition, data collected in each pullout test are presented in the form of a two-page test report.  Test reports for all 350 pullout tests conducted in Type B backfill are compiled in Volume 2 of this report.  Volume 2–Appendices F and G – includes all test reports for the 126 strip reinforcements.  Pullout test reports included in Appendix F represent strip reinforcements embedded in backfill compacted according to specifications (relative compaction = 95%) while those in Appendix G correspond to strips embedded in under-compacted backfill.

This section synthesizes and reviews these data.

#### 6.3.1.1 Presentation of F* Data for Strips in Type B Backfill

Figure 6.1 presents all data corresponding to ribbed strip reinforcements embedded in Type B backfill with 95% relative compaction.  This plot only includes data from reinforcements laid with zero skew angle.  Also shown in this plot is the AASHTO reference line for F* for strip reinforcement.  When plotting the AASHTO reference F* line, default soil parameters of $C_u = 4.0$ and $\phi = 34$-deg were used.   One observation that can be readily made is that nearly all of the measured F* values lie to the right hand side of the AASHTO reference line.  F* data obtained at shallow depths (*i.e.* depth < 20ft) plot to the right hand (conservative) side of the AASHTO reference line by a significant margin.
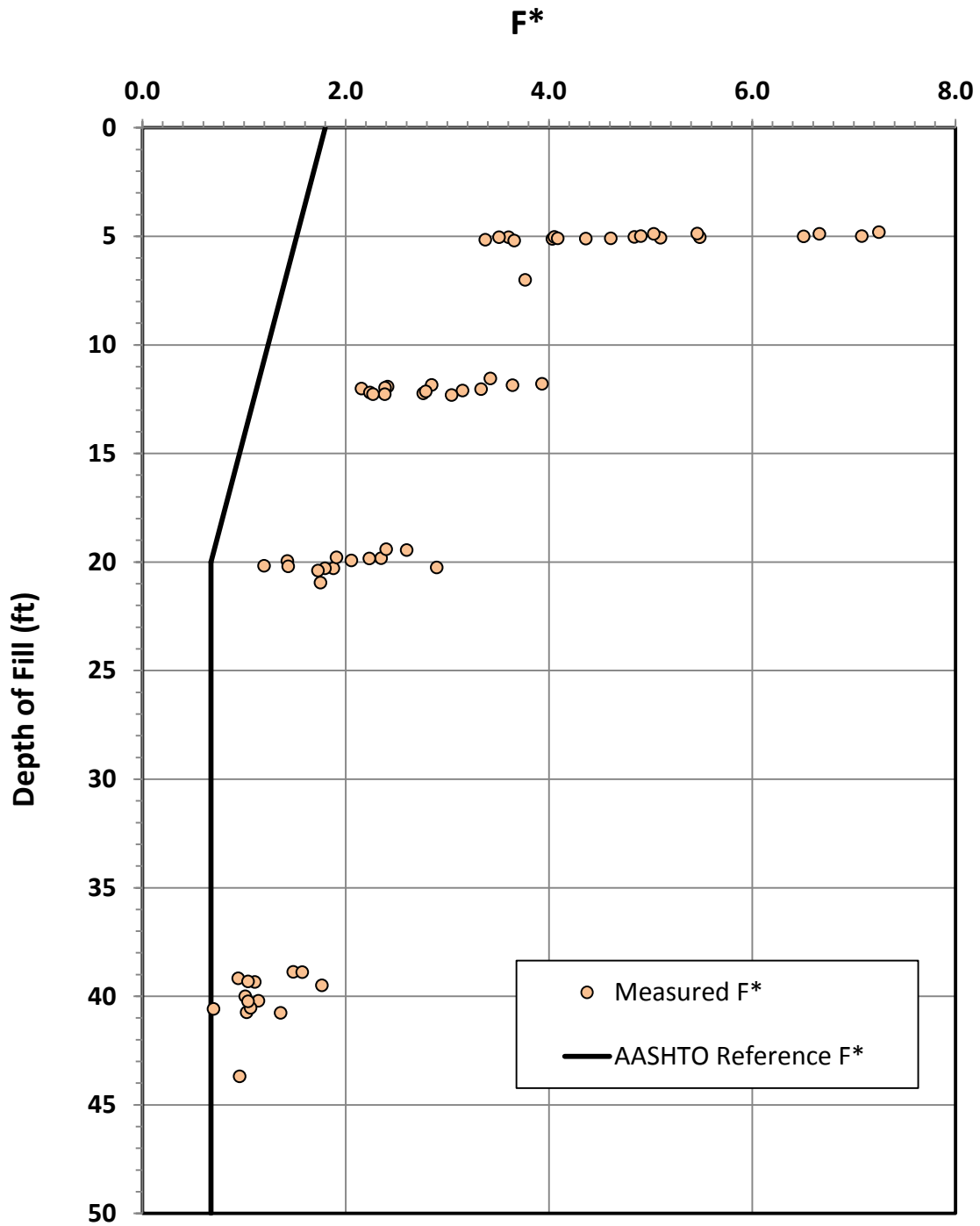
**Figure 6.1** F* versus Depth of Fill Chart for Ribbed Strip Reinforcement Embedded in Type B Backfill (Relative Compaction = 95%, Skew Angle = 0°)

*6.3.1.2 Predictive Model for F\* for Straight Strips in Type B Backfill*

The data presented in Figure 6.1 were subjected to systematic and detailed analysis using appropriate statistical analysis procedures. The primary objectives in this analysis were twofold: (a) analyze the database to identify those variables that have statistically significant influence on the measured F\*, and (b) develop an F\* prediction model and the corresponding prediction intervals based on the data set. The prediction limit corresponding to 95% confidence level would then be compared with the current AASHTO reference F\* line.

First, statistical analyses were performed on transformed F\*, i.e. *ln* (F\*), to develop an appropriate prediction model for F\*. In this analysis, *ln* (F\*) for all ribbed strip reinforcements was treated as the *dependent variable*. The most obvious among *independent variables* is the depth of fill. The dependence of F\* on depth of fill has been clearly established through previous test data, and is most pronounced over the depth range from 0 to 20ft. A second variable that was of interest was the length of reinforcement. Current AASHTO specifications assume that F\* is independent of the length of reinforcement. The length of reinforcement was included among the independent variables so that the validity of the assumption inherent in the current AASHTO specifications could be tested. Also included among the independent variables were a host of other variables that represent *test conditions* used during pullout testing. These variables included: the condition dictating the pullout load (0.75-in displacement or reinforcement rupture), the position of the reinforcement within the test box (top, middle or bottom layer), the order in which the tests were performed, maximum prior overburden stress, the number of times overburden stress on the reinforcement exceeded the test overburden stress, and the ratio between the maximum prior overburden stress and the test overburden stress. These test condition variables were included in the analysis so that any undue influence they may have on the measured F\* could be evaluated.

Table 6.2 presents the results from the ANOVA performed on the F\* data for straight strips. In this analysis the depth of fill emerged as the variable that has the most dominant influence on F\* (F = 101.19 and p=0.000). The effect of length of reinforcement was determined to be statistically insignificant (p=0.09). Among the test condition variables examined, the stress history, expressed in terms of ratio between the maximum prior

overburden stress and the test overburden stress (OSR), was identified as a significant variable influencing the measured F* (p=0.000). The test layer was found to be a second important variable (p=0.000).

**Table 6.2** Results from ANOVA: Straight Ribbed Steel Strips in Type B Backfill

**Analysis of Variance for log(F*), using Adjusted SS for Tests**

| Source | DF | Seq SS | Adj SS | Adj MS | F | P |
|---|---|---|---|---|---|---|
| OSR | 1 | 21.8005 | 1.0487 | 1.0487 | 28.71 | 0.000 |
| Test Layer | 2 | 0.1647 | 0.8755 | 0.4378 | 11.98 | 0.000 |
| Controlling Rupture Case | 1 | 1.0661 | 0.0151 | 0.0151 | 0.41 | 0.521 |
| Length | 3 | 2.8391 | 0.2434 | 0.0811 | 2.22 | 0.090 |
| Nominal Depth of Fill | 3 | 11.0893 | 11.0893 | 3.6964 | 101.19 | 0.000 |
| Error | 114 | 4.1643 | 4.1643 | 0.0365 | | |
| **Total** | **124** | **41.1240** | | | | |

The predictive model for F* should be free from any systematic influence from test condition variables. Therefore, standard test conditions were defined and then predictions made for these test conditions. The reinforcement placed in the middle layer would experience minimum interference from potential boundary effects and therefore, the middle layer was selected as the standard (or reference) test position. Similarly, a reinforcement on which the overburden stress never exceeded test overburden stress (maximum prior overburden stress equal to test overburden stress) was chosen as the reference.

Figure 6.2 shows the ribbed strip F* data along with the lower 95$^{th}$ predictive limit corresponding to the predictive model established for the data (dotted line). The solid line shown in this figure represents the AASHTO reference line for default F*. The predictive model and the corresponding 95% predictive limit represent standard test conditions for the laboratory test program. In other words, the F* predicted using the new model corresponds to the pullout resistance factor for a reinforcement embedded in the middle layer of the test box and tested using an overburden stress ratio of one. However, it should be noted that the F* data shown in Figure 6.2 represent the original, measured data.
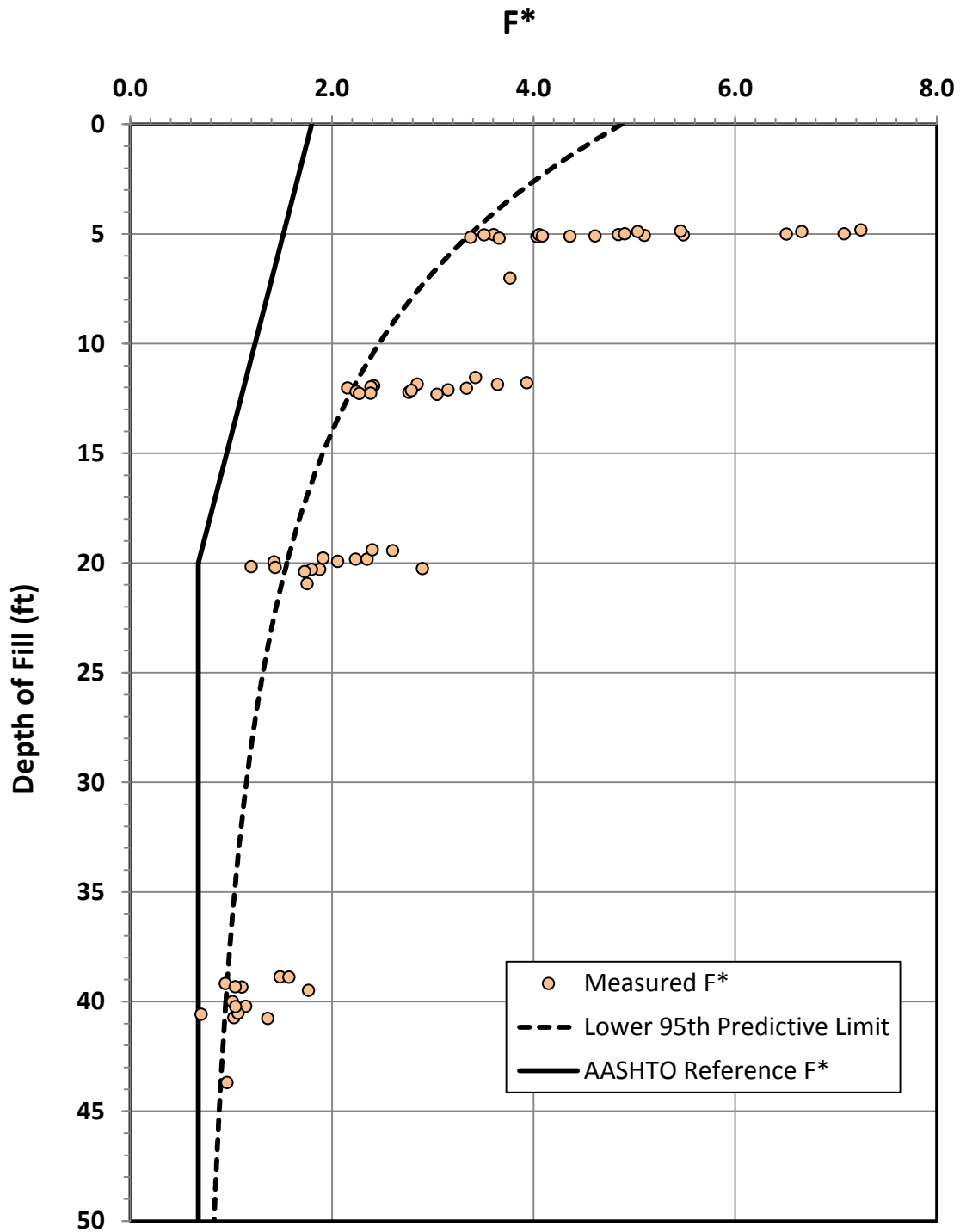
**Figure 6.2** Predictive Model for Ribbed Strip Reinforcement Embedded in Type B Backfill (Relative Compaction = 95%, Skew Angle = $0^0$)

### 6.3.1.3 Effect of Skewing on F* for Strips in Type B Backfill

As explained in Chapter 4, the test program on ribbed strip reinforcement also included a series of pullout tests on strips laid at skew angles of 15-deg and 30-deg. It should be noted that while pullout tests with zero skew were conducted over the entire depth range from 5ft to 40ft, pullout tests with 15-deg and 30-deg skew were conducted only at shallow depths (*i.e.*, 5ft and 12ft) where pullout behavior is most critical. Accordingly, the subset of F* data corresponding to 5 and 12ft of fill depth was analyzed using ANOVA to evaluate the effect of reinforcement skewing on pullout resistance.

ANOVA was conducted to determine possible influence due to skewing of strip reinforcement and considered two separate scenarios. In the first scenario, F* was calculated using the actual length of the reinforcement, L, rather than the reduced length in the direction of pull, L(cos β), in Figure 4.1. In this case, the pullout load capacity provided by the skew strip is directly compared to that provided by a strip of the same length but with no skew. Table 6.3 shows the results obtained by the ANOVA that examined the effect of skew with no adjustment made to the length of the reinforcement based on cosine projection.

**Table 6.3** Results from ANOVA: Effect of Skewing on F* for Ribbed Steel Strips in Type B Backfill (Without Cosine Projection)

**Analysis of Variance for log(F*), using Adjusted SS for Tests**

| Source | DF | Seq SS | Adj SS | Adj MS | F | P |
|---|---|---|---|---|---|---|
| OSR | 1 | 2.56093 | 0.10481 | 0.10481 | 2.05 | 0.173 |
| Test Layer | 2 | 0.57420 | 0.43696 | 0.21848 | 4.27 | 0.034 |
| Skew | 2 | 1.91101 | 0.49216 | 0.24608 | 4.81 | 0.024 |
| Nominal Depth of Fill | 1 | 2.24553 | 1.87229 | 1.87229 | 36.61 | 0.000 |
| Skew×Depth of Fill | 2 | 0.58710 | 0.58710 | 0.29355 | 5.74 | 0.014 |
| Error | 15 | 0.76703 | 0.76703 | 0.05114 | | |
| **Total** | **23** | **0.64579** | | | | |

The results from ANOVA shown in Table 6.3 indicate that, along with nominal depth of fill and test layer, the skew angle and an interaction term with skew and depth of fill are significant with p < 0.050. Accordingly, skewing of strip reinforcements has significant impact on their pullout resistance capacity. The presence of interaction between skew angle and depth of fill suggests that the effect of skewing will vary from one depth of fill to the

other.  This interaction effect is graphically shown in Fig. 6.3.
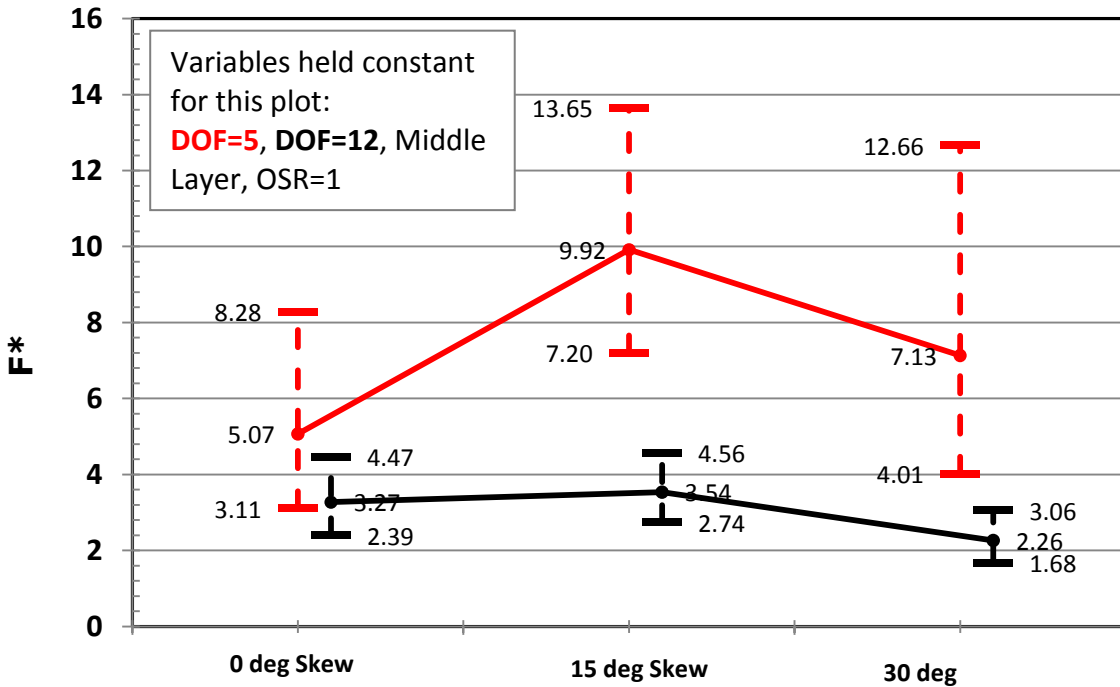


**Figure 6.3**  Effect of Skewing on the Pullout Resistance of Ribbed Strip Reinforcement Embedded in Type B Backfill (without Cosine Projection)

Further statistical analysis of the ln (F*) data using the *Tukey Method* provided the groupings shown in Table 6.4.  This table compares ln (F*) data for each depth of fill and skew angle.  The groups that do not share a letter are statistically different from each other.  This analysis shows that at 15-deg skew, ln (F*) are not statistically different from zero skew at both depths of fill.  At 30-deg skew a similar conclusion can be reached for a depth of fill of 5ft but not for a depth of fill of 12ft.

Next the analysis is repeated with F* values adjusted using cosine projection.  This represents AASHTO policy that requires an increase in the length of the reinforcement so that the projected length in the direction of pull will be the same as the length of a reinforcement with no skew.  Table 6.5 summarizes the findings from this ANOVA.

**Table 6.4** Results from Tukey Analysis: Effect of Skewing on F* for Ribbed Steel Strips in Type B Backfill (Without Cosine Projection)

| DOF | Skew (deg) | N | Mean Ln (F*) | Grouping | | | |
|---|---|---|---|---|---|---|---|
| 5 | 0 | 4 | 1.535 | A | B | | |
| | 15 | 3 | 2.171 | A | | | |
| | 30 | 3 | 1.732 | A | B | | |
| 12 | 0 | 5 | 1.097 | | B | | |
| | 15 | 5 | 1.140 | | B | | |
| | 30 | 4 | 0.585 | | | C | |

**Table 6.5** Results from ANOVA: Effect of Skewing on F* for Ribbed Steel Strips in Type B Backfill (With Cosine Projection)

**Analysis of Variance for ln(F*), using Adjusted SS for Tests**

| Source | DF | Seq SS | Adj SS | Adj MS | F | P |
|---|---|---|---|---|---|---|
| OSR | 1 | 2.62688 | 0.10481 | 0.10481 | 2.05 | 0.173 |
| Test Layer | 2 | 0.54667 | 0.43696 | 0.21848 | 4.27 | 0.034 |
| Skew | 2 | 1.62194 | 0.34835 | 0.17418 | 3.41 | 0.060 |
| Nominal Depth of Fill | 1 | 2.24553 | 1.87229 | 1.87229 | 36.61 | 0.000 |
| Skew×Depth of Fill | 2 | 0.58710 | 0.58710 | 0.29355 | 5.74 | 0.014 |
| Error | 15 | 0.76703 | 0.76703 | 0.05114 | | |
| **Total** | **23** | **8.39514** | | | | |

This analysis reveals that skew is marginally significant (p=0.060) and Skew×Depth of fill is significant (p=0.014). Figure 6.4 illustrates this effect. Subsequently, analysis was conducted using the Tukey Method to examine the effect of skewing at 15-deg versus 30-deg. Table 6.6 summarizes the results from this analysis. These result suggest that at each depth, one letter is shared among all three skew angles. This means, once the cosine projection is applied, there is no statistical difference between F* values obtained from reinforcements with 0, 15 and 30-deg skew. However, statistical difference exists between F* values obtained for 5ft of fill and 12 ft of fill.

Figure 6.5 compares F* values obtained for skewed strips versus the general population.
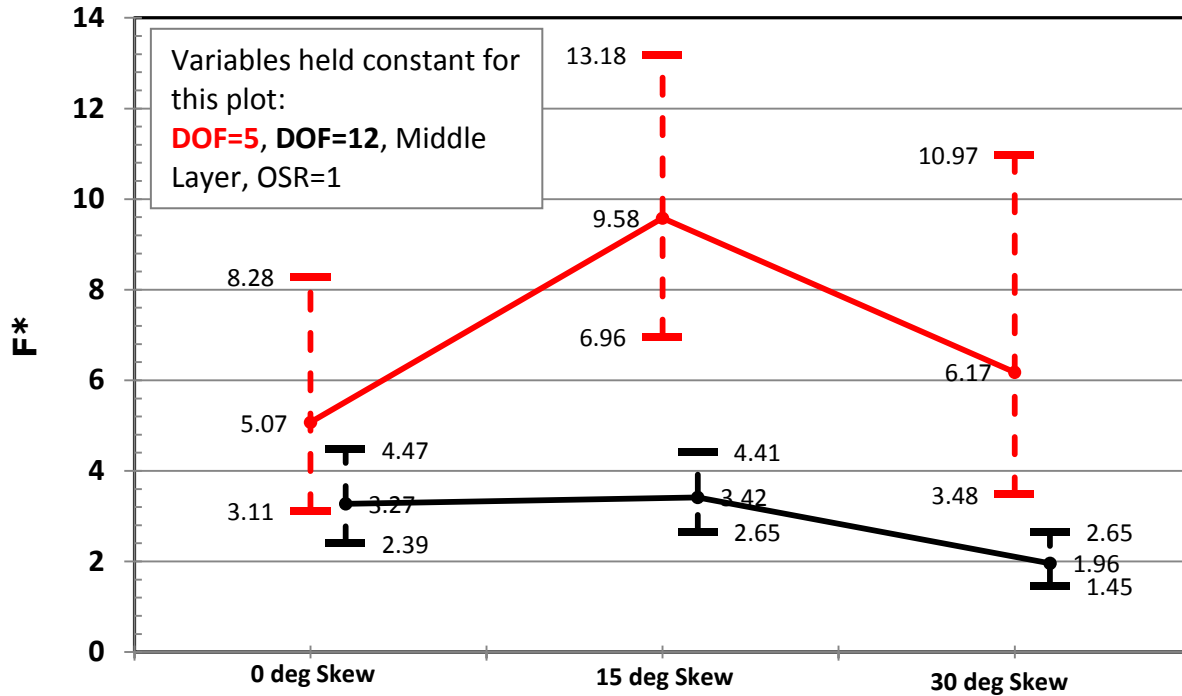
**Figure 6.4** Effect of Skewing on the Pullout Resistance of Ribbed Strip Reinforcement Embedded in Type B Backfill (with Cosine Projection)

**Table 6.6** Results from Tukey Analysis: Effect of Skewing on F* for Ribbed Steel Strips in Type B Backfill (With Cosine Projection)

| DOF | Skew (deg) | N | Mean Ln (F*) | Grouping | | | |
|-----|-----------|---|--------------|---|---|---|---|
| 5 | 0 | 4 | 1.535 | A | B | C | |
| | 15 | 3 | 2.206 | A | | | |
| | 30 | 3 | 1.876 | A | B | | |
| 12 | 0 | 5 | 1.097 | | | C | D |
| | 15 | 5 | 1.174 | | B | C | D |
| | 30 | 4 | 0.728 | | | | D |

**Figure 6.5**  F* versus Depth of Fill Chart for Ribbed Strip Reinforcement Embedded in Type B Backfill (Relative Compaction = 95%): Effect of Skewing

*6.3.1.4   Effect of Relative Compaction on F\* for Strips in Type B Backfill*

All of the data presented above were obtained from tests conducted using backfill Type B compacted to achieve a relative compaction of 95% in accordance with the requirements of TxDOT *Standard Specifications* Item No. 423.  The appropriate lift thickness and number of passes with the vibratory compactor needed to achieve this compaction level was determined by trial and error in early stages of the test program.

During this trial-and-error stage, several test set ups were completed using a different compaction protocol that yielded a lower level of compaction. This compaction protocol provided a relative compaction of 91%.  All of these pullout tests were later repeated at the 95% relative compaction.  However, the data obtained from those tests conducted at 91% relative compaction were retained, as this allowed general evaluation of the effect of compaction condition on the pullout resistance of ribbed strip reinforcements.

Figure 6.6 compares pullout resistance factors obtained at 91% relative compaction with those obtained at 95% relative compaction.  Based on the data presented in this figure, the backfill compaction level has significant influence on the pullout resistance factor of ribbed steel strips, lower compaction levels yielding lower F\* values.  This finding is confirmed by the results from ANOVA summarized in Table 6.7.   ANOVA shows that relative compaction is among the most significant variables (F=51.14, p=0.000).  Figure 6.6.7 provides a comparison between the 95% confidence intervals for the mean F\* for specified and under-compacted conditions for a depth of fill of 12ft.   It should be noted that the mean values and confidence limits shown in Figure 6.7 are values predicted by the model.  In other words, they represent the mean and confidence limits that are expected when all testing is performed under standard test conditions (*e.g.*, for reinforcements placed in the middle layer, overburden stress ratio = 1.0, etc).
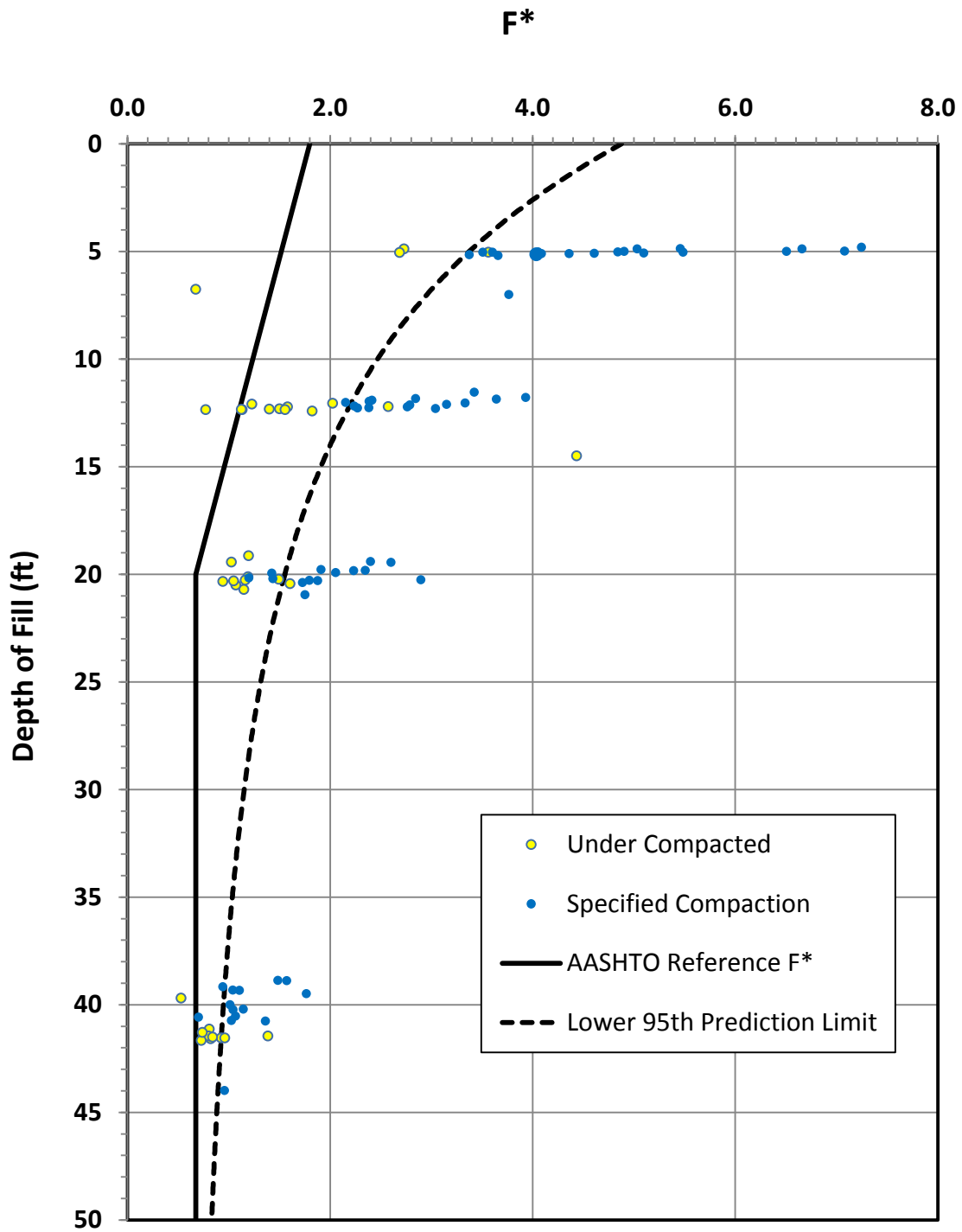
**Figure 6.6** F* versus Depth of Fill Chart for Ribbed Strip Reinforcement Embedded in Type B Backfill: Effect of Under-Compaction

**Table 6.7** Results from ANOVA: Effect of Under-Compaction on F\* for Ribbed Steel Strips
in Type B Backfill

**Analysis of Variance for ln(F\*), using Adjusted SS for Tests**

| Source | DF | Seq SS | Adj SS | Adj MS | F | P |
|---|---|---|---|---|---|---|
| OSR | 1 | 20.2536 | 1.2438 | 1.2438 | 15.95 | 0.000 |
| Test Layer | 2 | 0.0340 | 0.1824 | 0.0912 | 1.17 | 0.314 |
| Skew | 2 | 8.7226 | 2.3666 | 1.1833 | 15.18 | 0.000 |
| Nominal Depth of Fill | 3 | 11.6931 | 8.6047 | 2.8682 | 36.79 | 0.000 |
| Rupture | 1 | 0.0587 | 0.0023 | 0.0023 | 0.03 | 0.864 |
| Length | 4 | 1.0663 | 1.5086 | 0.3771 | 4.84 | 0.001 |
| Compaction Class | 1 | 3.9875 | 3.9875 | 3.9875 | 51.14 | 0.000 |
| Error | 111 | 8.6550 | 8.6550 | 0.0780 | | |
| **Total** | **125** | **54.4708** | | | | |
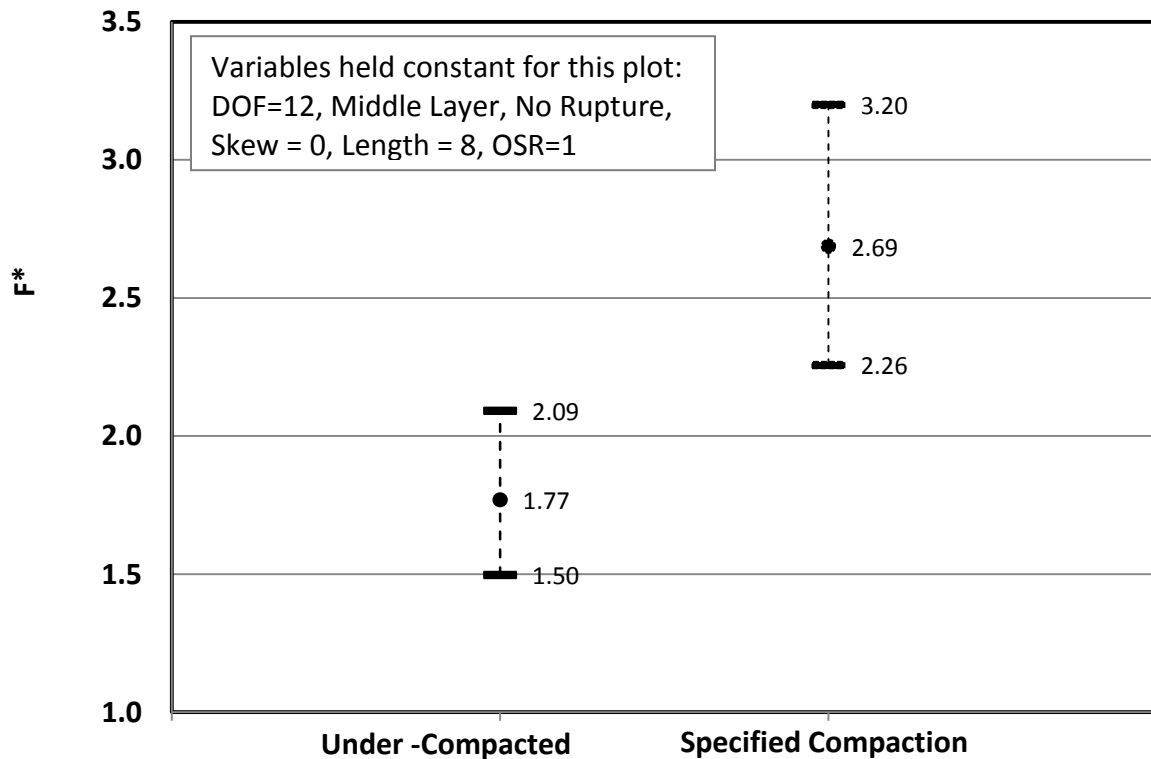


**Figure 6.7** 95% Confidence Intervals for the Mean F\* for Specified and Under-Compacted
Conditions (Depth of fill = 12ft, Length = 8ft)

### 6.3.2  F* for Grid Reinforcement Embedded in Type B Backfill

F* parameters obtained for the 207 welded steel grid reinforcements embedded in Type B backfill are summarized in Appendix C-Table C3 of this report. Report Volume 2-Appendix H includes all the test reports for grid reinforcements tested in Type B backfill. This section synthesizes and reviews these F* data.

#### 6.3.2.1  Presentation of F* Data for Grids in Type B Backfill

As noted previously, in AASHTO equations, F* for inextensible grids is expressed as a function of $t/S_t$ where t is the transverse bar diameter and $S_t$ is the transverse bar *spacing*. Normalization of F*, achieved by dividing F* by $t/S_t$, allows direct comparison of F* values for grids with various bar sizes and spacings. Therefore, all F* plots presented in this section are in the form of normalized F*, *i.e.* $F*S_t/t$, versus Depth of Fill charts.

Figure 6.8 presents data corresponding to all straight grid reinforcements embedded in Type B backfill. The dotted line represents the most conservative lower 95th percent predictive limit corresponding to grids typical of TxDOT MSE wall projects. Also shown in this plot is the AASHTO reference line for $F*S_t/t$ for grid reinforcement. It is important to note that these data have been determined for welded steel grids that have a wide range of longitudinal and transverse bar sizes and spacings. The data scatter seen in Figure 6.8 is primarily a result of this. Subsequent analyses show that data scatter is significantly less when groups of grids with similar bar spacings are considered. An important observation that can be made is that nearly all of the measured values of normalized F* data lie to the right hand side of the AASHTO reference line.

#### 6.3.2.2  Normalized F* for Straight Grids in Type B Backfill; Effect of Length

The AASHTO procedure for estimating F* for grid reinforcement assumes that the pullout resistance factor, F* is independent of the length of embedment of the reinforcement. Section 4.3.2.1 described the development of a test matrix to test the validity of this claim. Table 6.8 shows the results obtained from an ANOVA conducted on the data collected on the subset of grids tested for embedment length effect. According to the results obtained from the ANOVA, the embedment length of the grid was not statistically significant ($p=0.132>0.05$). In other words, the data collected in this research supported the underlying assumption in the AASHTO equation for F* for grid reinforcement embedded in Type B

backfill.  Figure 6.9 compares the 95% confidence intervals for the mean normalized F* for grids with lengths of 3ft, 6ft, 9ft and 12ft.
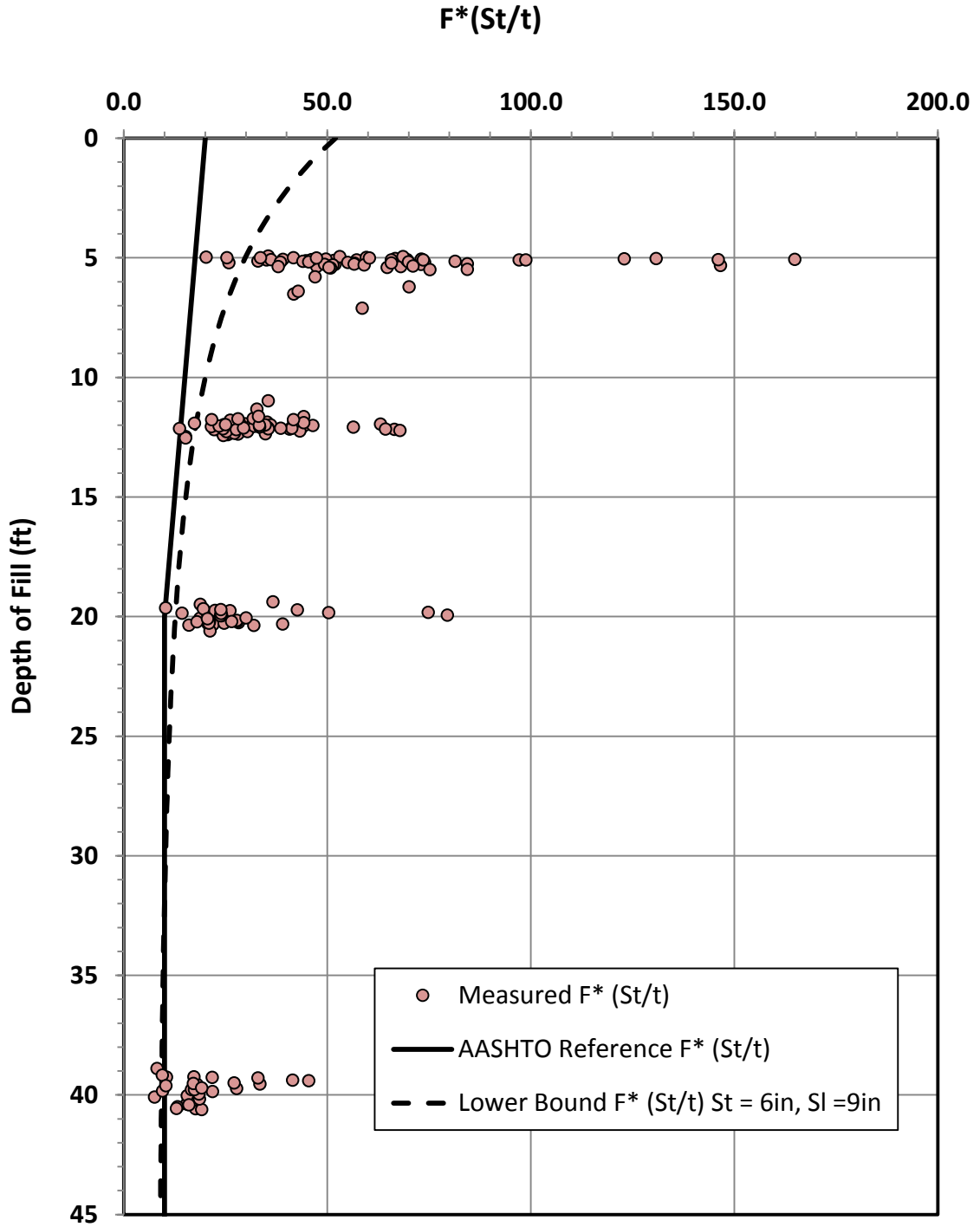


**Figure 6.8** Normalized F* versus Depth of Fill Chart for Grid Reinforcement Embedded in Type B Backfill (Relative Compaction = 95%, Splay Angle = 0°)

**Table 6.8** Results from ANOVA: Effect of Embedment Length on Normalized F* of Grid Reinforcement in Type B Backfill

**Analysis of Variance for log(Norm F*), using Adjusted SS for Tests**

| Source | DF | Seq SS | Adj SS | Adj MS | F | P |
|---|---|---|---|---|---|---|
| OSR | 1 | 1.02031 | 0.06031 | 0.06031 | 3.76 | 0.081 |
| Nominal Depth of Fill | 1 | 0.07356 | 0.15808 | 0.15808 | 9.85 | 0.011 |
| Length | 3 | 0.10887 | 0.11398 | 0.03799 | 2.37 | 0.132 |
| Test Layer | 2 | 0.03456 | 0.03456 | 0.01728 | 1.08 | 0.377 |
| Error | 10 | 0.16049 | 0.16049 | 0.01605 | | |
| **Total** | **17** | **1.39778** | | | | |
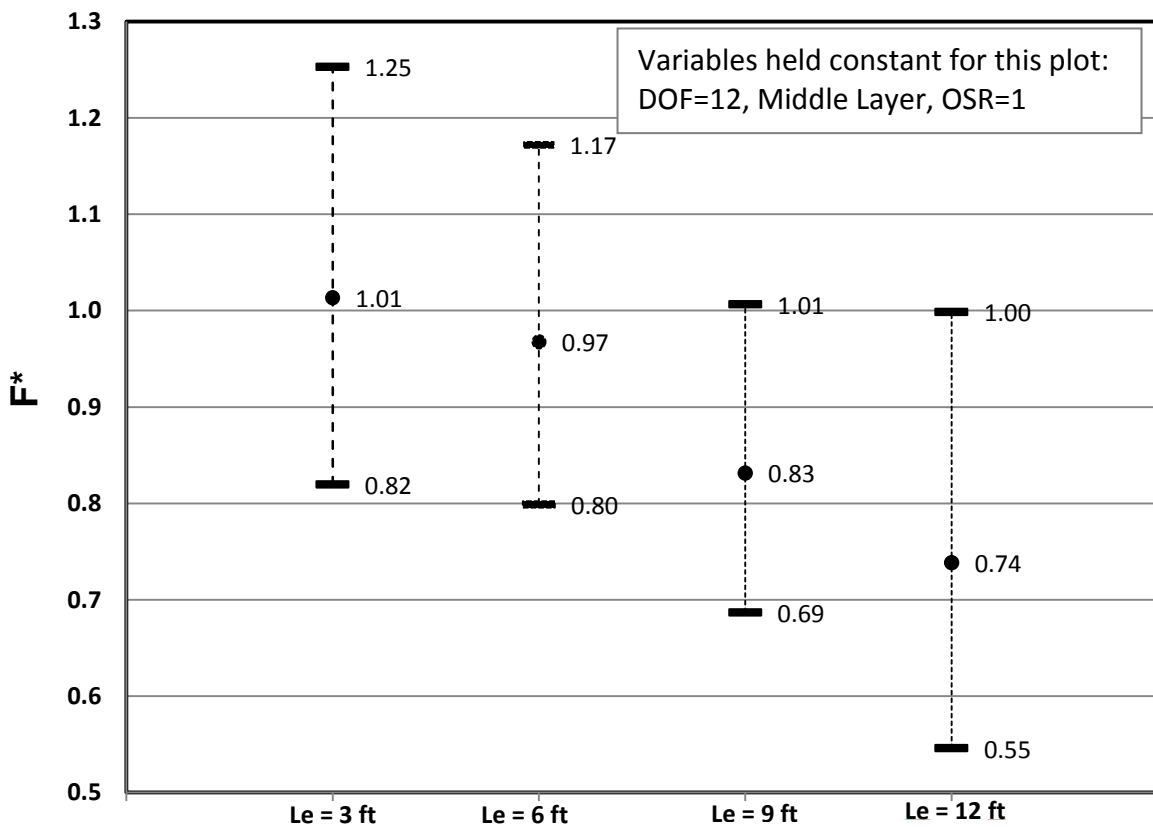


**Figure 6.9** Evaluating Length Effect of Welded Steel Grid in Type B Backfill Compacted to Specification and Zero Splay

### 6.3.2.3    Normalized F* for Straight Grids in Type B Backfill; Effect of Transverse Bar Size and Spacing

The next phase of data review and analysis explored the effect of transverse bar size and spacing.   According to the AASHTO design equation, F* for grids varies linearly with $t/S_t$, where t is the transverse bar diameter and $S_t$ is the transverse bar spacing.   Accordingly, the normalized F*, *i.e*. $F*(S_t/t)$ should be independent of both t and $S_t$.   The results from an ANOVA performed to test the validity of this premise are shown in Table 6.9.

The results from ANOVA, while supporting the view that normalized F* for grids is independent of the transverse bar diameter, shows definite influence of the transverse bar spacing (p=0.000).   Figure 6.10 shows the normalized F* data for each transverse bar spacing.   It also shows the lower 95th limits corresponding to predictive models developed for grids when differentiated by transverse bar spacing, 6, 12, 18 and 24-inches.   The predictive models indicate that the normalized F* was the lowest for grids with transverse bar spacing of 6-in.   A significant increase in normalized F* is observed when the transverse bar spacing is increased from 6-in to 12-in.   A transverse bar spacing of 18-in provides the highest normalized F* and therefore, appears to be the optimum.

**Table 6.9**  Results from ANOVA: Effect of Transverse Bar Diameter and Spacing on Normalized F* of Grid Reinforcement in Type B Backfill

| Analysis of Variance for ln (Norm F*), using Adjusted SS for Tests | | | | | | |
|---|---|---|---|---|---|---|
| **Source** | **DF** | **Seq  SS** | **Adj SS** | **Adj  MS** | **F** | **P** |
| **OSR** | 1 | 14.6936 | 0.1364 | 0.1364 | 4.94 | 0.029 |
| **Nominal Depth of Fill** | 4 | 9.1127 | 0.8682 | 2.9561 | 107.01 | 0.000 |
| **Test Layer** | 2 | 0.9263 | 1.2172 | 0.6086 | 22.03 | 0.000 |
| **Load-Displ Behavior Type** | 1 | 0.0838 | 0.0217 | 0.0217 | 0.79 | 0.377 |
| **Transverse Bar Diameter** | 2 | 0.1132 | 0.1628 | 0.0814 | 2.95 | 0.057 |
| **Transverse Bar Spacing** | 3 | 1.8351 | 1.8497 | 0.6166 | 22.32 | 0.000 |
| **Tran Bar Dia*Tran Bar Spac** | 6 | 0.1248 | 0.1248 | 0.0208 | 0.75 | 0.608 |
| **Error** | 97 | 2.7071 | 2.7071 | 0.0276 | | |
| **Total** | 116 | 29.5966 | | | | |
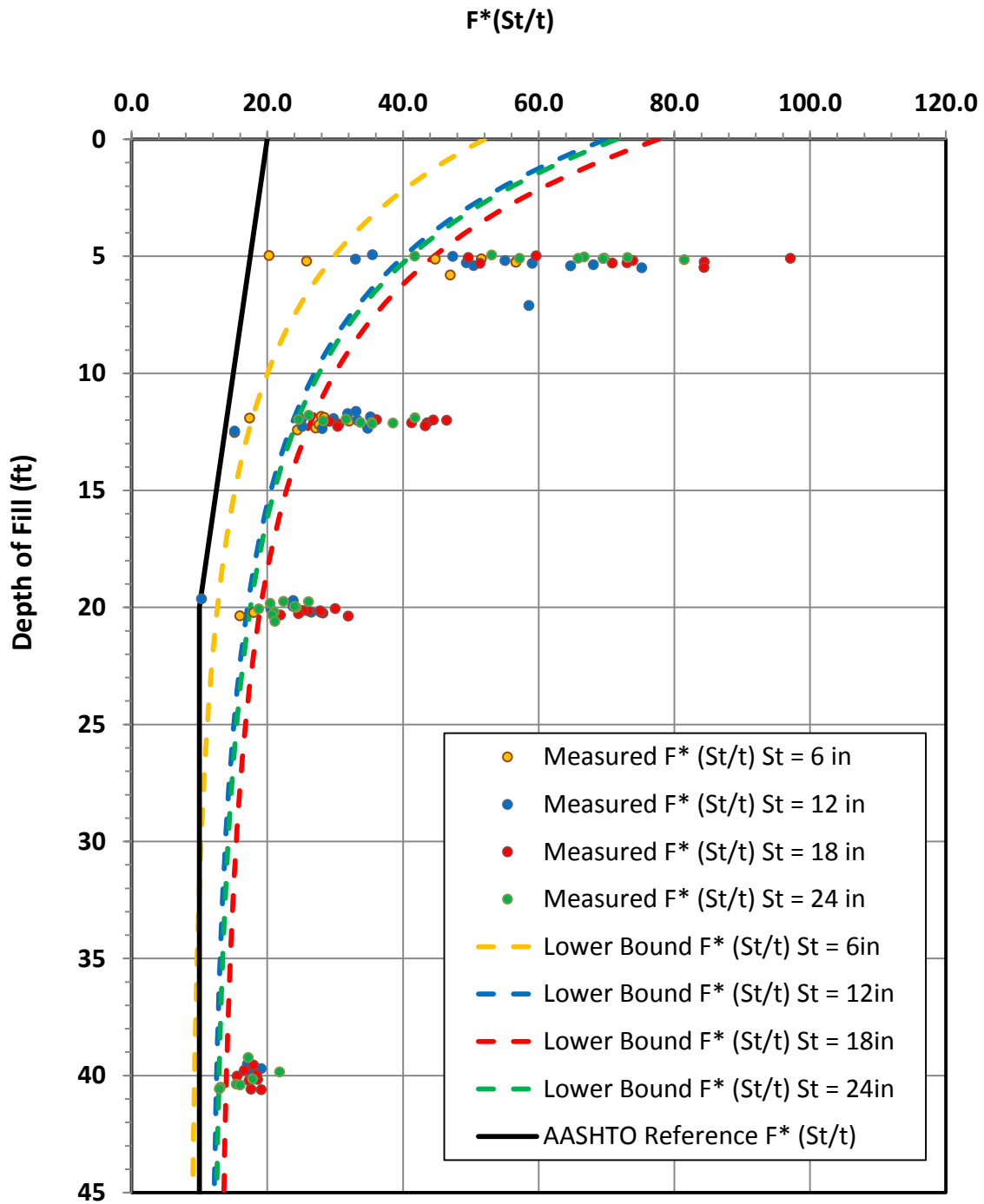
**Figure 6.10** Normalized F* versus Depth of Fill Chart for Grid Reinforcement Embedded in Type B Backfill: Effect of Transverse Bar Spacing
(Relative Compaction = 95%, Angle of Splay = 0°)

Published literature indicates that the optimum transverse bar spacing for inextensible grids is 6in or greater (*1, 2*). There are two mechanisms that may contribute to the observed increase in normalized F* from a transverse bar spacing of 6in to 18in. The first is increased frictional resistance provided by longer length of longitudinal bars in grids with larger transverse bar spacing. The second mechanism has to do with likely interaction that may be taking place between adjacent transverse bars. As the grid is pulled through compacted backfill, it is expected that large strains will develop within the material in the immediate vicinity of each transverse bar. When transverse bars are close to each other, the zones of disturbed material associated with adjacent bars may overlap with each other causing a reduction of the pullout capacity. The influence of transverse bar spacing on normalized F* is further illustrated in Figure 6.11. This figure compares the 95% confidence intervals for the mean normalized F* for grids with transverse bar spacing of 6in, 12in, 18in and 24in.
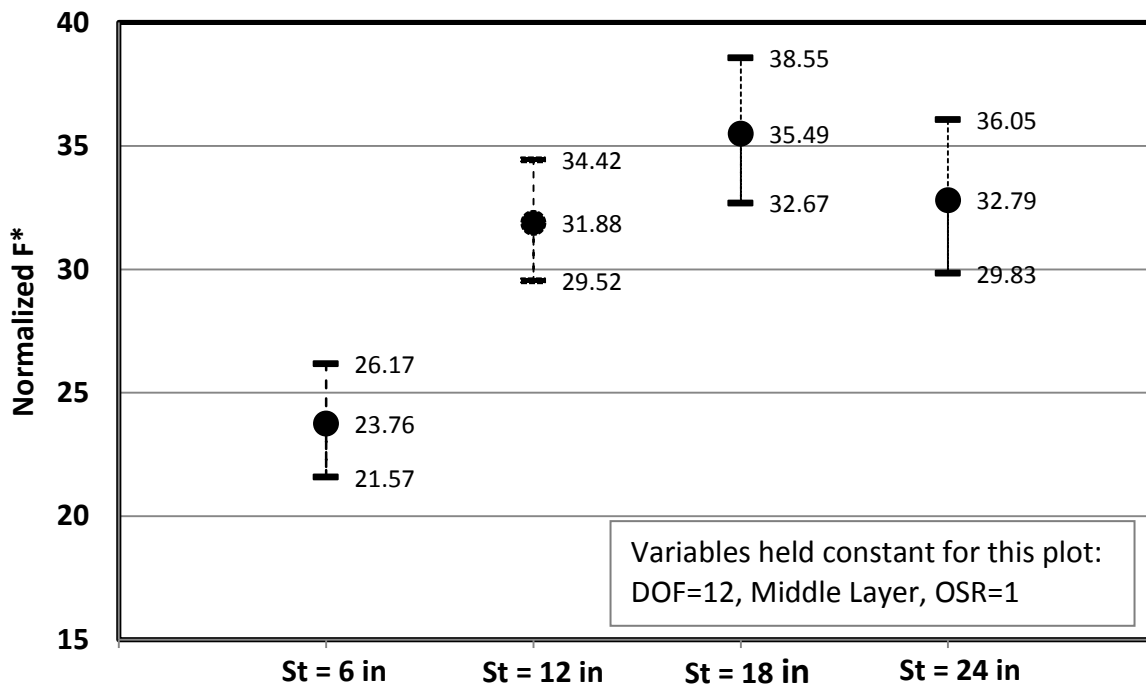


**Figure 6.11**  95% Confidence Intervals for the Mean Normalized F* for Transverse Bar Spacings of 6in, 12in, 18in and 24in (Depth of fill = 12ft)

*6.3.2.4  Normalized for F\* for Straight Grids in Type B Backfill; Effect of Longitudinal Bar Size and Spacing*

The next analysis of pullout resistance data on grids examined the influence of longitudinal bar size and spacing on normalized F\*.   According to conventional theory, these two parameters have no influence on the pullout resistance factor for grid reinforcement.  Accordingly, the current AASHTO and other procedures used in the estimation of F\* do not incorporate longitudinal bar size or spacing.

The results from the ANOVA on the influence of longitudinal bar size and spacing are shown in Table 6.10.  As described in Chapter 4, this portion of the pullout test program included grids with two longitudinal bar sizes, W9.5 and W20, and four different longitudinal bar spacings, 2, 6, 9 and 12-in.  The transverse bar size and spacing were kept constant at W11 and 12-in respectively.  The findings from the ANOVA show that the longitudinal bar spacing has significant influence on the normalized F\* (p=0.000) while the influence of the longitudinal bar size was not significant (p=0.780>0.05).   A grid that has closely spaced longitudinal bars would offer stiffer resistance during pullout because closely-spaced longitudinal bars restrain the transverse bars against deformation.  As a result, grids with smaller longitudinal bar spacings will yield higher normalized F\*. Figure 6.12 shows normalized F\* versus Depth of Fill plots for grids for different longitudinal bar spacing and the lower 95th prediction limits for grids with longitudinal bar spacings, 2, 6, 9 and 12-in.. Figure 6.13 compares the mean normalized F\* for these four grid categories for a depth of fill of 12ft.

**Table 6.10**  Results from ANOVA: Effect of Longitudinal Bar Diameter and Spacing on Normalized F* of Grid Reinforcement in Type B Backfill

**Analysis of Variance for log(Norm F*), using Adjusted SS for Tests**

| Source | DF | Seq SS | Adj SS | Adj MS | F | P |
|---|---|---|---|---|---|---|
| OSR | 1 | 7.0777 | 0.2938 | 0.2938 | 8.77 | 0.004 |
| Nominal Depth of Fill | 3 | 5.7446 | 3.0177 | 1.0059 | 30.04 | 0.000 |
| Test Layer | 2 | 0.4156 | 0.4727 | 0.2363 | 7.06 | 0.002 |
| Load-Displ Behavior Type | 1 | 6.7091 | 0.2291 | 0.2291 | 6.84 | 0.011 |
| Longitudinal Bar Diameter | 1 | 0.2643 | 0.0026 | 0.0026 | 0.08 | 0.780 |
| Longitudinal Bar Spacing | 3 | 6.3485 | 5.7332 | 1.9111 | 57.07 | 0.000 |
| Long Bar Dia*Long Bar Spac | 3 | 0.0286 | 0.0286 | 0.0095 | 0.29 | 0.836 |
| Error | 57 | 1.9087 | 1.9087 | 0.0335 | | |
| **Total** | **71** | **28.4972** | | | | |

**Figure 6.12** Normalized F* versus Depth of Fill Chart for Grid Reinforcement Embedded in Type B Backfill: Effect of Longitudinal Bar Spacing
(Relative Compaction = 95%, Angle of Splay = 0°)

**Figure 6.13** 95% Confidence Intervals for the Mean F* for Longitudinal Bar Spacings of 2in, 6in, 9in and 12in (Depth of fill = 12ft)

### 6.3.2.5  *Normalized for F\* for Cut and Splayed Grids in Type B Backfill*

This section evaluates the effect of cutting-and-splaying of grid reinforcement on the normalized pullout resistance factors.   Similar to the analysis conducted on skewed strip reinforcement, this analysis also considered two separate cases: effect of splaying when the cosine projection is not used, and effect of splaying when the cosine projection is used. Table 6.11 presents the results from the ANOVA conducted when no cosine projection was used.

**Table 6.11**  Results from ANOVA: Effect of Cut-and-Splay on Normalized F* of Grid Reinforcement in Type B Backfill (Without Cosine Projection)

| Analysis of Variance for ln (Norm F*), using Adjusted SS for Tests | | | | | | |
|---|---|---|---|---|---|---|
| Source | DF | Seq  SS | Adj SS | Adj  MS | F | P |
| OSR | 1 | 0.32656 | 0.00000 | 0.00000 | 0.00 | 0.993 |
| Nominal Depth of Fill | 1 | 1.57908 | 1.30633 | 1.30633 | 37.96 | 0.000 |
| Test Layer | 2 | 0.30428 | 0.25037 | 0.12518 | 3.64 | 0.061 |
| Splay | 2 | 0.07028 | 0.07028 | 0.03514 | 1.02 | 0.392 |
| Error | 11 | 0.37854 | 0.37854 | 0.03441 | | |
| Total | 17 | 2.65873 | | | | |

The results from the above analysis reveal that, for this case, the normalized F* for grids that are splayed was not significantly different from those measured for grids with no splay (p=0.392).  Figure 6.14 compares mean F* for grids with different splay angles.  Next the analysis was repeated for the case in which cosine projection was used.  The results from this second ANOVA are shown in Table 6.12.  Once again, the effect of splay is found to be not significant (p=0.194).  These results are shown graphically in Figure 6.15.  These observations suggest that when grid reinforcements in Type B backfill are cut-and-splayed, then the resulting F* values will not be significantly different from those of straight grids.

**Table 6.12**  Results from ANOVA: Effect of Cut-and-Splay on Normalized F* of Grid Reinforcement in Type B Backfill (With Cosine Projection)

| Analysis of Variance for ln (Norm F*), using Adjusted SS for Tests | | | | | | |
|---|---|---|---|---|---|---|
| Source | DF | Seq  SS | Adj SS | Adj  MS | F | P |
| OSR | 1 | 0.22793 | 0.00000 | 0.00000 | 0.00 | 0.993 |
| Nominal Depth of Fill | 1 | 1.70084 | 1.30633 | 1.30633 | 37.96 | 0.000 |
| Test Layer | 2 | 0.33266 | 0.25037 | 0.12518 | 3.64 | 0.061 |
| Splay | 1 | 0.13147 | 0.13147 | 0.06574 | 1.91 | 0.194 |
| Error | 1 | 0.37854 | 0.37854 | 0.03441 | | |
| Total | 17 | 2.77144 | | | | |
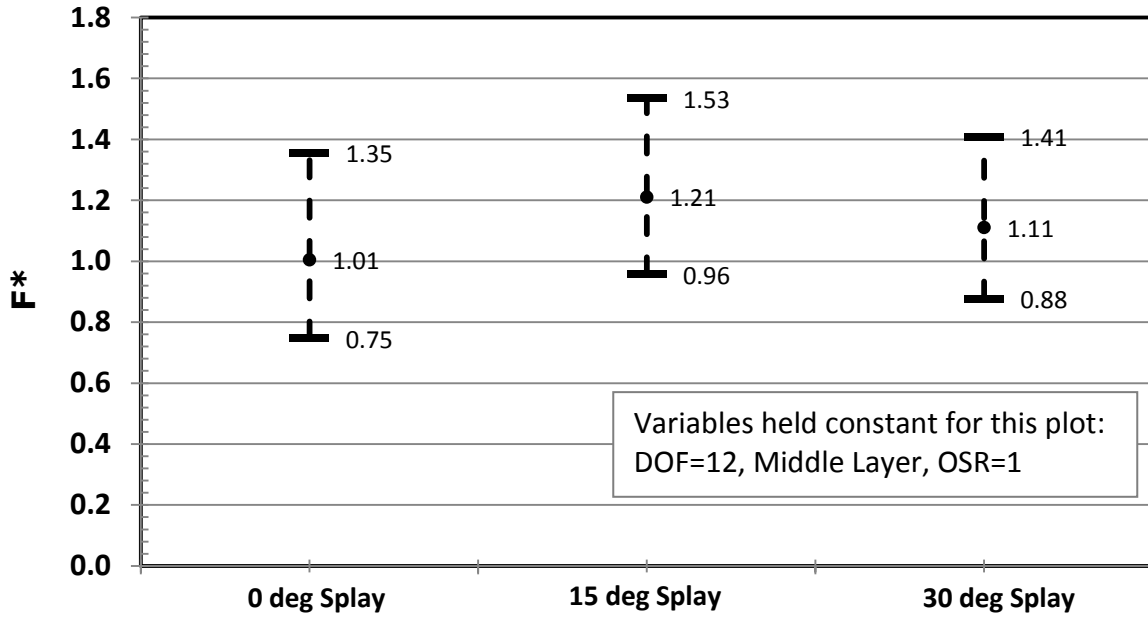
**Figure 6.14**  Mean F* for Grids in Type B Backfill with Splay Angles of 0, 15 and 30-deg when no Cosine Projection is Used (Depth of fill = 12ft)



**Figure 6.15**  Mean F* for Grids in Type B Backfill with Splay Angles of 0, 15 and 30-deg when Cosine Projection is Used (Depth of fill = 12ft)

### 6.3.3    F* for Smooth Straight Bars in Type B Backfill

As mentioned in Sec 4.3.2.5, the last series of pullout tests conducted in Type B backfill investigated the pullout resistance of smooth straight bars.  The test matrix for this test series, shown in Table 4.11, included eighteen pullout tests.   The pullout resistance factors for the smooth bars were calculated from the measured pullout loads using the same procedure as that used for strip reinforcement.  In this calculation, the cross section peripheral distance of $\pi D$ was used instead of the *2b* used in the case of strips.  The resulting F* values are provided in Table C4 of Appendix C.  The results obtained from ANOVA are given in Table 6.8.  This analysis shows that both depth of fill and length of reinforcement are significant at a level of 0.05.  The bar diameter, however, was not found to be significant. Figure 6.16 compares the mean normalized F* for smooth straight bars for lengths of 3ft and 6ft at a depth of fill of 12ft.

The primary objective of this test series was to evaluate the relative contribution of frictional resistance mobilized on longitudinal bars on the overall pullout resistance of welded steel grids.   Table 6.14 provides results from an analysis conducted to determine relative contribution to pullout capacity from longitudinal bars in a welded steel grid with three bars.  The third column in this table shows the pullout capacity expected from three longitudinal bars based on measured pullout resistance.  This capacity is then compared with the average pullout resistance measured for grids with the same length and at the same depth of fill.   The data shown reveal that the contribution from the frictional resistance on longitudinal bars can be quite significant in a typical grid with three longitudinal bars.

However, a more careful review of the underlying mechanisms governing pullout resistance suggests that such a conclusion may not be strictly valid.  First, the contact between the longitudinal bars and backfill will be different when transverse bars are present. In other words, the presence of transverse bars can alter the nature of the interaction that takes place between longitudinal bars and backfill.   Also, frictional and bearing resistance components of pullout resistance mobilize at different rates of relative displacement and therefore, their maximum values may not be reached simultaneously at the specified 0.75-in displacement.

**Table 6.13** Results from ANOVA: Pullout Resistance Factor, F* for Smooth Straight Bars in Type B Backfill

**Analysis of Variance for log(F*), using Adjusted SS for Tests**

| Source | DF | Seq SS | Adj SS | Adj MS | F | P |
|---|---|---|---|---|---|---|
| OSR | 1 | 1.78991 | 0.06254 | 0.06254 | 0.87 | 0.378 |
| Test Layer | 2 | 2.38403 | 0.43806 | 0.21903 | 3.05 | 0.104 |
| Length | 1 | 0.16041 | 0.62190 | 0.62190 | 8.66 | 0.019 |
| Bar Diameter | 1 | 0.69724 | 0.00902 | 0.00902 | 0.13 | 0.732 |
| Nominal Depth of Fill | 3 | 1.25305 | 1.25306 | 0.41768 | 5.82 | 0.021 |
| Error | 8 | 0.57452 | 0.57452 | 0.07182 | | |
| **Total** | **16** | **6.85916** | | | | |
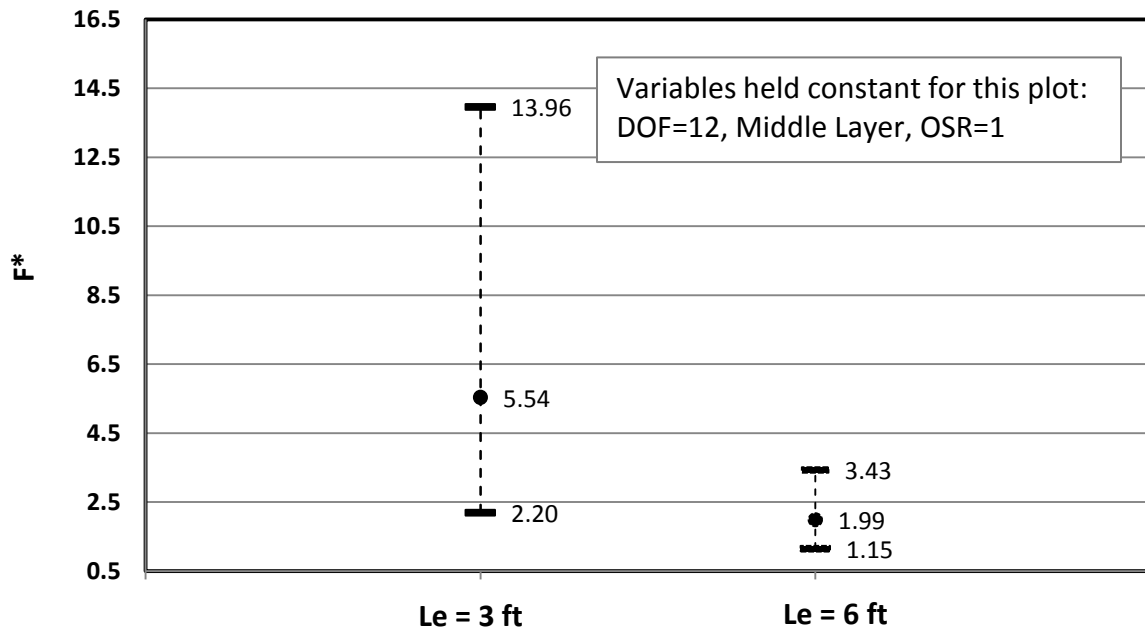


**Figure 6.16** 95% Confidence Intervals for the Mean F* for Straight Smooth Bars in Type B Backfill Compacted to Specification

**Table 6.14** Percent Contribution from Longitudinal Bars to Pullout Capacity of Welded Grids with Three Longitudinal Bars in Type B Backfill

| DOF, z (ft) | Longitudinal Bar Size | Pullout Resistance, Pr (lb) | 2" Longitudinal Bar Spacing Grid | 6" Longitudinal Bar Spacing Grid | 9" Longitudinal Bar Spacing Grid | 12" Longitudinal Bar Spacing Grid |
|---|---|---|---|---|---|---|
| 5 | W9.5 | 1762 | 47% | 29% | 33% | 34% |
| 12 | W9.5 | 3129 | 157% | 86% | 82% | 73% |
| 5 | W20 | 2813 | 100% | 51% | 41% | 45% |
| 12 | W20 | 3212 | 89% | 51% | 37% | 37% |
| 20 | W20 | 3902 | 59% | 32% | 44% | 47% |
| 40 | W20 | 2949 | 69% | 38% | 37% | 53% |

## 6.4 PULLOUT RESISTANCE FACTORS MEASURED IN TYPE A BACKFILL

This section presents a review of pullout resistance factor data collected for MSE reinforcements embedded in Type A backfill.   It is subdivided into three parts.  Section 6.4.1 reviews pullout test data for strip reinforcements. Section 6.4.2 reviews pullout test data for grid reinforcements.  The third and final section, Section 6.4.3 presents pullout test data corresponding to smooth straight bars.

### 6.4.1  F* for Strip Reinforcements Embedded in Type A Backfill

Test reports that include detailed data collected for each pullout test conducted in Type A backfill are included in Volume 3 of this report.   Volume 3-Appendix L includes all test reports for the 74 strip reinforcements tested.  Statistical analyses of these data are presented in the following sections.

### 6.4.1.1  *Presentation of F* Data for Straight Strips in Type A Backfill*

F* parameters calculated from strip reinforcement testing conducted in Type A backfill are listed in Table D1, Appendix D.  Figure 6.17 presents these data in the form of F* versus Depth of Fill chart.  Also shown in this plot is the 95th lower predictive limit for this data set.  The next figure, Figure 6.18, compares Type A ribbed strip data with the data obtained for ribbed strips embedded in Type B backfill.  It can be readily seen that the F* values measured for reinforcements embedded in Type A backfill are significantly higher than the corresponding F* for Type B.  The separation between the two curves is greatest at depths less than 20ft.

In the next step, Analysis of Variance (ANOVA) described in Sec. 6.2 was performed on the ribbed strip F* dataset to identify variables that have significant influence on the measured pullout resistance factors.  The variables included in this analysis were nominal depth of fill and the reinforcement length.  These variables were treated as *factors* in the ANOVA.  The covariates used in the above analysis included test layer (top, middle, bottom), overburden stress ratio (OSR) and controlling rupture case.  The last variable, *i.e.* controlling rupture case, was used to distinguish between those strip reinforcements that ruptured at displacements less than 0.75in and those that did not experience rupture.  Based on the definition used in this research, the pullout resistance factors were calculated using
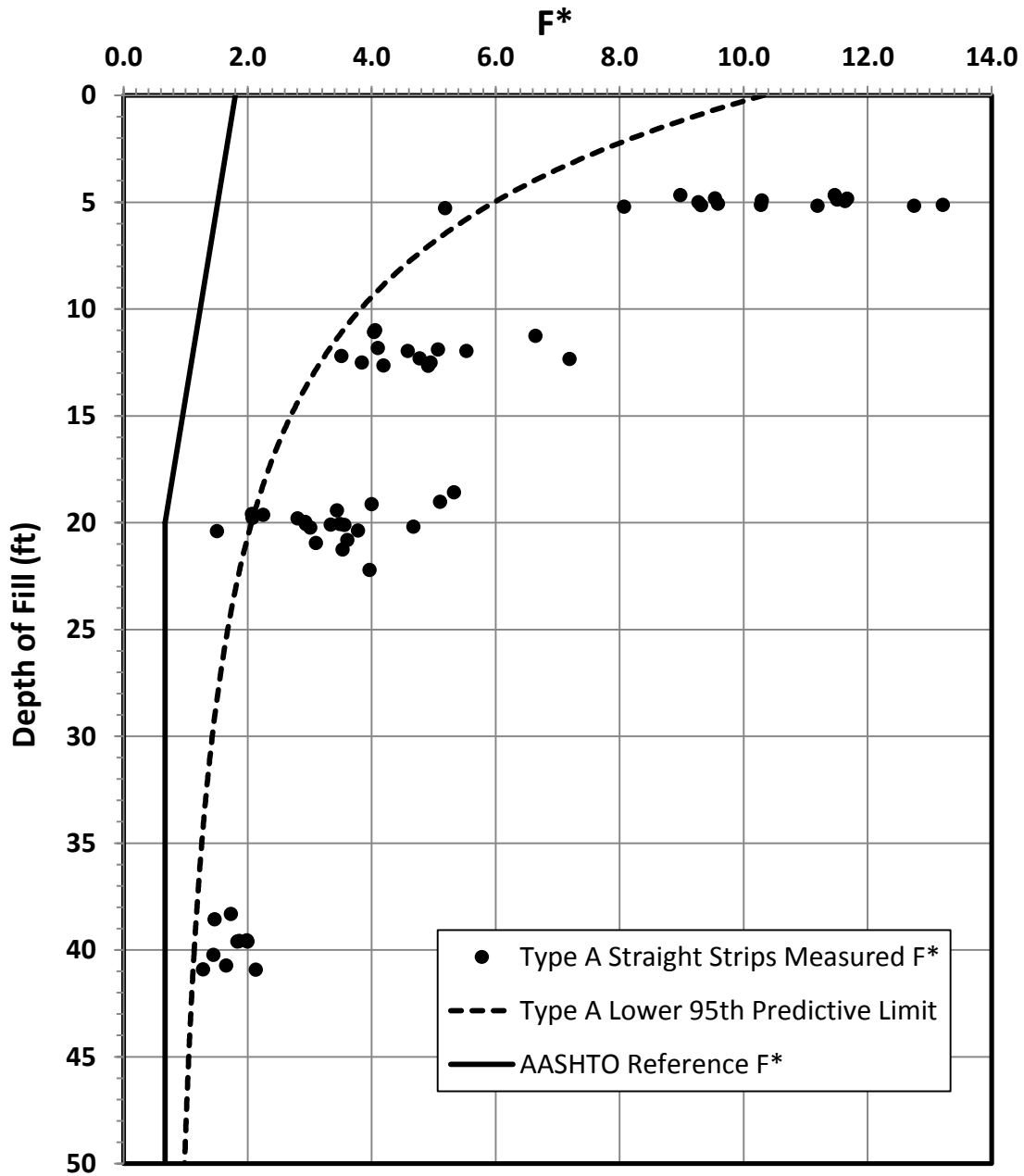
**Figure 6.17** F* versus Depth of Fill Chart for Ribbed Strip Reinforcements Embedded in Type A Backfill (Ordinary Compaction, Skew Angle = 0°)
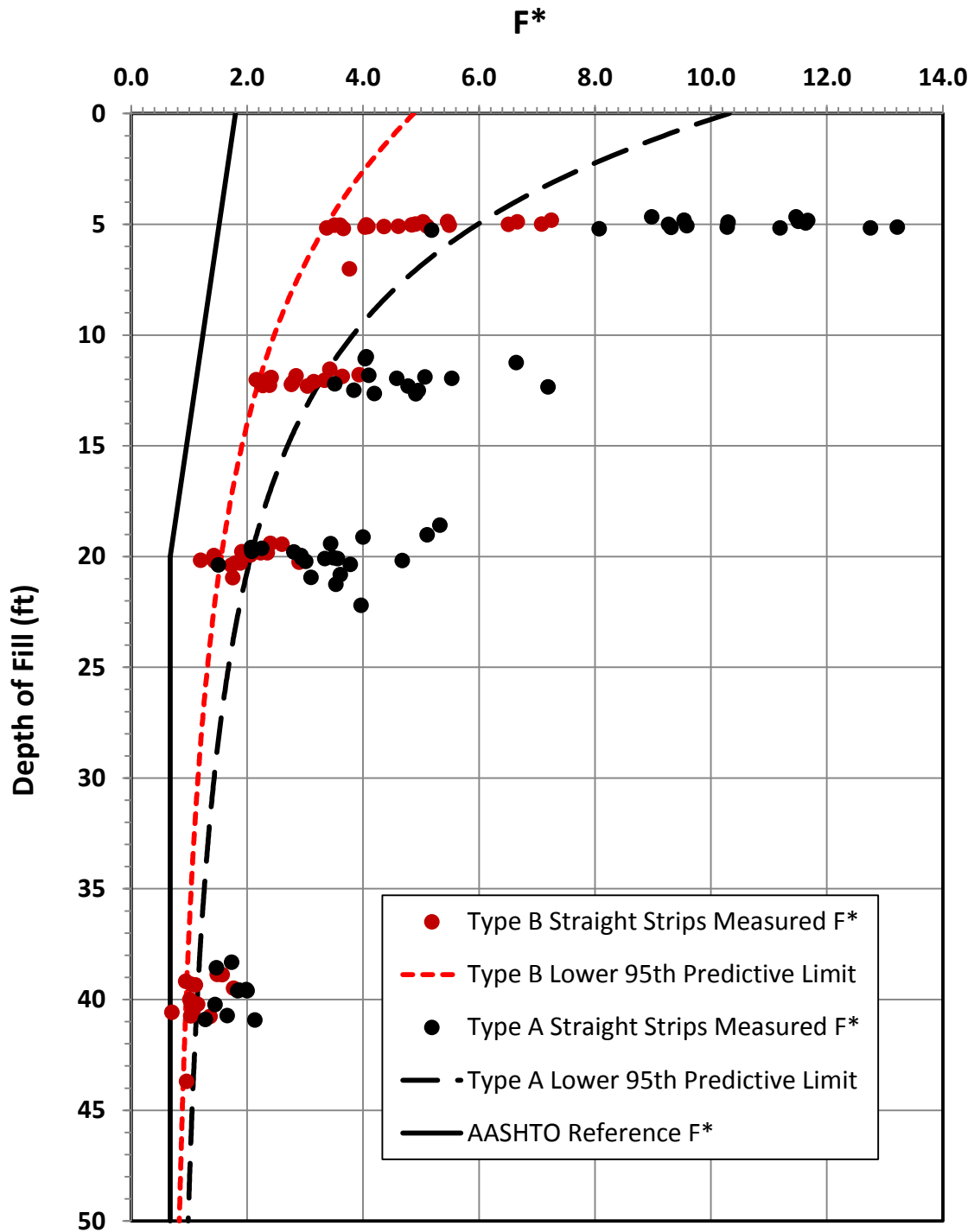
**Figure 6.18** Comparison of F* Data for Straight Ribbed Strip Reinforcement in Type A and Type B Backfills (Skew Angle = 0°)

the maximum pullout force measured at a displacement equal to or less than 0.75in (*2*).
Accordingly, when reinforcements experienced rupture before 0.75-in displacement, the F*
was calculated using pullout force at rupture displacement.  Therefore, it was of interest to
determine whether reinforcement rupture had significant influence on the measured F*.  The
results obtained from ANOVA are shown in Table 6.15.

**Table 6.15 Results from ANOVA: Straight Ribbed Steel Strips in Type A Backfill**

| Analysis of Variance for ln (F*), using Adjusted SS for Tests | | | | | | |
|---|---|---|---|---|---|---|
| **Source** | DF | Seq  SS | Adj SS | Adj  MS | F | P |
| **OSR** | 1 | 3.5515 | 0.1284 | 0.1284 | 3.98 | 0.052 |
| **Nominal Depth of Fill** | 3 | 18.2127 | 14.1852 | 4.7284 | 146.59 | 0.000 |
| **Test Layer** | 3 | 0.5109 | 0.3832 | 0.1916 | 5.94 | 0.005 |
| **Length** | 3 | 1.1592 | 1.0166 | 0.3389 | 10.51 | 0.000 |
| **Controlling Rupture Case** | 3 | 0.1361 | 0.1361 | 0.1361 | 4.22 | 0.045 |
| **Error** | 50 | 1.6128 | 1.6128 | 0.0323 | | |
| **Total** | 60 | 25.1832 | | | | |

The results from the ANOVA show that, once again, the nominal depth of fill has the
most dominant influence on pullout resistance factor, F* (F=146.59, p=0.000).
Reinforcement length emerged as a second significant variable (F=10.51, p=0.000) after the
depth of fill.  It is important to note that the dependence of measured F* on embedment
length of reinforcement is not consistent with the existing AASHTO F* formulation for
inextensible reinforcements.  Embedment length effect was observed in Type B test data
although not found to be statistically significant.  On the other hand, analysis of F* data
collected on both strips and grids in Type A backfill consistently showed that measured F*
varied with reinforcement length.  In all cases examined, the measured F* decreased with
increasing embedment length.  Fig. 6.19 shows F* versus Embedment Length, $L_e$ for straight
ribbed reinforcement corresponding to a 12ft depth of fill.   A definitive explanation for the
observed trend could not be established based on the data collected from this research study.
Plausible explanations involve boundary effects and ultimate limit state effects associated

with our large scale test system. The predictive models developed in this study used the longest reinforcement length which represented the most conservative conditions.
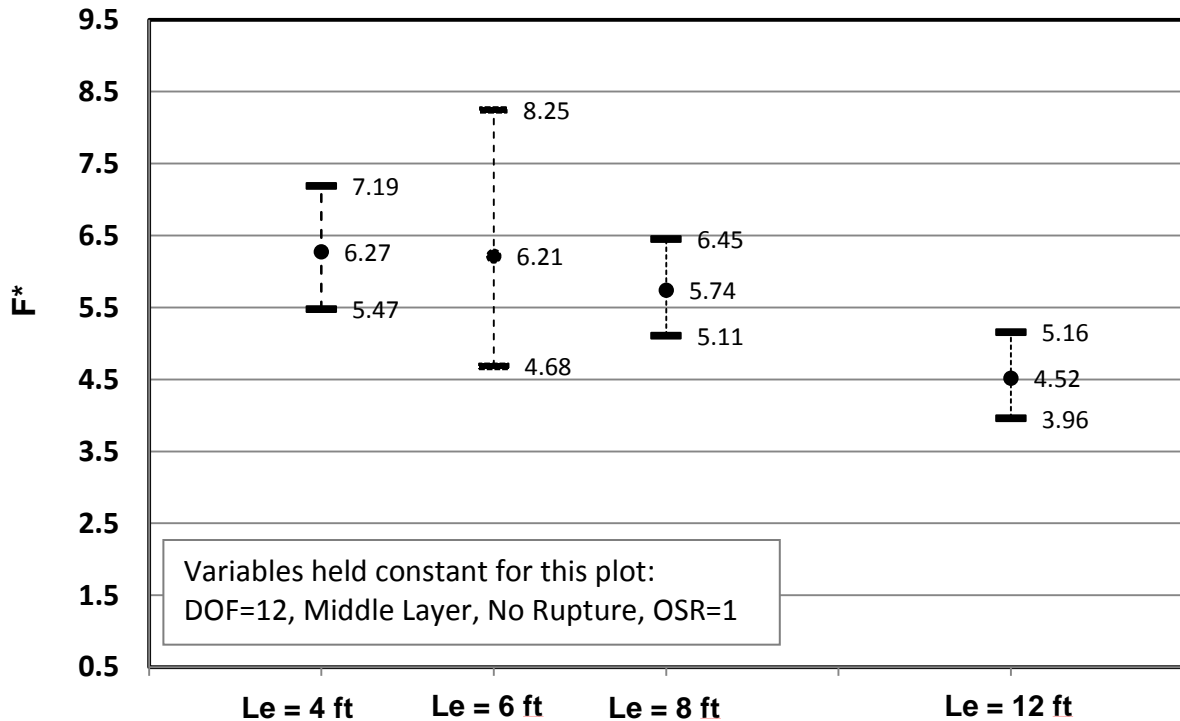


**Figure 6.19** Evaluating Length Effect for Ribbed Strips Embedded in Type A Backfill

In addition to the depth of fill and reinforcement length, the test layer was found to be a significant variable (p=0.005). Also, *Overburden Stress Ratio* (OSR) and *Controlling Rupture Case* were found to be marginally significant (p=0.052 and p=0.045 respectively). In subsequent statistical analysis that involved development of a predictive model and the lower 95th predictive limit for F*, these parameters were fixed at following values: embedment length = 12ft, Test Layer = Middle, OSR = 1.0 and Controlling Rupture Case = No Rupture. The lower 95th predictive limit that was established in this manner for straight strips embedded in Type A backfill is shown in Figure 6.18 as a long dashed line. This line yields lower-bound F* values that are significantly higher than those corresponding to AASHTO and Type B reference lines. The margin of separation between these lines is greatest at zero depth. The lines gradually converge at greater depths.

### 6.4.1.2 *Effect of Skewing on F* for Strips in Type A Backfill*

The next phase of ribbed strip reinforcement testing in Type A backfill investigated

the effect of skewing on pullout resistance capacity.   Accordingly, a series of pullout tests were performed with strips laid at skew angles of 15-deg and 30-deg.  Fig. 6.20 compares the F* data obtained from skewed strip reinforcement with F* data for straight strips.

The pullout tests for skewed reinforcements were conducted only at depths of 5ft and 12ft, while pullout tests with zero skew were conducted over the entire depth range.  The subset of F* data corresponding to 5ft and 12ft depths of fill were analyzed using ANOVA to evaluate the effect of reinforcement skewing on pullout resistance.  The data analysis to determine the effect of skew was conducted for two separate conditions.  The first condition represented situations in which the strip reinforcement will be placed at skew but with no adjustment made to the pullout force based on the cosine projection.   Table 6.16 shows the results obtained from the ANOVA conducted for this case.  This analysis shows that, along with nominal depth of fill and test layer, the skew angle and an interaction term with skew and depth of fill are all significant with $p < 0.050$.  In other words, skewing strip reinforcements have significant impact on their pullout resistance capacity.  Furthermore, the effect of skewing will vary from one depth of fill to the other.   This is graphically shown in Fig. 6.21.

**Table 6.16  Results from ANOVA: Effect of Skewing on F* for Ribbed Steel Strips in Type A Backfill (Without Cosine Projection)**

| Analysis of Variance for ln (F*), using Adjusted SS for Tests | | | | | | |
|---|---|---|---|---|---|---|
| **Source** | DF | Seq  SS | Adj SS | Adj  MS | F | P |
| **OCR** | 1 | 0.34303 | 0.00373 | 0.00373 | 0.18 | 0.672 |
| **Nominal Depth of Fill** | 1 | 3.85367 | 2.12713 | 2.12713 | 105.22 | 0.000 |
| **Test Layer** | 1 | 0.76267 | 0.64131 | 0.32065 | 15.86 | 0.000 |
| **Length** | 1 | 0.02775 | 0.00634 | 0.00634 | 0.31 | 0.582 |
| **Controlling Rupture Case** | 1 | 0.00375 | 0.00001 | 0.00001 | 0.00 | 0.982 |
| **Skew** | 2 | 0.36737 | 0.36797 | 0.18399 | 9.10 | 0.002 |
| **Nominal Depth of Fill*Skew** | 2 | 0.15593 | 0.15593 | 0.07797 | 3.86 | 0.038 |
| **Error** | 20 | 0.40431 | 0.40431 | 0.02022 | | |
| **Total** | 30 | 5.91847 | | | | |
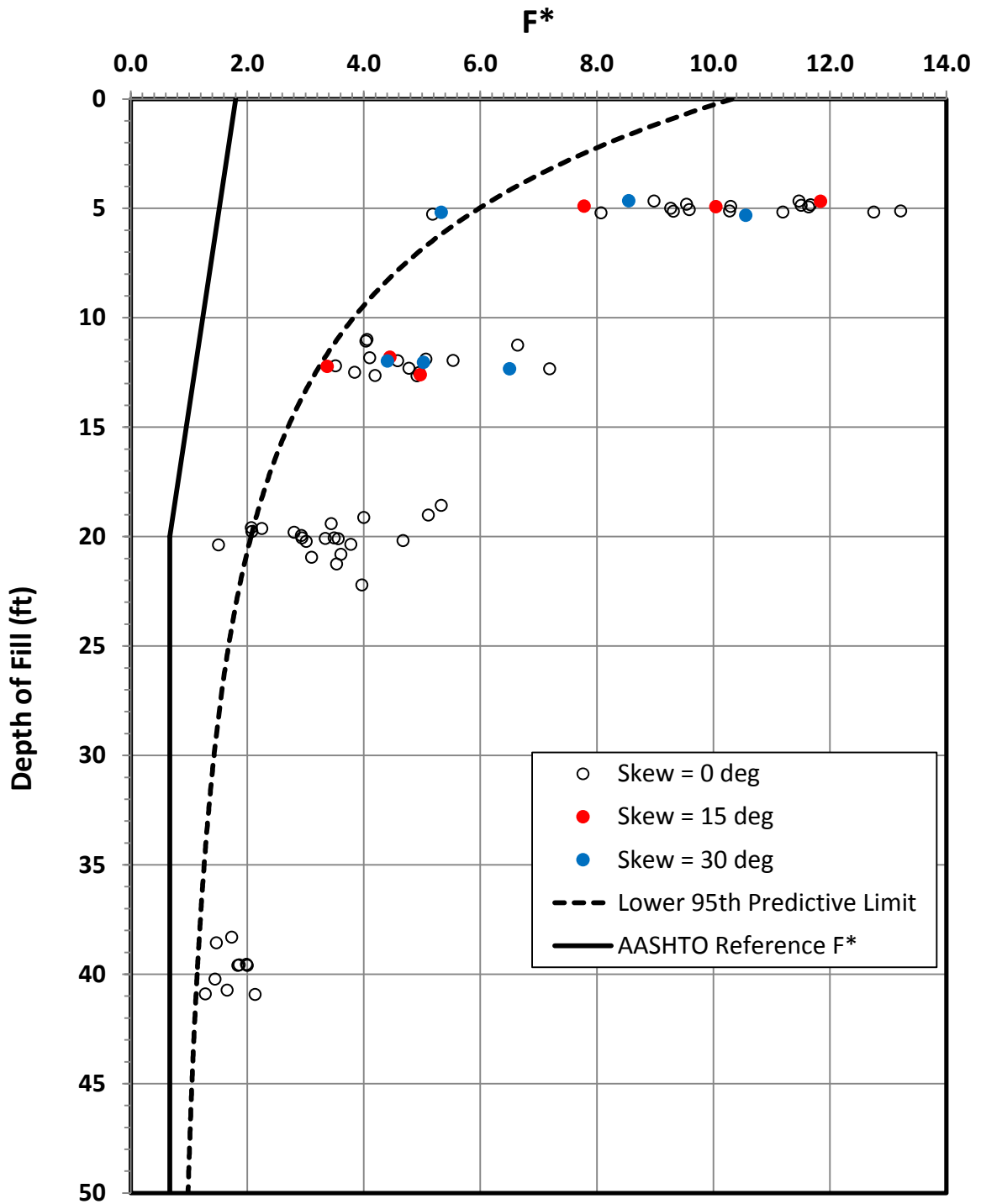
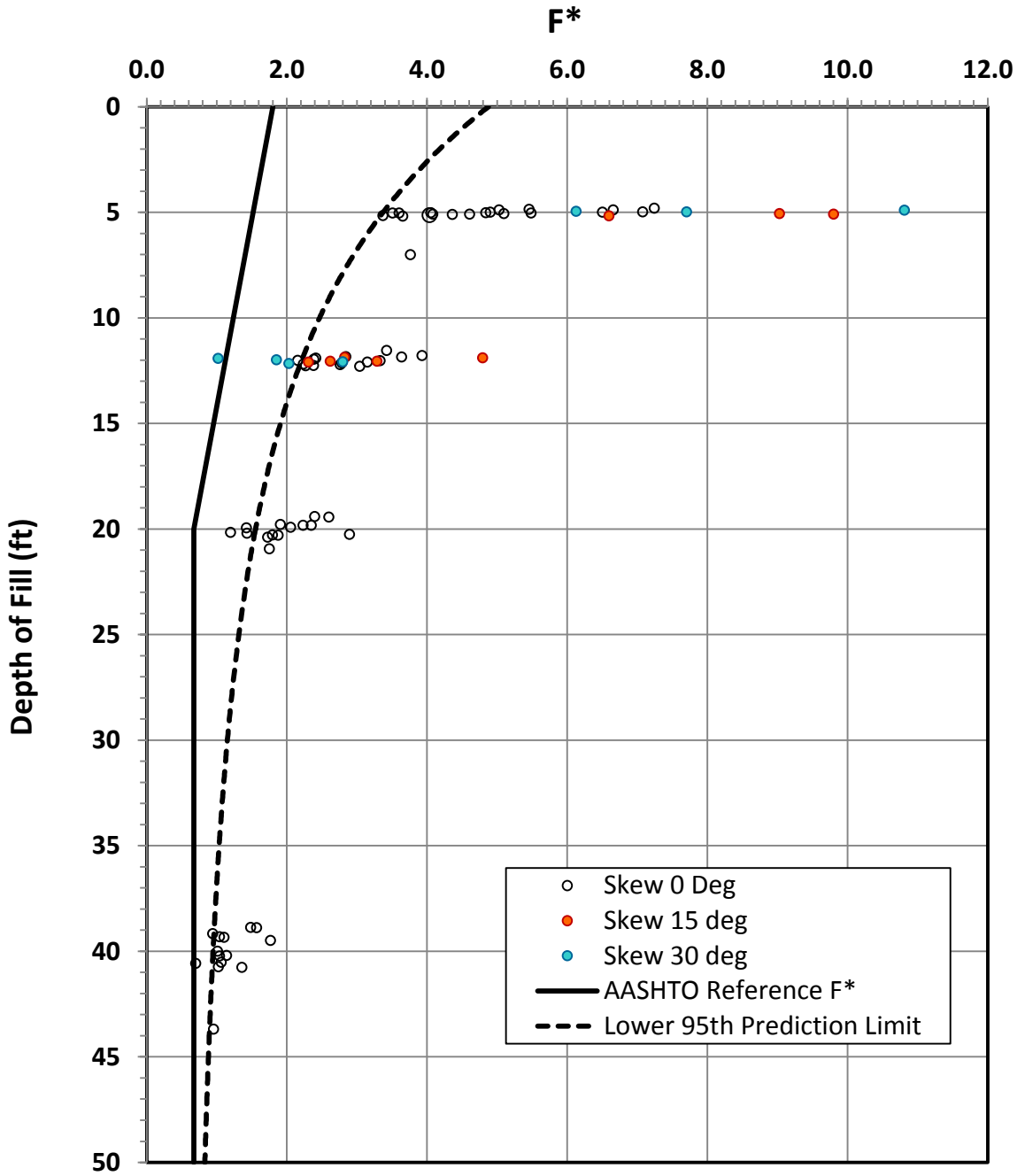**Figure 6.20** F* versus Depth of Fill Chart for Ribbed Strip Reinforcement Embedded in Type A Backfill (Ordinary Compaction): Effect of Skewing (without Cosine Projection)
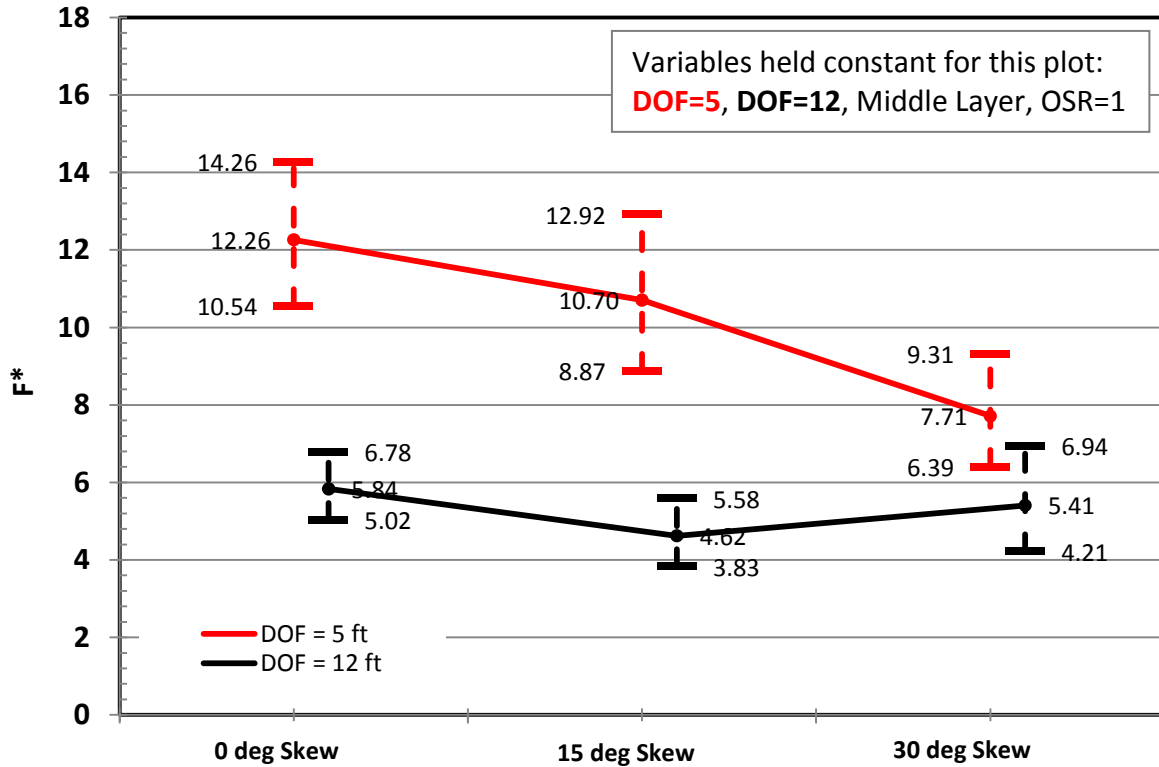
**Figure 6.21** Effect of Skewing on the Pullout Resistance of Ribbed Strip Reinforcement Embedded in Type A Backfill (without Cosine Projection)

Further statistical analysis of the ln (F*) data using the Tukey Method provided the groupings shown in Table 6.17. This table compares log (F*) data for each depth of fill and skew angle. The groups that do not share a letter are statistically different from each other. This analysis shows that at 15-deg skew, the ln (F*) is not statistically different from zero skew at both depths of fill.

**Table 6.17** Results from Tukey Analysis: Effect of Skewing on F* for Ribbed Steel Strips in Type A Backfill (Without Cosine Projection)

| DOF | Skew (deg) | N | Mean Log(F*) | Grouping | | | |
|---|---|---|---|---|---|---|---|
| 5 | 0 | 11 | 2.376 | A | | | |
| | 15 | 3 | 2.227 | A | B | | |
| | 30 | 3 | 1.900 | | B | C | |
| 12 | 0 | 8 | 1.623 | | | C | D |
| | 15 | 3 | 1.387 | | | | D |
| | 30 | 3 | 1.554 | | | C | D |

The same dataset was then analyzed again for the condition in which an adjustment was made to the pullout force based on the cosine projection. Table 6.18 shows the results obtained from the ANOVA conducted for this case. The findings are, once again, very similar to the case with no cosine projection. Accordingly, skew and the interaction term between skew and depth of fill are significant or marginally significant. Figure 6.22 further illustrate the influence skew for the two depths of fill, 5ft and 12ft.

**Table 6.18** Results from ANOVA: Effect of Skewing on F* for Ribbed Steel Strips in Type A Backfill (With Cosine Projection)

| Analysis of Variance for ln (F*), using Adjusted SS for Tests | | | | | | |
|---|---|---|---|---|---|---|
| Source | DF | Seq SS | Adj SS | Adj MS | F | P |
| OCR | 1 | 0.26961 | 0.00373 | 0.00373 | 0.18 | 0.672 |
| Nominal Depth of Fill | 1 | 3.83031 | 2.12713 | 2.12713 | 105.22 | 0.000 |
| Test Layer | 2 | 0.74787 | 0.64131 | 0.32065 | 15.86 | 0.000 |
| Length | 1 | 0.03770 | 0.00634 | 0.00634 | 0.31 | 0.582 |
| Controlling Rupture Case | 1 | 0.00159 | 0.00001 | 0.00001 | 0.00 | 0.982 |
| Skew | 2 | 0.10690 | 0.12377 | 0.06188 | 3.06 | 0.069 |
| Nominal Depth of Fill*Skew | 2 | 0.15593 | 0.15593 | 0.07797 | 3.86 | 0.038 |
| Error | 20 | 0.40431 | 0.40431 | 0.02022 | | |
| Total | 30 | 5.55422 | | | | |

The results obtained from analysis using the Tukey Method is shown in Table 6.19. This analysis shows that at 15-deg skew, the ln (F*) is not statistically different from zero skew at both depths of fill. This, however, is not true for a skew angle of 30-deg.

**Table 6.19** Results from Tukey Analysis: Effect of Skewing on F* for Ribbed Steel Strips in Type A Backfill (With Cosine Projection)

| DOF | Skew (deg) | N | Mean Log(F*) | Grouping | | | |
|---|---|---|---|---|---|---|---|
| 5 | 0 | 11 | 2.376 | A | | | |
| | 15 | 3 | 2.262 | A | B | | |
| | 30 | 3 | 2.043 | | B | C | |
| 12 | 0 | 8 | 1.623 | | | | D |
| | 15 | 3 | 1.422 | | | | D |
| | 30 | 3 | 1.698 | | | C | D |
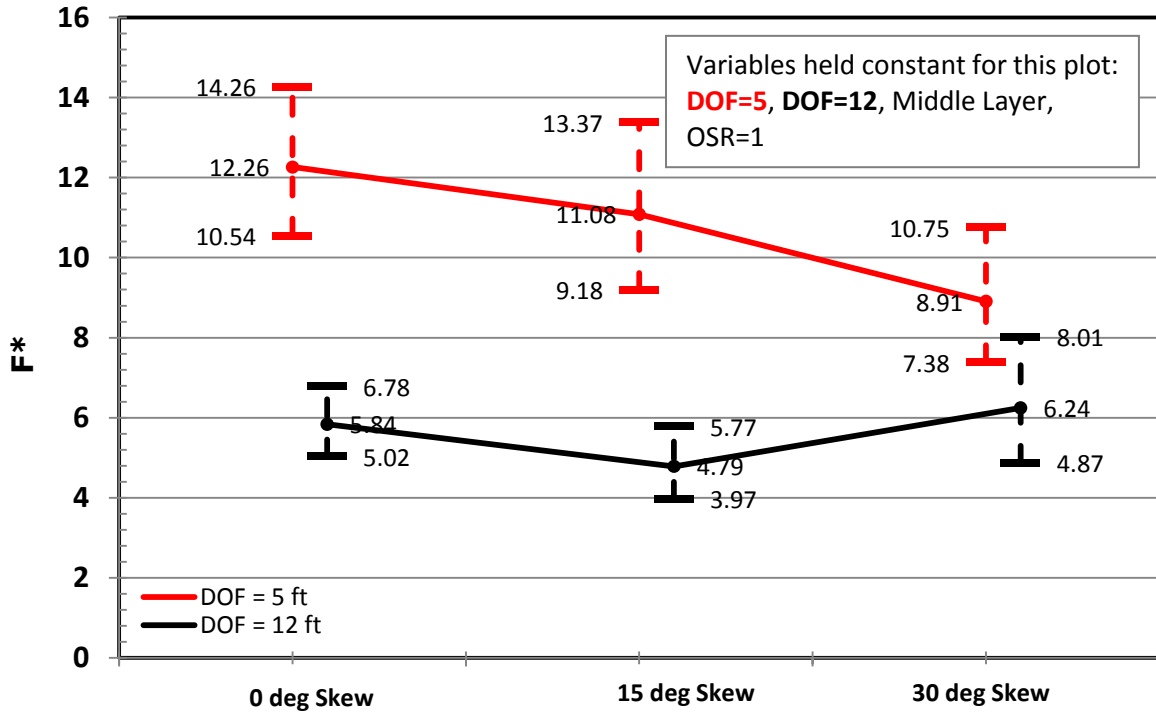
**Figure 6.22** Effect of Skewing on the Pullout Resistance of Ribbed Strip Reinforcement Embedded in Type A Backfill (with Cosine Projection)

### 6.4.2 F* for Grid Reinforcement Embedded in Type A Backfill

Volume 3-Appendix M includes the test reports for the 214 grid reinforcements tested in Type A backfill. This section synthesizes and reviews the above F* data.

*6.4.2.1 Presentation of F* Data for Grids in Type A Backfill*

F* data for all straight grid reinforcements embedded in Type A backfill are found in Table D2, Appendix D. Figure 6.23 presents this data in the form of an F* versus DOF chart. Since these data have been determined for welded steel grids that have a wide range of longitudinal and transverse bar sizes and spacings, the F* values are presented in the form of normalized pullout resistance factors, $F^*(S_t/t)$. Also shown in this plot is the AASHTO reference line for $F^*(S_t/t)$ for grid reinforcement. It can be seen that all of the measured values of normalized F* data lie to the right of the AASHTO reference line. Figure 6.24 compares the normalized F* data obtained for grids embedded in Type A and Type B backfill materials. The data clearly show that the pullout resistance factors for grid reinforcement embedded in Type A backfill is significantly higher than pullout resistance

factors for grids embedded in Type B backfill.

*6.4.2.2   Normalized F\* for Straight Grids in Type A Backfill; Effect of Length*

As described in Sec 4.3.2.1, the primary objective of the first test matrix in the grid test program was to investigate whether the length of embedment of the reinforcement has any influence on the pullout resistance factor, F\*.   Table 6.20 shows the results obtained from an ANOVA conducted on the data collected on the subset of grids tested for embedment length effect.  This analysis included Depth of Fill and Length as factors and Test Layer, Overburden Stress ratio (OSR), and Load-Displacement Behavior Type as covariates.  The last covariate, Load-Displacement Behavior Type, represented different types of load-displacement behavior observed during pullout testing of grid reinforcement as described in Chapter 5.  According to the results obtained from the ANOVA, the embedment length of the grid was found to be significant (p = 0.000).  This result is similar to that obtained for strips embedded in Type A backfill but contrary to the underlying assumption in the AASHTO equation for F\* for grid reinforcement.  A definitive explanation for the observed trend could not be established based on the data collected from this research study.  Plausible explanations involve boundary effects and ultimate limit state effects associated with our large scale test system.  Additional testing is necessary to establish the validity of apparent length effect finding.  The predictive models developed in this study used the longest reinforcement length which represented the most conservative conditions.  Figure 6.25 depicts the above normalized F\* versus length relationship.
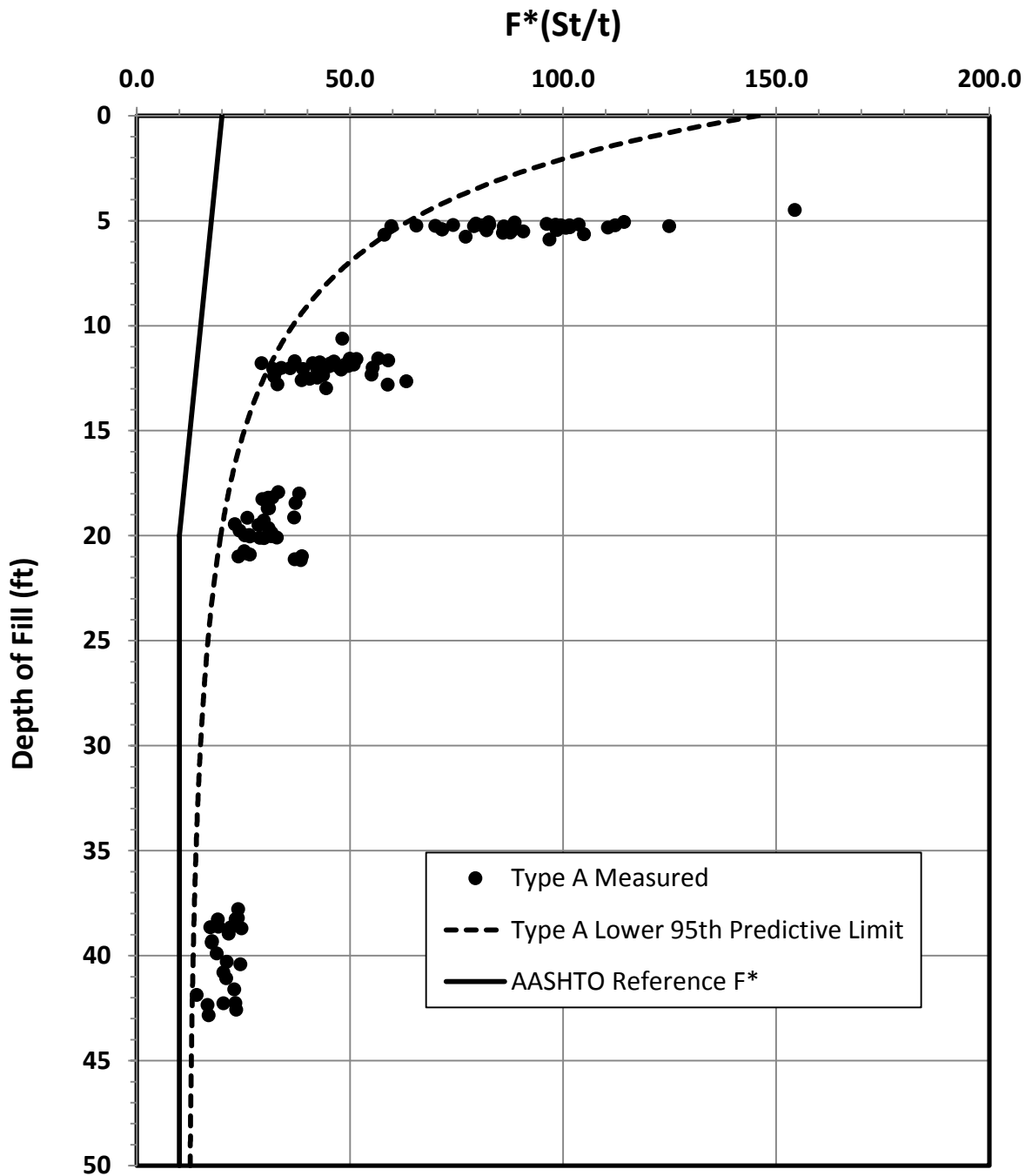
**Figure 6.23** Normalized F* versus Depth of Fill Chart for Grid Reinforcement Embedded in Type A Backfill (Ordinary Compaction; Splay Angle = 0°)
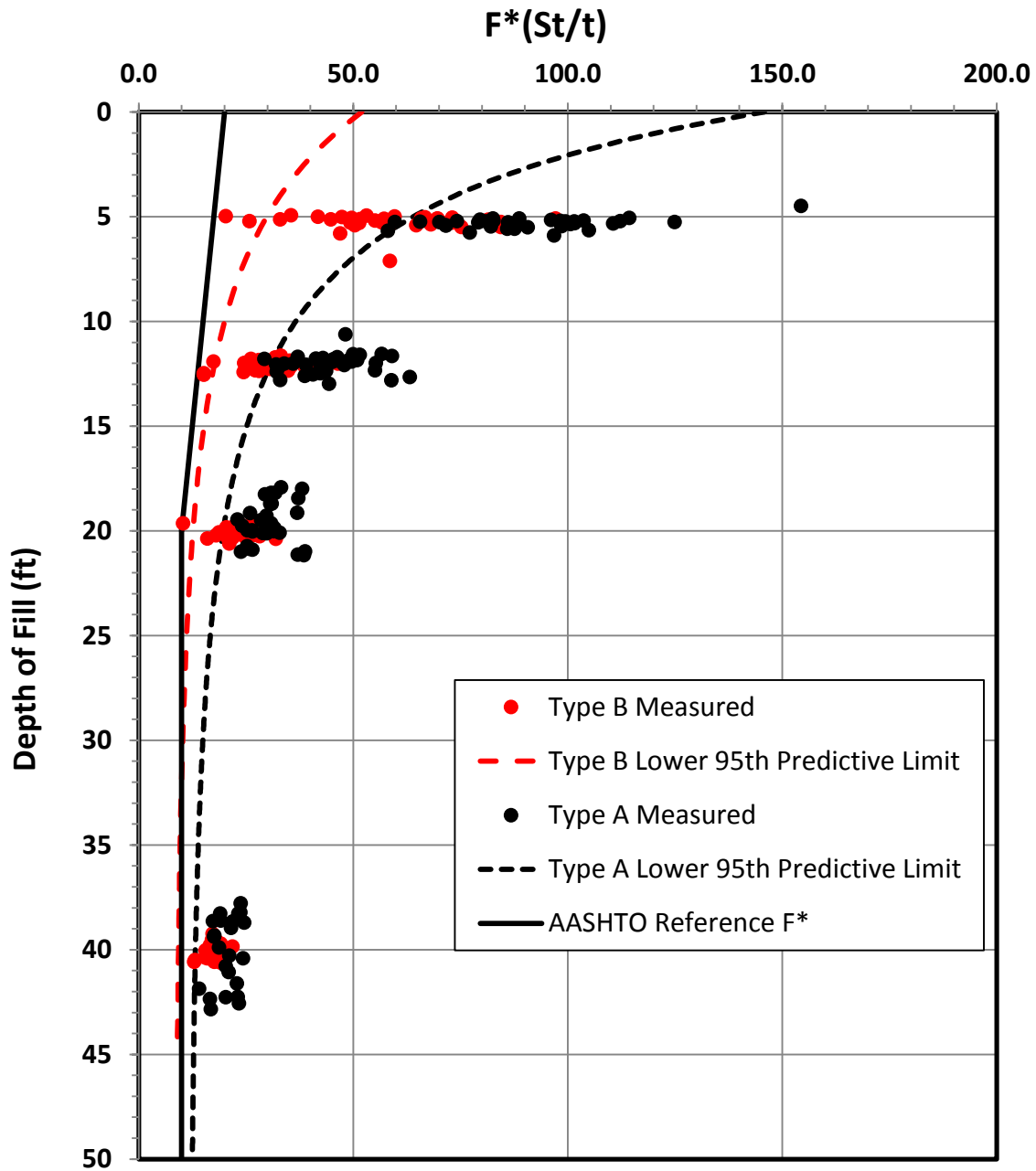
**Figure 6.24** Comparison of Normalized F* Data for Grid Reinforcement Embedded in Type A and Type B Backfills (Ordinary Compaction; Splay Angle = 0°)

**Table 6.20** Results from ANOVA: Effect of Embedment Length on Normalized F* of Grid Reinforcement in Type A Backfill

| Analysis of Variance for log(F*), using Adjusted SS for Tests | | | | | | |
|---|---|---|---|---|---|---|
| **Source** | DF | Seq SS | Adj SS | Adj MS | F | P |
| **OSR** | 1 | 0.26236 | 0.00020 | 0.00020 | 0.05 | 0.8330 |
| **Nominal Depth of Fill** | 1 | 1.63181 | 1.05884 | 1.05884 | 243.26 | 0.0000 |
| **Test Layer** | 2 | 0.14442 | 0.02234 | 0.01117 | 2.57 | 0.1220 |
| **Length** | 3 | 0.45976 | 0.51960 | 0.17320 | 39.79 | 0.0000 |
| **Load-Displ Behavior Type** | 2 | 0.14829 | 0.14829 | 0.07415 | 17.03 | 0.0000 |
| **Error** | 11 | 0.04788 | 0.04788 | 0.00435 | | |
| **Total** | 20 | 2.69452 | | | | |
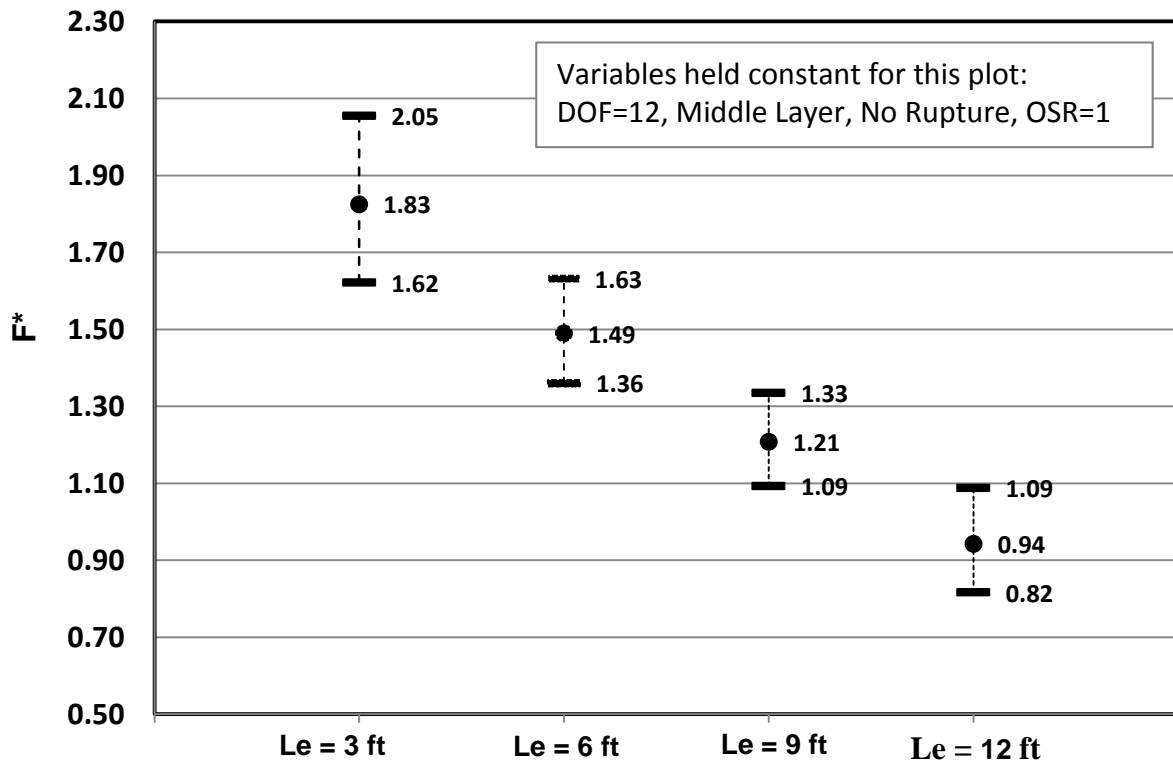


**Figure 6.25** Evaluating Length Effect for Welded Steel Grid in Type A Backfill

## 6.4.2.3 Normalized F* for Straight Grids in Type A Backfill; Effect of Transverse Bar Size and Spacing

The data review and analysis described in this section explores the effect of transverse bar size and spacing. Based on the AASHTO design equation, F* for grids varies linearly with $t/S_t$, and therefore, the normalized F*, i.e. $F^*(S_t/t)$ should be independent of both t and $S_t$. The results from an ANOVA performed to test the validity of this presupposition are shown in Table 6.21.

The results from the ANOVA revealed that all variables except overburden stress ratio had significant influence on the normalized F* (i.e. $p < 0.05$). Transverse bar spacing ($S_t$) and transverse bar diameter (t) were among the most significant (p=0.000) factors while the interaction term ($S_t \times t$) emerged as a marginally significant factor. Figure 6.26 further illustrates the influence of transverse bar spacing ($S_t$) and transverse bar diameter (t) on normalized F*. Figure 6.27 shows the lower 95th limits corresponding to three predictive models that represent the *worst*, *representative* and the *best* combination of parameters for $S_t$ and t.

**Table 6.21** Results from ANOVA: Effect of Transverse Bar Diameter and Spacing on Normalized F* of Grid Reinforcement in Type A Backfill

| Analysis of Variance for log(Norm F*), using Adjusted SS for Tests | | | | | | |
|---|---|---|---|---|---|---|
| Source | DF | Seq SS | Adj SS | Adj MS | F | P |
| OSR | 1 | 0.0023 | 0.0001 | 0.0001 | 0.01 | 0.907 |
| Nominal Depth of Fill | 3 | 36.7805 | 32.0070 | 10.6690 | 1188.08 | 0.000 |
| Test Layer | 2 | 0.3207 | 0.2753 | 0.1377 | 15.33 | 0.000 |
| Load-Displ Behavior Type | 2 | 0.9362 | 0.0595 | 0.0297 | 3.31 | 0.040 |
| Transverse Bar Diameter | 2 | 1.0575 | 1.0930 | 0.5465 | 60.86 | 0.000 |
| Transverse Bar Spacing | 3 | 0.4956 | 0.4784 | 0.1595 | 17.76 | 0.000 |
| Tran Bar Dia*Tran Bar Spac | 6 | 0.1229 | 0.1229 | 0.0205 | 2.28 | 0.041 |
| Error | 109 | 0.9788 | 0.9788 | 0.0090 | | |
| Total | 128 | 40.6947 | | | | |
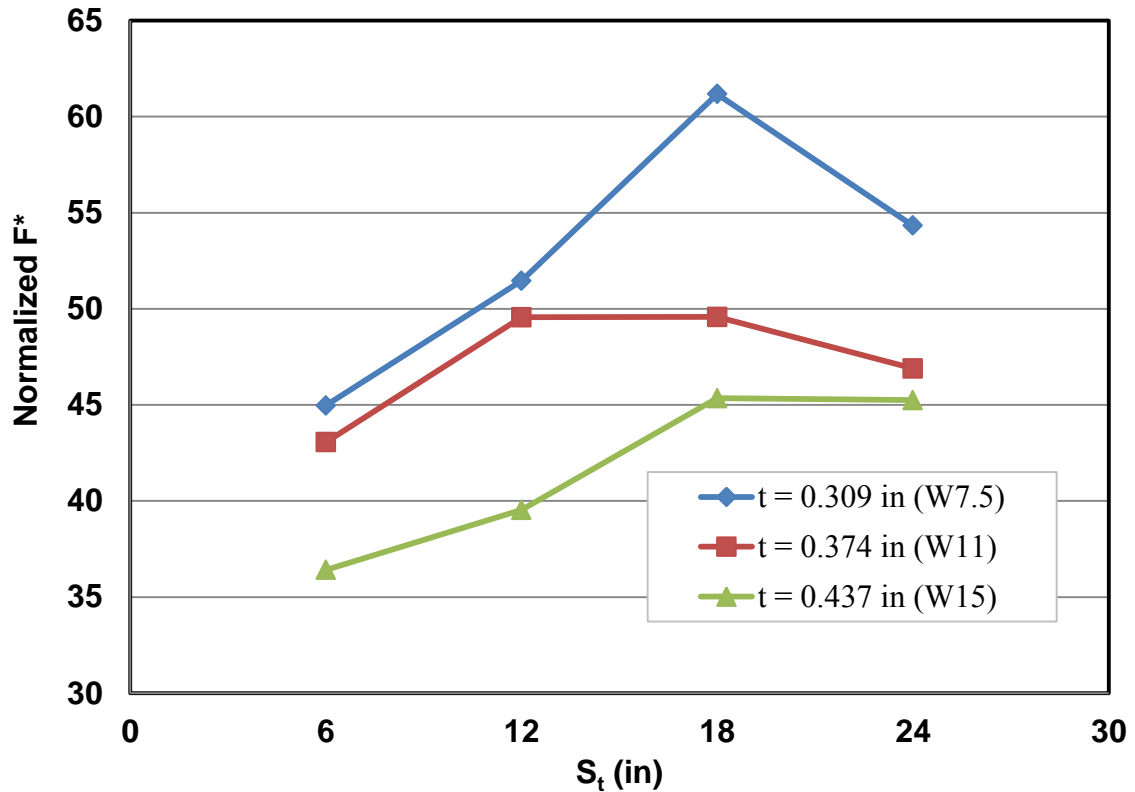
**Figure 6.26**  Mean Normalized F* for Transverse Bar Spacings of 6in, 12in, 18in and 24in (Depth of fill = 12ft)

### 6.4.2.4  *Normalized  F* for Straight Grids in Type A Backfill; Effect of Longitudinal Bar Size and Spacing*

The normalized F* data for grid reinforcement in Type A backfill was next analyzed to evaluate the influence of longitudinal bar size and spacing.   According to conventional theory, these two parameters have no influence on pullout resistance factor for grid reinforcement.  Accordingly, the current AASHTO formulation of F* does not incorporate longitudinal bar size or spacing.

The results from the ANOVA on the influence of longitudinal bar size and spacing are shown in Table 6.22.  The findings from the ANOVA show that the longitudinal bar spacing and bar diameter have dominant influence on the normalized F* along with nominal depth of fill (p=0.000).  Test Layer was the remaining variable that was significant (p=0.000).
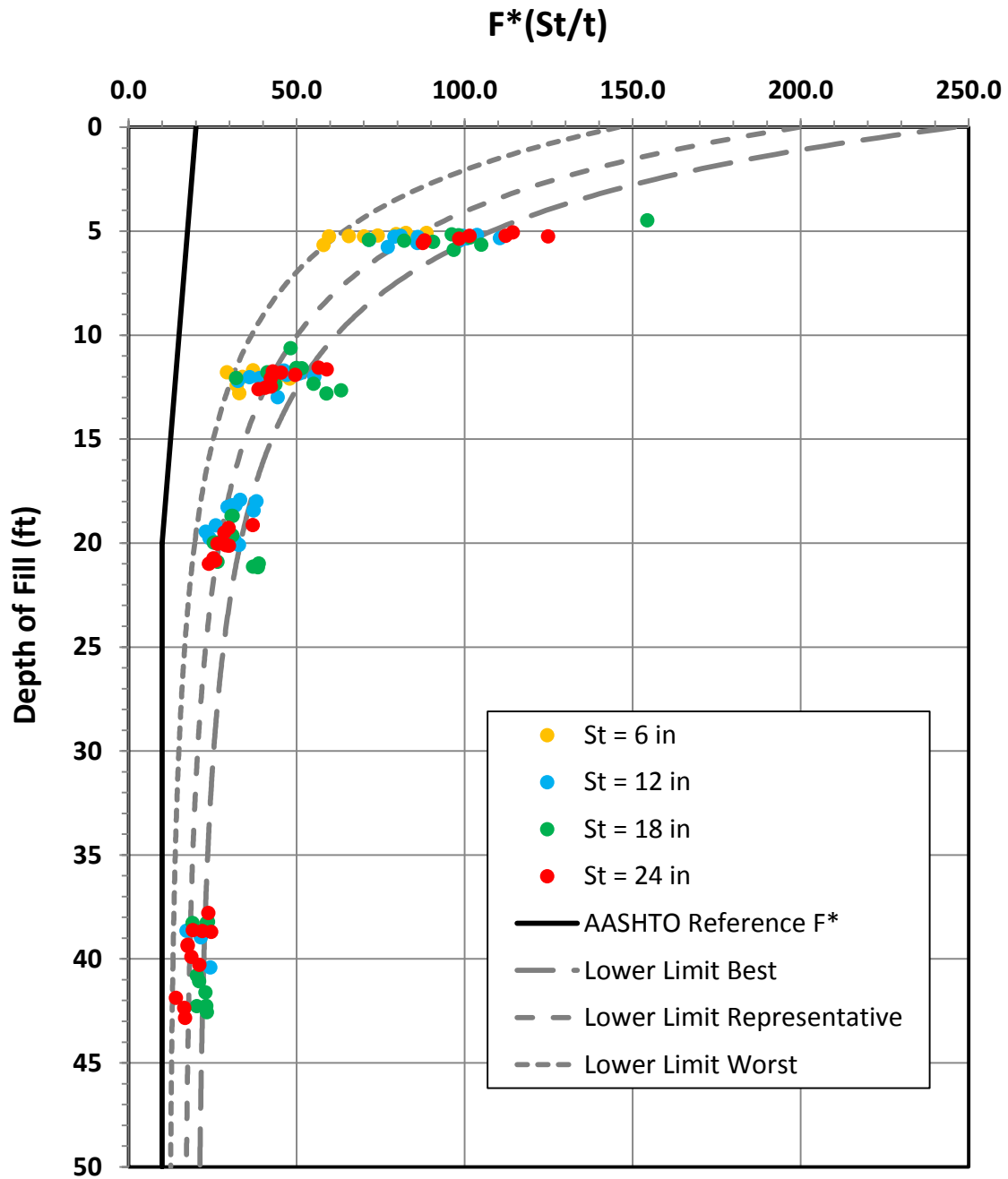
**Figure 6.27** Normalized F* versus Depth of Fill Chart for Grid Reinforcement Embedded in Type A Backfill: Effect of Transverse Bar Size and Spacing (Ordinary Compaction, Angle of Splay = 0°)

**Table 6.22**  Results from ANOVA: Effect of Longitudinal Bar Diameter and Spacing on
Normalized F* of Grid Reinforcement in Type A Backfill

| Analysis of Variance for log(Norm F*), using Adjusted SS for Tests | | | | | | |
|---|---|---|---|---|---|---|
| Source | DF | Seq  SS | Adj SS | Adj  MS | F | P |
| OSR | 1 | 7.2860 | 0.0673 | 0.0673 | 3.31 | 0.074 |
| Nominal Depth of Fill | 3 | 11.6397 | 5.9565 | 1.9855 | 97.57 | 0.000 |
| Test Layer | 2 | 0.8057 | 0.4687 | 0.2343 | 11.52 | 0.000 |
| Length | 1 | 0.3701 | 0.0393 | 0.0393 | 1.93 | 0.170 |
| Long Bar Diameter | 1 | 0.4630 | 0.6375 | 0.6375 | 31.33 | 0.000 |
| Long Bar Spacing | 3 | 16.8568 | 14.9384 | 4.9795 | 244.70 | 0.000 |
| Long Bar Dia*Long Bar Spac | 3 | 0.1210 | 0.1210 | 0.0403 | 1.98 | 0.126 |
| Error | 63 | 1.2820 | 1.2820 | 0.0203 | | |
| Total | 77 | 38.8245 | | | | |

Figure 6.28 shows the influence of longitudinal bar size and spacing on mean F*.
Figure 6.29 is the normalized F* versus Depth of Fill plot.  The lower 95th predictive limits
are shown for the least favorable, representative and most favorable combinations of
longitudinal bar spacing and bar size.
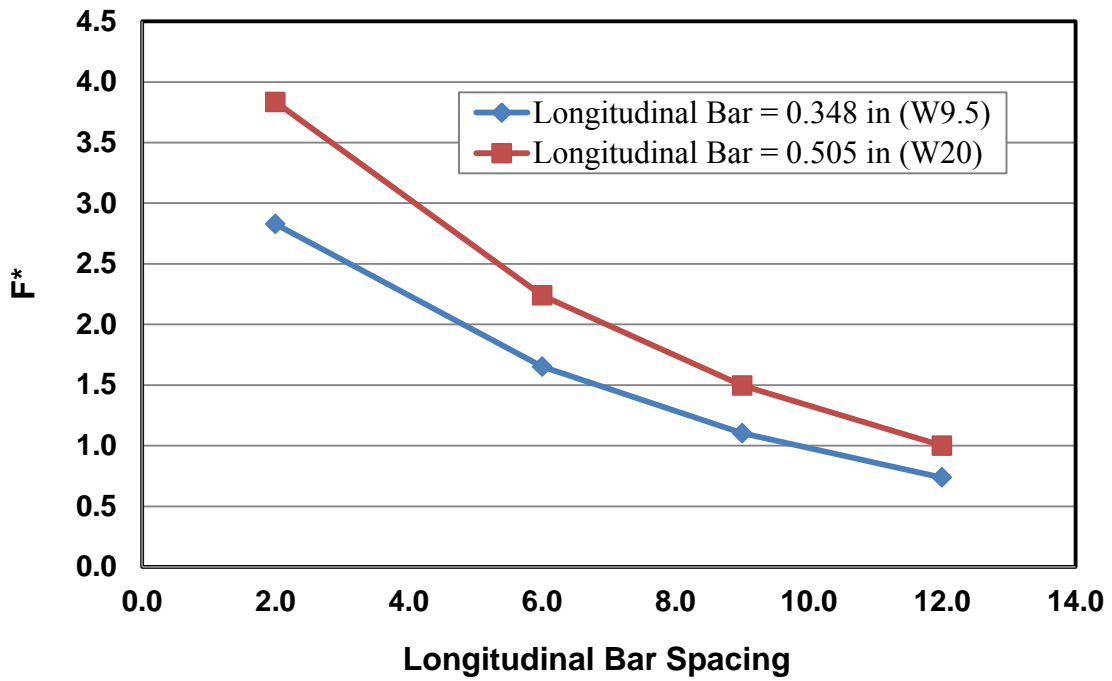
**Figure 6.28**  Mean F* for Longitudinal Bar Spacings of 2in, 6in, 9in and 12in and Longitudinal Bar Diameters 0.348in(W9.5) and 0.505in(W20) at Depth of fill = 12ft
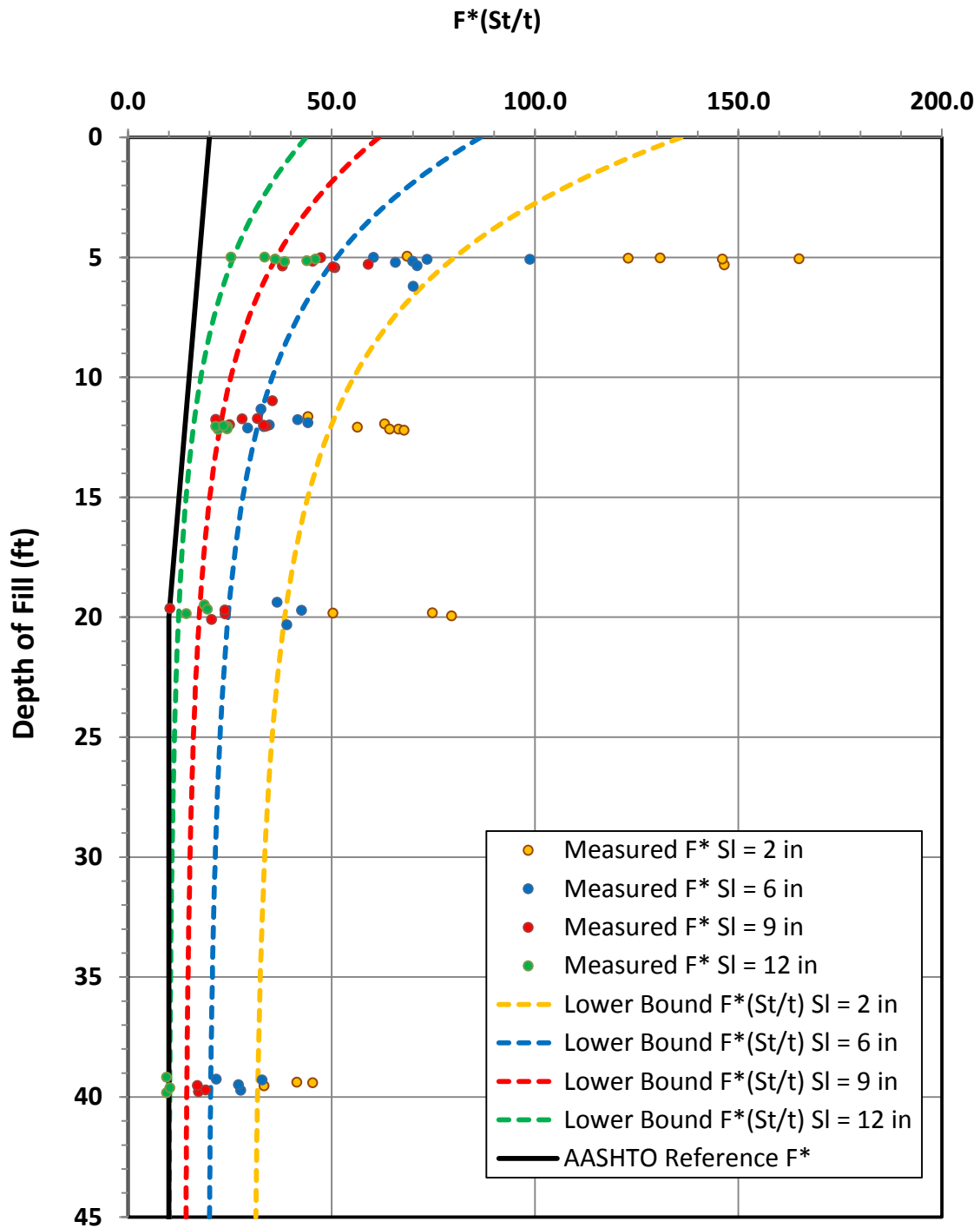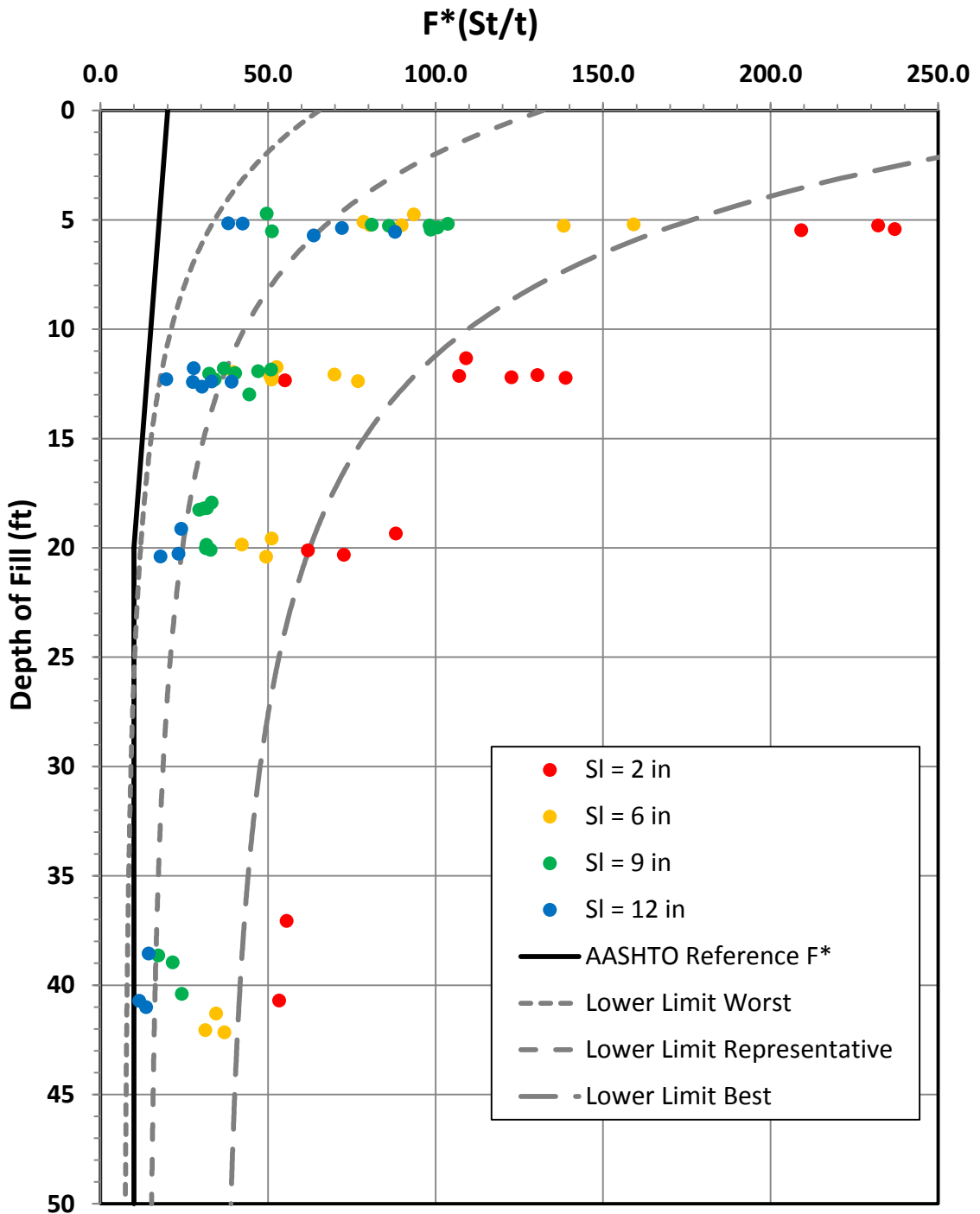
**Figure 6.29** Normalized F* versus Depth of Fill Chart for Grid Reinforcement Embedded in Type A Backfill: Effect of Longitudinal Bar Size and Spacing (Ordinary Compaction, Angle of Splay = 0°)
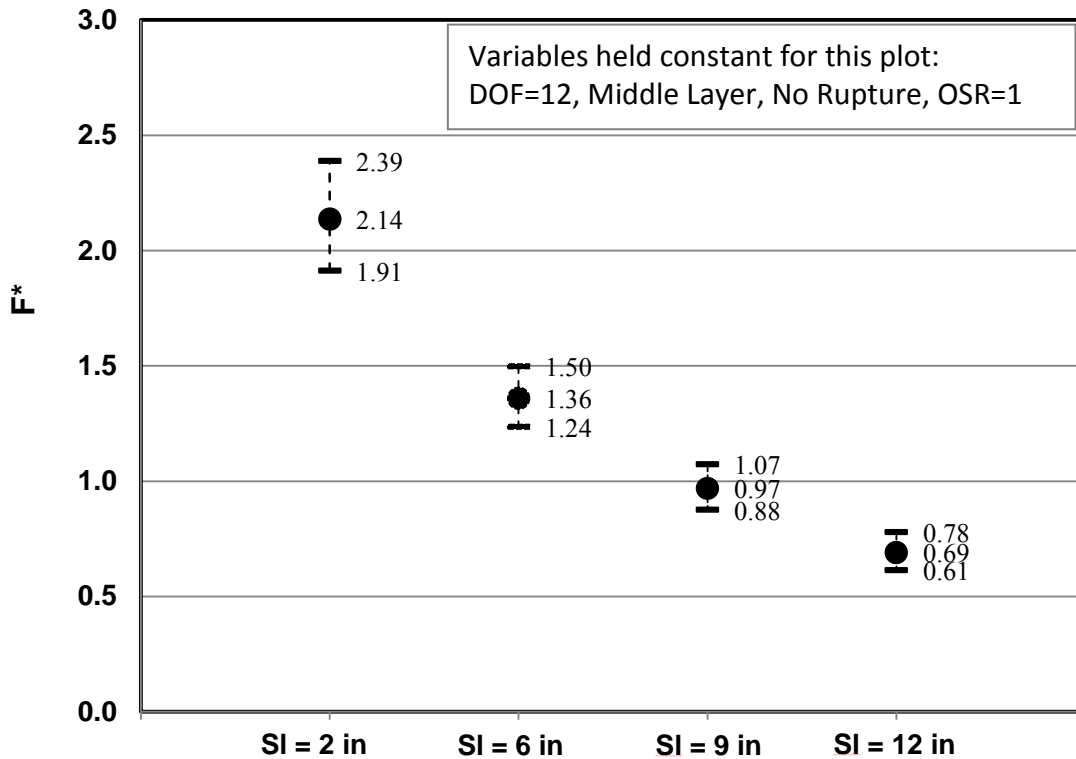
*6.4.2.5   Normalized F\* for Cut and Splayed Grids in Type A Backfill*

This section evaluates the effect of cutting and splaying of grid reinforcement on the normalized pullout resistance factors.   As described previously, this analysis considered two separate cases: effect of splaying when cosine projection is not used and effect of splaying when cosine projection is used.  Table 6.23 presents the results from the ANOVA conducted when no cosine projection was used.

**Table 6.23**  Results from ANOVA: Effect of Cut-and-Splay on Normalized F\* of Grid
Reinforcement in Type A Backfill (Without Cosine Projection)

| Analysis of Variance for log(Norm F\*), using Adjusted SS for Tests | | | | | | |
|---|---|---|---|---|---|---|
| **Source** | **DF** | **Seq  SS** | **Adj SS** | **Adj  MS** | **F** | **P** |
| **OSR** | 1 | 0.36891 | 0.00176 | 0.00176 | 0.25 | 0.625 |
| **Nominal Depth of Fill** | 1 | 2.26616 | 1.30323 | 1.30323 | 186.76 | 0.000 |
| **Test Layer** | 2 | 0.40383 | 0.28795 | 0.14397 | 20.63 | 0.000 |
| **Splay** | 2 | 0.15394 | 0.16735 | 0.08368 | 11.99 | 0.002 |
| **Load-Displ. Behavior Type** | 3 | 0.03180 | 0.03180 | 0.01060 | 1.52 | 0.264 |
| **Error** | 11 | 0.07676 | 0.07676 | 0.00698 | | |
| **Total** | 20 | 3.30140 | | | | |

The results from the above analysis reveal that normalized F\* for grids with splay was significantly different from normalized F\* for grids with no splay (p=0.002).  Figure 6.30 compares mean F\* for grids with different splay angles (we report F\* values for this data group because $S_t/t$ remained constant).

The analysis was repeated for the case in which cosine projection was used.  The results from this second ANOVA are shown in Table 6.24.  In this analysis, the effect of splay is found to be not significant (p=0.123).  These results are also shown graphically in Figure 6.31.  These observations indicate that when grid reinforcements in Type A backfill are cut and splayed, if the length of the grid is increased based on cosine projection, then the resulting F\* values will not be significantly different from F\* values for straight grids.

**Table 6.24** Results from ANOVA: Effect of Cut-and-Splay on Normalized F* of Grid Reinforcement in Type A Backfill (With Cosine Projection)

| Analysis of Variance for log(Norm F*), using Adjusted SS for Tests | | | | | | |
|---|---|---|---|---|---|---|
| Source | DF | Seq SS | Adj SS | Adj MS | F | P |
| OSR | 1 | 0.22593 | 0.00176 | 0.00176 | 0.25 | 0.625 |
| Nominal Depth of Fill | 1 | 2.25458 | 1.30323 | 1.30323 | 186.76 | 0.000 |
| Test Layer | 2 | 0.36492 | 0.28795 | 0.14397 | 20.63 | 0.000 |
| Splay | 2 | 0.02492 | 0.03560 | 0.01780 | 2.55 | 0.123 |
| Load-Displ. Behavior Type | 3 | 0.03180 | 0.03180 | 0.01060 | 1.52 | 0.264 |
| Error | 11 | 0.07676 | 0.07676 | 0.00698 | | |
| Total | 20 | 2.97891 | | | | |
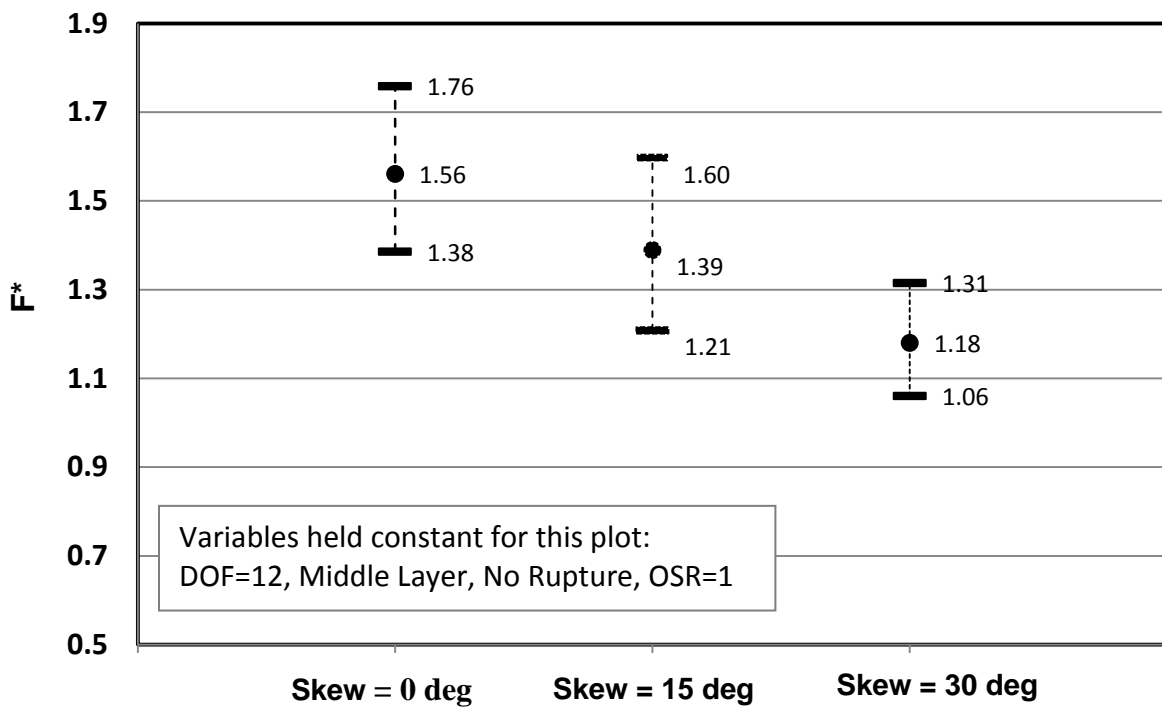


**Figure 6.30** Mean F* for Grids in Type A Backfill with Splay Angles of 0, 15 and 30-deg when no Cosine Projection is Used (Depth of fill = 12ft)
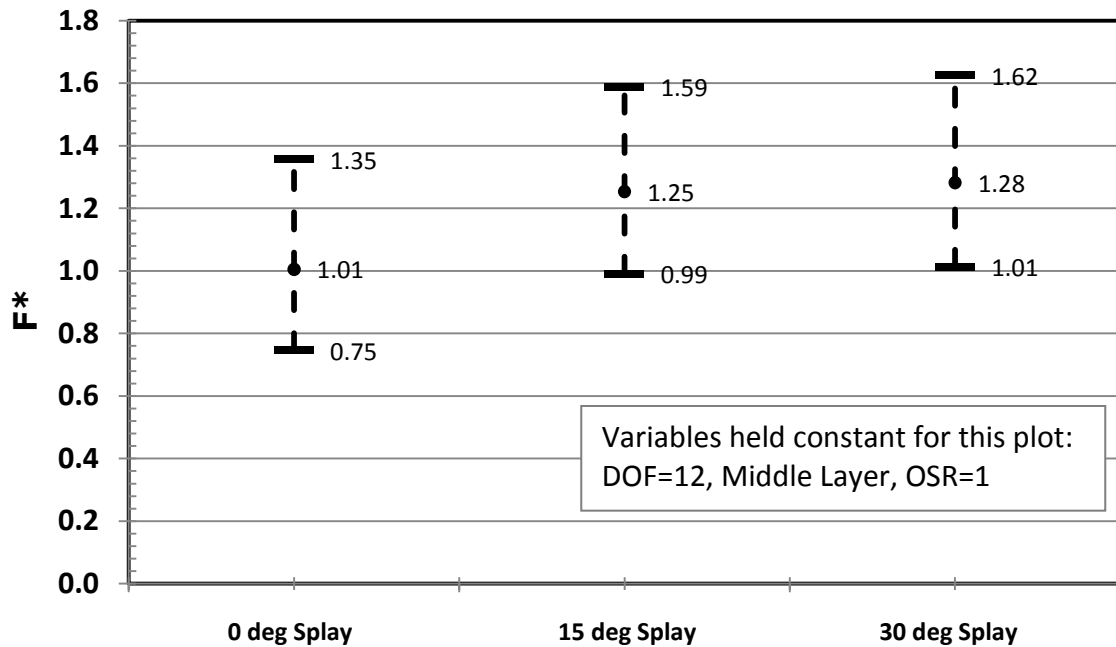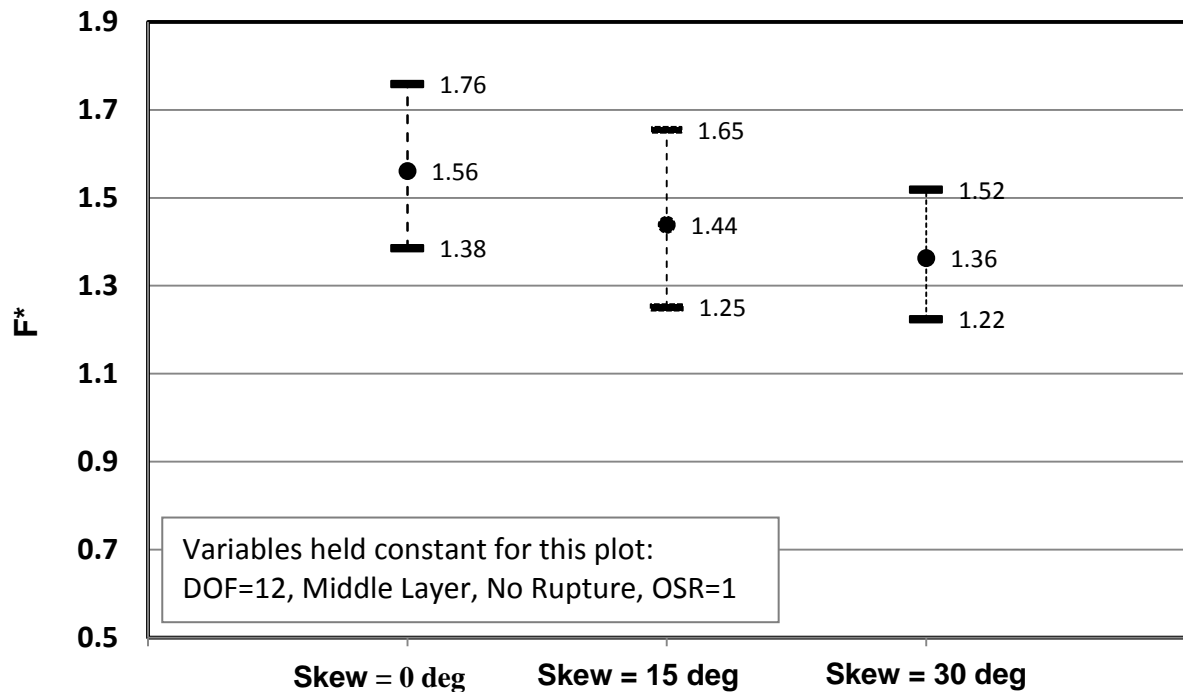
**Figure 6.31**   Mean F* for Grids in Type A Backfill with Splay Angles of 0, 15 and 30-deg when Cosine Projection is Used (Depth of fill = 12ft)

### 6.4.3    F* for Smooth Straight Bars in Type A Backfill

The last series of tests conducted in Type A backfill consisted of 16 pullout tests on smooth straight bars.  Pullout resistance factors for these bars were calculated by using the peripheral distance, $\pi D$ in place of 2b in the F* formula for ribbed steel strips.  These F* values are presented in Table D3 of Appendix D.  The results from an ANOVA performed on this limited dataset to determine factors influencing pullout resistance of smooth bars are summarized in Table 6.25.  The results indicate that nominal depth of fill is a significant variable (p=0.031).  None of the remaining factors demonstrated significant influence on the pullout resistance factors for smooth straight bars.

**Table 6.25** Results from ANOVA: Pullout Resistance Factor, F* of Smooth Bars in Type A Backfill

| Analysis of Variance for log(Norm F*), using Adjusted SS for Tests | | | | | | |
|---|---|---|---|---|---|---|
| **Source** | DF | Seq SS | Adj SS | Adj MS | F | P |
| **OSR** | 1 | 0.2111 | 0.0016 | 0.0016 | 0.01 | 0.916 |
| **Nominal Depth of Fill** | 3 | 3.2377 | 2.1756 | 0.7252 | 5.38 | 0.031 |
| **Test Layer** | 2 | 0.1434 | 0.0825 | 0.0412 | 0.31 | 0.746 |
| **Length** | 1 | 0.6217 | 0.5706 | 0.5706 | 4.23 | 0.079 |
| **Diameter** | 1 | 0.0811 | 0.0811 | 0.0811 | 0.60 | 0.464 |
| **Error** | 7 | 0.9442 | 0.9442 | 0.1349 | | |
| **Total** | 15 | 5.2391 | | | | |

The primary reason for undertaking pullout testing of smooth straight bars was to evaluate the relative contribution made by the longitudinal bars towards the overall pullout resistance capacity of welded grid reinforcement.  Accordingly, the percent contribution was calculated by first taking the average of pullout capacities measured for smooth bars of given length and diameter, then multiplying by three and expressing this quantity as a percentage of the average pullout capacity measured for grids with identical longitudinal bars.  The results from this analysis are shown in Table 6.26.  As the data reveal, the relative contribution is larger for narrower grids and then gradually decreases as the grid width increases.  For a typical 9-in wide grid in Type A backfill, the relative contribution from longitudinal bars will be in the range of 7%- 32%.  However, it should be noted that this finding will be strictly valid only if the transverse bars present in a welded steel grid do not alter the interaction that takes place between the longitudinal bars and the backfill material.

**Table 6.26** Percent Contribution from Longitudinal Bars to Pullout Capacity of Welded Grids with Three Longitudinal Bars in Type A Backfill

| DOF, z (ft) | Longitudinal Bar Size | Pullout Resistance, Pr (lb) | 2" Longitudinal Bar Spacing Grid | 6" Longitudinal Bar Spacing Grid | 9" Longitudinal Bar Spacing Grid | 12" Longitudinal Bar Spacing Grid |
|---|---|---|---|---|---|---|
| 5 | W9.5 | 645 | 10% | 19% | 15% | 18% |
| 12 | W9.5 | 996 | 33% | 36% | 32% | 28% |
| 5 | W20 | 1156 | 16% | 11% | 11% | 9% |
| 12 | W20 | 1289 | 17% | 11% | 11% | 15% |
| 20 | W20 | 873 | 11% | 6% | 7% | 6% |
| 40 | W20 | 1479 | 27% | 14% | 16% | 28% |

## 6.5 REVIEW OF STRAIN GAGE DATA

This section reviews the data collected from pullout testing of strain gaged MSE reinforcements. Strain gaged reinforcement testing was conducted in both types of backfill materials. Strain gaged reinforcement testing conducted in Type B backfill consisted of 15 successfully completed pullout tests on strain-gaged strips and 11 tests on strain-gaged grids. The test program in Type A backfill included three strain-gaged tests on strip reinforcement and six strain-gaged tests on grid reinforcement. The data collected from each test program are discussed in the following sections. Appendix E, Volume 1 includes tables that provide test parameters for all strain gaged reinforcements. Detailed test reports for strain gaged strips and grids in Type B backfill are found in Appendices J and K, respectively, in Volume 2. Similarly, tests reports for strain gaged strips and grids in Type A backfill are included in Appendices O and P, respectively, in Volume 3.

### 6.5.1 Strain Gage Data for Strip Reinforcements

For strip reinforcements, strain gages were installed along the length of the reinforcement at 2ft intervals as shown in Figure 5.26. At each gage location, strain gages were mounted on the top and bottom of the reinforcement. Pairing gages in this manner provided necessary redundancy. More importantly, it allowed elimination of potential error due to bending of the reinforcement. Strain measurements were made at each gage location as the pullout load was increased. The measured strains were then averaged over 500-lb load increments and converted to axial tensile forces. The axial tensile forces corresponding to each strain gage were then plotted against the applied pullout load. A representative example of an axial tensile force versus an applied pullout load plot based on data obtained from Test No. TS29.07-S-L12-Z20-M is shown in Figure 6.32. In this plot, the data from strain gages mounted on the top and bottom of the reinforcement are plotted separately.

In the next step, the tensile forces at each gage location were calculated based on the average strain for the top and bottom strain gages. These data are shown in Figure 6.33. As expected, the gage locations closer to the leading end of the reinforcement register higher axial tensile forces (plot closer the 45-deg line) and those farther from the leading end of the reinforcement register lower tensile forces. For example, in Figure 6.33 the axial force in the reinforcement at a location 1ft behind the wall (purple dotted line) is almost the same as the

applied pullout force.  At a distance of 7.0ft (yellow line), the axial force is about one-third of the applied pullout force.  The difference is the resistance that developed within the first 7ft of the reinforcement.  Whenever gage failure occurred, the data from the surviving gage was retained in the plot but denoted by an asterisk (*). Our analysis approach was to retain as much data as possible, realizing that results obtained from a single surviving gage will likely be less reliable than results from gage pairs.
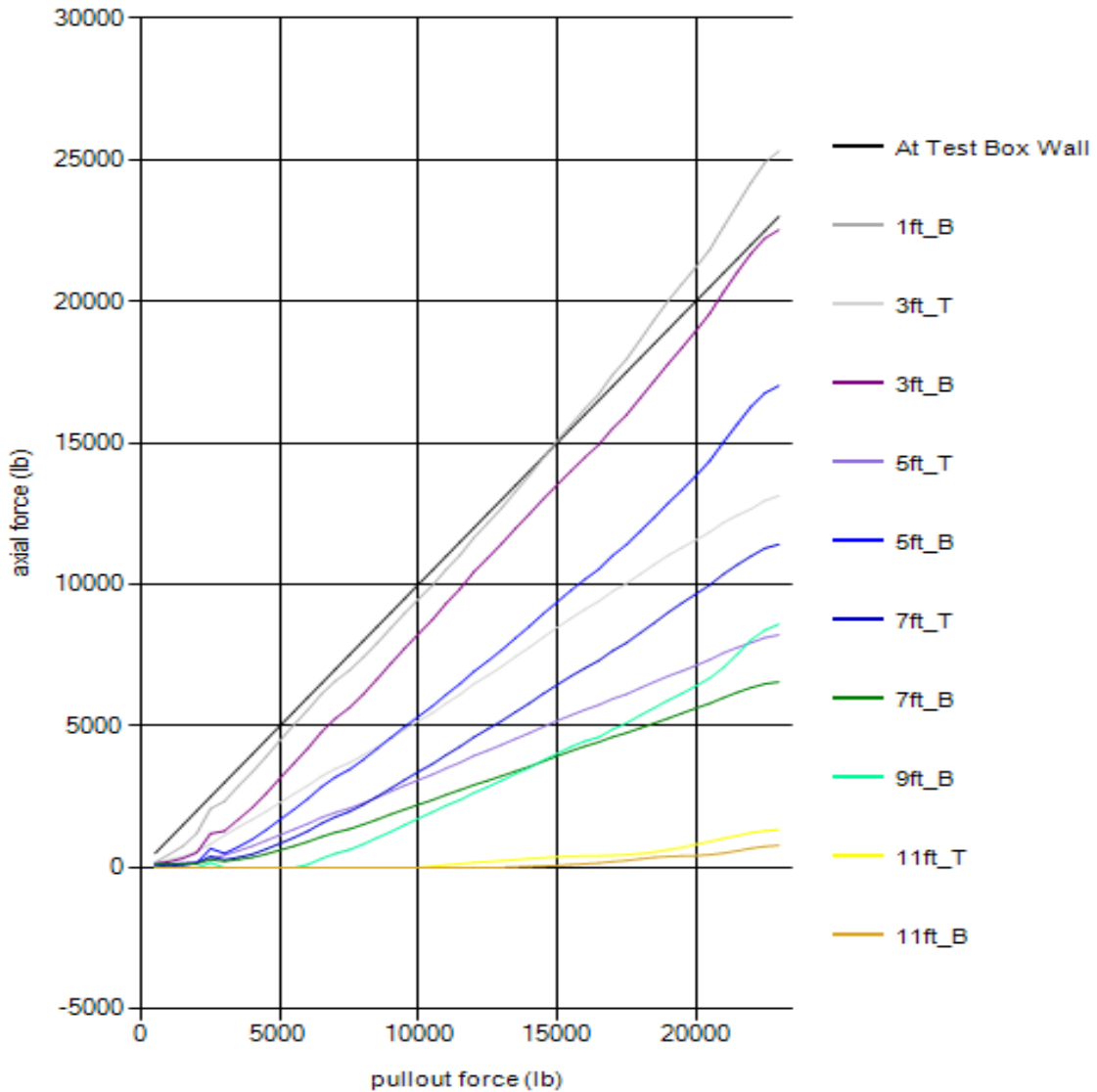


**Figure 6.32**  Axial Tensile Force Calculated Based on Strains Measured at the Top and Bottom of the Reinforcement versus Applied Pullout Load for Test No. TS29.07-S-L12-Z20-M
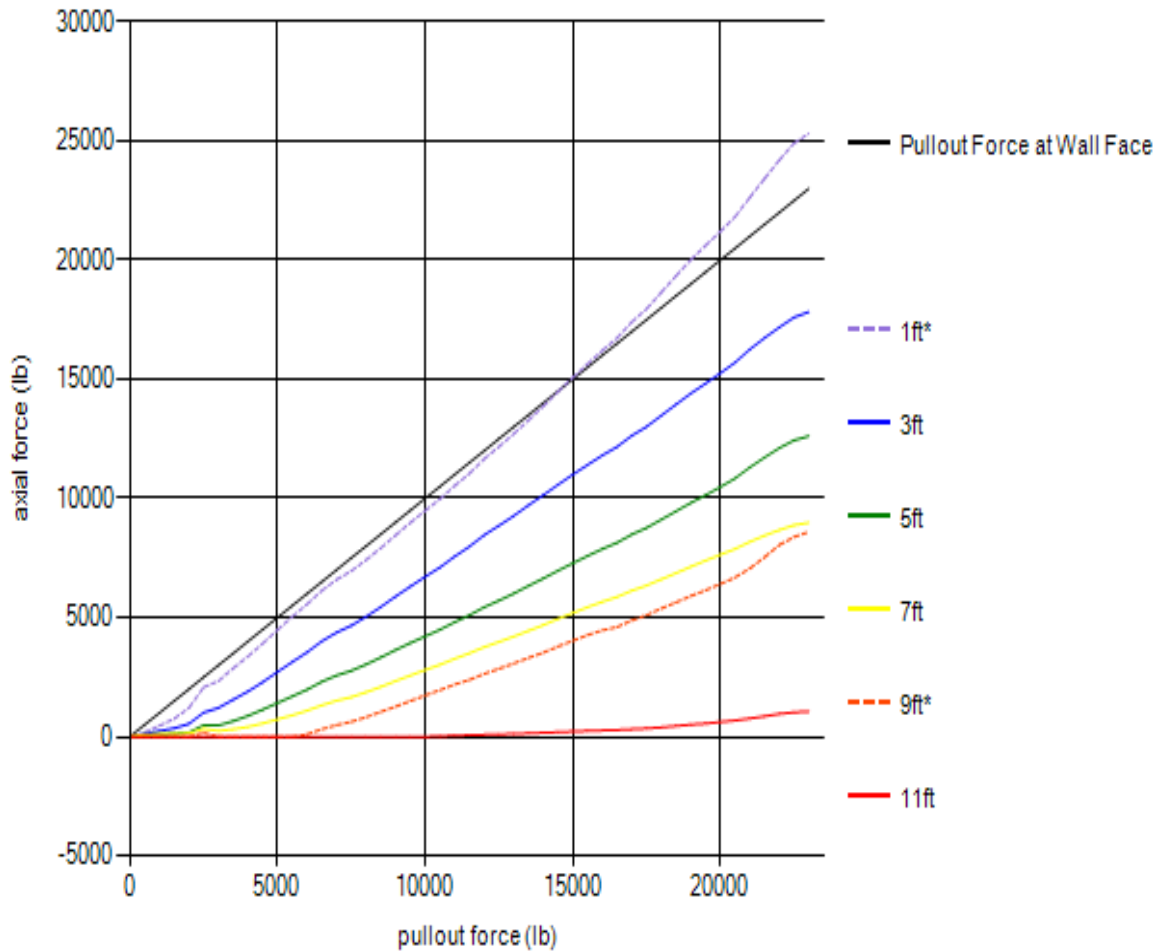
**Figure 6.33** Axial Tensile Force Calculated at Each Gage Location versus Applied Pullout Load for Test No. TS29.07-S-L12-Z20-M

The data presented in Figure 6.33 are also shown in the form of a plot of axial tensile force versus distance from the front wall of the pullout box (Figure 6.34). It should be noted that this plot only includes data within the service load range; that is, pullout forces no higher than 8,000 pounds. This is because strain data began to show more erratic behavior as the pullout loads were increased beyond service load levels. It is believed that this erratic strain behavior is largely a result of strain gage failure.

The linear trend seen in Figure 6.34 suggests that the pullout resistance is mobilized uniformly along the length of the strip reinforcement. Accordingly, this data supports the view that ribbed strip reinforcements behave in an inextensible manner with uniform displacement along their length; that is, the same displacement exists at the leading and

trailing ends of the reinforcement. This type of reinforcement-backfill interaction is assumed in the coherent gravity method used in the design of MSE retaining walls.
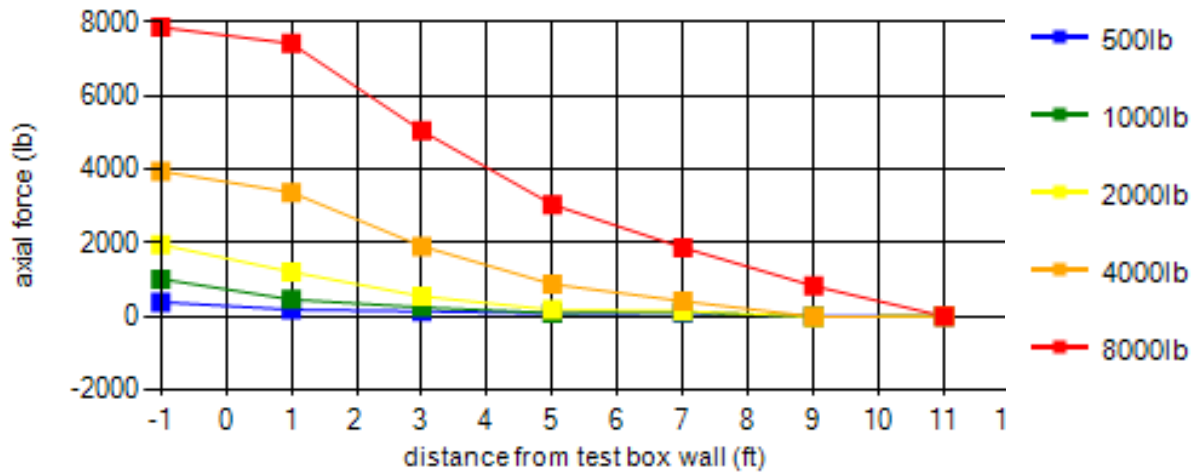


**Figure 6.34** Axial Tensile Force at Each Gage Location versus Distance from Front Wall of Test Box for No. TS29.07-S-L12-Z20-M

Results for strain-gaged pullout tests on steel MSE reinforcement strips in both Type B and Type A materials showed similar trends. In both cases, the reinforcements behave in an inextensible manner with uniform displacement along their length, consistent with the coherent gravity method used in the design of MSE retaining walls.

## 6.5.2 Strain Gage Data for Grid Type Reinforcements

The research program included strain-gaged pullout tests in both Type B and Type A backfill materials. As described in Section 5.5, the gaging plan used for grids embedded in Type A was different from the gaging plan used for grids in Type B backfill. These gaging plans were designed to provide three different types of data: (a) data on the distribution of axial load between the middle and outside longitudinal bars, (b) data on the distribution of axial load along the longitudinal bars, (c) data on the distribution of moments along transverse bars. The gaging plan used in Type B testing was only partially successful in providing reliable data in all three data categories. Therefore, necessary improvements in the gaging plan were made prior to Type A testing.

An important observation made during review of strain gage data was that the gages lost ability to provide reliable and valid data rapidly once the applied loads were increased beyond service loads. It was apparent that the the steel and wire connections to the gages began to break down as the pullout displacements increased. For this reason, the analysis of strain gage data was limited to the service load domain; that is, pullout forces no higher than 8,000 pounds.

Figure 6.35 is a representative plot showing the strain gage data converted to equivalent axial force for all strain gages mounted on a single longitudinal bar. Note that strain gages were installed in pairs on the inside and outside of the bar. At a given location the longitudinal bar may carry both axial tensile force as well as a bending moment transferred from the transverse bar. The net negative forces represent axial forces calculated based on strain gages that registered net compressive strains due to effects of bending.
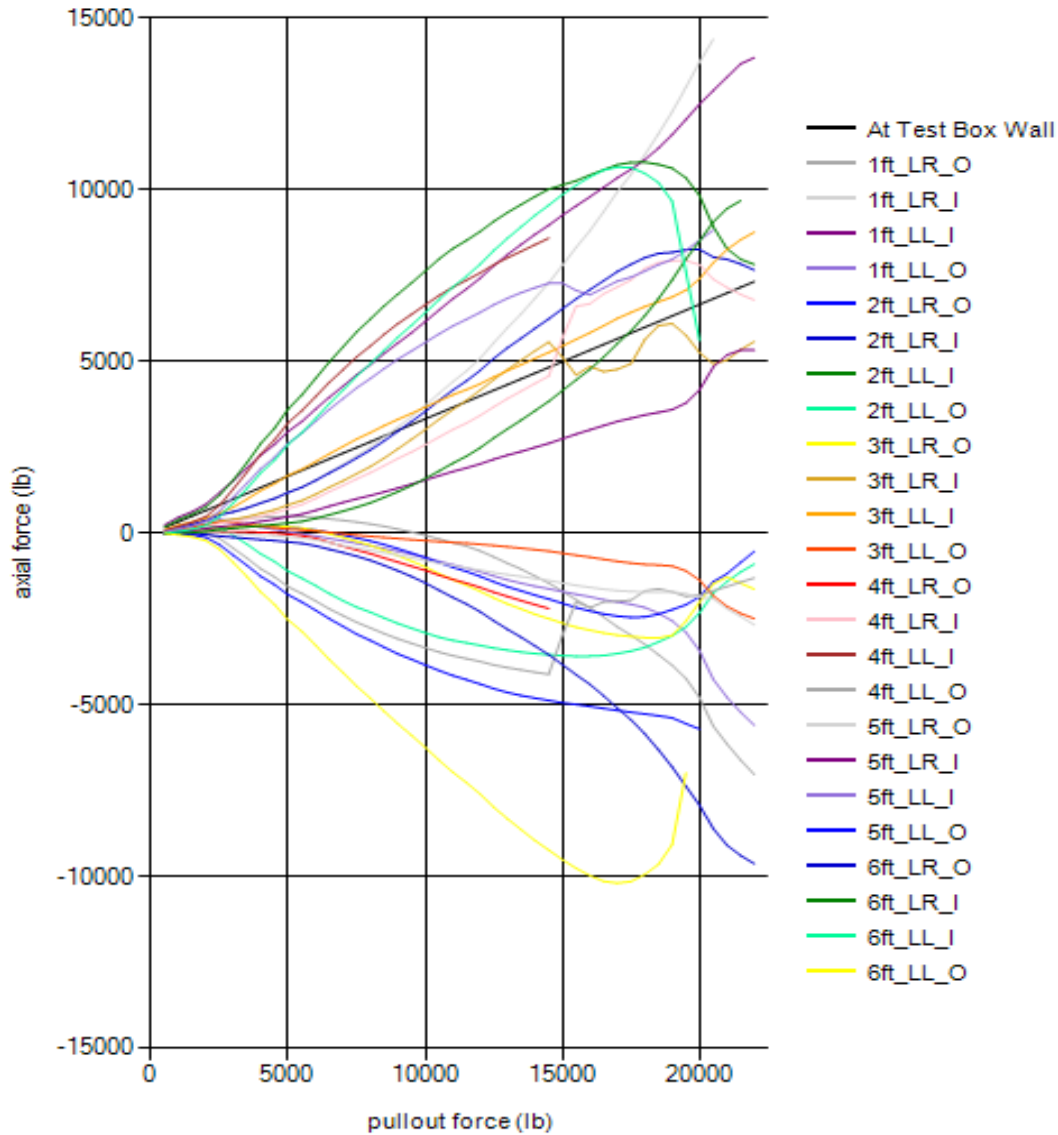
**Figure 6.35** Axial Forces Calculated Based on Strains Measured on the Inside and Outside of Longitudinal Bars versus Applied Pullout Load [TS25.02-G-9X12-W20xW11-L6-Z5-T]

In Figure 6.36, the same data are re-plotted after averaging the strains corresponding to matching gage pairs on the inside and outside of longitudinal bars. The averaging process filters out the effects of bending. The results are similar to those obtained for strip type reinforcements. As expected, the gages closer to the leading end of the reinforcement yield larger axial forces. Also as noted previously in strip reinforcements, the data begins to deviate from expected linear trend as the pullout loads are increased beyond service loads. This anomalous behavior is attributed to gage failure at larger strains.
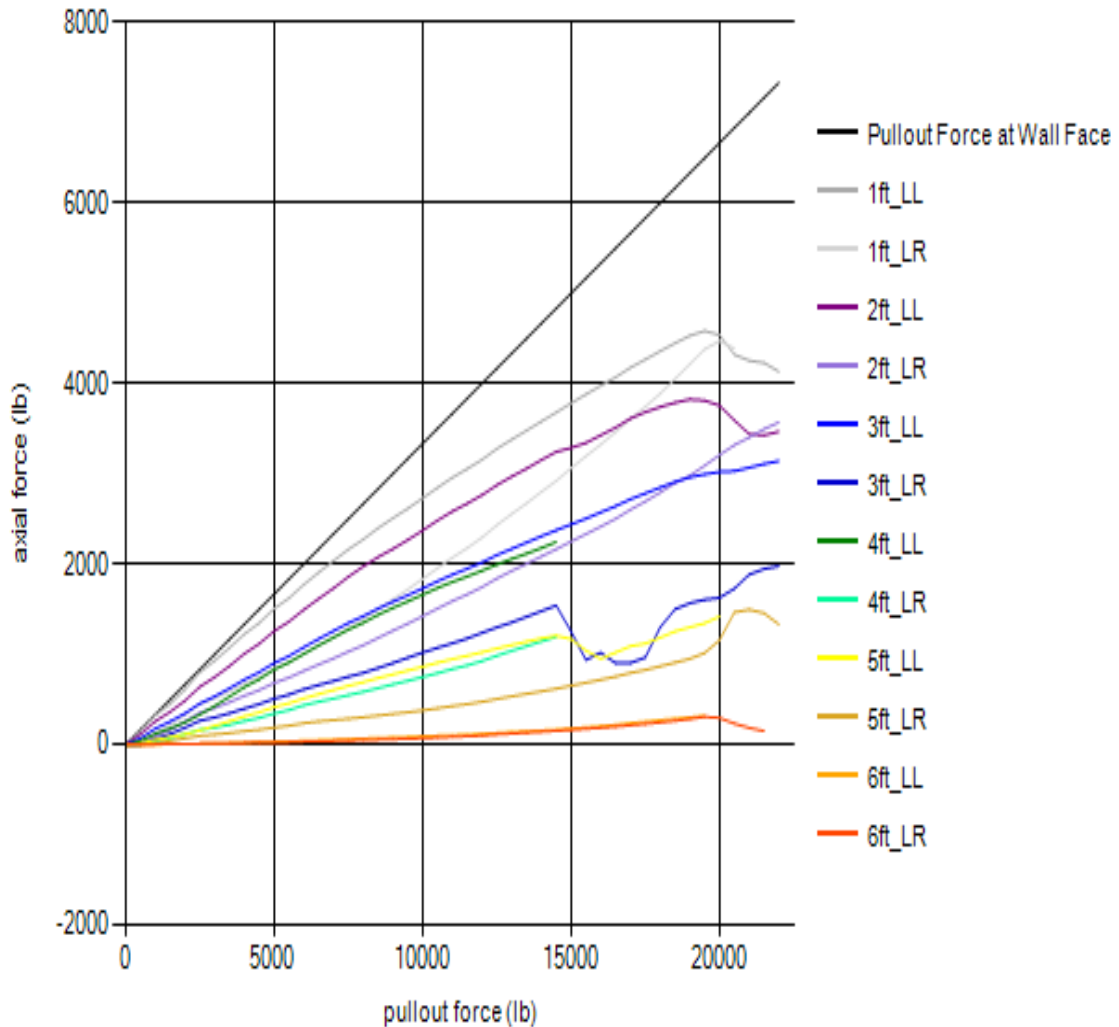
**Figure 6.36** Axial Forces Calculated Based on the Average of Strains Measured on the Inside and Outside of Longitudinal Bars versus Applied Pullout Load [TS25.02-G-9X12-W20xW11-L6-Z5-T]

In the next step, the strain measurements on the outside longitudinal bars as well as the transverse bars were reanalyzed to obtain bending moments. This was accomplished by first filtering the data. For the longitudinal bars, the difference between inside and outside strains from matching gage pairs was used to identify bending moments. In the transverse bars, the axial force was assumed to be zero and the single gage reading was relied upon when calculating bending moments. The bending moments in Figure 6.37 were plotted

against the corresponding applied pullout forces.  As expected, the various moments increase in magnitude with increased pullout force. Also, it can be seen that negative bending moments develop at some locations on the transverse bar (tension on the side nearest to the pullout force on transverse bars or toward the centerline on longitudinal bars) while positive bending moments developed at other locations.
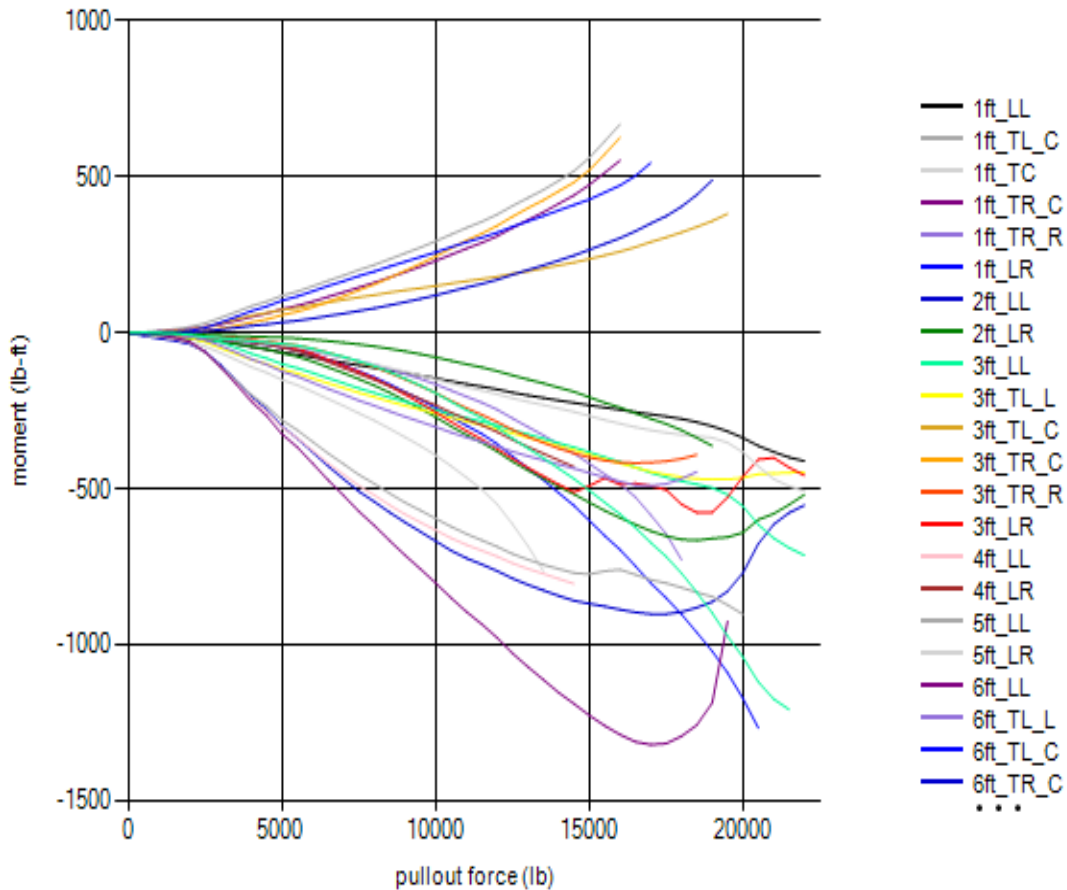


**Figure 6.37** Bending Moments Calculated Based on Strains Measured on the Inside and Outside of Longitudinal Bars versus Applied Pullout Load [TS25.02-G-9X12-W20xW11-L6-Z5-T]

The raw data plot shown above retains all potentially meaningful data collected. From these data sets additional plots were developed to facilitate analysis and observations on the behavior of grid type reinforcing under pullout.  The plots shown in this report represent some of the best and most complete datasets.  Data collected from other tests were not as complete due to progressive or complete strain gage failures. Nevertheless, the

observations described herein are generally supported by the strain gage data collected for all tests conducted in both Type B and Type A backfills. Complete strain gage reports for all strain gaged pullout tests can be found in Appendix K in Volume 2 and Appendix P in Volume 3 of this report.

*6.5.2.1  Distribution of Axial Forces in Longitudinal Bars Along the Length*

The variation of axial forces in the longitudinal bars as a function of distance from the front of the box is shown in Figure 6.38. This chart presents axial force measurements for all three longitudinal bars in the grid at various levels of applied pullout force. This is why each pullout force (color) in the chart differentiates three points for each measured distance – one is for the middle bar (the highest force) and the others for each outside bar.  The axial force shown at a distance of -1.0ft represents one-third of the applied pullout load.  This is the axial force that each longitudinal bar would be carrying if the applied pullout force is evenly distributed among the three longitudinal bars, an assumption common in MSE wall design. The axial forces shown at 0-ft are the axial forces measured at the front wall of the MSE test box.  The figure also shows the axial forces measured at each gage location inside the test box.
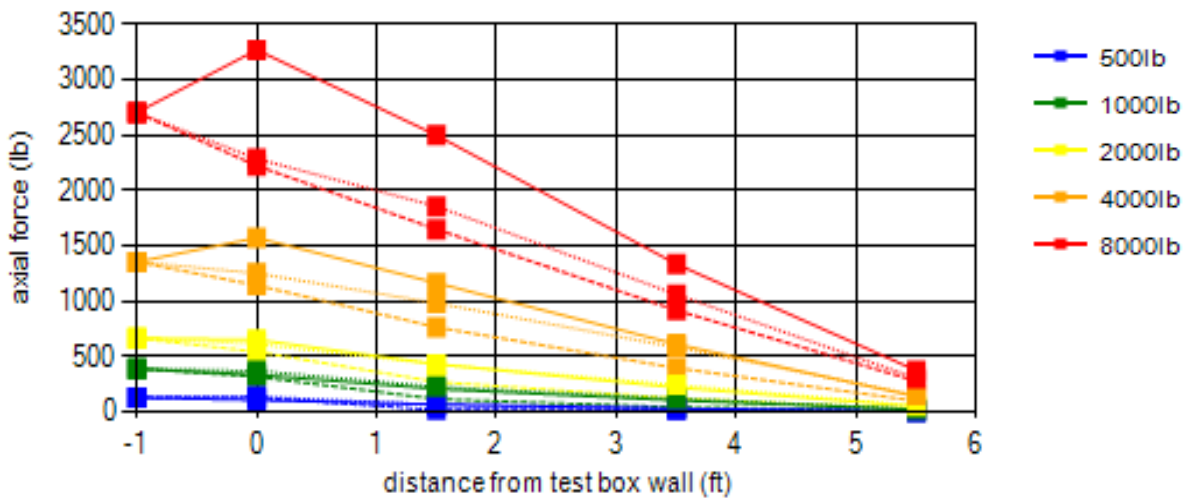


**Figure 6.38** Axial Tensile Force on Longitudinal Bars versus Distance from Front Wall of Test Box [TS48.11-G-9x12-W20xW11-L6-Z5-B]

The most important observation from this plot is that, as seen previously for strip reinforcements, the axial forces in longitudinal bars of welded steel grid reinforcements are distributed linearly along the length of the grid. This observation supports the view that steel grid reinforcement behaves in an inextensible manner. In other words, the relative displacement of the reinforcement with respect to the backfill remains nearly constant allowing the pullout resistance to develop uniformly.

An important corollary to this observation is that each transverse bar must develop approximately the same amount of pullout force. This will also be highlighted in the discussion about bending moments developed in the transverse bars. This observation is consistent with the AASHTO formulation for pullout resistance which functionally equates pullout resistance as linearly increasing with the number of transverse bars embedded in the backfill.

### 6.5.2.2 *Distribution of Axial Forces between Longitudinal Bars*

The AASHTO formulation for rupture capacity of grid type reinforcement assumes that the total pullout load on the grid is equally divided among longitudinal bars. Accordingly, in a three bar grid, each longitudinal bar would carry one third of the total load. The gage plans used in this research were designed to investigate the validity of this hypothesis. However, in the testing conducted in Type B materials, the gages on the center longitudinal bar proved unreliable due to local stress concentrations. In pullout testing conducted in Type A backfill, additional strain gage pairs were installed on each longitudinal bar outside the test box. Furthermore, the gage plan used in Type A testing also included gage pairs at three locations on each longitudinal bar inside the box, and this is mentioned in the discussion of Figure 6.38. This gage plan provided a very clear and complete picture of the distribution axial force between the middle and outside longitudinal bars.

Figure 6.39 presents this pullout test data in the form of cross sectional axial force diagrams at each gage location. Type A data show that the center longitudinal bar carries a greater share of the axial pullout force compared to the outside bars. Rather than sharing the total force equally among the three bars (*i.e.*, outside 33%, middle 33%, outside 33%), the actual distribution was closer to outside 30%, middle 40%, outside 30%. This finding

suggests that the AASHTO assumptions may be slightly unconservative on this point. Furthermore, this observation has important implications on the design of the connection between the steel grid and the facing panel; that is, the connection design should take into account that actual forces in the connections are not uniformly distributed .
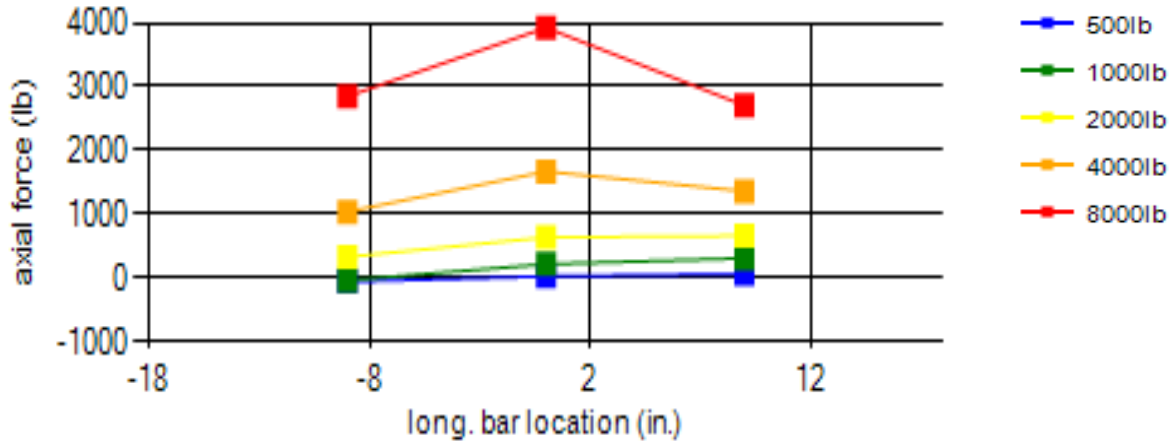


**Figure 6.39** Comparison of Axial Tensile Forces between the Left, Middle and Right Longitudinal Bars [TS48.11-G-9x12-W20xW11-L6-Z5-B Outside the Test Box]

Our gaging plan for reinforcements embedded in Type B backfill did not facilitate these same axial force measurements, but it is reasonable to assume that the axial force distribution for longitudinal bars of grids embedded in Type B backfill would behave similarly.

The strain gage data captured in the service load domain correlate well with observations made in the ultimate load domain during pullout testing. For example, the displacements measured on the center bar were typically lower than the outside bar displacements. This was particularly noticeable for pullout testing conducted in Type A backfill. This differential displacement in pullout testing would be caused by greater pullout resistance developed on the center bar. Additionally, the center bar was frequently observed yielding and rupturing well before the outside bars. This behavior is consistent with a force distribution for a 3-bar grid where the center bar is carrying a proportionally larger share of the axial force.

## 6.5.2.3 *Distribution of Bending Moments along Transverse Bars*

The bending moment data for welded steel grids as plotted in Figure 6.37 were used to investigate the bending behavior of the transverse bars in these grids. The findings were similar for reinforcements embedded in both Type A and Type B backfill. Figure 6.40 shows a representative example of a bending moment diagram for a transverse bar. The data trend seen in this plot is consistent with the expected behavior. The transverse bars experience negative bending moments at connections and positive bending moments at mid-points between connections. These plots show how the bending moments increase with increasing pullout loads. Moreover, it could be observed that bending moments calculated for different transverse bars on the same grid were similar in magnitude, indicating that transverse bars contributed equally to the overall pullout resistance of the grid. This finding is consistent with the observations of axial force along the longitudinal bars.
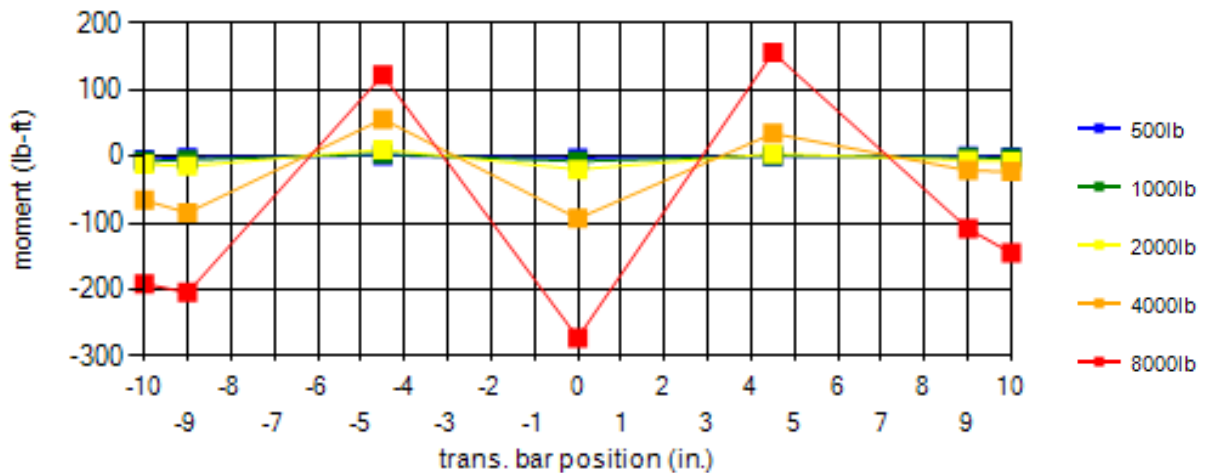


**Figure 6.40** Bending Moment Diagram for a Transverse Bar of a Grid Reinforcement [TS48.05-G-9x12-W20xW11-L6-Z5-M Transverse Bar at 3ft from the Test Box Wall]

Bending behavior of transverse bars obtained from analysis of strain gage data are well corroborated by observations collected during pullout testing and observations made on exhumed grids. For example, Figure 5.32 and Figure 5.33 illustrate plastic deformation of transverse bars and voids formed behind transverse bars during bending.

Figure 6.41 shows the ultimate permanent deformation of transverse bars in a grid exhumed after pullout testing. The deformation pattern in this grid is consistent with the

observations based on strain gage data. The center longitudinal bar is slightly behind the outside longitudinal bars indicating a concentration of pullout resistance in the center longitudinal bar. Each transverse bar is deformed as indicated by the moment distribution plot shown in Figure 6.40. Additionally each transverse bar has deformed by the same degree indicating that each transverse bar developed the same amount of pullout resistance.



**Figure 6.41** Transverse Bar Deformation of an Exhumed Grid Reinforcement

# CHAPTER 7
# CONCLUSIONS AND RECOMMENDATIONS

## 7.1 OVERVIEW

This research study was initiated to explore questions related to pullout resistance behavior of steel strip and grid type reinforcements used in TxDOT mechanically stabilized earth (MSE) wall construction. In current TxDOT MSE wall design practice, pullout resistance factors (F* values) are estimated using equations published by the AASHTO *Standard Specifications for Highway Bridges* (*21*) and are not based on project-specific pullout tests. AASHTO default values for F* have been developed from testing performed many decades ago on MSE reinforcement-backfill combinations that are not representative of materials used in TxDOT wall construction projects. Therefore, these AASHTO F* parameters may not be representative for wall systems built in Texas. Since pullout often governs the internal stability of wall systems that utilize metallic reinforcements, it is important to determine pullout resistance factors for specific reinforcement-backfill combinations used in TxDOT projects.

A second research question has to do with alternative reinforcement layouts used to avoid conflict between reinforcement and vertical obstructions located within the reinforced fill. Such alternative reinforcement layouts have the potential to impact the pullout resistance of the MSE reinforcement. Little or no data are available in published literature on the influence of alternative reinforcement details on pullout resistance.

In this study, the research team conducted an extensive pullout resistance test program to address the questions described above. A large scale test system including a test box with dimensions 12ft (length) x 12ft (width) x 4ft (height) and ability to accommodate three layers of MSE reinforcement in a single filling was specially designed and constructed. The test system had the capability to simulate overburden pressures corresponding to a maximum of 40ft of compacted backfill. Two types of granular backfill, Type A and Type B, and two types of metallic MSE reinforcement, ribbed strips and welded steel grids were included in the test program. The reinforcements were tested in typical design configurations with no skew or splay as well as with 15-deg and 30-deg skew and splay. In addition to the above, a limited number of pullout tests were conducted on smooth bars. A separate series of

pullout tests were conducted on strips and grids that were instrumented with electrical strain gages. The pullout test program conducted in this research study consisted of a total of 347 pullout tests in Type B backfill and 303 tests in Type A backfill. The data collected from this extensive test program were subjected to systematic and detailed statistical analyses.

This chapter presents the conclusions and the recommendations from this research study.

## 7.2    CONCLUSIONS

Conclusions about the pullout resistance behavior of inextensible MSE reinforcements embedded in backfills typically used in Texas can be summarized in three groups. Section 7.2.1 of this report presents conclusions from tests conducted in Type B (sandy) backfill on strips, grids and smooth bars. Section 7.2.1 presents conclusions from tests conducted in Type A (gravelly) backfill. Section 7.2.3 provides observations and conclusions from all strain gaged reinforcement testing.

### 7.2.1    Conclusions from Pullout Tests Conducted in Type B Backfill

The Type B test program consisted of a total of 347 pullout tests conducted on MSE reinforcements embedded in a sandy backfill that marginally met TxDOT specifications for Type B MSE select backfill. The test program included 126 pullout tests on ribbed strips, 204 pullout tests on welded steel grids and 17 pullout tests on smooth bars. The most important findings from this pullout test program are summarized below.

(a) Pullout resistance factors (F* values) determined from tests conducted on ribbed strip reinforcement embedded in sandy backfill are significantly higher than those predicted by the AASHTO equations for default F* when the soil is compacted to a relative compaction of 95%. The margin of separation between the lower 95th prediction limit established for the data from this study and the AASHTO reference line for F* is highest at depths of fill less than 20ft. The two lines converge at a depth of fill of 40ft.

(b) Analysis of Variance (ANOVA) conducted on the Type B ribbed strip dataset revealed that *depth of fill* is highly significant in determining the measured F* ($p=0.000$). The length of reinforcement was included among the independent

variables in the ANOVA so that the validity of the assumption inherent in the current AASHTO specifications could be tested. ANOVA results indicated that the reinforcement length was not a statistically-significant factor (p=0.090). This finding supports the assumptions used in the existing AASHTO formulation for pullout resistance factor for ribbed strips.

(c) The test program included 48 pullout tests performed on ribbed strips embedded in under-compacted Type B backfill with a relative compaction of approximately 91%. ANOVA conducted on the ribbed strip database shows that compaction is a highly-significant independent variable (p=0.000). Moreover, review of F* data collected show that "slight" under-compaction (only 4% below specification) can *significantly* lower MSE pullout resistance for ribbed strips (reduction of 34%). Data for the under-compacted pullout tests approached the AASHTO reference line.

(d) Relative to avoidance of vertical obstructions, ANOVA conducted on pullout test data for ribbed strip reinforcements placed at 0, 15 and 30-deg horizontal skew revealed that, at a skew angle of 15-deg, reinforcement skewing did not significantly impact the pullout resistance factor, with or without adjustment based on cosine projection. For a skew angle of 30-deg, the data indicate that pullout resistance factors without cosine projection adjustment are less than pullout resistance factors for straight strips. With cosine adjustment, the pullout resistance factors at 30-deg skew do not statistically differ from the pullout resistance factors for straight strips. .

(e) Pullout resistance factors (F* values) determined from pullout tests conducted on welded steel grid reinforcements embedded in Type B MSE select backfill were transformed into normalized F* by dividing by $t/S_t$. Such normalization was done so that F* data could be combined in a single plot and evaluated in one ANOVA. Results show that the measured normalized F* values obtained from this study are significantly higher than those predicted by the AASHTO equations when the soil is compacted to a relative compaction of 95%. The margin of separation between the lower 95th predicted limit established for the data obtained from this study and the AASHTO reference line was highest at depths of fill less than 20ft.

(f) ANOVA conducted on the Type B welded steel grid data revealed that depth of fill is statistically significant (p=0.011) and negatively correlated with normalized pullout resistance factor. The relationship between F* and depth of fill is consistent with AASHTO and most pronounced over the depth range from 0 to 20ft. ANOVA conducted on this data set further shows that embedment length is not statistically significant (p=0.132). This observation is also consistent with the AASHTO equation for F* for grids.

(g) According to AASHTO, F* for inextensible grids varies linearly with transverse bar spacing/transverse bar diameter ratio (*i.e.*, t/$S_t$). Accordingly, the normalized F* parameter would be independent of ($S_t$/t) ratio. However, ANOVA results from this study show that *transverse bar spacing* has significant influence (p=0.000) on the normalized F* (*i.e.*, F*$S_t$/t). The normalized F* was highest at a transverse bar spacing of 18 inches. Published literature indicates that the optimum transverse bar spacing for inextensible grids is 6in or greater (*1, 2*). There are two mechanisms that may contribute to the observed increase in normalized F* from a transverse bar spacing of 6in to 18in. The first is the frictional resistance provided by longer length of longitudinal bars in grids with larger transverse bar spacing. The second mechanism has to do with likely interaction that may be taking place between adjacent transverse bars. As the grid is pulled through compacted backfill, it is expected that large strains will develop within the material in the immediate vicinity of each transverse bar. When transverse bars are close to each other, the zones of disturbed material associated with adjacent bars may overlap with each other causing a reduction of the pullout capacity. The *transverse bar diameter* was not shown to be statistically significant (p=0.113) for normalized F* which is consistent with the AASHTO formulation.

(h) ANOVA for data from pullout tests on welded grid reinforcements embedded in Type B backfill show that the *longitudinal bar spacing* is a highly significant variable influencing normalized F* (p=0.000). The longitudinal bar size was not shown to be statistically significant (p=0.812). Longitudinal bar spacing is negatively correlated with the normalized pullout resistance factor. Normalized F* values are lowest at 12-inch spacing and highest at 2-inch spacing. A grid that has closely spaced longitudinal

bars would offer stiffer resistance during pullout because the transverse bars in these grids will not undergo as much deformation. As a result, grids with smaller longitudinal bar spacings will yield higher normalized F*. The significant impact that longitudinal bar spacing has on the pullout resistance factor of grid reinforcement is not reflected in the current AASHTO F* equation.

(i)  ANOVA conducted on pullout test data for welded steel grid reinforcements that were cut and splayed in the horizontal plane at splay angles of 0, 15-deg, and 30-deg revealed that, at splay angles of up to 30-deg, splaying did not significantly impact the pullout resistance. In other words, the pullout resistance factors for cut and splayed grid mats did not statistically differ from the pullout resistance factors for straight grid mats for splay angles up to 30-deg, with or without adjustment for cosine projection.

### 7.2.2   Conclusions from Pullout Tests Conducted in Type A Backfill

The Type A test program consisted of a total of 303 successfully-completed pullout tests on MSE reinforcements embedded in a gravelly backfill that marginally met TxDOT specifications for Type A MSE select backfill. Guidelines provided in TxDOT construction specifications for ordinary compaction were followed when placing and compacting the backfill material in the pullout test box. The test program included 73 pullout tests on ribbed strips, 214 pullout tests on welded steel grids and 16 pullout tests on smooth steel bars. The key findings from this pullout test program are summarized below.

(a)  Pullout resistance factors (F* values) determined from tests conducted on ribbed strip reinforcement embedded in Type A backfill are significantly higher than pullout resistance factors measured for strips in Type B as well as pullout resistance factors predicted by the AASHTO reference equation. The margin of separation between the lower 95th predicted limits for Type A and Type B backfills is greatest at shallow depths of fill. At a depth of fill of 5ft, measured F* values for pullout tests in Type A material are approximately double the F* values for tests in Type B material. The margin of separation decreases with depth, and at a depth of fill of 40ft, the F* values for the two predictive limits are comparable. A possible explanation is that for shallower depths of fill, the grain size, dilatancy effects, and

compaction conditions govern the pullout resistance.  As the depth of fill increases, the overburden stress begins to play a more dominant role.

(b) ANOVA conducted on the Type A ribbed strip dataset revealed that *depth of fill* is highly significant in determining the measured F* values (p=0.000).  The relationship between F* and depth of fill is consistent with AASHTO and most pronounced over the depth range from 0 to 20ft. However, unlike findings from the Type B analysis, ANOVA results for strips in Type A backfill indicate that the length of reinforcement *is* statistically significant (p=0.000). The pullout resistance factors decrease with increasing reinforcement length. This finding is not consistent with the assumptions made in the existing AASHTO formulation for pullout resistance factor for ribbed strips. A definitive explanation for the observed trend could not be established based on the data collected from this research study. Plausible explanations involve boundary effects and ultimate limit state effects associated with our large scale test system.  Additional testing is necessary to establish the validity of apparent length effect finding.  The predictive models developed in this study used the longest reinforcement length which represented the most conservative conditions.

(c) ANOVA conducted on pullout test data for ribbed strip reinforcement placed at horizontal skew angles of 0, 15-deg and 30-deg skew identified evidence of interaction between reinforcement skew angle and depth of fill.  ANOVA results indicate that, at a skew angle of 15-deg, reinforcement skewing does not significantly impact the pullout resistance at depths of fill of 5ft and 12ft, with or without adjustment for cosine projection.  However, F* values measured at a skew angle of 30-deg were found to be significantly different (lower) compared to those measured at zero skew, with or without adjustment for cosine projection.

(d) Pullout resistance factors (F* values) determined from pullout tests conducted on welded steel grid reinforcement embedded in Type A backfill were transformed to obtain normalized F* by dividing by $t/S_t$.  As explained previously, such normalization allows F* data to be combined in a single plot. ANOVA results show that the normalized F* values for grid reinforcements in Type A backfill are

significantly higher than F* values obtained for reinforcements in Type B backfill. The margin of separation between the lower 95th predicted limits established for Type A and Type B data is highest at shallow depths of fill.  In the depth range from 0ft to 5ft, Type A F* values are larger than Type B F* values by a factor of two or more.

(e)  ANOVA conducted on normalized F* data for welded steel grids in Type A backfill revealed that *depth of fill* is significant (p=0.000) and negatively correlated with normalized pullout resistance factor.  The relationship between F* and depth of fill is consistent with AASHTO and most pronounced over the depth range from 0 to 20ft. Findings from the ANOVA with regard to the influence of reinforcement length are similar to that observed for strip reinforcements in Type A backfill.  In other words, the ANOVA indicates that embedment length is a statistically-significant independent variable (p=0.000).  This observation is not consistent with the underlying assumptions of the AASHTO F*equation for grids.  As noted for strips, plausible explanations involve boundary effects and ultimate limit state effects associated with our large scale test system, but additional testing is necessary to establish the validity of apparent length effect finding.

(f)  The results from ANOVA conducted on the normalized F* dataset to determine effects of transverse bar spacing and diameter showed that both the *transverse bar spacing* and *transverse bar diameter* have significant influence (both p=0.000).  The normalized F* increases with increasing transverse bar spacing and reaches a peak value at 18 inches. The transverse bar diameter is inversely correlated to the normalized F*.  The influence of transverse bar spacing on normalized F* for grids in Type A is similar to that observed for grids in Type B backfill.  Two mechanisms may contribute:  (1) frictional resistance provided by longer length of longitudinal bars in grids with larger transverse bar spacing, and (2) likely interaction between adjacent transverse bars.

(g)  ANOVA conducted to investigate the influence of *longitudinal bar spacing* on pullout resistance of welded grid reinforcement in Type A backfill indicated that the longitudinal bar spacing is a highly significant variable influencing normalized F* (p=0.000).  This finding agrees closely with results obtained for grids in Type B backfill.

Longitudinal bar spacing is negatively correlated with the normalized pullout resistance factor. Accordingly, the normalized F* values are smallest at 12-inch longitudinal bar spacing and largest at 2-inch longitudinal bar spacing. In addition, the *longitudinal bar diameter* was also found to be statistically significant (p=0.000) with larger bar diameters resulting in higher normalized F* values.

(h) ANOVA conducted on pullout test data for welded grid reinforcement (bar mats) that were cut and splayed at horizontal splay angles of 0, 15-deg and 30-deg revealed that splaying has a significant impact on the pullout resistance (p=0.002). However, when the normalized F* was recalculated using adjustment for the cosine effect, the effect of splaying was observed to be not statistically significant (p=0.123).

### 7.2.3 Conclusions from Pullout Tests Conducted on Strain Gaged Reinforcements

This section presents conclusions from the pullout tests conducted on strain gaged MSE reinforcements which were performed to gain better insight on interactions that take place between the MSE reinforcement and backfill under pullout loading. The test program included 15 gaged strips in Type B backfill and 3 gaged strips in Type A backfill. The program also included 11 gaged grid reinforcements in Type B backfill and 6 gaged grid reinforcements in Type A backfill. The conclusions from this test program are summarized below.

(a) Data obtained from strain gages installed at intervals along the length of strip and grid reinforcements confirm that axial tensile force decreases linearly from a maximum value equal to the applied pullout force at the leading end (application of pull force) to zero at the trailing end of the reinforcement. This linear distribution of axial force is consistent with coherent gravity theory which holds that pullout resistance is mobilized uniformly along the length of inextensible reinforcements. Evidence of this was clear for pullout loads within the service load range. The data are less consistent at higher pullout loads primarily because of failure of strain gages.

(b) Strain gaged testing on grid reinforcements evaluated the magnitudes of axial loads carried by each longitudinal bar during pullout loading. Comparison of axial forces measured on the center bar and the two outside bars of three-bar grid reinforcements shows that the pullout load is not distributed evenly among the three longitudinal bars. Rather, the center bar carries approximately 40 percent of the total load while the remaining 60 percent of the load is divided equally between the two outside bars.

(c) Strain gaged tests on grid reinforcements also examined the direction and magnitude of bending moments on transverse bars during loading. The data confirm that positive bending moments develop on the transverse bars at mid-span (between connections to the longitudinal bars) and negative bending moments exist in the vicinity of welded connections to the longitudinal bars. These observations are consistent with the deformed shapes observed in steel grid elements that were exhumed after pullout tests had been completed.

(d) Measured strains were used to calculate bending moments for instrumented transverse bars in a steel grid mat. The magnitudes of these bending moments were then compared to determine their relative contribution to the total pullout capacity. The comparison reveals that the pullout load is distributed fairly evenly among different transverse bars.

## 7.3 RECOMMENDATIONS

The findings from TxDOT research project 0-6493 support the following recommendations for implementation and further study.

(a) Pullout resistance factor data for steel strip and grid type reinforcements developed from this research study clearly demonstrate that the requirements stipulated in TxDOT *Standard Specifications* Item 423 for the selection and compaction of Type A and Type B MSE select backfill are adequate in terms of providing a safe wall design relative to pullout resistance. Therefore, no changes in TxDOT specifications for MSE backfill material selection and compaction are recommended.

(b) The pullout resistance factors measured for strip and grid reinforcement embedded in properly compacted Type B material are significantly higher than the default F* parameters obtained using AASHTO equations.   For both strip and grid type reinforcements embedded in Type B backfill at fill depths of up to 20ft, the measured F* values are approximately twice as large as the AASHTO default F* estimates. Accordingly, if construction specifications are adhered to, the actual factor of safety against pullout failure for MSE walls built using Type B backfill will be twice as large as the design factor of safety.  This means that for wall systems designed using the allowable stress design method, the actual factor of safety against pullout failure will be about 3.0 instead of 1.5.   It recommended that TxDOT take this finding into consideration relative to their processes and procedures for MSE retaining wall design, construction, and quality control.

(c) The pullout resistance factors measured for strip and grid reinforcement embedded in properly compacted Type A material are even higher than those measured for strips and grids in Type B backfill within the depth of fill range where pullout resistance may control the design (*i.e.*, the top 20ft of the wall).  For strip type reinforcements embedded in Type A (gravelly) backfill, the ratio between the F* values obtained by the 95th lower predictive limit established from this research and the default F* parameters obtained using AASHTO equations is in the range of 3 to 4.  For grid type reinforcement, the corresponding ratio is in the range of 1.8 to 3.6.  These findings suggest that the actual margin of safety against pullout failure is significantly higher than the design factor of safety.  It recommended that TxDOT take this finding into consideration relative to their processes and procedures for MSE retaining wall design, construction, and quality control.

(d) Observation of grid reinforcement behavior during pullout testing revealed that transverse bars undergo significant bending deformation, especially at large displacements.   Bending of transverse bars in turn generates rotational movements and excessive shear stresses at connections between transverse and longitudinal bars.   The rate of failure of the welded connections was significantly high due to the effects of these rotational movements.   Therefore, it is recommended that the weld connection test

methods used for the quality control testing of grid reinforcements simulate the actual deformation behavior of the grid reinforcement under the effects of pullout loading.

(e) Pullout resistance data for steel grid type reinforcements provide clear evidence that the current AASHTO equations for default F* do not adequately account for all relevant grid parameters.  The most noteworthy parameter among those not considered in the current AASHTO equations is the *longitudinal bar spacing*.  According to the AASHTO equation, the default F* value for grids is independent of the longitudinal bar spacing.  Thus, a grid with 12-in longitudinal bar spacing ought to provide twice the pullout resistance of a grid with 6-in longitudinal bar spacing because it has twice the width.  However, data collected in this study show that F* values for narrow grids are much higher than F* values obtained for the wider grids.  This effect partially offsets the reduction in pullout resistance capacity due to difference in grid width.  In other words, narrow grids represent a more efficient system in terms of pullout resistance gained for the amount of steel used.  Therefore, it is recommended that TxDOT consider allowing alternative predictive models that account for the influence of longitudinal bar spacing on F* in their MSE wall design procedure.

(f) A second grid parameter not properly accounted for in the AASHTO equations is the *transverse bar spacing*.  The current AASHTO equation indicates that F* for grids is inversely proportional to transverse bar spacing.  This relationship is based on the belief that the pullout resistance capacity of grid reinforcement is solely dependent on the number of transverse bars embedded in the backfill rather than on grid length. By this view, according to the AASHTO equation, a grid with transverse bar spacing of 6-in ought to provide three times the pullout resistance of a grid with transverse bar spacing of 18-in and the same length.  However, data collected in this research for both Type A and Type B backfills clearly demonstrate that, for three wire grids with 9-in longitudinal bar spacing, the optimum pullout resistance performance is achieved at a transverse bar spacing of 18-in.  The actual ratio is approximately 2.0 for grids embedded in Type B backfill and 2.4 for grids in Type A backfill.  The influence of transverse bar spacing on pullout resistance factor is not as pronounced as that of longitudinal bar spacing.  Nevertheless, the implementation of the F* predictive model developed in this research

to account for transverse bar spacing would allow further optimization of the wall design.

(g) Based on the statistical comparison of F* values measured for ribbed strip reinforcements embedded in Type B (sandy) and Type A (gravelly) backfill and laid at 0, 15-deg and 30-deg skew angles, the findings of this study are consistent with AASHTO policy which allows rotation of strip reinforcement at pinned connections for skew angles up to 15-deg to avoid vertical obstructions. At skew angles of 15-deg or less, length adjustment based on cosine projection is not necessary. This finding assumes that the backfill has been compacted according to specification. The focus of this part of the study was to evaluate the influence of skew angle on pullout resistance. This study did not explore other factors associated with skewing such as interaction between the reinforcement and the obstruction, induced bending in the reinforcement, connection impacts, degradation of corrosion protection, or other factors associated with skewing that might affect MSE wall performance. Therefore, it is recommended that implementation of the findings of this research on skewing of MSE strip reinforcement be accomplished in association with due consideration to potential impact that these non-pullout resistance related factors may have on the performance of an MSE wall with skewed reinforcement.

(h) This study evaluated the influence of splay angle on pullout resistance for welded steel grids (*i.e.*, bar mats with three longitudinal bars) where the transverse bars were cut to allow the longitudinal bars to be splayed around vertical obstructions for splay angles of up to 30-deg. For steel grid reinforcements embedded in Type B (sandy) and Type A (gravelly) backfill with transverse bars cut and longitudinal bars splayed at 0, 15-deg and 30-deg splay angles, no statistically significant difference in pullout resistance was measured when the length of reinforcement was adjusted for cosine projection. This finding assumes (a) the backfill is compacted according to specification, (b) splaying originates at least two transverse bars from the wall face, (c) after being cut, the cantilevered portions of the transverse bars remain attached to the longitudinal bars, and (d) the longitudinal bars are bent smoothly to achieve the necessary splay angle. The focus of this part of the study was to evaluate the influence of splay angle on pullout

resistance. This study did not investigate potential impact that cutting and splaying may have on distribution of lateral earth pressure on wall panels. Also, this study did not explore other factors associated with cutting and splaying grid reinforcements such as method(s) used to splay the longitudinal bars, interaction between the grid reinforcement and the obstruction, induced bending in the grid reinforcements, connection impacts, degradation of corrosion protection caused by cutting and bending the grid, or other factors associated with cutting and splaying that might affect MSE wall performance. . Therefore, it is recommended that implementation of the findings of this research on splaying of MSE grid reinforcement be accomplished in association with due consideration to potential impact that these non-pullout resistance related factors may have on the performance of an MSE wall with splayed grid reinforcement.

(i)     This research focused on the pullout behavior of MSE reinforcements embedded in backfill materials that met the specification requirements for material quality as well as compaction.  This study did not investigate the influence of possible departures from specifications that may occur in the field.  However, a change in the test protocol used in the initial stages of testing led to the accidental discovery that F* values for strips embedded in sandy backfill are highly sensitive to the level of compaction in the fill. Data show that a small reduction in compaction level (approximately 4 percent reduction in relative compaction) resulted in a significant reduction in the pullout resistance capacity (34 percent).   This finding highlights the importance of proper compaction during field construction.  It is recommended that the effects of under-compaction be more completely and systematically evaluated through further research.   Such research should also investigate the influence of backfill compaction levels on the pullout resistance of grid type reinforcements.  The research design should also examine whether pullout resistance of strip and grid reinforcements show similar sensitivity to Type A backfill placement conditions.

**REFERENCES**

1. Elias, V., B.R. Christopher and R.R. Berg, *Mechanically Stabilized Earth Walls and Reinforced Soil Slopes Design and Construction Guidelines*, FHWA-NHI-00-043, National Highway Institute, Federal Highway Administration, U.S. Department of Transportation, Washington, D.C., March 2001.

2. Berg, R.R, B.R. Christopher, and N. C. Samtani. *Design of Mechanically Stabilized Earth Walls and Reinforced Soil Slopes – Volume I*, FHWA NHI-10-024-Vol I, National Highway Institute, Federal Highway Administration, U.S. Department of Transportation, Washington, D.C., November 2009.

3. Texas Department of Transportation, Powerpoint Presentation made at the Pre-proposal meeting for Project 0-6784: Creep Behavior of Soil Nails in High Plasticity Index Soils, Presentation made by Marcus Galvan, P.E. Geotechnical Branch Manager, TxDOT Bridge Division, February 2012.

4. AASHTO LRFD Bridge Design Specifications - 5th Edition, Section 11: Abutments, Piers, and Walls, American Association of State Highway and Transportation Officials, Washington D.C., 2010.

5. TxDOT Standard Specifications 2004, ITEM 423: Retaining Walls, ftp://ftp.dot.state.tx.us/pub/txdot-info/cmd/cserve/specs/2004/standard/s423.pdf

6. Vidal, H. The Principle of Reinforced Earth. *Highway Research Record No 282,* Washington, D. C., 1969.

7. Peterson, L. M. Pullout Resistance of Welded Wire Mesh Embedded in Soil. *M.S. Thesis,* Utah State University, Logan, Utah, 1980.

8. Chang, J. C., Hannon, J. B., & Forsyth, R. A. Pull Resistance and Interaction of Earthwork Reinforcement and Soil. *Transportation Research Board 56th Annual Meeting* 10, 1977

9. Bishop, J.A. and Anderson L.R., Performance of a Welded Wire Retaining Wall, *Report Submitted to the Hilfiker Company,* Utah State University, Logan, Utah, 1979.

10. Jewell, R.A., Milligan, G.W.E., Sarsby, R.W. and Dubois, D., Interaction Between Soil and Reinforcement, *Proceedings, Symposium on Polymer Grid Reinforcement in Civil Engineering*, Thornton Tellford Ltd., London, UN, pp. 19-29, 1984.

11. Bergado D.T., Lo K., Chai J.C., Shivankar, R., Alfaro, M., Anderson, L.R., Pullout Tests Using Steel Grid Reinforcements with Low Quality Backfill. *Journal of Geotechnical Engineering.* Vol. 18, No. 7. pp. 1047-1063, 1992.

12. TxDOT Standard Specifications 2004, ITEM 423: Retaining Walls, ftp://ftp.dot.state.tx.us/pub/txdot-info/cmd/cserve/specs/2004/standard/s423.pdf

13. Geotechnical Manual, Texas Department of Transportation, August 2006, http://onlinemanuals.txdot.gov/txdotmanuals/geo/index.htm

14. Test Procedure for Particle Size Analysis of Soils, TxDOT Designation: Tex-110-E, ftp://ftp.dot.state.tx.us/pub/txdot-info/cst/TMS/100-E_series/pdfs/soi110.pdf.

15. Test Procedure for Soundness of Aggregate using Sodium or Magnesium Sulfate, TxDOT Designation: Tex-411-A, ftp://ftp.dot.state.tx.us/pub/txdot-info/cst/TMS/400-A_series/pdfs/cnn411.pdf

16. Test Procedure for Determining Soil pH, TxDOT Designation: Tex-128-E, ftp://ftp.dot.state.tx.us/pub/txdot-info/cst/TMS/100-E_series/pdfs/soi128.pdf

17. Test Procedure for Measuring Resistivity of Soil Materials, TxDOT Designation: Tex-129-E, ftp://ftp.dot.state.tx.us/pub/txdot-info/cst/TMS/100-E_series/pdfs/soi129.pdf

18. Test Procedure for Determining Chloride and Sulfate Contents in Soil, TxDOT Designation: Tex-620-J, ftp://ftp.dot.state.tx.us/pub/txdot-info/cst/TMS/600-J_series/pdfs/chm620.pdf.

19. Test Procedure for Laboratory Compaction Characteristics and Moisture-Density Relationship of Subgrade, Embankment Soil and Backfill Material, TxDOT Designation: Tex-114-E, ftp://ftp.dot.state.tx.us/pub/txdot-info/cst/TMS/100-E_series/pdfs/soi114.pdf.

20. TxDOT Standard Specifications 2004, ITEM 132: Embankment, ftp://ftp.dot.state.tx.us/pub/txdot-info/cmd/cserve/specs/2004/standard/s132.pdf

21. Section 5: Retaining Walls, AASHTO Standard Specifications for Highway Bridges, 17th Edition, 2002.

22. Nielsen, M. R., & Anderson, L. R., Pullout Resistance of Wire Mats Embedded in Soil, *Report Submitted to the Hilfiker Company,* Utah State University Logan, Utah 1984.

23. Hannon, J. B., & Forsyth, R. A., Performance of an Earthwork Reinforcement System Constructed with Low-Quality Backfill. *Transportation Research Record 965* , 55-64, 1984.

24. VSL Corporation, Pullout Test Report Submitted to *Texas Department of Highways and Public Transportation*, Project: Interstate 35, Bexar County, July 1983.

25. VSL Corporation, Pullout Test Report Submitted to *Texas Department of Highways and Public Transportation*, Project: Loop 1, Travis County, January 1984.

26. VSL Corporation, Pullout Test Report Submitted to *Texas Department of Highways and Public Transportation*, Project: Loop 820, Tarrant County, March 1984.

27. VSL Corporation, Pullout Test Report Submitted to *Texas Department of Highways and Public Transportation*, Project: Loop 1, Austin, April 1984.

28. VSL Corporation, Pullout Test Report Submitted to *Texas Department of Highways and Public Transportation*, Project: Loop 1, Travis County, May 1984.

29. VSL Corporation, Pullout Test Report Submitted to *Texas Department of Highways and Public Transportation*, Project: Interstate 35, San Antonio, December 1984.

30. Bergado, D.T., Sampaco, C.L., Shivankar, R., Alfaro, M., Anderson, L.R., & Balasubramaniam A. S., Interaction of Welded Reinforcement with Poor Quality Backfill. *Proceedings: Southeast Asian Geotechical Conference, Taipei,* Vol. 1, Southeast Asian Geotechnical Society, Taipei, Taiwan, pp. 29-34, 1990.

31. Bergado D.T., Hardiyatimo H.C., Cisneros C.B., Chun C.J., Alfaro M.C., Balasubramaniam A. S. and Anderson L.R., Pullout Resistance of Steel Geogrids with Weathered Clay as Backfill Material. *Geotechnical Testing Journal*, GTJODJ, Vol. 15, No.1, pp 33-46, 1992.

32. Bergado, D.T., Chai J.C., Abeira H.O., Alfaro M.C., Balasubramaniam A. S., Interaction Between Cohesive Frictional Soil and Various Grid Reinforcements. *Geotextiles and Geomembranes*. Vol. 12, pp. 327-349, 1993.

33. Bergado, D.T., Chai J.C., Miura N., Prediction of Pullout Resistance and Pullout Force Displacement Relationship for Inextensible Grids. *Soils and Foundations*, Vol. 36, No.4, Japanese Technical Society, pp. 11-22, 1996.

34. Matsui T., San K.C, Nabeshima Y., and Amin U.N., Ultimate Pullout Loads of Steel Mesh in Sand. *Technology Reports of Osaka University*, Vol. 46, No. 2240, 1996a.

35. Matsui T., San K.C., Nabeshima Y., & Amin U.N., Bearing Mechanism of Steel Grid Reinforcement in Pullout Test . *Earth Reinforcement: Proceedings of the 3$^{rd}$ International Symposium on Earth Reinforcement,* Fukuoka, Kyushu, Japan. Vol. 1, pp. 269-274, 1996b.

36. Matsui T., Nabeshima Y., & Amin U.N., Reinforcing Effect of Steel Grid Reinforcement in Granular Soil, *International Conference on Urban Engineering in Asian Cities in the 21$^{st}$ Century,* Bangkok, Thailand, pp. B37-B42, 1996c.

37. Nabeshima Y., Matsui T., Bearing Resistance of Inextensible Grid Reinforcements. *The Proceedings of the Eighth International Offshore and Polar Engineering Conference.* Vol. 1. pp. 521-526, 1998.

38. Teerawattanasuk C., Bergado D.T., Kongkitkul W., Analytical and Numerical Modeling of Pullout Capacity and Interaction Between Hexagonal Wire Mesh and Silty Sand Backfill Under an In-soil Pullout Test. *Canadian Geotechnical Journal.* Vol. 40, pp. 886-899, 2003.

39. Lee H.S., Bobet A., (2005) Laboratory Evaluation of Pullout Capacity of Reinforced Silty Sands in Drained and Undrained Conditions. *Geotechnical Testing Journal.* Volume 28, No.4., pp. 370-379, 2003.

40. Horpibulsuk S., Niramitkornburee A., Pullout Resistance of Bearing Reinforcement Embedded in Sand. *Soils and Foundations,* Vol. 50, No. 2, pp. 215-226, 2010.

41. The Reinforced Earth Company, Technical Bulletin: MSE-6, Apparent Coefficient of Friction, f* to be Used in the Design of Reinforced Earth Structures, 1995.

42. Bergado, D.T., Sampaco, C.L., Shivashankar, R., Alfaro, M.C., Anderson, L.R., and Balasubramanium, A.S., Interaction of Welded Wire Wall with Poor Quality Backfills on Soft Clay, " ASCE Geotechnical Engineering Congress, ASCE, New York, NY, 1991.

43. Bergado D.T., Hardiyatimo H.C., Cisneros C.B., Chun C.J., Alfaro M.C., Balasubramaniam A. S. and Anderson L.R., Pullout Resistance of Steel Geogrids with Weathered Clay as Backfill Material. *Geotechnical Testing Journal*, GTJODJ, Vol. 15, No.1., pp 33-46, 1992.

44. ASTM (2008), Annual Book of Standards, Vol. 4.13, Geosynthetics, ASTM D 6706: Standard Test Method for Measuring Geosynthetic Pullout Resistance Testing in Soil, ASTM International, Philadelphia, PA.

45. —. *The Reinforced Earth Company Design Manual.* Vienna, VA: The Reinforced Earth Company, 2005.

46. Lyons, Louis, "A Practical Guide to Data Analysis for Physical Science Students," Cambridge University Press, Cambridge, UK, 1991.

Appendix A

Type B Backfill Gradation Data

**Table A-1: Type B Backfill Gradation Data**

**TYPE B**

|  | Pre TS 0 % Passing | Pre TS 0 % Retained | Post TS 15 % Passing | Post TS 15 % Retained | Post TS 30 % Passing | Post TS 30 % Retained |
|---|---|---|---|---|---|---|
| 3/8-in | 100 | 0 | 100 | 0 | 100 | 0 |
| # 4 | 99 | 1 | 99 | 1 | 99 | 1 |
| # 10 | 93 | 7 | 93 | 7 | 94 | 6 |
| # 20 | 84 | 16 | 84 | 16 | 86 | 14 |
| # 40 | 66 | 34 | 67 | 33 | 68 | 32 |
| # 100 | 19 | 81 | 22 | 78 | 21 | 79 |
| # 200 | 9 | 91 | 13 | 87 | 10 | 90 |
| Pan | 0 | 100 | **0** | **100** | **0** | **100** |

## Table A-2: Type A Backfill Gradation Data

### TYPE A Batch 1

|  | Pre TS 30 % Passing | Pre TS 30 % Retained | Pre TS 34 % Passing | Pre TS 34 % Retained | Post TS 37 % Passing | Post TS 37 % Retained |
|---|---|---|---|---|---|---|
| 1. 1/2-in | 100 | 0 | 100 | 0 | 100 | 0 |
| 1-in | 100 | 0 | 100 | 0 | 100 | 0 |
| 3/4-in | 83 | 17 | 94 | 6 | 84 | 16 |
| 1/2-in | 59 | 41 | 76 | 24 | 66 | 34 |
| 3/8-in | 49 | 52 | 55 | 45 | 57 | 43 |
| # 4 | 29 | 71 | 38 | 62 | 41 | 59 |
| # 10 | 17 | 83 | 24 | 76 | 28 | 72 |
| # 40 | 7 | 93 | 13 | 87 | 17 | 84 |
| # 200 | 1 | 99 | 4 | 96 | 7 | 93 |

### Type A Batch 2

|  | Pre TS 38 % Passing | Pre TS 38 % Retained | Pre TS 42 % Passing | Pre TS 42 % Retained | Post TS 44 % Passing | Post TS 44 % Retained |
|---|---|---|---|---|---|---|
| 1. 1/2-in | 100 | 0 | 100 | 0 | 100 | 0 |
| 1-in | 96 | 4 | 98 | 2 | 99 | 2 |
| 3/4-in | 63 | 37 | 72 | 28 | 80 | 20 |
| 1/2-in | 40 | 60 | 53 | 47 | 61 | 39 |
| 3/8-in | 32 | 68 | 43 | 57 | 53 | 47 |
| # 4 | 18 | 82 | 30 | 71 | 39 | 61 |
| # 10 | 11 | 89 | 20 | 80 | 27 | 73 |
| # 40 | 5 | 95 | 11 | 89 | 16 | 84 |
| # 200 | 2 | 98 | 6 | 94 | 9 | 91 |

### Type A Batch 3

|  | Pre TS 45 % Passing | Pre TS 45 % Retained | Pre TS 48 % Passing | Pre TS 48 % Retained | Post TS 50 % Passing | Post TS50 % Retained |
|---|---|---|---|---|---|---|
| 1. 1/2-in | 100 | 0 | 100 | 0 | 100 | 0 |
| 1-in | 97 | 3 | 96 | 4 | 99 | 1 |
| 3/4-in | 72 | 28 | 72 | 28 | 79 | 21 |
| 1/2-in | 51 | 49 | 52 | 49 | 57 | 43 |
| 3/8-in | 42 | 58 | 43 | 57 | 48 | 52 |
| # 4 | 29 | 71 | 30 | 70 | 35 | 65 |
| # 10 | 18 | 82 | 21 | 80 | 26 | 74 |
| # 40 | 9 | 91 | 11 | 89 | 17 | 83 |
| # 200 | 4 | 96 | 6 | 95 | 10 | 90 |

# Appendix B

# Summary of Quality Control Data for Reinforcements

# Table B2. Summary of Quality Control Data for Ribbed Strip Reinforcements

| Strips Recd. on February 26, 2012 | | | Strips Recd. on Nov. 10, 2012 | | | Strips Recd. on May 20, 2012 | | | Strips Recd. on January 09, 2012 | | |
|---|---|---|---|---|---|---|---|---|---|---|---|
| Lbs/feet: - | | | Lbs/feet: - | | | Lbs/feet: 1.124 | | | Lbs/feet: 1.124 | | |
| Thickness: - | | | Thickness: - | | | Thickness: 0.157 | | | Thickness: 0.157 | | |
| Width (in): - | | | Width (in): - | | | Width (in): 1.969 | | | Width (in): 1.969 | | |
| Yield Strength (ksi) | Tensile Strength (ksi) | % Elong. 8 in. | Yield Strength (ksi) | Tensile Strength (ksi) | % Elong. 8 in. | Yield Strength (ksi) | Tensile Strength (ksi) | % Elong. 8 in. | Yield Strength (ksi) | Tensile Strength (ksi) | % Elong. 8 in. |
| 60.3 | 103.9 | 12% | 76.1 | 103.6 | 13% | 84.0 | 104.8 | 13% | 79.7 | 104.7 | 11% |
| 77.9 | 104.5 | 12% | 78.2 | 106.9 | 12% | 81.5 | 103.9 | 13% | 86.7 | 104.5 | 12% |
| 76.5 | 102.4 | 13% | 79.2 | 105.1 | 9% | 83.1 | 105.1 | 13% | 79.7 | 106.9 | 12% |
| 86.0 | 105.0 | 11% | 76.4 | 101.8 | 13% | 80.9 | 102.4 | 13% | 78.5 | 99.6 | 13% |
| 83.0 | 101.0 | 13% | 90.3 | 110.8 | 11% | 79.7 | 105.4 | 11% | 81.5 | 101.5 | 11% |
| 75.8 | 105.4 | 11% | 76.4 | 104.2 | 9% | 79.2 | 102.7 | 13% | 81.2 | 101.5 | 11% |
| 78.2 | 105.7 | 13% | 76.4 | 106.3 | 12% | 79.4 | 103.6 | 11% | 80.6 | 101.2 | 10% |
| 93.0 | 105.1 | 12% | 77.0 | 104.2 | 12% | 80.1 | 103.6 | 12% | 77.9 | 100.3 | 12% |
| 76.7 | 106.0 | 10% | 77.6 | 106.9 | 11% | 78.5 | 102.7 | 10% | 80.4 | 100.9 | 11% |
| 78.5 | 103.9 | 12% | 76.7 | 105.1 | 14% | 81.5 | 103.0 | 12% | 79.7 | 105.1 | 12% |
| 77.6 | 102.7 | 11% | 75.8 | 105.4 | 11% | 81.3 | 103.9 | 11% | | | |
| 91.5 | 107.6 | 13% | 79.8 | 105.7 | 12% | 82.1 | 102.7 | 13% | | | |
| 79.9 | 105.7 | 11% | 83.0 | 107.5 | 10% | 77.3 | 100.9 | 13% | | | |
| 77.6 | 106.3 | 10% | 76.4 | 105.0 | 15% | 76.1 | 101.2 | 13% | | | |
| 81.8 | 100.6 | 13% | 76.4 | 104.2 | 12% | 79.5 | 102.1 | 13% | | | |
| 90.9 | 105.7 | 12% | 85.4 | 102.7 | 11% | 80.4 | 103.0 | 11% | | | |
| 78.5 | 105.7 | 11% | 79.8 | 109.7 | 13% | 78.8 | 105.7 | 10% | | | |
| 86.1 | 106.0 | 12% | | | | | | | | | |
| 89.7 | 109.6 | 12% | | | | | | | | | |
| 76.6 | 103.3 | 12% | | | | | | | | | |

**Table B2.  Summary of Quality Control Data for Welded Steel Grid Reinforcements**

| | | Original | | Tensile | Yield | Reduced | | | Bend | Weld | Weld | Weld | Weld | Required |
|---|---|---|---|---|---|---|---|---|---|---|---|---|---|---|
| | | Diam. | Area | Strength | Strength | Diam. | Area | % Area | Test | Shear | Shear | Shear | Shear | Weld |
| | | in | in$^2$ | ksi | ksi | in | in$^2$ | % | | Test 1 | Test 2 | Test 3 | Test 4 | Shear |
| Grids Received on July 7, 2010 | Line Wire | 0.505 | 0.200 | 94.5 | -- | 0.364 | 0.104 | 48 | ok | 8881 | 8542 | 7038 | 7937 | 7011 |
| | Cross Wire | 0.374 | 0.110 | 96.5 | -- | 0.242 | 0.045 | 58 | | | | | | |
| | Line Wire | 0.348 | 0.095 | 96.6 | -- | 0.206 | 0.033 | 65 | ok | 6516 | 6185 | 6107 | 5391 | 3850 |
| | Cross Wire | 0.374 | 0.110 | 97.8 | -- | 0.252 | 0.050 | 55 | | | | | | |
| | Line Wire | 0.505 | 0.200 | 91.6 | -- | 0.357 | 0.100 | 50 | ok | 8991 | 8785 | 8407 | 7556 | 7011 |
| | Cross Wire | 0.437 | 0.150 | 103.2 | -- | 0.333 | 0.087 | 42 | | | | | | |
| | Line Wire | 0.505 | 0.200 | 91.6 | -- | 0.357 | 0.100 | 50 | ok | 8991 | 8785 | 8407 | 7556 | 7011 |
| | Cross Wire | 0.437 | 0.150 | 103.2 | -- | 0.333 | 0.087 | 42 | | | | | | |
| | Line Wire | 0.505 | 0.200 | 91.6 | -- | 0.357 | 0.100 | 50 | ok | 8991 | 8785 | 8407 | 7556 | 7011 |
| | Cross Wire | 0.437 | 0.150 | 103.2 | -- | 0.333 | 0.087 | 42 | | | | | | |
| | Line Wire | 0.58 | 0.264 | 69.4 | -- | 0.357 | 0.100 | 62 | ok | 4991 | 8785 | 8407 | 7556 | 9247 |
| | Cross Wire | 0.437 | 0.150 | 103.2 | -- | 0.333 | 0.087 | 42 | | | | | | |
| | Line Wire | 0.505 | 0.200 | 91.6 | -- | 0.357 | 0.100 | 50 | ok | 8991 | 8785 | 8407 | 7556 | 7011 |
| | Cross Wire | 0.437 | 0.150 | 103.2 | -- | 0.333 | 0.087 | 42 | | | | | | |
| | Line Wire | 0.505 | 0.200 | 91.6 | -- | 0.357 | 0.100 | 50 | ok | 8991 | 8785 | 8407 | 7556 | 7011 |
| | Cross Wire | 0.437 | 0.150 | 103.2 | -- | 0.333 | 0.087 | 42 | | | | | | |
| | Line Wire | 0.505 | 0.200 | 91.3 | -- | 0.322 | 0.081 | 60 | ok | 8091 | 7979 | 7878 | 7642 | 7011 |
| | Cross Wire | 0.374 | 0.110 | 62.1 | -- | 0.199 | 0.031 | 72 | | | | | | |
| | Line Wire | 0.505 | 0.200 | 91.3 | -- | 0.322 | 0.081 | 60 | ok | 8091 | 7979 | 7878 | 7642 | 7011 |
| | Cross Wire | 0.309 | 0.075 | 92.3 | -- | 0.199 | 0.031 | 59 | | | | | | |
| | Line Wire | 0.505 | 0.200 | 91.3 | -- | 0.322 | 0.081 | 60 | ok | 8091 | 7979 | 7878 | 7642 | 7011 |
| | Cross Wire | 0.309 | 0.075 | 92.3 | -- | 0.199 | 0.031 | 59 | | | | | | |
| | Line Wire | 0.505 | 0.200 | 91.3 | -- | 0.322 | 0.081 | 60 | ok | 8091 | 7979 | 7878 | 7642 | 7011 |
| | Cross Wire | 0.309 | 0.075 | 92.3 | -- | 0.199 | 0.031 | 59 | | | | | | |
| | Line Wire | 0.505 | 0.200 | 91.3 | -- | 0.322 | 0.081 | 60 | ok | 8091 | 7979 | 7878 | 7642 | 7011 |
| | Cross Wire | 0.309 | 0.075 | 92.3 | -- | 0.199 | 0.031 | 59 | | | | | | |

**Table B2. Summary of Quality Control Data for Welded Steel Grid Reinforcements (Cont.)**

| | | Original | | Tensile | Yield | Reduced | | | Bend | Weld | Weld | Weld | Weld | Required |
|---|---|---|---|---|---|---|---|---|---|---|---|---|---|---|
| | | Diam. | Area | Strength | Strength | Diam. | Area | % Area | Test | Shear | Shear | Shear | Shear | Weld |
| | | in | in$^2$ | ksi | ksi | in | in$^2$ | % | | Test 1 | Test 2 | Test 3 | Test 4 | Shear |
| Grids Received on July 7, 2010 | Line Wire | 0.505 | 0.200 | 91.3 | -- | 0.322 | 0.081 | 60 | ok | 8091 | 7979 | 7878 | 7642 | 7011 |
| | Cross Wire | 0.309 | 0.075 | 92.3 | -- | 0.199 | 0.031 | 59 | | | | | | |
| | Line Wire | 0.505 | 0.200 | 94.5 | -- | 0.364 | 0.104 | 48 | ok | 8881 | 8542 | 7038 | 7937 | 7011 |
| | Cross Wire | 0.374 | 0.110 | 96.5 | -- | 0.242 | 0.045 | 58 | | | | | | |
| | Line Wire | 0.505 | 0.200 | 94.5 | -- | 0.364 | 0.104 | 48 | ok | 8881 | 8542 | 7038 | 7937 | 7011 |
| | Cross Wire | 0.374 | 0.110 | 96.5 | -- | 0.242 | 0.045 | 58 | | | | | | |
| | Line Wire | 0.505 | 0.200 | 94.5 | -- | 0.364 | 0.104 | 48 | ok | 8881 | 8542 | 7038 | 7937 | 7011 |
| | Cross Wire | 0.374 | 0.110 | 96.5 | -- | 0.242 | 0.045 | 58 | | | | | | |
| | Line Wire | 0.505 | 0.200 | 94.5 | -- | 0.364 | 0.104 | 48 | ok | 8881 | 8542 | 7038 | 7937 | 7011 |
| | Cross Wire | 0.374 | 0.110 | 96.5 | -- | 0.242 | 0.045 | 58 | | | | | | |
| | Line Wire | 0.505 | 0.200 | 94.5 | -- | 0.364 | 0.104 | 48 | ok | 8881 | 8542 | 7038 | 7937 | 7011 |
| | Cross Wire | 0.374 | 0.110 | 96.5 | -- | 0.242 | 0.045 | 58 | | | | | | |
| | Line Wire | 0.505 | 0.200 | 94.5 | -- | 0.364 | 0.104 | 48 | ok | 8881 | 8542 | 7038 | 7937 | 7011 |
| | Cross Wire | 0.374 | 0.110 | 96.5 | -- | 0.242 | 0.045 | 58 | | | | | | |
| | Line Wire | 0.505 | 0.200 | 94.5 | -- | 0.364 | 0.104 | 48 | ok | 8881 | 8542 | 7038 | 7937 | 7011 |
| | Cross Wire | 0.374 | 0.110 | 96.5 | -- | 0.242 | 0.045 | 58 | | | | | | |
| | Line Wire | 0.505 | 0.200 | 94.5 | -- | 0.364 | 0.104 | 48 | ok | 8881 | 8542 | 7038 | 7937 | 7011 |
| | Cross Wire | 0.374 | 0.110 | 96.5 | -- | 0.242 | 0.045 | 58 | | | | | | |
| | Line Wire | 0.505 | 0.200 | 94.5 | -- | 0.364 | 0.104 | 48 | ok | 8881 | 8542 | 7038 | 7937 | 7011 |
| | Cross Wire | 0.374 | 0.110 | 96.5 | -- | 0.242 | 0.045 | 58 | | | | | | |
| | Line Wire | 0.505 | 0.200 | 94.5 | -- | 0.364 | 0.104 | 48 | ok | 8881 | 8542 | 7038 | 7937 | 7011 |
| | Cross Wire | 0.374 | 0.110 | 96.5 | -- | 0.242 | 0.045 | 58 | | | | | | |
| | Line Wire | 0.505 | 0.200 | 94.5 | -- | 0.364 | 0.104 | 48 | ok | 8881 | 8542 | 7038 | 7937 | 7011 |
| | Cross Wire | 0.374 | 0.110 | 96.5 | -- | 0.242 | 0.045 | 58 | | | | | | |

**Table B2. Summary of Quality Control Data for Welded Steel Grid Reinforcements (Cont.)**

| | | Original | | Tensile | Yield | Reduced | | | Bend | Weld | Weld | Weld | Weld | Required |
|---|---|---|---|---|---|---|---|---|---|---|---|---|---|---|
| | | Diam. | Area | Strength | Strength | Diam. | Area | % Area | Test | Shear | Shear | Shear | Shear | Weld |
| | | in | in$^2$ | ksi | ksi | in | in$^2$ | % | | Test 1 | Test 2 | Test 3 | Test 4 | Shear |
| | Line Wire | 0.505 | 0.200 | 94.5 | -- | 0.364 | 0.104 | 48 | ok | 8881 | 8542 | 7038 | 7937 | 7011 |
| | Cross Wire | 0.374 | 0.110 | 96.5 | -- | 0.242 | 0.045 | 58 | | | | | | |
| | Line Wire | 0.505 | 0.200 | 94.5 | -- | 0.364 | 0.104 | 48 | ok | 8881 | 8542 | 7038 | 7937 | 7011 |
| | Cross Wire | 0.374 | 0.110 | 96.5 | -- | 0.242 | 0.045 | 58 | | | | | | |
| | Line Wire | 0.348 | 0.095 | 96.6 | -- | 0.206 | 0.033 | 65 | ok | 6516 | 6185 | 6107 | 5391 | 3850 |
| | Cross Wire | 0.374 | 0.110 | 97.8 | -- | 0.252 | 0.050 | 55 | | | | | | |
| | Line Wire | 0.348 | 0.095 | 96.6 | -- | 0.206 | 0.033 | 65 | ok | 6516 | 6185 | 6107 | 5391 | 3850 |
| | Cross Wire | 0.374 | 0.110 | 97.8 | -- | 0.252 | 0.050 | 55 | | | | | | |
| Grids Received on July 7, 2010 | Line Wire | 0.348 | 0.095 | 96.6 | -- | 0.206 | 0.033 | 65 | ok | 6516 | 6185 | 6107 | 5391 | 3850 |
| | Cross Wire | 0.374 | 0.110 | 97.8 | -- | 0.252 | 0.050 | 55 | | | | | | |
| | Line Wire | 0.348 | 0.095 | 96.6 | -- | 0.206 | 0.033 | 65 | ok | 6516 | 6185 | 6107 | 5391 | 3850 |
| | Cross Wire | 0.374 | 0.110 | 97.8 | -- | 0.252 | 0.050 | 55 | | | | | | |
| | Line Wire | 0.348 | 0.095 | 96.6 | -- | 0.206 | 0.033 | 65 | ok | 6516 | 6185 | 6107 | 5391 | 3850 |
| | Cross Wire | 0.374 | 0.110 | 97.8 | -- | 0.252 | 0.050 | 55 | | | | | | |
| | Line Wire | 0.348 | 0.095 | 96.6 | -- | 0.206 | 0.033 | 65 | ok | 6516 | 6185 | 6107 | 5391 | 3850 |
| | Cross Wire | 0.374 | 0.110 | 97.8 | -- | 0.252 | 0.050 | 55 | | | | | | |
| | Line Wire | 0.348 | 0.095 | 96.6 | -- | 0.206 | 0.033 | 65 | ok | 6516 | 6185 | 6107 | 5391 | 3850 |
| | Cross Wire | 0.374 | 0.110 | 97.8 | -- | 0.252 | 0.050 | 55 | | | | | | |
| | Line Wire | 0.348 | 0.095 | 96.6 | -- | 0.206 | 0.033 | 65 | ok | 6516 | 6185 | 6107 | 5391 | 3850 |
| | Cross Wire | 0.374 | 0.110 | 97.8 | -- | 0.252 | 0.050 | 55 | | | | | | |

**Table B2.  Summary of Quality Control Data for Welded Steel Grid Reinforcements (Cont.)**

| | | Original | | Tensile | Yield | Reduced | | | Bend | Weld | Weld | Weld | Weld | Required |
|---|---|---|---|---|---|---|---|---|---|---|---|---|---|---|
| | | Diam. | Area | Strength | Strength | Diam. | Area | % Area | Test | Shear | Shear | Shear | Shear | Weld |
| | | in | in$^2$ | ksi | ksi | in | in$^2$ | % | | Test 1 | Test 2 | Test 3 | Test 4 | Shear |
| Grids Received on June 28, 2011 | Line Wire | 0.505 | 0.200 | 89.2 | 81.584 | 0.332 | 0.087 | 56.78 | ok | 9072 | 8921 | 8663 | 8314 | 7010 |
| | Cross Wire | 0.374 | 0.110 | 105.5 | 96.204 | 0.230 | 0.042 | 62.18 | | | | | | |
| | Line Wire | 0.505 | 0.200 | 91.2 | 83.055 | 0.340 | 0.091 | 54.67 | ok | 9086 | 8914 | 8861 | 8457 | 7010 |
| | Cross Wire | 0.437 | 0.150 | 102.0 | 93.341 | 0.283 | 0.063 | 58.06 | | | | | | |
| | Line Wire | 0.348 | 0.095 | 103.7 | 94.961 | 0.210 | 0.035 | 63.59 | ok | 5618 | 5042 | 4819 | 4783 | 3845 |
| | Cross Wire | 0.374 | 0.110 | 103.7 | 95.254 | 0.237 | 0.044 | 59.84 | | | | | | |
| | Line Wire | 0.505 | 0.200 | 90.8 | 83.152 | 0.351 | 0.097 | 51.69 | ok | 9143 | 8876 | 8516 | 8491 | 7010 |
| | Cross Wire | 0.309 | 0.075 | 91.8 | 90.961 | 0.187 | 0.028 | 63.38 | | | | | | |
| Grids Received on February 6, 2012 | Line Wire | 0.505 | 0.200 | 102.6 | 96.052 | 0.297 | 0.069 | 66 | ok | 8361 | 8248 | 7926 | 7843 | 7011 |
| | Cross Wire | 0.374 | 0.110 | 101.2 | 94.65 | 0.221 | 0.038 | 65 | | | | | | |
| | Line Wire | 0.505 | 0.200 | 102.6 | 96.052 | 0.297 | 0.069 | 66 | ok | 8361 | 8248 | 7926 | 7843 | 7011 |
| | Cross Wire | 0.374 | 0.110 | 101.2 | 94.65 | 0.221 | 0.038 | 65 | | | | | | |
| | Line Wire | 0.505 | 0.200 | 102.6 | 96.052 | 0.297 | 0.069 | 66 | ok | 8361 | 8248 | 7926 | 7843 | 7011 |
| | Cross Wire | 0.374 | 0.110 | 101.2 | 94.65 | 0.221 | 0.038 | 65 | | | | | | |
| | Line Wire | 0.505 | 0.200 | 102.6 | 96.052 | 0.297 | 0.069 | 66 | ok | 8361 | 8248 | 7926 | 7843 | 7011 |
| | Cross Wire | 0.374 | 0.110 | 101.2 | 94.65 | 0.221 | 0.038 | 65 | | | | | | |
| | Line Wire | 0.505 | 0.200 | 102.6 | 96.052 | 0.297 | 0.069 | 66 | ok | 8361 | 8248 | 7926 | 7843 | 7011 |
| | Cross Wire | 0.374 | 0.110 | 101.2 | 94.65 | 0.221 | 0.038 | 65 | | | | | | |
| | Line Wire | 0.505 | 0.200 | 102.6 | 96.052 | 0.297 | 0.069 | 66 | ok | 8361 | 8248 | 7926 | 7843 | 7011 |
| | Cross Wire | 0.374 | 0.110 | 101.2 | 94.65 | 0.221 | 0.038 | 65 | | | | | | |
| | Line Wire | 0.505 | 0.200 | 102.6 | 96.052 | 0.297 | 0.069 | 66 | ok | 8361 | 8248 | 7926 | 7843 | 7011 |
| | Cross Wire | 0.374 | 0.110 | 101.2 | 94.65 | 0.221 | 0.038 | 65 | | | | | | |
| | Line Wire | 0.505 | 0.200 | 102.6 | 96.052 | 0.297 | 0.069 | 66 | ok | 8361 | 8248 | 7926 | 7843 | 7011 |
| | Cross Wire | 0.374 | 0.110 | 101.2 | 94.65 | 0.221 | 0.038 | 65 | | | | | | |
| | Line Wire | 0.505 | 0.200 | 102.6 | 96.052 | 0.297 | 0.069 | 66 | ok | 8361 | 8248 | 7926 | 7843 | 7011 |
| | Cross Wire | 0.374 | 0.110 | 101.2 | 94.65 | 0.221 | 0.038 | 65 | | | | | | |

# Appendix C

## Summary Data for MSE Reinforcement Pullout Tests

**Ribbed Strips in Type B Backfill**

**Ribbed Strips in Type B Backfill – Under-Compacted**

**Welded Steel Grids in Type B Backfill**

**Smooth Steel Bars in Type B Backfill**

**TABLE C1: SUMMARY DATA FOR MSE REINFORCEMENT PULLOUT TESTS**
**RIBBED STRIPS IN TYPE B BACKFILL**

| TestID | Length, Le (ft) | Width, b (in.) | Skew, β (°) | Reinforcement Behavior | Displacement (in.) | Overburden, σv (psf) | DOF, z (ft) | Load, Pr (lb) | F* |
|---|---|---|---|---|---|---|---|---|---|
| TS09.13-S-L4-Z5-T | 4 | 2 | 0 | Pullout | 0.65 | 637 | 5.1 | 3429 | 4.03 |
| TS09.14-S-L4-Z5-T | 4 | 2 | 0 | Pullout | 0.51 | 642 | 5.2 | 2890 | 3.38 |
| TS09.15-S-L4-Z5-B | 4 | 2 | 0 | Pullout | 0.74 | 627 | 5 | 3012 | 3.61 |
| TS13.13-S-L4-Z5-B | 4 | 2 | 0 | Pullout | 0.63 | 885 | 7 | 4447 | 3.77 |
| TS13.14-S-L4-Z5-T | 4 | 2 | 0 | Pullout | 0.75 | 635 | 5 | 4098 | 4.84 |
| TS17.13-S-L4-Z5-T | 4 | 2 | 0 | Pullout | 0.75 | 639 | 5.1 | 3917 | 4.6 |
| TS17.15-S-L4-Z5-M | 4 | 2 | 0 | Pullout | 0.73 | 629 | 5 | 5225 | 6.23 |
| TS17.17-S-L4-Z5-B | 4 | 2 | 0 | Pullout | 0.73 | 632 | 5 | 4603 | 5.46 |
| TS20.13-S-L8-Z5-T | 8 | 2 | 0 | Pullout | 0.74 | 632 | 5 | 8266 | 4.9 |
| TS20.17-S-L8-Z5-B | 8 | 2 | 0 | Pullout | 0.25 | 637 | 5 | 5968 | 3.51 |
| TS29.09-S-L8-Z5-M | 8 | 2 | 0 | Pullout | 0.72 | 635 | 4.9 | 11278 | 6.66 |
| TS29.13-S-L8-Z5-B | 8 | 2 | 0 | Pullout | 0.74 | 634 | 4.8 | 12255 | 7.25 |
| TS10.14-S-L12-Z5-T | 12 | 2 | 0 | Pullout | 0.75 | 645 | 5 | 10457 | 4.06 |
| TS10.16-S-L12-Z5-B | 12 | 2 | 0 | Pullout | 0.74 | 653 | 5.1 | 10679 | 4.09 |
| TS11.13-S-L12-Z5-T | 12 | 2 | 0 | Pullout | 0.74 | 637 | 5.1 | 11117 | 4.36 |
| TS18.14-S-L12-Z5-T | 12 | 2 | 0 | Pullout | 0.74 | 652 | 5.2 | 9537 | 3.66 |
| TS18.17-S-L12-Z5-M | 12 | 2 | 0 | Pullout | 0.54 | 626 | 5 | 17741 | 7.08 |
| TS18.20-S-L12-Z5-B | 12 | 2 | 0 | Pullout | 0.74 | 636 | 5.1 | 12985 | 5.1 |
| TS29.01-S-L12-Z5-T | 12 | 2 | 0 | Pullout | 0.75 | 626 | 4.9 | 12595 | 5.03 |
| TS29.05-S-L12-Z5-T | 12 | 2 | 0 | Pullout | 0.75 | 623 | 4.9 | 13611 | 5.46 |

| TestID | Length, Le (ft) | Width, b (in.) | Skew, β (°) | Reinforcement Behavior | Displacement (in.) | Overburden, σv (psf) | DOF, z (ft) | Load, Pr (lb) | F* |
|---|---|---|---|---|---|---|---|---|---|
| TS10.13-S-L4-Z12-T | 4 | 2 | 0 | Pullout | 0.71 | 1517 | 11.8 | 5757 | 2.85 |
| TS10.15-S-L4-Z12-B | 4 | 2 | 0 | Pullout | 0.7 | 1526 | 11.9 | 4914 | 2.42 |
| TS17.14-S-L4-Z12-T | 4 | 2 | 0 | Pullout | 0.69 | 1500 | 12 | 4770 | 2.38 |
| TS17.16-S-L4-Z12-M | 4 | 2 | 0 | Pullout | 0.72 | 1510 | 12 | 6710 | 3.33 |
| TS17.18-S-L4-Z12-B | 4 | 2 | 0 | Pullout | 0.65 | 1517 | 12.1 | 6363 | 3.15 |
| TS20.14-S-L8-Z12-T | 8 | 2 | 0 | Pullout | 0.72 | 1520 | 12 | 8738 | 2.16 |
| TS20.16-S-L8-Z12-M | 8 | 2 | 0 | Pullout | 0.22 | 1542 | 12.2 | 9204 | 2.24 |
| TS20.18-S-L8-Z12-B | 8 | 2 | 0 | Pullout | 0.65 | 1546 | 12.2 | 11396 | 2.76 |
| TS29.10-S-L8-Z12-M | 8 | 2 | 0 | Pullout | 0.74 | 1529 | 11.8 | 16037 | 3.93 |
| TS29.14-S-L8-Z12-B | 8 | 2 | 0 | Pullout | 0.75 | 1520 | 11.6 | 13887 | 3.43 |
| TS18.15-S-L12-Z12-T | 12 | 2 | 0 | Pullout | 0.74 | 1539 | 12.3 | 14685 | 2.39 |
| TS18.18-S-L12-Z12-M | 12 | 2 | 0 | Pullout | 0.74 | 1544 | 12.3 | 18795 | 3.04 |
| TS18.21-S-L12-Z12-B | 12 | 2 | 0 | Pullout | 0.74 | 1523 | 12.1 | 16996 | 2.79 |
| TS29.02-S-L12-Z12-T | 12 | 2 | 0 | Pullout | 0.75 | 1569 | 12.3 | 14261 | 2.27 |
| TS29.06-S-L12-Z12-M | 12 | 2 | 0 | Rupture | 0.51 | 1539 | 11.9 | 22427 | 3.64 |
| TS19.13-S-L4-Z20-T | 4 | 2 | 0 | Pullout | 0.75 | 2502 | 20 | 4762 | 1.43 |
| TS19.16-S-L4-Z20-M | 4 | 2 | 0 | Pullout | 0.74 | 2545 | 20.3 | 6382 | 1.88 |
| TS19.19-S-L4-Z20-B | 4 | 2 | 0 | Pullout | 0.71 | 2534 | 20.2 | 4852 | 1.44 |
| TS20.15-S-L8-Z20-M | 8 | 2 | 0 | Pullout | 0.74 | 2649 | 21 | 12390 | 1.75 |
| TS21.14-S-L8-Z20-T | 8 | 2 | 0 | Pullout | 0.74 | 2550 | 19.8 | 15983 | 2.35 |
| TS21.16-S-L8-Z20-M | 8 | 2 | 0 | Pullout | 0.73 | 2606 | 20.3 | 20133 | 2.9 |
| TS21.18-S-L8-Z20-B | 8 | 2 | 0 | Pullout | 0.75 | 2545 | 19.8 | 12973 | 1.91 |
| TS29.11-S-L8-Z20-B | 8 | 2 | 0 | Pullout | 0.75 | 2560 | 19.5 | 17762 | 2.6 |

| TestID | Length, Le (ft) | Width, b (in.) | Skew, β (°) | Reinforcement Behavior | Displacement (in.) | Overburden, σv (psf) | DOF, z (ft) | Load, Pr (lb) | F* |
|---|---|---|---|---|---|---|---|---|---|
| TS29.15-S-L8-Z20-B | 8 | 2 | 0 | Pullout | 0.75 | 2555 | 19.4 | 16350 | 2.4 |
| TS19.15-S-L12-Z20-T | 12 | 2 | 0 | Pullout | 0.73 | 2530 | 20.2 | 12136 | 1.2 |
| TS19.18-S-L12-Z20-M | 12 | 2 | 0 | Pullout | 0.73 | 2545 | 20.3 | 18313 | 1.8 |
| TS19.21-S-L12-Z20-B | 12 | 2 | 0 | Pullout | 0.74 | 2557 | 20.4 | 17685 | 1.73 |
| TS29.03-S-L12-Z20-T | 12 | 2 | 0 | Pullout | 0.74 | 2547 | 19.9 | 20972 | 2.06 |
| TS29.07-S-L12-Z20-M | 12 | 2 | 0 | Rupture | 0.5 | 2573 | 19.8 | 23009 | 2.24 |
| TS21.13-S-L4-Z40-T | 4 | 2 | 0 | Pullout | 0.74 | 5060 | 39.3 | 7473 | 1.11 |
| TS21.15-S-L4-Z40-M | 4 | 2 | 0 | Pullout | 0.48 | 5079 | 39.5 | 11974 | 1.77 |
| TS21.17-S-L4-Z40-B | 4 | 2 | 0 | Pullout | 0.55 | 5038 | 39.2 | 6342 | 0.94 |
| TS09.16-S-L6-Z40-B | 6 | 2 | 0 | Pullout | 0.74 | 5064 | 40.7 | 10400 | 1.03 |
| TS18.13-S-L6-Z40-T | 6 | 2 | 0 | Pullout | 0.72 | 5089 | 40.6 | 7151 | 0.7 |
| TS18.16-S-L6-Z40-M | 6 | 2 | 0 | Pullout | 0.29 | 5112 | 40.8 | 13928 | 1.36 |
| TS18.19-S-L6-Z40-B | 6 | 2 | 0 | Pullout | 0.4 | 5043 | 40.2 | 11546 | 1.14 |
| TS19.14-S-L8-Z40-T | 8 | 2 | 0 | Pullout | 0.74 | 5016 | 40 | 13551 | 1.01 |
| TS19.17-S-L8-Z40-M | 8 | 2 | 0 | Pullout | 0.73 | 5083 | 40.5 | 14469 | 1.07 |
| TS19.20-S-L8-Z40-B | 8 | 2 | 0 | Pullout | 0.75 | 5046 | 40.2 | 14029 | 1.04 |
| TS29.12-S-L8-Z40-B | 8 | 2 | 0 | Pullout | 0.74 | 5116 | 38.9 | 20289 | 1.49 |
| TS29.16-S-L8-Z40-B | 8 | 2 | 0 | Rupture | 0.36 | 5118 | 38.9 | 21479 | 1.57 |
| TS29.04-S-L12-Z40-T | 12 | 2 | 0 | Rupture | 0.74 | 5026 | 39.3 | 20954 | 1.04 |
| TS29.08-S-L12-Z40-M | 12 | 2 | 0 | Rupture | 0.34 | 5667 | 43.7 | 21725 | 0.96 |
| TS22.07-S-L8-ß15°-Z5-T | 8 | 2 | 15 | Pullout | 0.72 | 639 | 5.2 | 10865 | 6.38 |
| TS22.08-S-L8-ß15°-Z5-M | 8 | 2 | 15 | Pullout | 0.72 | 629 | 5.1 | 15880 | 9.47 |
| TS22.09-S-L8-ß15°-Z5-B | 8 | 2 | 15 | Pullout | 0.73 | 626 | 5.1 | 14562 | 8.73 |

| TestID | Length, Le (ft) | Width, b (in.) | Skew, β (°) | Reinforcement Behavior | Displacement (in.) | Overburden, σv (psf) | DOF, z (ft) | Load, Pr (lb) | F* |
|---|---|---|---|---|---|---|---|---|---|
| TS23.07-S-L4.5-ß15°-Z12-T | 4.5 | 2 | 15 | Pullout | 0.29 | 1528 | 12.1 | 5120 | 2.23 |
| TS23.08-S-L4.5-ß15°-Z12-M | 4.5 | 2 | 15 | Pullout | 0.75 | 1504 | 11.9 | 10447 | 4.63 |
| TS23.09-S-L4.5-ß15°-Z12-B | 4.5 | 2 | 15 | Pullout | 0.09 | 1500 | 11.9 | 6147 | 2.73 |
| TS24.14-S-L4.5-ß15°-Z12-M | 4.5 | 2 | 15 | Pullout | 0.73 | 1526 | 12.1 | 7271 | 3.18 |
| TS24.15-S-L4.5-ß15°-Z12-B | 4.5 | 2 | 15 | Pullout | 0.7 | 1527 | 12.1 | 5797 | 2.53 |
| TS27.07-S-L8-ß30°-Z5-T | 8 | 2 | 30 | Pullout | 0.74 | 642 | 5 | 9086 | 5.31 |
| TS27.08-S-L8-ß30°-Z5-M | 8 | 2 | 30 | Pullout | 0.75 | 646 | 5 | 11504 | 6.68 |
| TS27.09-S-L8-ß30°-Z5-B | 8 | 2 | 30 | Pullout | 0.74 | 636 | 4.9 | 15872 | 9.37 |
| TS24.13-S-L4.5-ß30°-Z12-T | 4.5 | 2 | 30 | Pullout | 0.72 | 1517 | 12 | 3656 | 1.61 |
| TS25.13-S-L4.5-ß30°-Z12-T | 4.5 | 2 | 30 | Pullout | 0.66 | 1516 | 11.9 | 2015 | 0.89 |
| TS25.14-S-L4.5-ß30°-Z12-M | 4.5 | 2 | 30 | Pullout | 0.75 | 1535 | 12.1 | 5587 | 2.43 |
| TS25.15-S-L4.5-ß30°-Z12-B | 4.5 | 2 | 30 | Pullout | 0.75 | 1546 | 12.2 | 4087 | 1.76 |

**TABLE C2: SUMMARY DATA FOR MSE REINFORCEMENT PULLOUT TESTS**
**RIBBED STRIPS IN TYPE B BACKFILL – UNDER-COMPACTED**

| TestID | Length, Le (ft) | Width, b (in.) | Skew, β (°) | Reinforcement Behavior | Displacement (in.) | Overburden, σv (psf) | DOF, z (ft) | Load, Pr (lb) | F* |
|---|---|---|---|---|---|---|---|---|---|
| TS01.04-S-L8-Z5-T | 8 | 2 | 0 | Pullout | 0.72 | 597 | 4.9 | 4352 | 2.73 |
| TS01.05-S-L8-Z5-T | 8 | 2 | 0 | Pullout | 0.69 | 617 | 5 | 5867 | 3.57 |
| TS01.06-S-L8-Z5-M | 8 | 2 | 0 | Pullout | 0.72 | 827 | 6.8 | 1490 | 0.68 |
| TS05.10-S-L8-Z5-B | 8 | 2 | 0 | Pullout | 0.63 | 616 | 5.1 | 4416 | 2.69 |
| TS01.10-S-L4-Z12-B | 4 | 2 | 0 | Pullout | 0.75 | 1773 | 14.5 | 10488 | 4.44 |
| TS01.11-S-L4-Z12-B | 4 | 2 | 0 | Pullout | 0.58 | 1506 | 12.3 | 3017 | 1.5 |
| TS01.12-S-L4-Z12-B | 4 | 2 | 0 | Pullout | 0.59 | 1518 | 12.4 | 3694 | 1.83 |
| TS05.11-S-L4-Z12-B | 4 | 2 | 0 | Pullout | 0.38 | 1507 | 12.4 | 1553 | 0.77 |
| TS01.13-S-L8-Z12-B | 8 | 2 | 0 | Pullout | 0.67 | 1510 | 12.4 | 4570 | 1.13 |
| TS01.14-S-L8-Z12-B | 8 | 2 | 0 | Pullout | 0.74 | 1508 | 12.3 | 5631 | 1.4 |
| TS02.01-S-L8-Z12-T | 8 | 2 | 0 | Pullout | 0.7 | 1493 | 12.2 | 10249 | 2.58 |
| TS05.12-S-L8-Z12-B | 8 | 2 | 0 | Pullout | 0.62 | 1507 | 12.3 | 4523 | 1.13 |
| TS02.02-S-L12-Z12-T | 12 | 2 | 0 | Pullout | 0.74 | 1479 | 12.1 | 7280 | 1.23 |
| TS02.03-S-L12-Z12-T | 12 | 2 | 0 | Pullout | 0.74 | 1473 | 12.1 | 11953 | 2.03 |
| TS02.04-S-L12-Z12-T | 12 | 2 | 0 | Pullout | 0.74 | 1494 | 12.2 | 9456 | 1.58 |
| TS05.13-S-L12-Z12-B | 12 | 2 | 0 | Pullout | 0.71 | 1508 | 12.4 | 9394 | 1.56 |
| TS02.05-S-L4-Z20-T | 4 | 2 | 0 | Pullout | 0.71 | 2498 | 20.4 | 5349 | 1.61 |
| TS02.06-S-L4-Z20-M | 4 | 2 | 0 | Pullout | 0.48 | 2474 | 20.2 | 4933 | 1.5 |
| TS02.07-S-L4-Z20-M | 4 | 2 | 0 | Pullout | 0.7 | 2458 | 20.1 | 3902 | 1.19 |
| TS02.08-S-L8-Z20-M | 8 | 2 | 0 | Pullout | 0.74 | 2340 | 19.1 | 7473 | 1.2 |

| TestID | Length, Le (ft) | Width, b (in.) | Skew, β (°) | Reinforcement Behavior | Displacement (in.) | Overburden, σv (psf) | DOF, z (ft) | Load, Pr (lb) | F* |
|---|---|---|---|---|---|---|---|---|---|
| TS02.09-S-L8-Z20-M | 8 | 2 | 0 | Pullout | 0.59 | 2485 | 20.3 | 6250 | 0.94 |
| TS02.10-S-L8-Z20-B | 8 | 2 | 0 | Pullout | 0.74 | 2376 | 19.4 | 6504 | 1.03 |
| TS05.14-S-L8-Z20-B | 8 | 2 | 0 | Pullout | 0.73 | 2527 | 20.7 | 7761 | 1.15 |
| TS02.11-S-L12-Z20-B | 12 | 2 | 0 | Pullout | 0.7 | 2478 | 20.3 | 11539 | 1.16 |
| TS02.12-S-L12-Z20-B | 12 | 2 | 0 | Pullout | 0.52 | 2506 | 20.5 | 10743 | 1.07 |
| TS02.13-S-L12-Z20-B | 12 | 2 | 0 | Pullout | 0.74 | 2483 | 20.3 | 10419 | 1.05 |
| TS02.14-S-L4-Z40-B | 4 | 2 | 0 | Pullout | 0.62 | 4852 | 39.7 | 3431 | 0.53 |
| TS05.01-S-L4-Z40-T | 4 | 2 | 0 | Pullout | 0.73 | 5070 | 41.6 | 6256 | 0.93 |
| TS05.02-S-L4-Z40-T | 4 | 2 | 0 | Pullout | 0.63 | 5019 | 41.1 | 5406 | 0.81 |
| TS05.03-S-L4-Z40-T | 4 | 2 | 0 | Pullout | 0.66 | 5074 | 41.6 | 5564 | 0.82 |
| TS05.04-S-L4-Z40-T | 4 | 2 | 0 | Pullout | 0.74 | 5059 | 41.5 | 9365 | 1.39 |
| TS05.05-S-L6-Z40-T | 6 | 2 | 0 | Pullout | 0.75 | 5058 | 41.5 | 8113 | 0.8 |
| TS05.06-S-L6-Z40-M | 6 | 2 | 0 | Pullout | 0.7 | 5084 | 41.7 | 7426 | 0.73 |
| TS05.07-S-L8-Z40-M | 8 | 2 | 0 | Pullout | 0.73 | 5070 | 41.6 | 13003 | 0.96 |
| TS05.08-S-L8-Z40-M | 8 | 2 | 0 | Pullout | 0.68 | 5064 | 41.5 | 11355 | 0.84 |
| TS05.09-S-L8-Z40-M | 8 | 2 | 0 | Pullout | 0.73 | 5038 | 41.3 | 9949 | 0.74 |
| TS03.07-S-L8-ß15°-Z5-M | 8 | 2 | 15 | Pullout | 0.75 | 551 | 4.5 | 6396 | 4.35 |
| TS04.07-S-L8-ß15°-Z5-M | 8 | 2 | 15 | Pullout | 0.75 | 608 | 5 | 6001 | 3.7 |
| TS04.11-S-L8-ß15°-Z5-B | 8 | 2 | 15 | Pullout | 0.74 | 628 | 5.1 | 6113 | 3.65 |
| TS03.03-S-L4.5-ß15°-Z12-T | 4.5 | 2 | 15 | Pullout | 0.74 | 1478 | 12.1 | 3620 | 1.63 |
| TS03.11-S-L4.5-ß15°-Z12-B | 4.5 | 2 | 15 | Pullout | 0.74 | 1509 | 12.3 | 3468 | 1.53 |
| TS04.03-S-L4.5-ß15°-Z12-T | 4.5 | 2 | 15 | Pullout | 0.74 | 1521 | 12.5 | 4926 | 2.16 |
| TS03.01-S-L8-ß30°-Z5-T | 8 | 2 | 30 | Pullout | 0.74 | 632 | 5.2 | 5469 | 3.25 |

| TestID | Length, Le (ft) | Width, b (in.) | Skew, β (°) | Reinforcement Behavior | Displacement (in.) | Overburden, σv (psf) | DOF, z (ft) | Load, Pr (lb) | F* |
|---|---|---|---|---|---|---|---|---|---|
| TS03.09-S-L8-ß30°-Z5-B | 8 | 2 | 30 | Pullout | 0.73 | 626 | 5.1 | 5720 | 3.42 |
| TS04.01-S-L8-ß30°-Z5-T | 8 | 2 | 30 | Pullout | 0.75 | 624 | 5.1 | 4972 | 2.99 |
| TS03.05-S-L4.5-ß30°-Z12-M | 4.5 | 2 | 30 | Pullout | 0.74 | 1516 | 12.4 | 3359 | 1.48 |
| TS04.05-S-L4.5-ß30°-Z12-M | 4.5 | 2 | 30 | Pullout | 0.74 | 1503 | 12.3 | 3700 | 1.64 |
| TS04.09-S-L4.5-ß30°-Z12-B | 4.5 | 2 | 30 | Pullout | 0.75 | 1506 | 12.3 | 3782 | 1.67 |

**TABLE C3: SUMMARY DATA FOR MSE REINFORCEMENT PULLOUT TESTS**
**WELDED STEEL GRIDS IN TYPE B BACKFILL**

| TestID | Length, Le (ft) | Width, b (in.) | Skew, β (°) | Trans. Bar # | Trans. Bar Diameter, t (in.) | Trans. Bar Spacing, St (in.) | Long. Bar # | Long. Bar Diameter, tl (in.) | Long. Bar Spacing, Sl (in.) | Reinforcement Behavior | Displacement (in.) | Overburden, σv (psf) | DOF, z (ft) | Load, Pr (lb) | F* |
|---|---|---|---|---|---|---|---|---|---|---|---|---|---|---|---|
| TS19.01-G-2x12-W9.5xW11-L6-Z5-T | 6 | 4 | 0 | 6 | 0.374 | 12 | 3 | 0.348 | 2 | Pullout | 0.75 | 631 | 5 | 10297 | 4.08 |
| TS19.05-G-2x12-W9.5xW11-L6-Z5-M | 6 | 4 | 0 | 6 | 0.374 | 12 | 3 | 0.348 | 2 | Pullout | 0.75 | 667 | 5.3 | 12198 | 4.57 |
| TS19.09-G-2x12-W9.5xW11-L6-Z5-B | 6 | 4 | 0 | 6 | 0.374 | 12 | 3 | 0.348 | 2 | Pullout | 0.74 | 636 | 5.1 | 13078 | 5.14 |
| TS20.09-G-2x12-W9.5xW11-L6-Z5-B | 6 | 4 | 0 | 6 | 0.374 | 12 | 3 | 0.348 | 2 | Pullout | 0.74 | 638 | 5 | 9779 | 3.83 |
| TS19.03-G-2x12-W9.5xW11-L3-Z12-T | 3 | 4 | 0 | 3 | 0.374 | 12 | 3 | 0.348 | 2 | Pullout | 0.75 | 1527 | 12.2 | 6330 | 2.07 |
| TS19.07-G-2x12-W9.5xW11-L3-Z12-M | 3 | 4 | 0 | 3 | 0.374 | 12 | 3 | 0.348 | 2 | Pullout | 0.75 | 1516 | 12.1 | 5330 | 1.76 |
| TS19.11-G-2x12-W9.5xW11-L3-Z12-B | 3 | 4 | 0 | 3 | 0.374 | 12 | 3 | 0.348 | 2 | Pullout | 0.75 | 1532 | 12.2 | 6482 | 2.12 |
| TS20.01-G-2x12-W20xW11-L6-Z5-T | 6 | 4 | 0 | 6 | 0.374 | 12 | 3 | 0.505 | 2 | Pullout | 0.73 | 627 | 5 | 5364 | 2.14 |
| TS20.05-G-2x12-W20xW11-L6-Z5-M | 6 | 4 | 0 | 6 | 0.374 | 12 | 3 | 0.505 | 2 | Pullout | 0.74 | 643 | 5.1 | 11709 | 4.55 |
| TS20.03-G-2x12-W20xW11-L6-Z12-T | 6 | 4 | 0 | 6 | 0.374 | 12 | 3 | 0.505 | 2 | Pullout | 0.7 | 1472 | 11.6 | 8120 | 1.38 |
| TS20.07-G-2x12-W20xW11-L6-Z12-M | 6 | 4 | 0 | 6 | 0.374 | 12 | 3 | 0.505 | 2 | Pullout | 0.74 | 1511 | 12 | 11891 | 1.97 |
| TS20.11-G-2x12-W20xW11-L6-Z12-B | 6 | 4 | 0 | 6 | 0.374 | 12 | 3 | 0.505 | 2 | Pullout | 0.75 | 1538 | 12.2 | 12332 | 2 |
| TS21.01-G-2x12-W20xW11-L6-Z20-T | 6 | 4 | 0 | 6 | 0.374 | 12 | 3 | 0.505 | 2 | Pullout | 0.75 | 2551 | 19.8 | 16023 | 1.57 |
| TS21.05-G-2x12-W20xW11-L6-Z20-M | 6 | 4 | 0 | 6 | 0.374 | 12 | 3 | 0.505 | 2 | Pullout | 0.75 | 2549 | 19.8 | 23781 | 2.33 |
| TS21.09-G-2x12-W20xW11-L6-Z20-B | 6 | 4 | 0 | 6 | 0.374 | 12 | 3 | 0.505 | 2 | Pullout | 0.6 | 2565 | 19.9 | 25442 | 2.48 |
| TS21.03-G-2x12-W20xW11-L3-Z40-T | 3 | 4 | 0 | 3 | 0.374 | 12 | 3 | 0.505 | 2 | Pullout | 0.75 | 5066 | 39.4 | 13104 | 1.29 |
| TS21.07-G-2x12-W20xW11-L3-Z40-M | 3 | 4 | 0 | 3 | 0.374 | 12 | 3 | 0.505 | 2 | Pullout | 0.75 | 5086 | 39.5 | 10601 | 1.04 |
| TS21.11-G-2x12-W20xW11-L3-Z40-B | 3 | 4 | 0 | 3 | 0.374 | 12 | 3 | 0.505 | 2 | Pullout | 0.74 | 5068 | 39.4 | 14352 | 1.42 |
| TS24.01-G-6x12-W9.5xW11-L6-Z5-T | 6 | 12 | 0 | 6 | 0.374 | 12 | 3 | 0.348 | 6 | Pullout | 0.74 | 660 | 5.2 | 16242 | 2.05 |
| TS24.05-G-6x12-W9.5xW11-L6-Z5-B | 6 | 12 | 0 | 6 | 0.374 | 12 | 3 | 0.348 | 6 | Pullout | 0.75 | 787 | 6.2 | 20628 | 2.19 |

| TestID | Length, Le (ft) | Width, b (in.) | Skew, β (°) | Trans. Bar # | Trans. Bar Diameter, t (in.) | Trans. Bar Spacing, St (in.) | Long. Bar # | Long. Bar Diameter, tl (in.) | Long. Bar Spacing, Sl (in.) | Reinforcement Behavior | Displacement (in.) | Overburden, σv (psf) | DOF, z (ft) | Load, Pr (lb) | F* |
|---|---|---|---|---|---|---|---|---|---|---|---|---|---|---|---|
| TS24.09-G-6x12-W9.5xW11-L6-Z5-B | 6 | 12 | 0 | 6 | 0.374 | 12 | 3 | 0.348 | 6 | Progressive Rupture | 0.64 | 655 | 5.2 | 17144 | 2.18 |
| TS27.05-G-6x12-W9.5xW11-L6-Z5-B | 6 | 12 | 0 | 6 | 0.374 | 12 | 3 | 0.348 | 6 | Progressive Rupture | 0.53 | 659 | 5.1 | 24368 | 3.08 |
| TS24.03-G-6x12-W9.5xW11-L3-Z12-T | 3 | 12 | 0 | 3 | 0.374 | 12 | 3 | 0.348 | 6 | Pullout | 0.74 | 1534 | 12.1 | 8449 | 0.92 |
| TS24.07-G-6x12-W9.5xW11-L3-Z12-M | 3 | 12 | 0 | 3 | 0.374 | 12 | 3 | 0.348 | 6 | Pullout | 0.74 | 1505 | 11.9 | 12458 | 1.38 |
| TS24.11-G-6x12-W9.5xW11-L3-Z12-B | 3 | 12 | 0 | 3 | 0.374 | 12 | 3 | 0.348 | 6 | Pullout | 0.75 | 1489 | 11.8 | 11614 | 1.3 |
| TS25.01-G-6x12-W20xW11-L6-Z5-T | 6 | 12 | 0 | 6 | 0.374 | 12 | 3 | 0.505 | 6 | Pullout | 0.74 | 647 | 5.1 | 17811 | 2.29 |
| TS25.05-G-6x12-W20xW11-L6-Z5-M | 6 | 12 | 0 | 6 | 0.374 | 12 | 3 | 0.505 | 6 | Pullout | 0.75 | 680 | 5.4 | 18071 | 2.21 |
| TS25.09-G-6x12-W20xW11-L6-Z5-B | 6 | 12 | 0 | 6 | 0.374 | 12 | 3 | 0.505 | 6 | Pullout | 0.74 | 636 | 5 | 14367 | 1.88 |
| TS25.03-G-6x12-W20xW11-L6-Z12-T | 6 | 12 | 0 | 6 | 0.374 | 12 | 3 | 0.505 | 6 | Pullout | 0.74 | 1523 | 12 | 19804 | 1.08 |
| TS25.07-G-6x12-W20xW11-L6-Z12-M | 6 | 12 | 0 | 6 | 0.374 | 12 | 3 | 0.505 | 6 | Pullout | 0.74 | 1533 | 12.1 | 19154 | 1.04 |
| TS25.11-G-6x12-W20xW11-L6-Z12-B | 6 | 12 | 0 | 6 | 0.374 | 12 | 3 | 0.505 | 6 | Pullout | 0.74 | 1439 | 11.3 | 17627 | 1.02 |
| TS26.01-G-6x12-W20xW11-L6-Z20-T | 6 | 12 | 0 | 6 | 0.374 | 12 | 3 | 0.505 | 6 | Pullout | 0.75 | 2490 | 19.4 | 34156 | 1.14 |
| TS26.05-G-6x12-W20xW11-L6-Z20-M | 6 | 12 | 0 | 6 | 0.374 | 12 | 3 | 0.505 | 6 | Progressive Rupture | 0.62 | 2609 | 20.3 | 38133 | 1.22 |
| TS26.09-G-6x12-W20xW11-L6-Z20-B | 6 | 12 | 0 | 6 | 0.374 | 12 | 3 | 0.505 | 6 | Progressive Rupture | 0.61 | 2533 | 19.7 | 40429 | 1.33 |
| TS26.03-G-6x12-W20xW11-L3-Z40-T | 3 | 12 | 0 | 3 | 0.374 | 12 | 3 | 0.505 | 6 | Pullout | 0.75 | 5102 | 39.7 | 26451 | 0.86 |
| TS26.07-G-6x12-W20xW11-L3-Z40-M | 3 | 12 | 0 | 3 | 0.374 | 12 | 3 | 0.505 | 6 | Progressive Rupture | 0.64 | 5072 | 39.5 | 25761 | 0.85 |
| TS26.11-G-6x12-W20xW11-L3-Z40-B | 3 | 12 | 0 | 3 | 0.374 | 12 | 3 | 0.505 | 6 | Pullout | 0.74 | 5046 | 39.3 | 31150 | 1.03 |
| TS27.04-G-6x12-W20xW11-L3-Z40-M | 3 | 12 | 0 | 3 | 0.374 | 12 | 3 | 0.505 | 6 | Progressive Rupture | 0.63 | 5082 | 39.3 | 20680 | 0.68 |
| TS10.03-G-9x6-W20xW7.5-L3-Z5-T | 3 | 18 | 0 | 6 | 0.309 | 6 | 3 | 0.505 | 9 | Pullout | 0.75 | 637 | 5 | 5986 | 1.04 |
| TS10.07-G-9x6-W20xW7.5-L3-Z5-M | 3 | 18 | 0 | 6 | 0.309 | 6 | 3 | 0.505 | 9 | Pullout | 0.74 | 655 | 5.1 | 15658 | 2.66 |
| TS10.11-G-9x6-W20xW7.5-L3-Z5-B | 3 | 18 | 0 | 6 | 0.309 | 6 | 3 | 0.505 | 9 | Pullout | 0.74 | 656 | 5.1 | 13622 | 2.31 |
| TS10.04-G-9x6-W20xW7.5-L3-Z12-T | 3 | 18 | 0 | 6 | 0.309 | 6 | 3 | 0.505 | 9 | Pullout | 0.75 | 1525 | 11.9 | 12316 | 0.9 |
| TS10.08-G-9x6-W20xW7.5-L3-Z12-M | 3 | 18 | 0 | 6 | 0.309 | 6 | 3 | 0.505 | 9 | Pullout | 0.75 | 1517 | 11.9 | 19684 | 1.44 |

| TestID | Length, Le (ft) | Width, b (in.) | Skew, β (°) | Trans. Bar # | Trans. Bar Diameter, t (in.) | Trans. Bar Spacing, St (in.) | Long. Bar # | Long. Bar Diameter, tl (in.) | Long. Bar Spacing, Sl (in.) | Reinforcement Behavior | Displacement (in.) | Overburden, σv (psf) | DOF, z (ft) | Load, Pr (lb) | F* |
|---|---|---|---|---|---|---|---|---|---|---|---|---|---|---|---|
| TS10.12-G-9x6-W20xW7.5-L3-Z12-B | 3 | 18 | 0 | 6 | 0.309 | 6 | 3 | 0.505 | 9 | Pullout | 0.75 | 1523 | 11.9 | 20084 | 1.47 |
| TS18.07-G-9x6-W20xW11-L3-Z5-M | 3 | 18 | 0 | 6 | 0.374 | 6 | 3 | 0.505 | 9 | Pullout | 0.75 | 728 | 5.8 | 19188 | 2.93 |
| TS18.11-G-9x6-W20xW11-L3-Z5-B | 3 | 18 | 0 | 6 | 0.374 | 6 | 3 | 0.505 | 9 | Pullout | 0.72 | 660 | 5.3 | 20991 | 3.53 |
| TS18.08-G-9x6-W20xW11-L3-Z12-M | 3 | 18 | 0 | 6 | 0.374 | 6 | 3 | 0.505 | 9 | Progressive Rupture | 0.75 | 1511 | 12 | 27192 | 2 |
| TS18.12-G-9x6-W20xW11-L3-Z12-B | 3 | 18 | 0 | 6 | 0.374 | 6 | 3 | 0.505 | 9 | Progressive Rupture | 0.7 | 1528 | 12.2 | 23714 | 1.72 |
| TS18.03-G-9x6-W20xW11-L3-Z20-T | 3 | 18 | 0 | 6 | 0.374 | 6 | 3 | 0.505 | 9 | Pullout | 0.75 | 2554 | 20.4 | 22927 | 1 |
| TS18.04-G-9x6-W20xW11-L3-Z20-T | 3 | 18 | 0 | 6 | 0.374 | 6 | 3 | 0.505 | 9 | Pullout | 0.74 | 2536 | 20.2 | 25647 | 1.12 |
| TS15.03-G-9x6-W20xW15-L3-Z5-T | 3 | 18 | 0 | 6 | 0.437 | 6 | 3 | 0.505 | 9 | Pullout | 0.74 | 637 | 5.2 | 10780 | 1.88 |
| TS15.11-G-9x6-W20xW15-L3-Z5-B | 3 | 18 | 0 | 6 | 0.437 | 6 | 3 | 0.505 | 9 | Pullout | 0.74 | 640 | 5.2 | 23790 | 4.13 |
| TS15.04-G-9x6-W20xW15-L3-Z12-T | 3 | 18 | 0 | 6 | 0.437 | 6 | 3 | 0.505 | 9 | Pullout | 0.74 | 1533 | 12.5 | 15260 | 1.11 |
| TS15.08-G-9x6-W20xW15-L3-Z12-M | 3 | 18 | 0 | 6 | 0.437 | 6 | 3 | 0.505 | 9 | Pullout | 0.73 | 1519 | 12.4 | 24373 | 1.78 |
| TS15.12-G-9x6-W20xW15-L3-Z12-B | 3 | 18 | 0 | 6 | 0.437 | 6 | 3 | 0.505 | 9 | Pullout | 0.75 | 1509 | 12.3 | 26872 | 1.98 |
| TS24.02-G-9x12-W9.5xW11-L6-Z5-T | 6 | 18 | 0 | 6 | 0.374 | 12 | 3 | 0.348 | 9 | Pullout | 0.74 | 679 | 5.4 | 14469 | 1.18 |
| TS24.06-G-9x12-W9.5xW11-L6-Z5-M | 6 | 18 | 0 | 6 | 0.374 | 12 | 3 | 0.348 | 9 | Progressive Rupture | 0.67 | 687 | 5.4 | 19614 | 1.58 |
| TS24.10-G-9x12-W9.5xW11-L6-Z5-B | 6 | 18 | 0 | 6 | 0.374 | 12 | 3 | 0.348 | 9 | Progressive Rupture | 0.62 | 655 | 5.2 | 16693 | 1.42 |
| TS24.04-G-9x12-W9.5xW11-L3-Z12-T | 3 | 18 | 0 | 3 | 0.374 | 12 | 3 | 0.348 | 9 | Pullout | 0.75 | 1489 | 11.8 | 9021 | 0.67 |
| TS24.08-G-9x12-W9.5xW11-L3-Z12-M | 3 | 18 | 0 | 3 | 0.374 | 12 | 3 | 0.348 | 9 | Pullout | 0.75 | 1389 | 11 | 13844 | 1.11 |
| TS24.12-G-9x12-W9.5xW11-L3-Z12-B | 3 | 18 | 0 | 3 | 0.374 | 12 | 3 | 0.348 | 9 | Pullout | 0.74 | 1523 | 12 | 14538 | 1.06 |
| TS27.02-G-9x12-W9.5xW11-L3-Z12-T | 3 | 18 | 0 | 3 | 0.374 | 12 | 3 | 0.348 | 9 | Pullout | 0.74 | 1519 | 11.7 | 11974 | 0.88 |
| TS10.01-G-9x12-W20xW7.5-L6-Z5-T | 6 | 18 | 0 | 6 | 0.309 | 12 | 3 | 0.505 | 9 | Pullout | 0.73 | 632 | 4.9 | 10412 | 0.92 |
| TS10.09-G-9x12-W20xW7.5-L6-Z5-B | 6 | 18 | 0 | 6 | 0.309 | 12 | 3 | 0.505 | 9 | Progressive Rupture | 0.72 | 911 | 7.1 | 24732 | 1.51 |
| TS18.01-G-9x12-W20xW7.5-L6-Z5-T | 6 | 18 | 0 | 6 | 0.309 | 12 | 3 | 0.505 | 9 | Pullout | 0.74 | 651 | 5.2 | 16620 | 1.42 |
| TS18.09-G-9x12-W20xW7.5-L6-Z5-B | 6 | 18 | 0 | 6 | 0.309 | 12 | 3 | 0.505 | 9 | Pullout | 0.75 | 690 | 5.5 | 24049 | 1.94 |

| TestID | Length, Le (ft) | Width, b (in.) | Skew, β (°) | Trans. Bar # | Trans. Bar Diameter, t (in.) | Trans. Bar Spacing, St (in.) | Long. Bar # | Long. Bar Diameter, tl (in.) | Long. Bar Spacing, Sl (in.) | Reinforcement Behavior | Displacement (in.) | Overburden, σv (psf) | DOF, z (ft) | Load, Pr (lb) | F* |
|---|---|---|---|---|---|---|---|---|---|---|---|---|---|---|---|
| TS10.06-G-9x12-W20xW7.5-L6-Z12-M | 6 | 18 | 0 | 6 | 0.309 | 12 | 3 | 0.505 | 9 | Pullout | 0.74 | 1520 | 11.9 | 24810 | 0.91 |
| TS10.10-G-9x12-W20xW7.5-L6-Z12-B | 6 | 18 | 0 | 6 | 0.309 | 12 | 3 | 0.505 | 9 | Pullout | 0.74 | 1529 | 11.9 | 21118 | 0.77 |
| TS27.01-G-9x12-W20xW7.5-L6-Z12-T | 6 | 18 | 0 | 6 | 0.309 | 12 | 3 | 0.505 | 9 | Pullout | 0.75 | 1506 | 11.6 | 23117 | 0.85 |
| TS18.05-G-9x12-W20xW7.5-L6-Z20-M | 6 | 18 | 0 | 6 | 0.309 | 12 | 3 | 0.505 | 9 | Progressive Rupture | 0.66 | 2535 | 20.2 | 31136 | 0.68 |
| TS25.02-G-9x12-W20xW11-L6-Z5-T | 6 | 18 | 0 | 6 | 0.374 | 12 | 3 | 0.505 | 9 | Pullout | 0.74 | 687 | 5.4 | 19417 | 1.57 |
| TS25.06-G-9x12-W20xW11-L6-Z5-M | 6 | 18 | 0 | 6 | 0.374 | 12 | 3 | 0.505 | 9 | Pullout | 0.74 | 674 | 5.3 | 22326 | 1.84 |
| TS25.10-G-9x12-W20xW11-L6-Z5-B | 6 | 18 | 0 | 6 | 0.374 | 12 | 3 | 0.505 | 9 | Pullout | 0.75 | 637 | 5 | 16930 | 1.48 |
| TS09.02-G-9x12-W20xW11-L9-Z5-T | 9 | 18 | 0 | 9 | 0.374 | 12 | 3 | 0.505 | 9 | Pullout | 0.75 | 633 | 5.1 | 18682 | 1.09 |
| TS09.06-G-9x12-W20xW11-L9-Z5-M | 9 | 18 | 0 | 9 | 0.374 | 12 | 3 | 0.505 | 9 | Pullout | 0.74 | 668 | 5.4 | 26666 | 1.48 |
| TS09.10-G-9x12-W20xW11-L9-Z5-B | 9 | 18 | 0 | 9 | 0.374 | 12 | 3 | 0.505 | 9 | Pullout | 0.75 | 656 | 5.3 | 28687 | 1.62 |
| TS09.01-G-9x12-W20xW11-L12-Z5-T | 12 | 18 | 0 | 12 | 0.374 | 12 | 3 | 0.505 | 9 | Pullout | 0.75 | 630 | 5.1 | 27653 | 1.22 |
| TS09.05-G-9x12-W20xW11-L12-Z5-M | 12 | 18 | 0 | 12 | 0.374 | 12 | 3 | 0.505 | 9 | Pullout | 0.74 | 811 | 6.5 | 38033 | 1.3 |
| TS09.09-G-9x12-W20xW11-L12-Z5-B | 12 | 18 | 0 | 12 | 0.374 | 12 | 3 | 0.505 | 9 | Progressive Rupture | 0.69 | 795 | 6.4 | 38289 | 1.34 |
| TS09.04-G-9x12-W20xW11-L3-Z12-T | 3 | 18 | 0 | 3 | 0.374 | 12 | 3 | 0.505 | 9 | Pullout | 0.73 | 1542 | 12.4 | 11061 | 0.8 |
| TS09.08-G-9x12-W20xW11-L3-Z12-M | 3 | 18 | 0 | 3 | 0.374 | 12 | 3 | 0.505 | 9 | Pullout | 0.75 | 1519 | 12.2 | 12531 | 0.92 |
| TS09.12-G-9x12-W20xW11-L3-Z12-B | 3 | 18 | 0 | 3 | 0.374 | 12 | 3 | 0.505 | 9 | Pullout | 0.73 | 1512 | 12.2 | 17275 | 1.27 |
| TS25.04-G-9x12-W20xW11-L6-Z12-T | 6 | 18 | 0 | 6 | 0.374 | 12 | 3 | 0.505 | 9 | Pullout | 0.75 | 1489 | 11.7 | 26622 | 0.99 |
| TS25.08-G-9x12-W20xW11-L6-Z12-M | 6 | 18 | 0 | 6 | 0.374 | 12 | 3 | 0.505 | 9 | Pullout | 0.75 | 1525 | 12 | 28502 | 1.04 |
| TS25.12-G-9x12-W20xW11-L6-Z12-B | 6 | 18 | 0 | 6 | 0.374 | 12 | 3 | 0.505 | 9 | Pullout | 0.75 | 1522 | 12 | 21370 | 0.78 |
| TS09.03-G-9x12-W20xW11-L9-Z12-T | 9 | 18 | 0 | 9 | 0.374 | 12 | 3 | 0.505 | 9 | Pullout | 0.75 | 1515 | 12.2 | 29385 | 0.72 |
| TS09.07-G-9x12-W20xW11-L9-Z12-M | 9 | 18 | 0 | 9 | 0.374 | 12 | 3 | 0.505 | 9 | Pullout | 0.75 | 1536 | 12.4 | 33179 | 0.8 |
| TS09.11-G-9x12-W20xW11-L9-Z12-B | 9 | 18 | 0 | 9 | 0.374 | 12 | 3 | 0.505 | 9 | Progressive Rupture | 0.67 | 1518 | 12.2 | 36425 | 0.89 |
| TS26.02-G-9x12-W20xW11-L6-Z20-T | 6 | 18 | 0 | 6 | 0.374 | 12 | 3 | 0.505 | 9 | Progressive Rupture | 0.61 | 2522 | 19.6 | 14623 | 0.32 |

| TestID | Length, Le (ft) | Width, b (in.) | Skew, β (°) | Trans. Bar # | Trans. Bar Diameter, t (in.) | Trans. Bar Spacing, St (in.) | Long. Bar # | Long. Bar Diameter, tl (in.) | Long. Bar Spacing, Sl (in.) | Reinforcement Behavior | Displacement (in.) | Overburden, σv (psf) | DOF, z (ft) | Load, Pr (lb) | F* |
|---|---|---|---|---|---|---|---|---|---|---|---|---|---|---|---|
| TS26.06-G-9x12-W20xW11-L6-Z20-M | 6 | 18 | 0 | 6 | 0.374 | 12 | 3 | 0.505 | 9 | Progressive Rupture | 0.69 | 2581 | 20.1 | 29809 | 0.64 |
| TS26.10-G-9x12-W20xW11-L6-Z20-B | 6 | 18 | 0 | 6 | 0.374 | 12 | 3 | 0.505 | 9 | Progressive Rupture | 0.4 | 2552 | 19.9 | 34230 | 0.75 |
| TS27.03-G-9x12-W20xW11-L6-Z20-M | 6 | 18 | 0 | 6 | 0.374 | 12 | 3 | 0.505 | 9 | Progressive Rupture | 0.56 | 2551 | 19.7 | 34138 | 0.74 |
| TS26.04-G-9x12-W20xW11-L3-Z40-T | 3 | 18 | 0 | 3 | 0.374 | 12 | 3 | 0.505 | 9 | Progressive Rupture | 0.72 | 5108 | 39.8 | 24919 | 0.54 |
| TS26.08-G-9x12-W20xW11-L3-Z40-M | 3 | 18 | 0 | 3 | 0.374 | 12 | 3 | 0.505 | 9 | Progressive Rupture | 0.74 | 5075 | 39.5 | 24347 | 0.53 |
| TS26.12-G-9x12-W20xW11-L3-Z40-B | 3 | 18 | 0 | 3 | 0.374 | 12 | 3 | 0.505 | 9 | Progressive Rupture | 0.52 | 5099 | 39.7 | 27395 | 0.6 |
| TS22.01-G-9x12-W20xW11-L6-ß15°-Z5-T | 6 | 18 | 15 | 6 | 0.374 | 12 | 3 | 0.505 | 9 | Pullout | 0.66 | 627 | 5.1 | 17322 | 1.54 |
| TS22.03-G-9x12-W20xW11-L6-ß15°-Z5-M | 6 | 18 | 15 | 6 | 0.374 | 12 | 3 | 0.505 | 9 | Pullout | 0.75 | 630 | 5.1 | 25942 | 2.29 |
| TS22.05-G-9x12-W20xW11-L6-ß15°-Z5-B | 6 | 18 | 15 | 6 | 0.374 | 12 | 3 | 0.505 | 9 | Progressive Rupture | 0.57 | 628 | 5.1 | 29235 | 2.59 |
| TS23.01-G-9x12-W20xW11-L6-ß15°-Z12-T | 6 | 18 | 15 | 6 | 0.374 | 12 | 3 | 0.505 | 9 | Progressive Rupture | 0.68 | 1532 | 12.1 | 24754 | 0.9 |
| TS23.03-G-9x12-W20xW11-L6-ß15°-Z12-M | 6 | 18 | 15 | 6 | 0.374 | 12 | 3 | 0.505 | 9 | Pullout | 0.75 | 1395 | 11 | 30046 | 1.2 |
| TS23.05-G-9x12-W20xW11-L6-ß15°-Z12-B | 6 | 18 | 15 | 6 | 0.374 | 12 | 3 | 0.505 | 9 | Pullout | 0.74 | 1526 | 12.1 | 29511 | 1.07 |
| TS22.04-G-9x12-W20xW11-L5-ß30°-Z5-M | 5 | 18 | 30 | 5 | 0.374 | 12 | 3 | 0.505 | 9 | Progressive Rupture | 0.69 | 630 | 5.1 | 19798 | 2.09 |
| TS22.06-G-9x12-W20xW11-L5-ß30°-Z5-B | 5 | 18 | 30 | 5 | 0.374 | 12 | 3 | 0.505 | 9 | Pullout | 0.74 | 624 | 5.1 | 25329 | 2.71 |
| TS22.02-G-9x12-W20xW11-L6-ß30°-Z5-T | 6 | 18 | 30 | 6 | 0.374 | 12 | 3 | 0.505 | 9 | Pullout | 0.73 | 639 | 5.2 | 14612 | 1.27 |
| TS23.02-G-9x12-W20xW11-L5-ß30°-Z12-T | 5 | 18 | 30 | 5 | 0.374 | 12 | 3 | 0.505 | 9 | Progressive Rupture | 0.74 | 1528 | 12.1 | 18614 | 0.81 |
| TS23.04-G-9x12-W20xW11-L5-ß30°-Z12-M | 5 | 18 | 30 | 5 | 0.374 | 12 | 3 | 0.505 | 9 | Pullout | 0.74 | 1404 | 11.1 | 24761 | 1.18 |
| TS23.06-G-9x12-W20xW11-L5-ß30°-Z12-B | 5 | 18 | 30 | 5 | 0.374 | 12 | 3 | 0.505 | 9 | Progressive Rupture | 0.54 | 1522 | 12.1 | 20678 | 0.91 |
| TS15.01-G-9x12-W20xW15-L6-Z5-T | 6 | 18 | 0 | 6 | 0.437 | 12 | 3 | 0.505 | 9 | Pullout | 0.74 | 628 | 5.1 | 13582 | 1.2 |
| TS15.05-G-9x12-W20xW15-L6-Z5-M | 6 | 18 | 0 | 6 | 0.437 | 12 | 3 | 0.505 | 9 | Progressive Rupture | 0.71 | 661 | 5.4 | 28049 | 2.36 |
| TS15.07-G-9x12-W20xW15-L6-Z5-M | 6 | 18 | 0 | 6 | 0.437 | 12 | 3 | 0.505 | 9 | Pullout | 0.74 | 646 | 5.3 | 20893 | 1.8 |
| TS15.09-G-9x12-W20xW15-L6-Z5-B | 6 | 18 | 0 | 6 | 0.437 | 12 | 3 | 0.505 | 9 | Progressive Rupture | 0.69 | 656 | 5.4 | 29296 | 2.48 |
| TS15.02-G-9x12-W20xW15-L6-Z12-T | 6 | 18 | 0 | 6 | 0.437 | 12 | 3 | 0.505 | 9 | Pullout | 0.74 | 1525 | 12.5 | 15215 | 0.55 |

| TestID | Length, Le (ft) | Width, b (in.) | Skew, β (°) | Trans. Bar # | Trans. Bar Diameter, t (in.) | Trans. Bar Spacing, St (in.) | Long. Bar # | Long. Bar Diameter, tl (in.) | Long. Bar Spacing, Sl (in.) | Reinforcement Behavior | Displacement (in.) | Overburden, σv (psf) | DOF, z (ft) | Load, Pr (lb) | F* |
|---|---|---|---|---|---|---|---|---|---|---|---|---|---|---|---|
| TS15.06-G-9x12-W20xW15-L6-Z12-M | 6 | 18 | 0 | 6 | 0.437 | 12 | 3 | 0.505 | 9 | Pullout | 0.75 | 1512 | 12.4 | 27835 | 1.02 |
| TS15.10-G-9x12-W20xW15-L6-Z12-B | 6 | 18 | 0 | 6 | 0.437 | 12 | 3 | 0.505 | 9 | Pullout | 0.75 | 1510 | 12.4 | 34492 | 1.27 |
| TS18.02-G-9x12-W20xW15-L6-Z12-T | 6 | 18 | 0 | 6 | 0.437 | 12 | 3 | 0.505 | 9 | Pullout | 0.74 | 1539 | 12.3 | 25426 | 0.92 |
| TS18.06-G-9x12-W20xW15-L6-Z20-M | 6 | 18 | 0 | 6 | 0.437 | 12 | 3 | 0.505 | 9 | Progressive Rupture | 0.73 | 2504 | 20 | 39085 | 0.87 |
| TS18.10-G-9x12-W20xW15-L6-Z20-B | 6 | 18 | 0 | 6 | 0.437 | 12 | 3 | 0.505 | 9 | Progressive Rupture | 0.47 | 2543 | 20.3 | 34880 | 0.76 |
| TS11.01-G-9x18-W20xW7.5-L9-Z5-T | 9 | 18 | 0 | 6 | 0.309 | 18 | 3 | 0.505 | 9 | Pullout | 0.75 | 631 | 5.1 | 14524 | 0.85 |
| TS11.05-G-9x18-W20xW7.5-L9-Z5-M | 9 | 18 | 0 | 6 | 0.309 | 18 | 3 | 0.505 | 9 | Pullout | 0.74 | 654 | 5.3 | 25610 | 1.45 |
| TS11.09-G-9x18-W20xW7.5-L9-Z5-B | 9 | 18 | 0 | 6 | 0.309 | 18 | 3 | 0.505 | 9 | Pullout | 0.75 | 634 | 5.1 | 28564 | 1.67 |
| TS11.02-G-9x18-W20xW7.5-L9-Z12-T | 9 | 18 | 0 | 6 | 0.309 | 18 | 3 | 0.505 | 9 | Pullout | 0.75 | 1518 | 12.2 | 21531 | 0.53 |
| TS11.06-G-9x18-W20xW7.5-L9-Z12-M | 9 | 18 | 0 | 6 | 0.309 | 18 | 3 | 0.505 | 9 | Pullout | 0.75 | 1511 | 12.1 | 30522 | 0.75 |
| TS11.10-G-9x18-W20xW7.5-L9-Z12-B | 9 | 18 | 0 | 6 | 0.309 | 18 | 3 | 0.505 | 9 | Pullout | 0.74 | 1496 | 12 | 30865 | 0.76 |
| TS11.03-G-9x18-W20xW7.5-L9-Z20-T | 9 | 18 | 0 | 6 | 0.309 | 18 | 3 | 0.505 | 9 | Pullout | 0.75 | 2534 | 20.3 | 25790 | 0.38 |
| TS11.07-G-9x18-W20xW7.5-L9-Z20-M | 9 | 18 | 0 | 6 | 0.309 | 18 | 3 | 0.505 | 9 | Pullout | 0.75 | 2524 | 20.3 | 33041 | 0.48 |
| TS11.11-G-9x18-W20xW7.5-L9-Z20-B | 9 | 18 | 0 | 6 | 0.309 | 18 | 3 | 0.505 | 9 | Pullout | 0.74 | 2539 | 20.4 | 37640 | 0.55 |
| TS11.04-G-9x18-W20xW7.5-L4.5-Z40-T | 4.5 | 18 | 0 | 3 | 0.309 | 18 | 3 | 0.505 | 9 | Pullout | 0.75 | 4929 | 39.6 | 20538 | 0.31 |
| TS11.08-G-9x18-W20xW7.5-L4.5-Z40-M | 4.5 | 18 | 0 | 3 | 0.309 | 18 | 3 | 0.505 | 9 | Pullout | 0.75 | 5057 | 40.6 | 20661 | 0.3 |
| TS11.12-G-9x18-W20xW7.5-L4.5-Z40-B | 4.5 | 18 | 0 | 3 | 0.309 | 18 | 3 | 0.505 | 9 | Pullout | 0.74 | 5061 | 40.6 | 22456 | 0.33 |
| TS13.01-G-9x18-W20xW11-L9-Z5-T | 9 | 18 | 0 | 6 | 0.374 | 18 | 3 | 0.505 | 9 | Pullout | 0.74 | 629 | 5 | 21067 | 1.24 |
| TS13.05-G-9x18-W20xW11-L9-Z5-M | 9 | 18 | 0 | 6 | 0.374 | 18 | 3 | 0.505 | 9 | Pullout | 0.74 | 669 | 5.3 | 26606 | 1.47 |
| TS13.09-G-9x18-W20xW11-L9-Z5-B | 9 | 18 | 0 | 6 | 0.374 | 18 | 3 | 0.505 | 9 | Pullout | 0.74 | 656 | 5.2 | 27185 | 1.54 |
| TS13.02-G-9x18-W20xW11-L9-Z12-T | 9 | 18 | 0 | 6 | 0.374 | 18 | 3 | 0.505 | 9 | Pullout | 0.75 | 1523 | 12.1 | 24928 | 0.61 |
| TS13.06-G-9x18-W20xW11-L9-Z12-M | 9 | 18 | 0 | 6 | 0.374 | 18 | 3 | 0.505 | 9 | Pullout | 0.75 | 1546 | 12.3 | 37546 | 0.9 |
| TS13.10-G-9x18-W20xW11-L9-Z12-B | 9 | 18 | 0 | 6 | 0.374 | 18 | 3 | 0.505 | 9 | Pullout | 0.75 | 1513 | 12 | 30671 | 0.75 |

| TestID | Length, Le (ft) | Width, b (in.) | Skew, β (°) | Trans. Bar # | Trans. Bar Diameter, t (in.) | Trans. Bar Spacing, St (in.) | Long. Bar # | Long. Bar Diameter, tl (in.) | Long. Bar Spacing, Sl (in.) | Reinforcement Behavior | Displacement (in.) | Overburden, σv (psf) | DOF, z (ft) | Load, Pr (lb) | F* |
|---|---|---|---|---|---|---|---|---|---|---|---|---|---|---|---|
| TS13.03-G-9x18-W20xW11-L9-Z20-T | 9 | 18 | 0 | 6 | 0.374 | 18 | 3 | 0.505 | 9 | Pullout | 0.75 | 2544 | 20.2 | 37209 | 0.54 |
| TS13.07-G-9x18-W20xW11-L9-Z20-M | 9 | 18 | 0 | 6 | 0.374 | 18 | 3 | 0.505 | 9 | Pullout | 0.74 | 2551 | 20.2 | 39930 | 0.58 |
| TS13.11-G-9x18-W20xW11-L9-Z20-B | 9 | 18 | 0 | 6 | 0.374 | 18 | 3 | 0.505 | 9 | Pullout | 0.75 | 2542 | 20.1 | 36100 | 0.53 |
| TS13.04-G-9x18-W20xW11-L4.5-Z40-T | 4.5 | 18 | 0 | 3 | 0.374 | 18 | 3 | 0.505 | 9 | Pullout | 0.74 | 5076 | 40.2 | 24699 | 0.36 |
| TS13.08-G-9x18-W20xW11-L4.5-Z40-M | 4.5 | 18 | 0 | 3 | 0.374 | 18 | 3 | 0.505 | 9 | Pullout | 0.74 | 5070 | 40.2 | 26447 | 0.39 |
| TS13.12-G-9x18-W20xW11-L4.5-Z40-B | 4.5 | 18 | 0 | 3 | 0.374 | 18 | 3 | 0.505 | 9 | Progressive Rupture | 0.73 | 5052 | 40 | 22095 | 0.32 |
| TS16.01-G-9x18-W20xW15-L9-Z5-T | 9 | 18 | 0 | 6 | 0.437 | 18 | 3 | 0.505 | 9 | Pullout | 0.74 | 672 | 5.3 | 22636 | 1.25 |
| TS16.05-G-9x18-W20xW15-L9-Z5-M | 9 | 18 | 0 | 6 | 0.437 | 18 | 3 | 0.505 | 9 | Progressive Rupture | 0.75 | 669 | 5.3 | 32030 | 1.77 |
| TS16.09-G-9x18-W20xW15-L9-Z5-B | 9 | 18 | 0 | 6 | 0.437 | 18 | 3 | 0.505 | 9 | Pullout | 0.75 | 695 | 5.5 | 38480 | 2.05 |
| TS16.02-G-9x18-W20xW15-L9-Z12-T | 9 | 18 | 0 | 6 | 0.437 | 18 | 3 | 0.505 | 9 | Pullout | 0.75 | 1555 | 12.3 | 31007 | 0.74 |
| TS16.06-G-9x18-W20xW15-L9-Z12-M | 9 | 18 | 0 | 6 | 0.437 | 18 | 3 | 0.505 | 9 | Pullout | 0.75 | 1536 | 12.1 | 41589 | 1 |
| TS16.10-G-9x18-W20xW15-L9-Z12-B | 9 | 18 | 0 | 6 | 0.437 | 18 | 3 | 0.505 | 9 | Pullout | 0.75 | 1522 | 12 | 46352 | 1.13 |
| TS16.03-G-9x18-W20xW15-L9-Z20-T | 9 | 18 | 0 | 6 | 0.437 | 18 | 3 | 0.505 | 9 | Pullout | 0.75 | 2569 | 20.3 | 41513 | 0.6 |
| TS16.07-G-9x18-W20xW15-L9-Z20-M | 9 | 18 | 0 | 6 | 0.437 | 18 | 3 | 0.505 | 9 | Pullout | 0.74 | 2554 | 20.2 | 46607 | 0.68 |
| TS16.11-G-9x18-W20xW15-L9-Z20-B | 9 | 18 | 0 | 6 | 0.437 | 18 | 3 | 0.505 | 9 | Pullout | 0.75 | 2541 | 20.1 | 50062 | 0.73 |
| TS16.08-G-9x18-W20xW15-L4.5-Z40-M | 4.5 | 18 | 0 | 3 | 0.437 | 18 | 3 | 0.505 | 9 | Pullout | 0.75 | 5064 | 40 | 30628 | 0.45 |
| TS16.12-G-9x18-W20xW15-L4.5-Z40-B | 4.5 | 18 | 0 | 3 | 0.437 | 18 | 3 | 0.505 | 9 | Pullout | 0.74 | 5041 | 39.8 | 27501 | 0.4 |
| TS16.04-G-9x18-W20xW15-L9-Z40-T | 9 | 18 | 0 | 6 | 0.437 | 18 | 3 | 0.505 | 9 | Progressive Rupture | 0.66 | 5079 | 40.1 | 25303 | 0.18 |
| TS12.01-G-9x24-W20xW7.5-L12-Z5-T | 12 | 18 | 0 | 6 | 0.309 | 24 | 3 | 0.505 | 9 | Progressive Rupture | 0.75 | 634 | 5 | 19615 | 0.86 |
| TS12.05-G-9x24-W20xW7.5-L12-Z5-M | 12 | 18 | 0 | 6 | 0.309 | 24 | 3 | 0.505 | 9 | Pullout | 0.74 | 642 | 5.1 | 17031 | 0.74 |
| TS12.09-G-9x24-W20xW7.5-L12-Z5-B | 12 | 18 | 0 | 6 | 0.309 | 24 | 3 | 0.505 | 9 | Progressive Rupture | 0.66 | 640 | 5.1 | 20686 | 0.9 |
| TS12.02-G-9x24-W20xW7.5-L12-Z12-T | 12 | 18 | 0 | 6 | 0.309 | 24 | 3 | 0.505 | 9 | Progressive Rupture | 0.71 | 1507 | 12 | 22115 | 0.41 |
| TS12.06-G-9x24-W20xW7.5-L12-Z12-M | 12 | 18 | 0 | 6 | 0.309 | 24 | 3 | 0.505 | 9 | Progressive Rupture | 0.73 | 1516 | 12 | 19876 | 0.36 |

| TestID | Length, Le (ft) | Width, b (in.) | Skew, β (°) | Trans. Bar # | Trans. Bar Diameter, t (in.) | Trans. Bar Spacing, St (in.) | Long. Bar # | Long. Bar Diameter, tl (in.) | Long. Bar Spacing, Sl (in.) | Reinforcement Behavior | Displacement (in.) | Overburden, σv (psf) | DOF, z (ft) | Load, Pr (lb) | F* |
|---|---|---|---|---|---|---|---|---|---|---|---|---|---|---|---|
| TS12.10-G-9x24-W20xW7.5-L12-Z12-B | 12 | 18 | 0 | 6 | 0.309 | 24 | 3 | 0.505 | 9 | Progressive Rupture | 0.6 | 1526 | 12.1 | 23879 | 0.43 |
| TS12.03-G-9x24-W20xW7.5-L12-Z20-T | 12 | 18 | 0 | 6 | 0.309 | 24 | 3 | 0.505 | 9 | Progressive Rupture | 0.68 | 2548 | 20.2 | 24887 | 0.27 |
| TS12.07-G-9x24-W20xW7.5-L12-Z20-M | 12 | 18 | 0 | 6 | 0.309 | 24 | 3 | 0.505 | 9 | Progressive Rupture | 0.72 | 2530 | 20.1 | 22015 | 0.24 |
| TS12.11-G-9x24-W20xW7.5-L12-Z20-B | 12 | 18 | 0 | 6 | 0.309 | 24 | 3 | 0.505 | 9 | Progressive Rupture | 0.71 | 2522 | 20 | 28425 | 0.31 |
| TS12.04-G-9x24-W20xW7.5-L6-Z40-T | 6 | 18 | 0 | 3 | 0.309 | 24 | 3 | 0.505 | 9 | Progressive Rupture | 0.66 | 5058 | 40.1 | 20954 | 0.23 |
| TS12.08-G-9x24-W20xW7.5-L6-Z40-M | 6 | 18 | 0 | 3 | 0.309 | 24 | 3 | 0.505 | 9 | Progressive Rupture | 0.56 | 5088 | 40.4 | 18229 | 0.2 |
| TS12.12-G-9x24-W20xW7.5-L6-Z40-B | 6 | 18 | 0 | 3 | 0.309 | 24 | 3 | 0.505 | 9 | Progressive Rupture | 0.71 | 5022 | 39.9 | 25425 | 0.28 |
| TS14.01-G-9x24-W20xW11-L12-Z5-T | 12 | 18 | 0 | 6 | 0.374 | 24 | 3 | 0.505 | 9 | Pullout | 0.74 | 633 | 5 | 18860 | 0.83 |
| TS14.05-G-9x24-W20xW11-L12-Z5-M | 12 | 18 | 0 | 6 | 0.374 | 24 | 3 | 0.505 | 9 | Progressive Rupture | 0.67 | 646 | 5.1 | 26500 | 1.14 |
| TS14.09-G-9x24-W20xW11-L12-Z5-B | 12 | 18 | 0 | 6 | 0.374 | 24 | 3 | 0.505 | 9 | Pullout | 0.74 | 658 | 5.2 | 30084 | 1.27 |
| TS14.02-G-9x24-W20xW11-L12-Z12-T | 12 | 18 | 0 | 6 | 0.374 | 24 | 3 | 0.505 | 9 | Progressive Rupture | 0.68 | 1508 | 11.8 | 22130 | 0.41 |
| TS14.06-G-9x24-W20xW11-L12-Z12-M | 12 | 18 | 0 | 6 | 0.374 | 24 | 3 | 0.505 | 9 | Progressive Rupture | 0.65 | 1547 | 12.1 | 30750 | 0.55 |
| TS14.10-G-9x24-W20xW11-L12-Z12-B | 12 | 18 | 0 | 6 | 0.374 | 24 | 3 | 0.505 | 9 | Progressive Rupture | 0.55 | 1522 | 11.9 | 35689 | 0.65 |
| TS14.03-G-9x24-W20xW11-L12-Z20-T | 12 | 18 | 0 | 6 | 0.374 | 24 | 3 | 0.505 | 9 | Pullout | 0.72 | 2535 | 19.8 | 29098 | 0.32 |
| TS14.07-G-9x24-W20xW11-L12-Z20-M | 12 | 18 | 0 | 6 | 0.374 | 24 | 3 | 0.505 | 9 | Progressive Rupture | 0.71 | 2524 | 19.8 | 31778 | 0.35 |
| TS14.11-G-9x24-W20xW11-L12-Z20-B | 12 | 18 | 0 | 6 | 0.374 | 24 | 3 | 0.505 | 9 | Progressive Rupture | 0.37 | 2525 | 19.8 | 36983 | 0.41 |
| TS14.04-G-9x24-W20xW11-L6-Z40-T | 6 | 18 | 0 | 3 | 0.374 | 24 | 3 | 0.505 | 9 | Pullout | 0.72 | 5015 | 39.2 | 24225 | 0.27 |
| TS14.08-G-9x24-W20xW11-L12-Z40-M | 12 | 18 | 0 | 6 | 0.374 | 24 | 3 | 0.505 | 9 | Progressive Rupture | 0.6 | 4971 | 38.9 | 22856 | 0.13 |
| TS14.12-G-9x24-W20xW11-L12-Z40-B | 12 | 18 | 0 | 6 | 0.374 | 24 | 3 | 0.505 | 9 | Progressive Rupture | 0.59 | 5017 | 39.3 | 29480 | 0.16 |
| TS17.01-G-9x24-W20xW15-L12-Z5-T | 12 | 18 | 0 | 6 | 0.437 | 24 | 3 | 0.505 | 9 | Pullout | 0.74 | 627 | 5 | 17150 | 0.76 |
| TS17.05-G-9x24-W20xW15-L12-Z5-M | 12 | 18 | 0 | 6 | 0.437 | 24 | 3 | 0.505 | 9 | Progressive Rupture | 0.69 | 638 | 5.1 | 27510 | 1.2 |
| TS17.09-G-9x24-W20xW15-L12-Z5-B | 12 | 18 | 0 | 6 | 0.437 | 24 | 3 | 0.505 | 9 | Progressive Rupture | 0.4 | 640 | 5.1 | 29197 | 1.27 |
| TS17.02-G-9x24-W20xW15-L12-Z12-T | 12 | 18 | 0 | 6 | 0.437 | 24 | 3 | 0.505 | 9 | Pullout | 0.74 | 1502 | 12 | 24192 | 0.45 |

| TestID | Length, Le (ft) | Width, b (in.) | Skew, β (°) | Trans. Bar # | Trans. Bar Diameter, t (in.) | Trans. Bar Spacing, St (in.) | Long. Bar # | Long. Bar Diameter, tl (in.) | Long. Bar Spacing, Sl (in.) | Reinforcement Behavior | Displacement (in.) | Overburden, σv (psf) | DOF, z (ft) | Load, Pr (lb) | F* |
|---|---|---|---|---|---|---|---|---|---|---|---|---|---|---|---|
| TS17.06-G-9x24-W20xW15-L12-Z12-M | 12 | 18 | 0 | 6 | 0.437 | 24 | 3 | 0.505 | 9 | Pullout | 0.73 | 1524 | 12.2 | 35449 | 0.65 |
| TS17.10-G-9x24-W20xW15-L12-Z12-B | 12 | 18 | 0 | 6 | 0.437 | 24 | 3 | 0.505 | 9 | Progressive Rupture | 0.65 | 1520 | 12.1 | 38436 | 0.7 |
| TS17.03-G-9x24-W20xW15-L12-Z20-T | 12 | 18 | 0 | 6 | 0.437 | 24 | 3 | 0.505 | 9 | Pullout | 0.75 | 2546 | 20.3 | 34624 | 0.38 |
| TS17.07-G-9x24-W20xW15-L12-Z20-M | 12 | 18 | 0 | 6 | 0.437 | 24 | 3 | 0.505 | 9 | Progressive Rupture | 0.64 | 2502 | 20 | 39474 | 0.44 |
| TS17.11-G-9x24-W20xW15-L12-Z20-B | 12 | 18 | 0 | 6 | 0.437 | 24 | 3 | 0.505 | 9 | Progressive Rupture | 0.53 | 2582 | 20.6 | 35930 | 0.39 |
| TS17.04-G-9x24-W20xW15-L6-Z40-T | 6 | 18 | 0 | 3 | 0.437 | 24 | 3 | 0.505 | 9 | Progressive Rupture | 0.5 | 5075 | 40.5 | 21974 | 0.24 |
| TS17.08-G-9x24-W20xW15-L6-Z40-M | 6 | 18 | 0 | 3 | 0.437 | 24 | 3 | 0.505 | 9 | Progressive Rupture | 0.55 | 5064 | 40.4 | 26638 | 0.29 |
| TS17.12-G-9x24-W20xW15-L6-Z40-B | 6 | 18 | 0 | 3 | 0.437 | 24 | 3 | 0.505 | 9 | Progressive Rupture | 0.6 | 5083 | 40.6 | 21558 | 0.24 |
| TS19.02-G-12x12-W9.5xW11-L6-Z5-T | 6 | 24 | 0 | 6 | 0.374 | 12 | 3 | 0.348 | 12 | Progressive Rupture | 0.58 | 637 | 5.1 | 17266 | 1.13 |
| TS19.06-G-12x12-W9.5xW11-L6-Z5-M | 6 | 24 | 0 | 6 | 0.374 | 12 | 3 | 0.348 | 12 | Progressive Rupture | 0.6 | 627 | 5 | 15775 | 1.05 |
| TS19.10-G-12x12-W9.5xW11-L6-Z5-B | 6 | 24 | 0 | 6 | 0.374 | 12 | 3 | 0.348 | 12 | Progressive Rupture | 0.66 | 650 | 5.2 | 18729 | 1.2 |
| TS19.04-G-12x12-W9.5xW11-L3-Z12-T | 3 | 24 | 0 | 3 | 0.374 | 12 | 3 | 0.348 | 12 | Pullout | 0.73 | 1528 | 12.2 | 12706 | 0.69 |
| TS19.08-G-12x12-W9.5xW11-L3-Z12-M | 3 | 24 | 0 | 3 | 0.374 | 12 | 3 | 0.348 | 12 | Progressive Rupture | 0.71 | 1513 | 12.1 | 13883 | 0.76 |
| TS19.12-G-12x12-W9.5xW11-L6-Z12-B | 6 | 24 | 0 | 6 | 0.374 | 12 | 3 | 0.348 | 12 | Progressive Rupture | 0.67 | 1523 | 12.1 | 15592 | 0.43 |
| TS20.02-G-12x12-W20xW11-L6-Z5-T | 6 | 24 | 0 | 6 | 0.374 | 12 | 3 | 0.505 | 12 | Pullout | 0.74 | 632 | 5 | 11990 | 0.79 |
| TS20.06-G-12x12-W20xW11-L6-Z5-M | 6 | 24 | 0 | 6 | 0.374 | 12 | 3 | 0.505 | 12 | Pullout | 0.74 | 642 | 5.1 | 22137 | 1.44 |
| TS20.10-G-12x12-W20xW11-L6-Z5-B | 6 | 24 | 0 | 6 | 0.374 | 12 | 3 | 0.505 | 12 | Pullout | 0.75 | 651 | 5.1 | 21421 | 1.37 |
| TS20.04-G-12x12-W20xW11-L6-Z12-T | 6 | 24 | 0 | 6 | 0.374 | 12 | 3 | 0.505 | 12 | Pullout | 0.74 | 1524 | 12.1 | 24596 | 0.67 |
| TS20.08-G-12x12-W20xW11-L6-Z12-M | 6 | 24 | 0 | 6 | 0.374 | 12 | 3 | 0.505 | 12 | Progressive Rupture | 0.61 | 1537 | 12.2 | 28024 | 0.76 |
| TS20.12-G-12x12-W20xW11-L6-Z12-B | 6 | 24 | 0 | 6 | 0.374 | 12 | 3 | 0.505 | 12 | Pullout | 0.74 | 1521 | 12 | 26711 | 0.73 |
| TS21.02-G-12x12-W20xW11-L6-Z20-T | 6 | 24 | 0 | 6 | 0.374 | 12 | 3 | 0.505 | 12 | Progressive Rupture | 0.44 | 2555 | 19.9 | 27431 | 0.45 |
| TS21.06-G-12x12-W20xW11-L6-Z20-M | 6 | 24 | 0 | 6 | 0.374 | 12 | 3 | 0.505 | 12 | Progressive Rupture | 0.59 | 2507 | 19.5 | 35235 | 0.59 |
| TS21.10-G-12x12-W20xW11-L6-Z20-B | 6 | 24 | 0 | 6 | 0.374 | 12 | 3 | 0.505 | 12 | Progressive Rupture | 0.57 | 2530 | 19.7 | 37054 | 0.61 |

| TestID | Length, Le (ft) | Width, b (in.) | Skew, β (°) | Trans. Bar # | Trans. Bar Diameter, t (in.) | Trans. Bar Spacing, St (in.) | Long. Bar # | Long. Bar Diameter, tl (in.) | Long. Bar Spacing, Sl (in.) | Reinforcement Behavior | Displacement (in.) | Overburden, σv (psf) | DOF, z (ft) | Load, Pr (lb) | F* |
|---|---|---|---|---|---|---|---|---|---|---|---|---|---|---|---|
| TS21.04-G-12x12-W20xW11-L3-Z40-T | 3 | 24 | 0 | 3 | 0.374 | 12 | 3 | 0.505 | 12 | Progressive Rupture | 0.57 | 5039 | 39.2 | 17895 | 0.3 |
| TS21.08-G-12x12-W20xW11-L3-Z40-M | 3 | 24 | 0 | 3 | 0.374 | 12 | 3 | 0.505 | 12 | Progressive Rupture | 0.47 | 5123 | 39.8 | 18273 | 0.3 |
| TS21.12-G-12x12-W20xW11-L3-Z40-B | 3 | 24 | 0 | 3 | 0.374 | 12 | 3 | 0.505 | 12 | Progressive Rupture | 0.27 | 5095 | 39.6 | 19709 | 0.32 |

## TABLE C4: SUMMARY DATA FOR MSE REINFORCEMENT PULLOUT TESTS
## SMOOTH STEEL BARS IN TYPE B BACKFILL

| TestID | Length, Le (ft) | Long. Bar Diameter, tl (in.) | Reinforcement Behavior | Displacement (in.) | Overburden, σv (psf) | DOF, z (ft) | Load, Pr (lb) | F* |
|---|---|---|---|---|---|---|---|---|
| TS27.17-B-W9.5-L6-Z5-M | 6 | 0.348 | Pullout | 0.63 | 642 | 5 | 1585 | 4.52 |
| TS27.22-B-W9.5-L6-Z5-B | 6 | 0.348 | Pullout | 0.64 | 663 | 5.1 | 1932 | 5.33 |
| TS27.24-B-W9.5-L6-Z5-B | 6 | 0.348 | Pullout | 0.58 | 639 | 4.9 | 2095 | 6 |
| TS27.18-B-W9.5-L3-Z12-M | 3 | 0.348 | Pullout | 0.68 | 1570 | 12.1 | 2800 | 6.53 |
| TS27.25-B-W9.5-L3-Z12-B | 3 | 0.348 | Pullout | 0.7 | 1596 | 12.3 | 3686 | 8.45 |
| TS27.10-B-W20-L6-Z5-T | 6 | 0.505 | Pullout | 0.44 | 659 | 5.1 | 2763 | 5.34 |
| TS27.15-B-W20-L6-Z5-M | 6 | 0.505 | Pullout | 0.63 | 646 | 5 | 2927 | 5.77 |
| TS27.21-B-W20-L6-Z5-B | 6 | 0.505 | Pullout | 0.59 | 653 | 5 | 3081 | 6.01 |
| TS27.11-B-W20-L6-Z12-T | 6 | 0.505 | Pullout | 0.33 | 1551 | 12 | 4358 | 3.58 |
| TS27.16-B-W20-L6-Z12-M | 6 | 0.505 | Pullout | 0.13 | 1532 | 11.8 | 2080 | 1.73 |
| TS27.23-B-W20-L6-Z12-B | 6 | 0.505 | Pullout | 0.7 | 1539 | 11.9 | 4150 | 3.44 |
| TS27.14-B-W20-L6-Z20-T | 6 | 0.505 | Pullout | 0.07 | 2577 | 19.9 | 2552 | 1.26 |
| TS27.20-B-W20-L6-Z20-M | 6 | 0.505 | Pullout | 0.27 | 2549 | 19.7 | 3857 | 1.93 |
| TS27.27-B-W20-L6-Z20-B | 6 | 0.505 | Pullout | 0.73 | 2568 | 19.8 | 5883 | 2.92 |
| TS27.13-B-W20-L3-Z40-T | 3 | 0.505 | Pullout | 0.62 | 4977 | 38.5 | 3673 | 1.88 |
| TS27.19-B-W20-L3-Z40-M | 3 | 0.505 | Pullout | 0.15 | 5114 | 39.5 | 1874 | 0.93 |
| TS27.26-B-W20-L3-Z40-B | 3 | 0.505 | Pullout | 0.73 | 4981 | 38.5 | 3562 | 1.82 |

# Appendix D


# Summary Data for MSE Reinforcement Pullout Tests

## Ribbed Strips in Type A Backfill

## Welded Steel Grids in Type A Backfill

## Smooth Steel Bars in Type B Backfill

**TABLE D1: SUMMARY DATA FOR MSE REINFORCEMENT PULLOUT TESTS**
**RIBBED STRIPS IN TYPE A BACKFILL**

| TestID | Length, Le (ft) | Width, b (in.) | Skew, β (°) | Reinforcement Behavior | Displacement (in.) | Overburden, σv (psf) | DOF, z (ft) | Load, Pr (lb) | F* |
|---|---|---|---|---|---|---|---|---|---|
| TS42.13-S-L4-Z5-T | 4 | 2 | 0 | Pullout | 0.75 | 621 | 5.1 | 8510 | 10.28 |
| TS42.16-S-L4-Z5-M | 4 | 2 | 0 | Pullout | 0.75 | 600 | 4.9 | 9306 | 11.64 |
| TS42.19-S-L4-Z5-B | 4 | 2 | 0 | Pullout | 0.7 | 644 | 4.8 | 10025 | 11.67 |
| TS50.25-S-L4-Z5-M | 4 | 2 | 0 | Pullout | 0.69 | 587 | 4.7 | 8975 | 11.47 |
| TS30.13-S-L8-Z5-T | 8 | 2 | 0 | Pullout | 0.51 | 601 | 5 | 14849 | 9.27 |
| TS30.14-S-L8-Z5-M | 8 | 2 | 0 | Rupture | 0.72 | 616 | 5.1 | 21703 | 13.22 |
| TS30.15-S-L8-Z5-B | 8 | 2 | 0 | Pullout | 0.74 | 621 | 5.2 | 21125 | 12.75 |
| TS42.14-S-L8-Z5-T | 8 | 2 | 0 | Pullout | 0.73 | 630 | 5.2 | 13568 | 8.07 |
| TS42.17-S-L8-Z5-M | 8 | 2 | 0 | Pullout | 0.74 | 627 | 5.2 | 18716 | 11.2 |
| TS42.20-S-L8-Z5-B | 8 | 2 | 0 | Pullout | 0.63 | 649 | 4.9 | 19910 | 11.51 |
| TS48.18-S-L8-Z5-B | 8 | 2 | 0 | Pullout | 0.73 | 604 | 4.9 | 16591 | 10.3 |
| TS31.13-S-L12-Z5-T | 12 | 2 | 0 | Pullout | 0.74 | 560 | 4.7 | 20137 | 8.98 |
| TS31.15-S-L12-Z5-M | 12 | 2 | 0 | Pullout | 0.73 | 578 | 4.8 | 22071 | 9.54 |
| TS45.13-S-L12-Z5-T | 12 | 2 | 0 | Pullout | 0.62 | 640 | 5.3 | 13281 | 5.19 |
| TS45.14-S-L12-Z5-M | 12 | 2 | 0 | Pullout | 0.75 | 625 | 5.1 | 23271 | 9.31 |
| TS45.15-S-L12-Z5-B | 12 | 2 | 0 | Pullout | 0.61 | 597 | 5.1 | 22908 | 9.59 |
| TS46.13-S-L4-Z12-T | 4 | 2 | 0 | Pullout | 0.72 | 1459 | 12.2 | 6841 | 3.52 |
| TS46.19-S-L4-Z12-B | 4 | 2 | 0 | Pullout | 0.75 | 1480 | 12.3 | 9427 | 4.78 |
| TS32.14-S-L8-Z12-T | 8 | 2 | 0 | Pullout | 0.74 | 1501 | 11.9 | 20291 | 5.07 |
| TS32.17-S-L8-Z12-M | 8 | 2 | 0 | Pullout | 0.74 | 1510 | 12 | 18453 | 4.58 |

| TestID | Length, Le (ft) | Width, b (in.) | Skew, β (°) | Reinforcement Behavior | Displacement (in.) | Overburden, σv (psf) | DOF, z (ft) | Load, Pr (lb) | F* |
|---|---|---|---|---|---|---|---|---|---|
| TS32.20-S-L8-Z12-B | 8 | 2 | 0 | Rupture | 0.67 | 1509 | 12 | 22271 | 5.53 |
| TS42.15-S-L8-Z12-T | 8 | 2 | 0 | Pullout | 0.75 | 1513 | 12.5 | 15508 | 3.84 |
| TS42.18-S-L8-Z12-M | 8 | 2 | 0 | Pullout | 0.73 | 1497 | 12.3 | 28710 | 7.19 |
| TS42.21-S-L8-Z12-B | 8 | 2 | 0 | Pullout | 0.74 | 1499 | 11.3 | 26551 | 6.64 |
| TS31.14-S-L12-Z12-T | 12 | 2 | 0 | Pullout | 0.58 | 1320 | 11 | 21423 | 4.06 |
| TS31.16-S-L12-Z12-M | 12 | 2 | 0 | Rupture | 0.52 | 1330 | 11.1 | 21487 | 4.04 |
| TS40.13-S-L12-Z12-T | 12 | 2 | 0 | Pullout | 0.75 | 1509 | 12.7 | 29665 | 4.91 |
| TS40.15-S-L12-Z12-M | 12 | 2 | 0 | Pullout | 0.74 | 1509 | 12.6 | 25309 | 4.19 |
| TS40.17-S-L12-Z12-B | 12 | 2 | 0 | Pullout | 0.73 | 1492 | 12.5 | 29568 | 4.95 |
| TS48.13-S-L12-Z12-T | 12 | 2 | 0 | Pullout | 0.75 | 1478 | 11.8 | 24260 | 4.1 |
| TS35.13-S-L4-Z20-T | 4 | 2 | 0 | Pullout | 0.73 | 2489 | 19 | 16951 | 5.11 |
| TS35.14-S-L4-Z20-M | 4 | 2 | 0 | Pullout | 0.74 | 2433 | 18.6 | 17283 | 5.33 |
| TS35.15-S-L4-Z20-B | 4 | 2 | 0 | Pullout | 0.72 | 2504 | 19.1 | 13352 | 4 |
| TS46.14-S-L4-Z20-T | 4 | 2 | 0 | Pullout | 0.65 | 2490 | 20.8 | 11986 | 3.61 |
| TS46.20-S-L4-Z20-B | 4 | 2 | 0 | Pullout | 0.74 | 2448 | 20.4 | 12340 | 3.78 |
| TS37.16-S-L8-Z20-T | 8 | 2 | 0 | Pullout | 0.74 | 2597 | 20.1 | 20365 | 2.94 |
| TS37.17-S-L8-Z20-M | 8 | 2 | 0 | Pullout | 0.75 | 2583 | 20 | 20195 | 2.93 |
| TS37.18-S-L8-Z20-B | 8 | 2 | 0 | Pullout | 0.74 | 2617 | 20.2 | 21016 | 3.01 |
| TS37.19-S-L8-Z20-B | 8 | 2 | 0 | Pullout | 0.61 | 2513 | 19.4 | 23059 | 3.44 |
| TS38.14-S-L8-Z20-M | 8 | 2 | 0 | Pullout | 0.75 | 2493 | 21.3 | 23494 | 3.53 |
| TS38.15-S-L8-Z20-B | 8 | 2 | 0 | Pullout | 0.75 | 2605 | 22.2 | 27560 | 3.97 |
| TS48.17-S-L8-Z20-M | 8 | 2 | 0 | Pullout | 0.75 | 2484 | 20.1 | 23130 | 3.49 |

| TestID | Length, Le (ft) | Width, b (in.) | Skew, β (°) | Reinforcement Behavior | Displacement (in.) | Overburden, σv (psf) | DOF, z (ft) | Load, Pr (lb) | F* |
|---|---|---|---|---|---|---|---|---|---|
| TS48.19-S-L8-Z20-B | 8 | 2 | 0 | Pullout | 0.75 | 2482 | 20.2 | 30950 | 4.68 |
| TS50.22-S-L8-Z20-T | 8 | 2 | 0 | Pullout | 0.74 | 2468 | 20.1 | 23451 | 3.56 |
| TS32.15-S-L12-Z20-T | 12 | 2 | 0 | Rupture | 0.3 | 2473 | 19.6 | 20500 | 2.07 |
| TS32.18-S-L12-Z20-M | 12 | 2 | 0 | Rupture | 0.53 | 2495 | 19.8 | 20768 | 2.08 |
| TS32.21-S-L12-Z20-B | 12 | 2 | 0 | Rupture | 0.38 | 2478 | 19.6 | 22318 | 2.25 |
| TS40.14-S-L12-Z20-T | 12 | 2 | 0 | Pullout | 0.74 | 2397 | 20.1 | 32024 | 3.34 |
| TS40.18-S-L12-Z20-B | 12 | 2 | 0 | Pullout | 0.74 | 2499 | 20.9 | 31021 | 3.1 |
| TS48.14-S-L12-Z20-T | 12 | 2 | 0 | Pullout | 0.73 | 2475 | 19.8 | 27795 | 2.81 |
| TS50.23-S-L12-Z20-T | 12 | 2 | 0 | Pullout | 0.74 | 2504 | 20.4 | 15085 | 1.51 |
| TS48.15-S-L4-Z40-T | 4 | 2 | 0 | Pullout | 0.67 | 4947 | 39.6 | 12297 | 1.86 |
| TS32.13-S-L6-Z40-T | 6 | 2 | 0 | Pullout | 0.74 | 4991 | 39.6 | 19849 | 1.99 |
| TS32.16-S-L6-Z40-M | 6 | 2 | 0 | Pullout | 0.75 | 4998 | 39.6 | 19996 | 2 |
| TS32.19-S-L6-Z40-B | 6 | 2 | 0 | Rupture | 0.45 | 4998 | 39.6 | 18380 | 1.84 |
| TS41.17-S-L8-Z40-M | 8 | 2 | 0 | Pullout | 0.73 | 5017 | 40.9 | 28562 | 2.13 |
| TS41.20-S-L8-Z40-B | 8 | 2 | 0 | Pullout | 0.71 | 4993 | 38.3 | 23075 | 1.73 |
| TS41.14-S-L12-Z40-T | 12 | 2 | 0 | Pullout | 0.74 | 4995 | 40.9 | 25618 | 1.28 |
| TS41.15-S-L12-Z40-T | 12 | 2 | 0 | Pullout | 0.75 | 4911 | 40.2 | 28464 | 1.45 |
| TS41.18-S-L12-Z40-M | 12 | 2 | 0 | Pullout | 0.74 | 4993 | 40.7 | 33076 | 1.66 |
| TS50.26-S-L12-Z40-B | 12 | 2 | 0 | Pullout | 0.74 | 4956 | 38.6 | 29151 | 1.47 |
| TS43.13-S-L8-ß15°-Z5-T | 8 | 2 | 15 | Pullout | 0.6 | 607 | 4.9 | 12181 | 7.52 |
| TS43.16-S-L8-ß15°-Z5-M | 8 | 2 | 15 | Pullout | 0.74 | 566 | 4.7 | 17268 | 11.44 |
| TS43.19-S-L8-ß15°-Z5-B | 8 | 2 | 15 | Pullout | 0.74 | 625 | 4.9 | 16178 | 9.7 |
| TS44.13-S-L8-ß15°-Z12-T | 8 | 2 | 15 | Pullout | 0.72 | 1510 | 12.2 | 13121 | 3.26 |

| TestID | Length, Le (ft) | Width, b (in.) | Skew, β (°) | Reinforcement Behavior | Displacement (in.) | Overburden, σv (psf) | DOF, z (ft) | Load, Pr (lb) | F* |
|---|---|---|---|---|---|---|---|---|---|
| TS49.14-S-L4.5-ß30°-Z12-M | 4.5 | 2 | 30 | Pullout | 0.66 | 1557 | 12.3 | 13148 | 5.63 |
| TS49.15-S-L4.5-ß30°-Z12-B | 4.5 | 2 | 30 | Pullout | 0.7 | 1511 | 12 | 9864 | 4.35 |

## TABLE D2: SUMMARY DATA FOR MSE REINFORCEMENT PULLOUT TESTS
## WELDED STEEL GRIDS IN TYPE A BACKFILL

| TestID | Length, Le (ft) | Width, b (in.) | Skew, β (°) | Trans. Bar # | Trans. Bar Diameter, t (in.) | Trans. Bar Spacing, St (in.) | Long. Bar # | Long. Bar Diameter, tl (in.) | Long. Bar Spacing, Sl (in.) | Reinforcement Behavior | Displacement (in.) | Overburden, σv (psf) | DOF, z (ft) | Load, Pr (lb) | F* |
|---|---|---|---|---|---|---|---|---|---|---|---|---|---|---|---|
| TS42.01-G-2x12-W9.5xW11-L6-Z5-T | 6 | 4 | 0 | 6 | 0.374 | 12 | 3 | 0.348 | 2 | Pullout | 0.75 | 664 | 5.5 | 17313 | 6.52 |
| TS42.05-G-2x12-W9.5xW11-L6-Z5-M | 6 | 4 | 0 | 6 | 0.374 | 12 | 3 | 0.348 | 2 | Pullout | 0.75 | 642 | 5.3 | 20036 | 7.81 |
| TS42.03-G-2x12-W9.5xW11-L3-Z12-T | 3 | 4 | 0 | 3 | 0.374 | 12 | 3 | 0.348 | 2 | Progressive Rupture | 0.75 | 1495 | 12.3 | 5131 | 1.72 |
| TS42.07-G-2x12-W9.5xW11-L3-Z12-M | 3 | 4 | 0 | 3 | 0.374 | 12 | 3 | 0.348 | 2 | Pullout | 0.75 | 1468 | 12.1 | 11935 | 4.07 |
| TS42.11-G-2x12-W9.5xW11-L3-Z12-B | 3 | 4 | 0 | 3 | 0.374 | 12 | 3 | 0.348 | 2 | Pullout | 0.75 | 1510 | 11.3 | 10277 | 3.4 |
| TS42.09-G-2x12-W9.5xW11-L6-Z20-B | 6 | 4 | 0 | 6 | 0.374 | 12 | 3 | 0.348 | 2 | Rupture | 0.43 | 2506 | 18.8 | 20198 | 2.01 |
| TS40.01-G-2x12-W20xW11-L6-Z5-T | 6 | 4 | 0 | 6 | 0.374 | 12 | 3 | 0.505 | 2 | Pullout | 0.74 | 647 | 5.4 | 19127 | 7.39 |
| TS40.05-G-2x12-W20xW11-L6-Z5-M | 6 | 4 | 0 | 6 | 0.374 | 12 | 3 | 0.505 | 2 | Pullout | 0.75 | 628 | 5.3 | 18160 | 7.23 |
| TS40.09-G-2x12-W20xW11-L6-Z5-B | 6 | 4 | 0 | 6 | 0.374 | 12 | 3 | 0.505 | 2 | Pullout | 0.74 | 634 | 5.3 | 26244 | 10.35 |
| TS40.03-G-2x12-W20xW11-L6-Z12-T | 6 | 4 | 0 | 6 | 0.374 | 12 | 3 | 0.505 | 2 | Pullout | 0.72 | 1456 | 12.2 | 22271 | 3.82 |
| TS40.07-G-2x12-W20xW11-L6-Z12-M | 6 | 4 | 0 | 6 | 0.374 | 12 | 3 | 0.505 | 2 | Pullout | 0.74 | 1448 | 12.1 | 19336 | 3.34 |
| TS40.11-G-2x12-W20xW11-L6-Z12-B | 6 | 4 | 0 | 6 | 0.374 | 12 | 3 | 0.505 | 2 | Pullout | 0.74 | 1459 | 12.2 | 25264 | 4.33 |
| TS41.01-G-2x12-W20xW11-L6-Z20-T | 6 | 4 | 0 | 6 | 0.374 | 12 | 3 | 0.505 | 2 | Pullout | 0.75 | 2457 | 20.1 | 18980 | 1.93 |
| TS41.05-G-2x12-W20xW11-L6-Z20-M | 6 | 4 | 0 | 6 | 0.374 | 12 | 3 | 0.505 | 2 | Pullout | 0.74 | 2492 | 20.3 | 22566 | 2.26 |
| TS41.09-G-2x12-W20xW11-L6-Z20-B | 6 | 4 | 0 | 6 | 0.374 | 12 | 3 | 0.505 | 2 | Pullout | 0.74 | 2521 | 19.4 | 27713 | 2.75 |
| TS41.07-G-2x12-W20xW11-L3-Z40-M | 3 | 4 | 0 | 3 | 0.374 | 12 | 3 | 0.505 | 2 | Pullout | 0.73 | 4991 | 40.7 | 16586 | 1.66 |
| TS41.11-G-2x12-W20xW11-L3-Z40-B | 3 | 4 | 0 | 3 | 0.374 | 12 | 3 | 0.505 | 2 | Pullout | 0.74 | 4830 | 37.1 | 16739 | 1.73 |
| TS41.03-G-2x12-W20xW11-L6-Z40-T | 6 | 4 | 0 | 6 | 0.374 | 12 | 3 | 0.505 | 2 | Pullout | 0.72 | 5021 | 41.1 | 14831 | 0.74 |
| TS49.01-G-6x12-W9.5xW11-L6-Z5-T | 6 | 12 | 0 | 6 | 0.374 | 12 | 3 | 0.348 | 6 | Pullout | 0.74 | 638 | 5.1 | 18722 | 2.45 |
| TS49.05-G-6x12-W9.5xW11-L6-Z5-M | 6 | 12 | 0 | 6 | 0.374 | 12 | 3 | 0.348 | 6 | Progressive Rupture | 0.39 | 600 | 4.8 | 20996 | 2.91 |

| TestID | Length, Le (ft) | Width, b (in.) | Skew, β (°) | Trans. Bar # | Trans. Bar Diameter, t (in.) | Trans. Bar Spacing, St (in.) | Long. Bar # | Long. Bar Diameter, tl (in.) | Long. Bar Spacing, Sl (in.) | Reinforcement Behavior | Displacement (in.) | Overburden, σv (psf) | DOF, z (ft) | Load, Pr (lb) | F* |
|---|---|---|---|---|---|---|---|---|---|---|---|---|---|---|---|
| TS49.09-G-6x12-W9.5xW11-L6-Z5-B | 6 | 12 | 0 | 6 | 0.374 | 12 | 3 | 0.348 | 6 | Progressive Rupture | 0.21 | 656 | 5.2 | 19740 | 2.51 |
| TS47.02-G-6x12-W9.5xW11-L3-Z12-T | 3 | 12 | 0 | 3 | 0.374 | 12 | 3 | 0.348 | 6 | Progressive Rupture | 0.58 | 1470 | 12.2 | 14085 | 1.6 |
| TS47.06-G-6x12-W9.5xW11-L3-Z12-M | 3 | 12 | 0 | 3 | 0.374 | 12 | 3 | 0.348 | 6 | Progressive Rupture | 0.38 | 1494 | 12.3 | 14286 | 1.59 |
| TS47.10-G-6x12-W9.5xW11-L3-Z12-B | 3 | 12 | 0 | 3 | 0.374 | 12 | 3 | 0.348 | 6 | Progressive Rupture | 0.26 | 1468 | 12 | 10892 | 1.24 |
| TS48.03-G-6x12-W9.5xW11-L3-Z12-T | 3 | 12 | 0 | 3 | 0.374 | 12 | 3 | 0.348 | 6 | Progressive Rupture | 0.38 | 1467 | 11.7 | 14434 | 1.64 |
| TS46.01-G-6x12-W20xW11-L6-Z5-T | 6 | 12 | 0 | 6 | 0.374 | 12 | 3 | 0.505 | 6 | Pullout | 0.75 | 627 | 5.2 | 21097 | 2.8 |
| TS46.05-G-6x12-W20xW11-L6-Z5-M | 6 | 12 | 0 | 6 | 0.374 | 12 | 3 | 0.505 | 6 | Pullout | 0.74 | 633 | 5.3 | 32739 | 4.31 |
| TS46.09-G-6x12-W20xW11-L6-Z5-B | 6 | 12 | 0 | 6 | 0.374 | 12 | 3 | 0.505 | 6 | Pullout | 0.75 | 627 | 5.2 | 37325 | 4.96 |
| TS46.02-G-6x12-W20xW11-L6-Z12-T | 6 | 12 | 0 | 6 | 0.374 | 12 | 3 | 0.505 | 6 | Pullout | 0.74 | 1451 | 12.1 | 27479 | 1.58 |
| TS46.06-G-6x12-W20xW11-L6-Z12-M | 6 | 12 | 0 | 6 | 0.374 | 12 | 3 | 0.505 | 6 | Pullout | 0.74 | 1448 | 12.1 | 37831 | 2.18 |
| TS46.10-G-6x12-W20xW11-L6-Z12-B | 6 | 12 | 0 | 6 | 0.374 | 12 | 3 | 0.505 | 6 | Pullout | 0.74 | 1488 | 12.4 | 42755 | 2.39 |
| TS46.03-G-6x12-W20xW11-L6-Z20-T | 6 | 12 | 0 | 6 | 0.374 | 12 | 3 | 0.505 | 6 | Pullout | 0.72 | 2375 | 19.9 | 37494 | 1.32 |
| TS46.07-G-6x12-W20xW11-L6-Z20-M | 6 | 12 | 0 | 6 | 0.374 | 12 | 3 | 0.505 | 6 | Pullout | 0.64 | 2348 | 19.6 | 44863 | 1.59 |
| TS46.11-G-6x12-W20xW11-L6-Z20-B | 6 | 12 | 0 | 6 | 0.374 | 12 | 3 | 0.505 | 6 | Pullout | 0.74 | 2454 | 20.4 | 45391 | 1.54 |
| TS46.04-G-6x12-W20xW11-L3-Z40-T | 3 | 12 | 0 | 3 | 0.374 | 12 | 3 | 0.505 | 6 | Pullout | 0.75 | 5031 | 42.1 | 29448 | 0.98 |
| TS46.08-G-6x12-W20xW11-L3-Z40-M | 3 | 12 | 0 | 3 | 0.374 | 12 | 3 | 0.505 | 6 | Pullout | 0.74 | 5056 | 42.2 | 34949 | 1.15 |
| TS46.12-G-6x12-W20xW11-L3-Z40-B | 3 | 12 | 0 | 3 | 0.374 | 12 | 3 | 0.505 | 6 | Pullout | 0.74 | 4964 | 41.3 | 32072 | 1.08 |
| TS32.03-G-9x6-W20xW7.5-L3-Z5-T | 3 | 18 | 0 | 6 | 0.309 | 6 | 3 | 0.505 | 9 | Progressive Rupture | 0.75 | 663 | 5.3 | 21541 | 3.61 |
| TS32.07-G-9x6-W20xW7.5-L3-Z5-M | 3 | 18 | 0 | 6 | 0.309 | 6 | 3 | 0.505 | 9 | Progressive Rupture | 0.75 | 656 | 5.2 | 25141 | 4.26 |
| TS32.11-G-9x6-W20xW7.5-L3-Z5-B | 3 | 18 | 0 | 6 | 0.309 | 6 | 3 | 0.505 | 9 | Progressive Rupture | 0.64 | 642 | 5.1 | 24557 | 4.25 |
| TS32.04-G-9x6-W20xW7.5-L3-Z12-T | 3 | 18 | 0 | 6 | 0.309 | 6 | 3 | 0.505 | 9 | Progressive Rupture | 0.74 | 1518 | 12 | 29885 | 2.19 |
| TS32.08-G-9x6-W20xW7.5-L3-Z12-M | 3 | 18 | 0 | 6 | 0.309 | 6 | 3 | 0.505 | 9 | Progressive Rupture | 0.74 | 1507 | 11.9 | 31519 | 2.32 |
| TS32.12-G-9x6-W20xW7.5-L3-Z12-B | 3 | 18 | 0 | 6 | 0.309 | 6 | 3 | 0.505 | 9 | Progressive Rupture | 0.75 | 1492 | 11.8 | 32154 | 2.4 |

| TestID | Length, Le (ft) | Width, b (in.) | Skew, β (°) | Trans. Bar # | Trans. Bar Diameter, t (in.) | Trans. Bar Spacing, St (in.) | Long. Bar # | Long. Bar Diameter, tl (in.) | Long. Bar Spacing, Sl (in.) | Reinforcement Behavior | Displacement (in.) | Overburden, σv (psf) | DOF, z (ft) | Load, Pr (lb) | F* |
|---|---|---|---|---|---|---|---|---|---|---|---|---|---|---|---|
| TS47.03-G-9x6-W20xW11-L3-Z5-T | 3 | 18 | 0 | 6 | 0.374 | 6 | 3 | 0.505 | 9 | Pullout | 0.75 | 637 | 5.3 | 21328 | 3.72 |
| TS47.07-G-9x6-W20xW11-L3-Z5-M | 3 | 18 | 0 | 6 | 0.374 | 6 | 3 | 0.505 | 9 | Pullout | 0.75 | 625 | 5.1 | 27914 | 4.96 |
| TS47.11-G-9x6-W20xW11-L3-Z5-B | 3 | 18 | 0 | 6 | 0.374 | 6 | 3 | 0.505 | 9 | Pullout | 0.73 | 625 | 5.1 | 31106 | 5.53 |
| TS47.04-G-9x6-W20xW11-L3-Z12-T | 3 | 18 | 0 | 6 | 0.374 | 6 | 3 | 0.505 | 9 | Progressive Rupture | 0.64 | 1487 | 12.3 | 35703 | 2.67 |
| TS47.08-G-9x6-W20xW11-L3-Z12-M | 3 | 18 | 0 | 6 | 0.374 | 6 | 3 | 0.505 | 9 | Progressive Rupture | 0.73 | 1460 | 12 | 35726 | 2.72 |
| TS47.12-G-9x6-W20xW11-L3-Z12-B | 3 | 18 | 0 | 6 | 0.374 | 6 | 3 | 0.505 | 9 | Progressive Rupture | 0.66 | 1484 | 12.1 | 39921 | 2.99 |
| TS37.03-G-9x6-W20xW15-L3-Z5-T | 3 | 18 | 0 | 6 | 0.437 | 6 | 3 | 0.505 | 9 | Pullout | 0.75 | 734 | 5.7 | 27964 | 4.23 |
| TS37.07-G-9x6-W20xW15-L3-Z5-M | 3 | 18 | 0 | 6 | 0.437 | 6 | 3 | 0.505 | 9 | Progressive Rupture | 0.47 | 675 | 5.2 | 32813 | 5.4 |
| TS37.11-G-9x6-W20xW15-L3-Z5-B | 3 | 18 | 0 | 6 | 0.437 | 6 | 3 | 0.505 | 9 | Progressive Rupture | 0.36 | 678 | 5.2 | 29166 | 4.78 |
| TS37.04-G-9x6-W20xW15-L3-Z12-T | 3 | 18 | 0 | 6 | 0.437 | 6 | 3 | 0.505 | 9 | Progressive Rupture | 0.6 | 1606 | 12.4 | 33901 | 2.34 |
| TS37.08-G-9x6-W20xW15-L3-Z12-M | 3 | 18 | 0 | 6 | 0.437 | 6 | 3 | 0.505 | 9 | Progressive Rupture | 0.56 | 1513 | 11.7 | 36764 | 2.7 |
| TS37.12-G-9x6-W20xW15-L3-Z12-B | 3 | 18 | 0 | 6 | 0.437 | 6 | 3 | 0.505 | 9 | Progressive Rupture | 0.44 | 1555 | 12 | 34594 | 2.47 |
| TS48.01-G-9x6-W20xW15-L3-Z12-T | 3 | 18 | 0 | 6 | 0.437 | 6 | 3 | 0.505 | 9 | Rupture | 0.22 | 1474 | 11.8 | 28298 | 2.13 |
| TS50.07-G-9x6-W20xW15-L3-Z12-T | 3 | 18 | 0 | 6 | 0.437 | 6 | 3 | 0.505 | 9 | Pullout | 0.73 | 1572 | 12.8 | 34015 | 2.4 |
| TS49.02-G-9x12-W9.5xW11-L6-Z5-T | 6 | 18 | 0 | 6 | 0.374 | 12 | 3 | 0.348 | 9 | Progressive Rupture | 0.74 | 591 | 4.7 | 16460 | 1.55 |
| TS49.06-G-9x12-W9.5xW11-L6-Z5-M | 6 | 18 | 0 | 6 | 0.374 | 12 | 3 | 0.348 | 9 | Progressive Rupture | 0.21 | 698 | 5.5 | 20050 | 1.59 |
| TS47.01-G-9x12-W9.5xW11-L3-Z12-T | 3 | 18 | 0 | 3 | 0.374 | 12 | 3 | 0.348 | 9 | Progressive Rupture | 0.39 | 1428 | 11.8 | 14754 | 1.15 |
| TS47.05-G-9x12-W9.5xW11-L3-Z12-M | 3 | 18 | 0 | 3 | 0.374 | 12 | 3 | 0.348 | 9 | Progressive Rupture | 0.42 | 1494 | 12.3 | 14294 | 1.06 |
| TS47.09-G-9x12-W9.5xW11-L3-Z12-B | 3 | 18 | 0 | 3 | 0.374 | 12 | 3 | 0.348 | 9 | Progressive Rupture | 0.27 | 1475 | 12 | 16621 | 1.25 |
| TS48.04-G-9x12-W9.5xW11-L3-Z12-T | 3 | 18 | 0 | 3 | 0.374 | 12 | 3 | 0.348 | 9 | Progressive Rupture | 0.47 | 1506 | 12 | 13703 | 1.01 |
| TS32.01-G-9x12-W20xW7.5-L6-Z5-T | 6 | 18 | 0 | 6 | 0.309 | 12 | 3 | 0.505 | 9 | Pullout | 0.75 | 704 | 5.6 | 28024 | 2.21 |
| TS32.05-G-9x12-W20xW7.5-L6-Z5-M | 6 | 18 | 0 | 6 | 0.309 | 12 | 3 | 0.505 | 9 | Pullout | 0.74 | 660 | 5.2 | 30427 | 2.56 |
| TS32.09-G-9x12-W20xW7.5-L6-Z5-B | 6 | 18 | 0 | 6 | 0.309 | 12 | 3 | 0.505 | 9 | Pullout | 0.74 | 673 | 5.3 | 34494 | 2.85 |

| TestID | Length, Le (ft) | Width, b (in.) | Skew, β (°) | Trans. Bar # | Trans. Bar Diameter, t (in.) | Trans. Bar Spacing, St (in.) | Long. Bar # | Long. Bar Diameter, tl (in.) | Long. Bar Spacing, Sl (in.) | Reinforcement Behavior | Displacement (in.) | Overburden, σv (psf) | DOF, z (ft) | Load, Pr (lb) | F* |
|---|---|---|---|---|---|---|---|---|---|---|---|---|---|---|---|
| TS32.02-G-9x12-W20xW7.5-L6-Z12-T | 6 | 18 | 0 | 6 | 0.309 | 12 | 3 | 0.505 | 9 | Pullout | 0.74 | 1478 | 11.7 | 31708 | 1.19 |
| TS32.06-G-9x12-W20xW7.5-L6-Z12-M | 6 | 18 | 0 | 6 | 0.309 | 12 | 3 | 0.505 | 9 | Pullout | 0.75 | 1497 | 11.9 | 33923 | 1.26 |
| TS32.10-G-9x12-W20xW7.5-L6-Z12-B | 6 | 18 | 0 | 6 | 0.309 | 12 | 3 | 0.505 | 9 | Pullout | 0.75 | 1514 | 12 | 38824 | 1.42 |
| TS31.05-G-9x12-W20xW7.5-L6-Z20-M | 6 | 18 | 0 | 6 | 0.309 | 12 | 3 | 0.505 | 9 | Pullout | 0.75 | 2161 | 18 | 38155 | 0.98 |
| TS31.09-G-9x12-W20xW7.5-L6-Z20-B | 6 | 18 | 0 | 6 | 0.309 | 12 | 3 | 0.505 | 9 | Pullout | 0.74 | 2215 | 18.4 | 38213 | 0.96 |
| TS31.03-G-9x12-W20xW11-L6-Z5-T | 6 | 18 | 0 | 6 | 0.374 | 12 | 3 | 0.505 | 9 | Pullout | 0.75 | 628 | 5.2 | 28519 | 2.52 |
| TS31.07-G-9x12-W20xW11-L6-Z5-M | 6 | 18 | 0 | 6 | 0.374 | 12 | 3 | 0.505 | 9 | Pullout | 0.74 | 655 | 5.5 | 36213 | 3.07 |
| TS31.11-G-9x12-W20xW11-L6-Z5-B | 6 | 18 | 0 | 6 | 0.374 | 12 | 3 | 0.505 | 9 | Pullout | 0.75 | 642 | 5.3 | 36279 | 3.14 |
| TS48.05-G-9x12-W20xW11-L6-Z5-M | 6 | 18 | 0 | 6 | 0.374 | 12 | 3 | 0.505 | 9 | Pullout | 0.75 | 652 | 5.3 | 35903 | 3.06 |
| TS48.07-G-9x12-W20xW11-L6-Z5-M | 6 | 18 | 0 | 6 | 0.374 | 12 | 3 | 0.505 | 9 | Pullout | 0.75 | 653 | 5.3 | 31567 | 2.68 |
| TS48.11-G-9x12-W20xW11-L6-Z5-B | 6 | 18 | 0 | 6 | 0.374 | 12 | 3 | 0.505 | 9 | Pullout | 0.74 | 638 | 5.2 | 37091 | 3.23 |
| TS30.03-G-9x12-W20xW11-L9-Z5-T | 9 | 18 | 0 | 9 | 0.374 | 12 | 3 | 0.505 | 9 | Pullout | 0.73 | 670 | 5.6 | 42099 | 2.33 |
| TS30.07-G-9x12-W20xW11-L9-Z5-M | 9 | 18 | 0 | 9 | 0.374 | 12 | 3 | 0.505 | 9 | Pullout | 0.75 | 650 | 5.4 | 43226 | 2.46 |
| TS30.11-G-9x12-W20xW11-L9-Z5-B | 9 | 18 | 0 | 9 | 0.374 | 12 | 3 | 0.505 | 9 | Pullout | 0.73 | 647 | 5.4 | 43780 | 2.5 |
| TS30.01-G-9x12-W20xW11-L12-Z5-T | 12 | 18 | 0 | 12 | 0.374 | 12 | 3 | 0.505 | 9 | Pullout | 0.6 | 653 | 5.4 | 44122 | 1.88 |
| TS30.05-G-9x12-W20xW11-L12-Z5-M | 12 | 18 | 0 | 12 | 0.374 | 12 | 3 | 0.505 | 9 | Pullout | 0.64 | 669 | 5.6 | 42504 | 1.77 |
| TS30.09-G-9x12-W20xW11-L12-Z5-B | 12 | 18 | 0 | 12 | 0.374 | 12 | 3 | 0.505 | 9 | Pullout | 0.73 | 636 | 5.3 | 44779 | 1.96 |
| TS31.08-G-9x12-W20xW11-L3-Z12-M | 3 | 18 | 0 | 3 | 0.374 | 12 | 3 | 0.505 | 9 | Pullout | 0.74 | 1320 | 11 | 22782 | 1.92 |
| TS31.12-G-9x12-W20xW11-L3-Z12-B | 3 | 18 | 0 | 3 | 0.374 | 12 | 3 | 0.505 | 9 | Pullout | 0.74 | 1457 | 12.1 | 23505 | 1.79 |
| TS48.02-G-9x12-W20xW11-L3-Z12-T | 3 | 18 | 0 | 3 | 0.374 | 12 | 3 | 0.505 | 9 | Progressive Rupture | 0.66 | 1501 | 12 | 13439 | 0.99 |
| TS30.04-G-9x12-W20xW11-L6-Z12-T | 6 | 18 | 0 | 6 | 0.374 | 12 | 3 | 0.505 | 9 | Pullout | 0.74 | 1560 | 13 | 38854 | 1.38 |
| TS30.08-G-9x12-W20xW11-L6-Z12-M | 6 | 18 | 0 | 6 | 0.374 | 12 | 3 | 0.505 | 9 | Pullout | 0.74 | 1423 | 11.9 | 40657 | 1.59 |
| TS30.12-G-9x12-W20xW11-L6-Z12-B | 6 | 18 | 0 | 6 | 0.374 | 12 | 3 | 0.505 | 9 | Rupture | 0.6 | 1432 | 11.9 | 37806 | 1.47 |

| TestID | Length, Le (ft) | Width, b (in.) | Skew, β (°) | Trans. Bar # | Trans. Bar Diameter, t (in.) | Trans. Bar Spacing, St (in.) | Long. Bar # | Long. Bar Diameter, tl (in.) | Long. Bar Spacing, Sl (in.) | Reinforcement Behavior | Displacement (in.) | Overburden, σv (psf) | DOF, z (ft) | Load, Pr (lb) | F* |
|---|---|---|---|---|---|---|---|---|---|---|---|---|---|---|---|
| TS30.02-G-9x12-W20xW11-L9-Z12-T | 9 | 18 | 0 | 9 | 0.374 | 12 | 3 | 0.505 | 9 | Pullout | 0.67 | 1418 | 11.8 | 44067 | 1.15 |
| TS30.06-G-9x12-W20xW11-L9-Z12-M | 9 | 18 | 0 | 9 | 0.374 | 12 | 3 | 0.505 | 9 | Rupture | 0.67 | 1424 | 11.9 | 45836 | 1.19 |
| TS30.10-G-9x12-W20xW11-L9-Z12-B | 9 | 18 | 0 | 9 | 0.374 | 12 | 3 | 0.505 | 9 | Pullout | 0.73 | 1433 | 11.9 | 45142 | 1.17 |
| TS31.01-G-9x12-W20xW11-L6-Z20-T | 6 | 18 | 0 | 6 | 0.374 | 12 | 3 | 0.505 | 9 | Pullout | 0.74 | 2184 | 18.2 | 38991 | 0.99 |
| TS31.02-G-9x12-W20xW11-L6-Z20-T | 6 | 18 | 0 | 6 | 0.374 | 12 | 3 | 0.505 | 9 | Pullout | 0.75 | 2153 | 17.9 | 40125 | 1.04 |
| TS31.06-G-9x12-W20xW11-L6-Z20-M | 6 | 18 | 0 | 6 | 0.374 | 12 | 3 | 0.505 | 9 | Progressive Rupture | 0.59 | 2194 | 18.3 | 36241 | 0.92 |
| TS31.10-G-9x12-W20xW11-L6-Z20-B | 6 | 18 | 0 | 6 | 0.374 | 12 | 3 | 0.505 | 9 | Progressive Rupture | 0.54 | 2185 | 18.2 | 37837 | 0.96 |
| TS48.06-G-9x12-W20xW11-L6-Z20-M | 6 | 18 | 0 | 6 | 0.374 | 12 | 3 | 0.505 | 9 | Progressive Rupture | 0.69 | 2479 | 20 | 43794 | 0.98 |
| TS48.08-G-9x12-W20xW11-L6-Z20-M | 6 | 18 | 0 | 6 | 0.374 | 12 | 3 | 0.505 | 9 | Pullout | 0.74 | 2460 | 19.9 | 43645 | 0.99 |
| TS48.10-G-9x12-W20xW11-L6-Z20-B | 6 | 18 | 0 | 6 | 0.374 | 12 | 3 | 0.505 | 9 | Pullout | 0.75 | 2460 | 20 | 44021 | 0.99 |
| TS48.12-G-9x12-W20xW11-L6-Z20-B | 6 | 18 | 0 | 6 | 0.374 | 12 | 3 | 0.505 | 9 | Pullout | 0.74 | 2472 | 20.1 | 45569 | 1.02 |
| TS49.04-G-9x12-W20xW11-L3-Z40-T | 3 | 18 | 0 | 3 | 0.374 | 12 | 3 | 0.505 | 9 | Progressive Rupture | 0.61 | 4839 | 38.6 | 23470 | 0.54 |
| TS49.08-G-9x12-W20xW11-L3-Z40-M | 3 | 18 | 0 | 3 | 0.374 | 12 | 3 | 0.505 | 9 | Progressive Rupture | 0.65 | 4917 | 39 | 29741 | 0.67 |
| TS49.12-G-9x12-W20xW11-L3-Z40-B | 3 | 18 | 0 | 3 | 0.374 | 12 | 3 | 0.505 | 9 | Progressive Rupture | 0.71 | 5067 | 40.4 | 34574 | 0.76 |
| TS43.01-G-9x12-W20xW11-L6-ß15°-Z5-T | 6 | 18 | 15 | 6 | 0.374 | 12 | 3 | 0.505 | 9 | Pullout | 0.74 | 624 | 5 | 21883 | 1.95 |
| TS43.05-G-9x12-W20xW11-L6-ß15°-Z5-M | 6 | 18 | 15 | 6 | 0.374 | 12 | 3 | 0.505 | 9 | Pullout | 0.75 | 626 | 5.2 | 28783 | 2.55 |
| TS43.09-G-9x12-W20xW11-L6-ß15°-Z5-B | 6 | 18 | 15 | 6 | 0.374 | 12 | 3 | 0.505 | 9 | Pullout | 0.74 | 624 | 4.9 | 38550 | 3.43 |
| TS44.01-G-9x12-W20xW11-L6-ß15°-Z12-T | 6 | 18 | 15 | 6 | 0.374 | 12 | 3 | 0.505 | 9 | Pullout | 0.74 | 1501 | 12.2 | 28254 | 1.05 |
| TS44.05-G-9x12-W20xW11-L6-ß15°-Z12-M | 6 | 18 | 15 | 6 | 0.374 | 12 | 3 | 0.505 | 9 | Progressive Rupture | 0.73 | 1437 | 11.5 | 34018 | 1.32 |
| TS44.09-G-9x12-W20xW11-L6-ß15°-Z12-B | 6 | 18 | 15 | 6 | 0.374 | 12 | 3 | 0.505 | 9 | Progressive Rupture 2 | 0.75 | 1526 | 11.8 | 44579 | 1.62 |
| TS43.02-G-9x12-W20xW11-L6-ß30°-Z5-T | 6 | 18 | 30 | 6 | 0.374 | 12 | 3 | 0.505 | 9 | Pullout | 0.75 | 631 | 5.1 | 20277 | 1.78 |
| TS43.06-G-9x12-W20xW11-L6-ß30°-Z5-M | 6 | 18 | 30 | 6 | 0.374 | 12 | 3 | 0.505 | 9 | Pullout | 0.74 | 609 | 5 | 24108 | 2.2 |
| TS43.10-G-9x12-W20xW11-L6-ß30°-Z5-B | 6 | 18 | 30 | 6 | 0.374 | 12 | 3 | 0.505 | 9 | Pullout | 0.75 | 621 | 4.9 | 28731 | 2.57 |

| TestID | Length, Le (ft) | Width, b (in.) | Skew, β (°) | Trans. Bar # | Trans. Bar Diameter, t (in.) | Trans. Bar Spacing, St (in.) | Long. Bar # | Long. Bar Diameter, tl (in.) | Long. Bar Spacing, Sl (in.) | Reinforcement Behavior | Displacement (in.) | Overburden, σv (psf) | DOF, z (ft) | Load, Pr (lb) | F* |
|---|---|---|---|---|---|---|---|---|---|---|---|---|---|---|---|
| TS44.02-G-9x12-W20xW11-L6-ß30°-Z12-T | 6 | 18 | 30 | 6 | 0.374 | 12 | 3 | 0.505 | 9 | Pullout | 0.74 | 1497 | 12.1 | 25531 | 0.95 |
| TS44.06-G-9x12-W20xW11-L6-ß30°-Z12-M | 6 | 18 | 30 | 6 | 0.374 | 12 | 3 | 0.505 | 9 | Pullout | 0.74 | 1487 | 11.9 | 34105 | 1.27 |
| TS44.10-G-9x12-W20xW11-L6-ß30°-Z12-B | 6 | 18 | 30 | 6 | 0.374 | 12 | 3 | 0.505 | 9 | Pullout | 0.74 | 1485 | 11.5 | 32266 | 1.21 |
| TS37.01-G-9x12-W20xW15-L6-Z5-T | 6 | 18 | 0 | 6 | 0.437 | 12 | 3 | 0.505 | 9 | Pullout | 0.74 | 701 | 5.4 | 32947 | 2.61 |
| TS37.05-G-9x12-W20xW15-L6-Z5-M | 6 | 18 | 0 | 6 | 0.437 | 12 | 3 | 0.505 | 9 | Pullout | 0.74 | 746 | 5.8 | 37734 | 2.81 |
| TS37.09-G-9x12-W20xW15-L6-Z5-B | 6 | 18 | 0 | 6 | 0.437 | 12 | 3 | 0.505 | 9 | Progressive Rupture | 0.64 | 681 | 5.3 | 35343 | 2.88 |
| TS37.02-G-9x12-W20xW15-L6-Z12-T | 6 | 18 | 0 | 6 | 0.437 | 12 | 3 | 0.505 | 9 | Progressive Rupture | 0.73 | 1579 | 12.2 | 33712 | 1.19 |
| TS37.06-G-9x12-W20xW15-L6-Z12-M | 6 | 18 | 0 | 6 | 0.437 | 12 | 3 | 0.505 | 9 | Pullout | 0.75 | 1556 | 12 | 36725 | 1.31 |
| TS37.10-G-9x12-W20xW15-L6-Z12-B | 6 | 18 | 0 | 6 | 0.437 | 12 | 3 | 0.505 | 9 | Pullout | 0.71 | 1562 | 12.1 | 39922 | 1.42 |
| TS49.03-G-9x12-W20xW15-L6-Z20-T | 6 | 18 | 0 | 6 | 0.437 | 12 | 3 | 0.505 | 9 | Progressive Rupture | 0.73 | 2474 | 19.8 | 39079 | 0.88 |
| TS49.07-G-9x12-W20xW15-L6-Z20-M | 6 | 18 | 0 | 6 | 0.437 | 12 | 3 | 0.505 | 9 | Progressive Rupture | 0.45 | 2456 | 19.5 | 37065 | 0.84 |
| TS49.11-G-9x12-W20xW15-L6-Z20-B | 6 | 18 | 0 | 6 | 0.437 | 12 | 3 | 0.505 | 9 | Progressive Rupture | 0.5 | 2402 | 19.2 | 40894 | 0.95 |
| TS38.01-G-9x18-W20xW7.5-L9-Z5-T | 9 | 18 | 0 | 6 | 0.309 | 18 | 3 | 0.505 | 9 | Pullout | 0.75 | 693 | 5.9 | 31073 | 1.66 |
| TS38.05-G-9x18-W20xW7.5-L9-Z5-M | 9 | 18 | 0 | 6 | 0.309 | 18 | 3 | 0.505 | 9 | Pullout | 0.75 | 663 | 5.7 | 32264 | 1.8 |
| TS38.09-G-9x18-W20xW7.5-L9-Z5-M | 9 | 18 | 0 | 6 | 0.309 | 18 | 3 | 0.505 | 9 | Pullout | 0.74 | 526 | 4.5 | 37671 | 2.65 |
| TS38.02-G-9x18-W20xW7.5-L9-Z12-T | 9 | 18 | 0 | 6 | 0.309 | 18 | 3 | 0.505 | 9 | Pullout | 0.75 | 1447 | 12.3 | 36946 | 0.95 |
| TS38.06-G-9x18-W20xW7.5-L9-Z12-M | 9 | 18 | 0 | 6 | 0.309 | 18 | 3 | 0.505 | 9 | Pullout | 0.74 | 1502 | 12.8 | 41018 | 1.01 |
| TS38.10-G-9x18-W20xW7.5-L9-Z12-B | 9 | 18 | 0 | 6 | 0.309 | 18 | 3 | 0.505 | 9 | Pullout | 0.73 | 1484 | 12.7 | 43508 | 1.09 |
| TS38.03-G-9x18-W20xW7.5-L9-Z20-T | 9 | 18 | 0 | 6 | 0.309 | 18 | 3 | 0.505 | 9 | Pullout | 0.74 | 2479 | 21.1 | 42588 | 0.64 |
| TS38.07-G-9x18-W20xW7.5-L9-Z20-M | 9 | 18 | 0 | 6 | 0.309 | 18 | 3 | 0.505 | 9 | Pullout | 0.73 | 2483 | 21.2 | 44338 | 0.66 |
| TS38.11-G-9x18-W20xW7.5-L9-Z20-B | 9 | 18 | 0 | 6 | 0.309 | 18 | 3 | 0.505 | 9 | Pullout | 0.66 | 2461 | 21 | 44223 | 0.67 |
| TS38.04-G-9x18-W20xW7.5-L4.5-Z40-T | 4.5 | 18 | 0 | 3 | 0.309 | 18 | 3 | 0.505 | 9 | Pullout | 0.74 | 4994 | 42.6 | 27021 | 0.4 |
| TS38.08-G-9x18-W20xW7.5-L4.5-Z40-M | 4.5 | 18 | 0 | 3 | 0.309 | 18 | 3 | 0.505 | 9 | Progressive Rupture | 0.5 | 4881 | 41.6 | 25895 | 0.39 |

| TestID | Length, Le (ft) | Width, b (in.) | Skew, β (°) | Trans. Bar # | Trans. Bar Diameter, t (in.) | Trans. Bar Spacing, St (in.) | Long. Bar # | Long. Bar Diameter, tl (in.) | Long. Bar Spacing, Sl (in.) | Reinforcement Behavior | Displacement (in.) | Overburden, σv (psf) | DOF, z (ft) | Load, Pr (lb) | F* |
|---|---|---|---|---|---|---|---|---|---|---|---|---|---|---|---|
| TS38.12-G-9x18-W20xW7.5-L4.5-Z40-B | 4.5 | 18 | 0 | 3 | 0.309 | 18 | 3 | 0.505 | 9 | Progressive Rupture | 0.67 | 4957 | 42.3 | 26556 | 0.4 |
| TS35.01-G-9x18-W20xW11-L9-Z5-T | 9 | 18 | 0 | 6 | 0.374 | 18 | 3 | 0.505 | 9 | Pullout | 0.73 | 722 | 5.5 | 36703 | 1.88 |
| TS35.05-G-9x18-W20xW11-L9-Z5-M | 9 | 18 | 0 | 6 | 0.374 | 18 | 3 | 0.505 | 9 | Pullout | 0.74 | 695 | 5.3 | 39624 | 2.11 |
| TS35.09-G-9x18-W20xW11-L9-Z5-B | 9 | 18 | 0 | 6 | 0.374 | 18 | 3 | 0.505 | 9 | Pullout | 0.75 | 681 | 5.2 | 37540 | 2.04 |
| TS35.02-G-9x18-W20xW11-L9-Z12-T | 9 | 18 | 0 | 6 | 0.374 | 18 | 3 | 0.505 | 9 | Pullout | 0.71 | 1391 | 10.6 | 37628 | 1 |
| TS35.06-G-9x18-W20xW11-L9-Z12-M | 9 | 18 | 0 | 6 | 0.374 | 18 | 3 | 0.505 | 9 | Pullout | 0.7 | 1518 | 11.6 | 43883 | 1.07 |
| TS35.10-G-9x18-W20xW11-L9-Z12-B | 9 | 18 | 0 | 6 | 0.374 | 18 | 3 | 0.505 | 9 | Pullout | 0.75 | 1516 | 11.6 | 42494 | 1.04 |
| TS35.03-G-9x18-W20xW11-L9-Z20-T | 9 | 18 | 0 | 6 | 0.374 | 18 | 3 | 0.505 | 9 | Progressive Rupture | 0.61 | 2448 | 18.7 | 42159 | 0.64 |
| TS35.07-G-9x18-W20xW11-L9-Z20-M | 9 | 18 | 0 | 6 | 0.374 | 18 | 3 | 0.505 | 9 | Pullout | 0.7 | 2571 | 19.6 | 44581 | 0.64 |
| TS35.11-G-9x18-W20xW11-L9-Z20-B | 9 | 18 | 0 | 6 | 0.374 | 18 | 3 | 0.505 | 9 | Pullout | 0.75 | 2448 | 18.7 | 42598 | 0.64 |
| TS35.04-G-9x18-W20xW11-L4.5-Z40-T | 4.5 | 18 | 0 | 3 | 0.374 | 18 | 3 | 0.505 | 9 | Pullout | 0.74 | 5002 | 38.2 | 33251 | 0.49 |
| TS35.08-G-9x18-W20xW11-L4.5-Z40-M | 4.5 | 18 | 0 | 3 | 0.374 | 18 | 3 | 0.505 | 9 | Pullout | 0.74 | 5010 | 38.3 | 32636 | 0.48 |
| TS35.12-G-9x18-W20xW11-L4.5-Z40-B | 4.5 | 18 | 0 | 3 | 0.374 | 18 | 3 | 0.505 | 9 | Progressive Rupture | 0.69 | 5010 | 38.3 | 26756 | 0.4 |
| TS45.01-G-9x18-W20xW15-L9-Z5-T | 9 | 18 | 0 | 6 | 0.437 | 18 | 3 | 0.505 | 9 | Pullout | 0.74 | 657 | 5.4 | 30815 | 1.74 |
| TS45.05-G-9x18-W20xW15-L9-Z5-M | 9 | 18 | 0 | 6 | 0.437 | 18 | 3 | 0.505 | 9 | Progressive Rupture | 0.55 | 664 | 5.5 | 35726 | 1.99 |
| TS45.09-G-9x18-W20xW15-L9-Z5-B | 9 | 18 | 0 | 6 | 0.437 | 18 | 3 | 0.505 | 9 | Progressive Rupture | 0.62 | 608 | 5.2 | 38314 | 2.33 |
| TS45.02-G-9x18-W20xW15-L9-Z12-T | 9 | 18 | 0 | 6 | 0.437 | 18 | 3 | 0.505 | 9 | Progressive Rupture | 0.75 | 1465 | 12.1 | 30774 | 0.78 |
| TS45.06-G-9x18-W20xW15-L9-Z12-M | 9 | 18 | 0 | 6 | 0.437 | 18 | 3 | 0.505 | 9 | Progressive Rupture | 0.52 | 1432 | 11.8 | 38775 | 1 |
| TS45.10-G-9x18-W20xW15-L9-Z12-B | 9 | 18 | 0 | 6 | 0.437 | 18 | 3 | 0.505 | 9 | Progressive Rupture | 0.55 | 1458 | 12.4 | 41774 | 1.06 |
| TS45.03-G-9x18-W20xW15-L9-Z20-T | 9 | 18 | 0 | 6 | 0.437 | 18 | 3 | 0.505 | 9 | Progressive Rupture | 0.46 | 2426 | 20 | 40363 | 0.62 |
| TS45.07-G-9x18-W20xW15-L9-Z20-M | 9 | 18 | 0 | 6 | 0.437 | 18 | 3 | 0.505 | 9 | Progressive Rupture | 0.37 | 2427 | 20 | 42035 | 0.64 |
| TS45.11-G-9x18-W20xW15-L9-Z20-B | 9 | 18 | 0 | 6 | 0.437 | 18 | 3 | 0.505 | 9 | Progressive Rupture | 0.23 | 2464 | 20.9 | 42835 | 0.64 |
| TS45.04-G-9x18-W20xW15-L4.5-Z40-T | 4.5 | 18 | 0 | 3 | 0.437 | 18 | 3 | 0.505 | 9 | Pullout | 0.75 | 4952 | 40.8 | 32972 | 0.49 |

| TestID | Length, Le (ft) | Width, b (in.) | Skew, β (°) | Trans. Bar # | Trans. Bar Diameter, t (in.) | Trans. Bar Spacing, St (in.) | Long. Bar # | Long. Bar Diameter, tl (in.) | Long. Bar Spacing, Sl (in.) | Reinforcement Behavior | Displacement (in.) | Overburden, σv (psf) | DOF, z (ft) | Load, Pr (lb) | F* |
|---|---|---|---|---|---|---|---|---|---|---|---|---|---|---|---|
| TS45.08-G-9x18-W20xW15-L4.5-Z40-M | 4.5 | 18 | 0 | 3 | 0.437 | 18 | 3 | 0.505 | 9 | Pullout | 0.74 | 4991 | 41.1 | 34340 | 0.51 |
| TS45.12-G-9x18-W20xW15-L4.5-Z40-B | 4.5 | 18 | 0 | 3 | 0.437 | 18 | 3 | 0.505 | 9 | Progressive Rupture | 0.74 | 4984 | 42.3 | 33184 | 0.49 |
| TS33.01-G-9x24-W20xW7.5-L12-Z5-T | 12 | 18 | 0 | 6 | 0.309 | 24 | 3 | 0.505 | 9 | Pullout | 0.75 | 658 | 5.1 | 34892 | 1.47 |
| TS33.09-G-9x24-W20xW7.5-L12-Z5-B | 12 | 18 | 0 | 6 | 0.309 | 24 | 3 | 0.505 | 9 | Pullout | 0.75 | 683 | 5.3 | 39563 | 1.61 |
| TS33.02-G-9x24-W20xW7.5-L12-Z12-T | 12 | 18 | 0 | 6 | 0.309 | 24 | 3 | 0.505 | 9 | Pullout | 0.75 | 1502 | 11.6 | 39434 | 0.73 |
| TS33.06-G-9x24-W20xW7.5-L12-Z12-M | 12 | 18 | 0 | 6 | 0.309 | 24 | 3 | 0.505 | 9 | Pullout | 0.75 | 1514 | 11.7 | 41424 | 0.76 |
| TS33.10-G-9x24-W20xW7.5-L12-Z12-B | 12 | 18 | 0 | 6 | 0.309 | 24 | 3 | 0.505 | 9 | Progressive Rupture | 0.6 | 1526 | 11.7 | 30370 | 0.55 |
| TS33.03-G-9x24-W20xW7.5-L12-Z20-T | 12 | 18 | 0 | 6 | 0.309 | 24 | 3 | 0.505 | 9 | Progressive Rupture | 0.52 | 2505 | 19.3 | 34617 | 0.38 |
| TS33.07-G-9x24-W20xW7.5-L12-Z20-M | 12 | 18 | 0 | 6 | 0.309 | 24 | 3 | 0.505 | 9 | Progressive Rupture | 0.47 | 2533 | 19.5 | 33516 | 0.37 |
| TS33.11-G-9x24-W20xW7.5-L12-Z20-B | 12 | 18 | 0 | 6 | 0.309 | 24 | 3 | 0.505 | 9 | Pullout | 0.75 | 2486 | 19.1 | 42554 | 0.48 |
| TS33.04-G-9x24-W20xW7.5-L6-Z40-T | 6 | 18 | 0 | 3 | 0.309 | 24 | 3 | 0.505 | 9 | Pullout | 0.75 | 5022 | 38.7 | 25577 | 0.28 |
| TS33.08-G-9x24-W20xW7.5-L6-Z40-M | 6 | 18 | 0 | 3 | 0.309 | 24 | 3 | 0.505 | 9 | Pullout | 0.75 | 5028 | 38.7 | 28652 | 0.32 |
| TS33.12-G-9x24-W20xW7.5-L6-Z40-B | 6 | 18 | 0 | 3 | 0.309 | 24 | 3 | 0.505 | 9 | Pullout | 0.75 | 4910 | 37.8 | 27065 | 0.31 |
| TS36.05-G-9x24-W20xW11-L12-Z5-M | 12 | 18 | 0 | 6 | 0.374 | 24 | 3 | 0.505 | 9 | Pullout | 0.72 | 699 | 5.4 | 38623 | 1.53 |
| TS36.09-G-9x24-W20xW11-L12-Z5-B | 12 | 18 | 0 | 6 | 0.374 | 24 | 3 | 0.505 | 9 | Progressive Rupture | 0.71 | 681 | 5.2 | 42876 | 1.75 |
| TS36.02-G-9x24-W20xW11-L12-Z12-T | 12 | 18 | 0 | 6 | 0.374 | 24 | 3 | 0.505 | 9 | Pullout | 0.75 | 1575 | 12.1 | 37430 | 0.66 |
| TS36.06-G-9x24-W20xW11-L12-Z12-M | 12 | 18 | 0 | 6 | 0.374 | 24 | 3 | 0.505 | 9 | Pullout | 0.75 | 1539 | 11.8 | 39193 | 0.71 |
| TS36.10-G-9x24-W20xW11-L12-Z12-B | 12 | 18 | 0 | 6 | 0.374 | 24 | 3 | 0.505 | 9 | Pullout | 0.74 | 1554 | 11.9 | 43262 | 0.77 |
| TS36.03-G-9x24-W20xW11-L12-Z20-T | 12 | 18 | 0 | 6 | 0.374 | 24 | 3 | 0.505 | 9 | Pullout | 0.73 | 2613 | 20 | 38863 | 0.41 |
| TS36.07-G-9x24-W20xW11-L12-Z20-M | 12 | 18 | 0 | 6 | 0.374 | 24 | 3 | 0.505 | 9 | Pullout | 0.71 | 2622 | 20.1 | 42537 | 0.45 |
| TS36.11-G-9x24-W20xW11-L12-Z20-B | 12 | 18 | 0 | 6 | 0.374 | 24 | 3 | 0.505 | 9 | Pullout | 0.73 | 2624 | 20.1 | 44006 | 0.47 |
| TS36.04-G-9x24-W20xW11-L6-Z40-T | 6 | 18 | 0 | 3 | 0.374 | 24 | 3 | 0.505 | 9 | Pullout | 0.75 | 5203 | 39.9 | 27362 | 0.29 |
| TS36.08-G-9x24-W20xW11-L6-Z40-M | 6 | 18 | 0 | 3 | 0.374 | 24 | 3 | 0.505 | 9 | Pullout | 0.74 | 5036 | 38.6 | 27045 | 0.3 |

| TestID | Length, Le (ft) | Width, b (in.) | Skew, β (°) | Trans. Bar # | Trans. Bar Diameter, t (in.) | Trans. Bar Spacing, St (in.) | Long. Bar # | Long. Bar Diameter, tl (in.) | Long. Bar Spacing, Sl (in.) | Reinforcement Behavior | Displacement (in.) | Overburden, σv (psf) | DOF, z (ft) | Load, Pr (lb) | F* |
|---|---|---|---|---|---|---|---|---|---|---|---|---|---|---|---|
| TS36.12-G-9x24-W20xW11-L6-Z40-B | 6 | 18 | 0 | 3 | 0.374 | 24 | 3 | 0.505 | 9 | Progressive Rupture | 0.37 | 5135 | 39.4 | 25355 | 0.27 |
| TS39.01-G-9x24-W20xW15-L12-Z5-T | 12 | 18 | 0 | 6 | 0.437 | 24 | 3 | 0.505 | 9 | Progressive Rupture | 0.54 | 646 | 5.4 | 37301 | 1.6 |
| TS39.05-G-9x24-W20xW15-L12-Z5-M | 12 | 18 | 0 | 6 | 0.437 | 24 | 3 | 0.505 | 9 | Progressive Rupture | 0.34 | 661 | 5.6 | 37964 | 1.59 |
| TS39.09-G-9x24-W20xW15-L12-Z5-B | 12 | 18 | 0 | 6 | 0.437 | 24 | 3 | 0.505 | 9 | Progressive Rupture | 0.33 | 619 | 5.2 | 41224 | 1.85 |
| TS39.02-G-9x24-W20xW15-L12-Z12-T | 12 | 18 | 0 | 6 | 0.437 | 24 | 3 | 0.505 | 9 | Progressive Rupture | 0.51 | 1494 | 12.6 | 37909 | 0.7 |
| TS39.06-G-9x24-W20xW15-L12-Z12-M | 12 | 18 | 0 | 6 | 0.437 | 24 | 3 | 0.505 | 9 | Progressive Rupture | 0.33 | 1487 | 12.5 | 39579 | 0.74 |
| TS39.10-G-9x24-W20xW15-L12-Z12-B | 12 | 18 | 0 | 6 | 0.437 | 24 | 3 | 0.505 | 9 | Progressive Rupture | 0.45 | 1480 | 12.5 | 41077 | 0.77 |
| TS39.03-G-9x24-W20xW15-L12-Z20-T | 12 | 18 | 0 | 6 | 0.437 | 24 | 3 | 0.505 | 9 | Progressive Rupture | 0.49 | 2490 | 21 | 38981 | 0.43 |
| TS39.07-G-9x24-W20xW15-L12-Z20-M | 12 | 18 | 0 | 6 | 0.437 | 24 | 3 | 0.505 | 9 | Progressive Rupture | 0.28 | 2473 | 20.9 | 41817 | 0.47 |
| TS39.11-G-9x24-W20xW15-L12-Z20-B | 12 | 18 | 0 | 6 | 0.437 | 24 | 3 | 0.505 | 9 | Progressive Rupture | 0.28 | 2460 | 20.7 | 40727 | 0.46 |
| TS39.04-G-9x24-W20xW15-L6-Z40-T | 6 | 18 | 0 | 3 | 0.437 | 24 | 3 | 0.505 | 9 | Progressive Rupture | 0.31 | 5082 | 42.8 | 28060 | 0.31 |
| TS39.08-G-9x24-W20xW15-L6-Z40-M | 6 | 18 | 0 | 3 | 0.437 | 24 | 3 | 0.505 | 9 | Progressive Rupture | 0.31 | 5023 | 42.4 | 27341 | 0.3 |
| TS39.12-G-9x24-W20xW15-L6-Z40-B | 6 | 18 | 0 | 3 | 0.437 | 24 | 3 | 0.505 | 9 | Progressive Rupture | 0.74 | 4966 | 41.9 | 22913 | 0.26 |
| TS50.14-G-9x24-W20xW15-L6-Z40-M | 6 | 18 | 0 | 3 | 0.437 | 24 | 3 | 0.505 | 9 | Pullout | 0.74 | 5061 | 40.3 | 35041 | 0.38 |
| TS50.21-G-9x24-W20xW15-L6-Z40-B | 6 | 18 | 0 | 3 | 0.437 | 24 | 3 | 0.505 | 9 | Progressive Rupture | 0.37 | 5053 | 39.3 | 29185 | 0.32 |
| TS42.02-G-12x12-W9.5xW11-L6-Z5-T | 6 | 24 | 0 | 6 | 0.374 | 12 | 3 | 0.348 | 12 | Progressive Rupture | 0.4 | 625 | 5.2 | 17842 | 1.19 |
| TS42.06-G-12x12-W9.5xW11-L6-Z5-M | 6 | 24 | 0 | 6 | 0.374 | 12 | 3 | 0.348 | 12 | Progressive Rupture | 0.28 | 627 | 5.2 | 19896 | 1.32 |
| TS42.04-G-12x12-W9.5xW11-L3-Z12-T | 3 | 24 | 0 | 3 | 0.374 | 12 | 3 | 0.348 | 12 | Progressive Rupture | 0.26 | 1489 | 12.3 | 10961 | 0.61 |
| TS42.08-G-12x12-W9.5xW11-L3-Z12-M | 3 | 24 | 0 | 3 | 0.374 | 12 | 3 | 0.348 | 12 | Progressive Rupture | 0.35 | 1507 | 12.4 | 15545 | 0.86 |
| TS42.12-G-12x12-W9.5xW11-L3-Z12-B | 3 | 24 | 0 | 3 | 0.374 | 12 | 3 | 0.348 | 12 | Progressive Rupture | 0.32 | 1570 | 11.8 | 16332 | 0.87 |
| TS42.10-G-12x12-W9.5xW11-L6-Z20-B | 6 | 24 | 0 | 6 | 0.374 | 12 | 3 | 0.348 | 12 | Rupture | 0.3 | 2529 | 19 | 23558 | 0.39 |
| TS40.02-G-12x12-W20xW11-L6-Z5-T | 6 | 24 | 0 | 6 | 0.374 | 12 | 3 | 0.505 | 12 | Pullout | 0.75 | 683 | 5.7 | 32498 | 1.98 |
| TS40.06-G-12x12-W20xW11-L6-Z5-M | 6 | 24 | 0 | 6 | 0.374 | 12 | 3 | 0.505 | 12 | Pullout | 0.75 | 642 | 5.4 | 34621 | 2.25 |

| TestID | Length, Le (ft) | Width, b (in.) | Skew, β (°) | Trans. Bar # | Trans. Bar Diameter, t (in.) | Trans. Bar Spacing, St (in.) | Long. Bar # | Long. Bar Diameter, tl (in.) | Long. Bar Spacing, Sl (in.) | Reinforcement Behavior | Displacement (in.) | Overburden, σv (psf) | DOF, z (ft) | Load, Pr (lb) | F* |
|---|---|---|---|---|---|---|---|---|---|---|---|---|---|---|---|
| TS40.10-G-12x12-W20xW11-L6-Z5-B | 6 | 24 | 0 | 6 | 0.374 | 12 | 3 | 0.505 | 12 | Pullout | 0.75 | 662 | 5.5 | 43538 | 2.74 |
| TS40.04-G-12x12-W20xW11-L6-Z12-T | 6 | 24 | 0 | 6 | 0.374 | 12 | 3 | 0.505 | 12 | Progressive Rupture | 0.43 | 1507 | 12.6 | 34132 | 0.94 |
| TS40.08-G-12x12-W20xW11-L6-Z12-M | 6 | 24 | 0 | 6 | 0.374 | 12 | 3 | 0.505 | 12 | Pullout | 0.74 | 1480 | 12.4 | 43342 | 1.22 |
| TS40.12-G-12x12-W20xW11-L6-Z12-B | 6 | 24 | 0 | 6 | 0.374 | 12 | 3 | 0.505 | 12 | Progressive Rupture | 0.42 | 1479 | 12.4 | 36777 | 1.04 |
| TS41.02-G-12x12-W20xW11-L6-Z20-T | 6 | 24 | 0 | 6 | 0.374 | 12 | 3 | 0.505 | 12 | Progressive Rupture | 0.61 | 2491 | 20.4 | 33413 | 0.56 |
| TS41.06-G-12x12-W20xW11-L6-Z20-M | 6 | 24 | 0 | 6 | 0.374 | 12 | 3 | 0.505 | 12 | Pullout | 0.73 | 2486 | 20.3 | 43369 | 0.73 |
| TS41.10-G-12x12-W20xW11-L6-Z20-B | 6 | 24 | 0 | 6 | 0.374 | 12 | 3 | 0.505 | 12 | Progressive Rupture | 0.6 | 2493 | 19.1 | 44959 | 0.75 |
| TS41.04-G-12x12-W20xW11-L3-Z40-T | 3 | 24 | 0 | 3 | 0.374 | 12 | 3 | 0.505 | 12 | Progressive Rupture | 0.52 | 5008 | 41 | 25478 | 0.42 |
| TS41.08-G-12x12-W20xW11-L3-Z40-M | 3 | 24 | 0 | 3 | 0.374 | 12 | 3 | 0.505 | 12 | Progressive Rupture | 0.41 | 4992 | 40.7 | 21608 | 0.36 |
| TS41.12-G-12x12-W20xW11-L3-Z40-B | 3 | 24 | 0 | 3 | 0.374 | 12 | 3 | 0.505 | 12 | Progressive Rupture | 0.55 | 5024 | 38.6 | 26982 | 0.45 |

## TABLE D3: SUMMARY DATA FOR MSE REINFORCEMENT PULLOUT TESTS
## SMOOTH STEEL BARS IN TYPE B BACKFILL

| TestID | Length, Le (ft) | Long. Bar Diameter, tl (in.) | Reinforcement Behavior | Displacement (in.) | Overburden, σv (psf) | DOF, z (ft) | Load, Pr (lb) | F* |
|---|---|---|---|---|---|---|---|---|
| TS50.01-B-W9.5-L6-Z5-T | 6 | 0.348 | 0 | 0 | 0 | 0 | 1 | 0.348 |
| TS50.08-B-W9.5-L6-Z5-M | 6 | 0.348 | 0 | 0 | 0 | 0 | 1 | 0.348 |
| TS50.15-B-W9.5-L6-Z5-B | 6 | 0.348 | 0 | 0 | 0 | 0 | 1 | 0.348 |
| TS50.06-B-W9.5-L3-Z12-T | 3 | 0.348 | 0 | 0 | 0 | 0 | 1 | 0.348 |
| TS50.13-B-W9.5-L3-Z12-M | 3 | 0.348 | 0 | 0 | 0 | 0 | 1 | 0.348 |
| TS50.20-B-W9.5-L3-Z12-B | 3 | 0.348 | 0 | 0 | 0 | 0 | 1 | 0.348 |
| TS50.02-B-W20-L6-Z5-T | 6 | 0.5 | 0 | 0 | 0 | 0 | 1 | 0.505 |
| TS50.09-B-W20-L6-Z5-M | 6 | 0.5 | 0 | 0 | 0 | 0 | 1 | 0.505 |
| TS50.16-B-W20-L6-Z5-B | 6 | 0.5 | 0 | 0 | 0 | 0 | 1 | 0.505 |
| TS50.03-B-W20-L6-Z12-T | 6 | 0.5 | 0 | 0 | 0 | 0 | 1 | 0.505 |
| TS50.10-B-W20-L6-Z12-M | 6 | 0.5 | 0 | 0 | 0 | 0 | 1 | 0.505 |
| TS50.17-B-W20-L6-Z12-B | 6 | 0.5 | 0 | 0 | 0 | 0 | 1 | 0.505 |
| TS50.04-B-W20-L6-Z20-T | 6 | 0.5 | 0 | 0 | 0 | 0 | 1 | 0.505 |
| TS50.05-B-W20-L3-Z40-T | 3 | 0.5 | 0 | 0 | 0 | 0 | 1 | 0.505 |
| TS50.12-B-W20-L3-Z40-M | 3 | 0.5 | 0 | 0 | 0 | 0 | 1 | 0.505 |
| TS50.19-B-W20-L3-Z40-B | 3 | 0.5 | 0 | 0 | 0 | 0 | 1 | 0.505 |

# Appendix E

# Summary Data for MSE Reinforcement Pullout Tests – Strain Gage Reports

## Ribbed Strips in Type B Backfill

## Welded Steel Grids in Type B Backfill

## Ribbed Strips in Type A Backfill

## Welded Steel Grids in Type A Backfill

**TABLE E1: SUMMARY DATA FOR MSE REINFORCEMENT PULLOUT TESTS**
**RIBBED STRIPS IN TYPE B BACKFILL**
**STRAIN GAGE REPORTS**

| TestID | Nominal Depth of Fill, z (ft) | Reinforcement Dimensions | | |
| --- | --- | --- | --- | --- |
| | | Length, Le (ft) | Width, b (in.) | Skew, β (°) |
| TS29.09-S-L8-Z5-M | 5 | 8 | 2 | 0 |
| TS29.13-S-L8-Z5-B | 5 | 8 | 2 | 0 |
| TS29.01-S-L12-Z5-T | 5 | 12 | 2 | 0 |
| TS29.05-S-L12-Z5-T | 5 | 12 | 2 | 0 |
| TS29.10-S-L8-Z12-M | 12 | 8 | 2 | 0 |
| TS29.14-S-L8-Z12-B | 12 | 8 | 2 | 0 |
| TS29.02-S-L12-Z12-T | 12 | 12 | 2 | 0 |
| TS29.06-S-L12-Z12-M | 12 | 12 | 2 | 0 |
| TS29.11-S-L8-Z20-B | 20 | 8 | 2 | 0 |
| TS29.03-S-L12-Z20-T | 20 | 12 | 2 | 0 |
| TS29.07-S-L12-Z20-M | 20 | 12 | 2 | 0 |
| TS29.12-S-L8-Z40-B | 40 | 8 | 2 | 0 |
| TS29.16-S-L8-Z40-B | 40 | 8 | 2 | 0 |
| TS29.04-S-L12-Z40-T | 40 | 12 | 2 | 0 |
| TS29.08-S-L12-Z40-M | 40 | 12 | 2 | 0 |

## TABLE E2: SUMMARY DATA FOR MSE REINFORCEMENT PULLOUT TESTS
## WELDED STEEL GRIDS IN TYPE B BACKFILL
## STRAIN GAGE REPORTS

| TestID | Nominal Depth of Fill, z (ft) | Length, Le (ft) | Width, b (in.) | Skew, β (°) | Trans. Bar # | Trans. Bar Diameter, t (in.) | Trans. Bar Spacing, St (in.) | Long. Bar # | Long. Bar Diameter, tl (in.) | Long. Bar Spacing, Sl (in.) |
|---|---|---|---|---|---|---|---|---|---|---|
| TS24.01-G-6x12-W9.5xW11-L6-Z5-T | 5 | 6 | 12 | 0 | 6 | 0.374 | 12 | 3 | 0.348 | 6 |
| TS25.01-G-6x12-W20xW11-L6-Z5-T | 5 | 6 | 12 | 0 | 6 | 0.374 | 12 | 3 | 0.505 | 6 |
| TS24.02-G-9x12-W9.5xW11-L6-Z5-T | 5 | 6 | 18 | 0 | 6 | 0.374 | 12 | 3 | 0.348 | 9 |
| TS25.02-G-9x12-W20xW11-L6-Z5-T | 5 | 6 | 18 | 0 | 6 | 0.374 | 12 | 3 | 0.505 | 9 |
| TS24.03-G-6x12-W9.5xW11-L3-Z12-T | 12 | 3 | 12 | 0 | 3 | 0.374 | 12 | 3 | 0.348 | 6 |
| TS25.03-G-6x12-W20xW11-L6-Z12-T | 12 | 6 | 12 | 0 | 6 | 0.374 | 12 | 3 | 0.505 | 6 |
| TS24.04-G-9x12-W9.5xW11-L3-Z12-T | 12 | 3 | 18 | 0 | 3 | 0.374 | 12 | 3 | 0.348 | 9 |
| TS25.04-G-9x12-W20xW11-L6-Z12-T | 12 | 6 | 18 | 0 | 6 | 0.374 | 12 | 3 | 0.505 | 9 |
| TS26.01-G-6x12-W20xW11-L6-Z20-T | 20 | 6 | 12 | 0 | 6 | 0.374 | 12 | 3 | 0.505 | 6 |
| TS26.02-G-9x12-W20xW11-L6-Z20-T | 20 | 6 | 18 | 0 | 6 | 0.374 | 12 | 3 | 0.505 | 9 |
| TS26.03-G-6x12-W20xW11-L3-Z40-T | 40 | 3 | 12 | 0 | 3 | 0.374 | 12 | 3 | 0.505 | 6 |

## TABLE E3: SUMMARY DATA FOR MSE REINFORCEMENT PULLOUT TESTS
## RIBBED STRIPS IN TYPE A BACKFILL
## STRAIN GAGE REPORTS

| TestID | Nominal Depth of Fill, z (ft) | Reinforcement Dimensions | | |
|---|---|---|---|---|
| | | Length, Le (ft) | Width, b (in.) | Skew, β (°) |
| TS48.18-S-L8-Z5-B | 5 | 8 | 2 | 0 |
| TS48.17-S-L8-Z20-M | 20 | 8 | 2 | 0 |
| TS48.19-S-L8-Z20-B | 20 | 8 | 2 | 0 |

## TABLE E4: SUMMARY DATA FOR MSE REINFORCEMENT PULLOUT TESTS
## WELDED STEEL GRIDS IN TYPE A BACKFILL
## STRAIN GAGE REPORTS

| TestID | Nominal Depth of Fill, z (ft) | Length, Le (ft) | Width, b (in.) | Skew, β (°) | Trans. Bar # | Trans. Bar Diameter, t (in.) | Trans. Bar Spacing, St (in.) | Long. Bar # | Long. Bar Diameter, tl (in.) | Long. Bar Spacing, Sl (in.) |
|---|---|---|---|---|---|---|---|---|---|---|
| | | | | | **Reinforcement Dimensions** | | | | | |
| TS48.05-G-9x12-W20xW11-L6-Z5-M | 5 | 6 | 18 | 0 | 6 | 0.374 | 12 | 3 | 0.505 | 9 |
| TS48.07-G-9x12-W20xW11-L6-Z5-M | 5 | 6 | 18 | 0 | 6 | 0.374 | 12 | 3 | 0.505 | 9 |
| TS48.11-G-9x12-W20xW11-L6-Z5-B | 5 | 6 | 18 | 0 | 6 | 0.374 | 12 | 3 | 0.505 | 9 |
| TS48.06-G-9x12-W20xW11-L6-Z20-M | 20 | 6 | 18 | 0 | 6 | 0.374 | 12 | 3 | 0.505 | 9 |
| TS48.10-G-9x12-W20xW11-L6-Z20-B | 20 | 6 | 18 | 0 | 6 | 0.374 | 12 | 3 | 0.505 | 9 |
| TS48.12-G-9x12-W20xW11-L6-Z20-B | 20 | 6 | 18 | 0 | 6 | 0.374 | 12 | 3 | 0.505 | 9 |
| TS48.05-G-9x12-W20xW11-L6-Z5-M | 5 | 6 | 18 | 0 | 6 | 0.374 | 12 | 3 | 0.505 | 9 |
| TS48.07-G-9x12-W20xW11-L6-Z5-M | 5 | 6 | 18 | 0 | 6 | 0.374 | 12 | 3 | 0.505 | 9 |
| TS48.11-G-9x12-W20xW11-L6-Z5-B | 5 | 6 | 18 | 0 | 6 | 0.374 | 12 | 3 | 0.505 | 9 |
| TS48.06-G-9x12-W20xW11-L6-Z20-M | 20 | 6 | 18 | 0 | 6 | 0.374 | 12 | 3 | 0.505 | 9 |

**TEXAS TECH UNIVERSITY**

## Multidisciplinary Research in Transportation

Texas Tech University | Lubbock, Texas 79409
P 806.742.3503 | F 806.742.4168